

**Investigation of the grade of calcined clays used
as clinker substitute
in Limestone Calcined Clay Cement (LC3)**

THÈSE N° 8143 (2017)

PRÉSENTÉE LE 10 NOVEMBRE 2017
À LA FACULTÉ DES SCIENCES ET TECHNIQUES DE L'INGÉNIEUR
LABORATOIRE DES MATÉRIAUX DE CONSTRUCTION
PROGRAMME DOCTORAL EN SCIENCE ET GÉNIE DES MATÉRIAUX

ÉCOLE POLYTECHNIQUE FÉDÉRALE DE LAUSANNE

POUR L'OBTENTION DU GRADE DE DOCTEUR ÈS SCIENCES

PAR

François Henri AVET

acceptée sur proposition du jury:

Dr L. Weber, président du jury
Prof. K. Scrivener, directrice de thèse
Dr B. Lothenbach, rapporteuse
Prof. J. Skibsted, rapporteur
Prof. P. Bowen, rapporteur



ÉCOLE POLYTECHNIQUE
FÉDÉRALE DE LAUSANNE

Suisse
2017

Acknowledgements

These four years of PhD were an unforgettable step of my life and I would really like to thank the people who made me enjoy it so much.

I would first like to thank the person who made this thesis possible, my thesis director, Prof. Karen Scrivener for the opportunity of doing a PhD, for her support and her extremely valuable advice during these four years of PhD. I would also like to thank the members of my jury for their comments and suggestions, Dr. Barbara Lothenbach, Prof. Jorgen Skibsted and Prof. Paul Bowen.

The LMC team made the everyday-life great. Lily and I were in between two "waves" of PhD students and we could enjoy both periods. From the old team, I would like to thank Elise and Berta for their daily smiles and the scientific discussions, John for TEM help and chocolate brownies, Arnaud for the help for $^1\text{H-NMR}$ and the amazing Europapark trips, Julien for the Ticino accent, Ruben for the great help with the R^3 test and Mathieu for all the calcined clay legacy.

From the younger team, I would like to thank Mink for her kindness, Wiola for the great dinners, Hamed for the chloride barbecues, Xuerun for the help for XRD, Yosra for the pleasant lab atmosphere, Emmanuelle for the TEM tough work, Frank for the Satellite trips, Adrien for your motivating attitude, Alex for the white board, Yan for Hui, Hui for the cactus and Shiyu for Jacques Dutronc. I would also like to wish the best to the latest LMC comers for their on-going PhDs: the famous Anna, So, Mahsa and Mariana. Thanks also to Ellina and Emilie from EMPA. I am also grateful for the help given by bachelor and master students for this project: Delphine, Aigoul and Joanne, my intern Benoît and my semester project students Dimitri, Gilles, Joris and Gauthier.

More generally, I would like to thank all members of the LC^3 team from Switzerland, Cuba and India. We always had very good interactions between Julien, Aurélie, Franco at EPFL, Geetika, A.Anuj, Yuvaraj, Sundar, Vineet, Sreejith and Arun from IITs, Ribalta, Abdel and Adrian from Havana. All our meetings and discussions brought new insight and new perspective for this amazing project.

I would also like to thank Maude and Anne-Sandra for their help in the organization for conferences, trips, lab hikes, ski seminars and many other things, Marie Alix for the Nanocem events, Jean, Paul and Tonio for the technical help and the funny discussions.

I could not put Hadi neither in the old nor the new team since he might still be around hidden. Thanks for all the great moments spent together! Lionel. Just entering your office was great. So many good stories, anecdotes and jokes heard. My dear officemate, Lily (Xiaoli), we started on the same day, and we almost finished on the same day. We shared many good memories and the MXG241 office quickly became the place to be in the lab.

Last but not least, I would like to really emphasize the bravery of my whole family for supporting me, especially during the last busy months of PhD.

Acknowledgements

The Swiss Agency for Development and Cooperation (SDC) is warmly thanked for funding this thesis through the LC³ project.

Abstract

The combination of calcined kaolinitic clays and limestone in Limestone Calcined Clay Cement (LC³) is a promising approach to reduce the cost and the CO₂ emissions of cement production by reducing the clinker content of cement. This thesis investigates the feasibility of using various grades of calcined clays in LC³. LC³-50 blends with a clinker content reduced to 50% are studied.

The factors controlling the reactivity of LC³-50 blends containing various grades of calcined kaolinitic clays were first studied. A benchmark test of mortar strength was developed. Similar strength to plain Portland cement (PC) can be obtained even for clays with 40% of calcined kaolinite only. Moreover, strengths are strongly dependent on the calcined kaolinite content of the calcined clay. The development of the new Rapid, Relevant and Reliable (R³) pozzolanic test allows the evaluation of the reactivity of calcined clays after only 24 h by isothermal calorimetry and 3 days simply using an oven, and it allows the prediction of the strength development of LC³-50 mortars.

To explain strength results, a phase assemblage study was carried out. In order to determine the amount of reacted metakaolin, three methods were tested and mass balance was found to be the most reliable one. The phase assemblage study showed that a critical refinement of pore connectivity is reached already at 3 days for LC³-50 blends with high calcined kaolinite content. From this point on, clinker hydration is slowed down, and the formation of crystalline hydration products is limited. The on-going reaction of metakaolin leads to the higher incorporation of aluminium in the calcium alumino silicate hydrate (C-A-S-H). The C-A-S-H was fully characterized in terms of composition, morphology and density. No change in morphology was observed by Transmission Electron Microscopy. The C-A-S-H density determined by ¹H-Nuclear Magnetic Resonance was also found to be similar between PC and LC³-50 with different calcined kaolinite content. Combining all this information, a good relationship is obtained between strength and gel space ratio for PC and for the LC³-50 blends.

Finally, the chloride resistance was tested through ponding and chloride binding isotherm tests. The results also support previous findings for the use of calcined clays with a calcined kaolinite content of at least 40% to get a better chloride resistance than PC. These results are mainly explained by the pore connectivity refinement of LC³-50 blends compared with PC. The chloride binding is the highest for clays with 40-50% of calcined kaolinite.

Keywords

Limestone Calcined Clay Cement, hydration, microstructure development

Résumé

Une approche prometteuse pour réduire le coût et les émissions de CO₂ de la production de ciment consiste à partiellement remplacer le clinker du ciment par de l'argile calcinée et du calcaire pour la formulation des ciments calcaire argiles calcinées (LC³). Dans ce travail de thèse, les systèmes LC³-50 sont étudiés, dans lesquels le contenu en clinker est réduit à 50%. Le but de cette thèse est de mettre en lumière l'influence de la qualité de l'argile calcinée sur les propriétés des mélanges LC³-50.

Les facteurs déterminant la réactivité des mélanges LC³-50 contenant différentes argiles kaoliniques ont d'abord été étudiés. Un test comparatif de référence pour mesurer la résistance à la compression sur mortier a été lancé. Les résultats montrent que des résistances similaires au ciment de référence (PC) sont obtenues même pour des systèmes LC³-50 ayant des argiles calcinées avec un contenu initial en kaolinite de 40% seulement. De plus, les résistances obtenues indiquent une claire dépendance au contenu en kaolinite calcinée de l'argile. En parallèle de cette étude sur mortiers, un nouveau test pouzzolanique (nommé R³) a été développé afin de prédire le développement de la résistance des mortiers de manière beaucoup plus rapide. Ce test est réalisé en évaluant la réactivité des argiles calcinées en 24 h par calorimétrie isotherme ou en 3 jours en utilisant simplement un four.

Pour expliquer les résultats en compression obtenus, la microstructure et l'assemblage de phase durant l'hydratation ont été étudiés sur pâte de ciment. Afin de déterminer le degré de réaction du métakaolin, trois méthodes ont été utilisées et la conservation de masse s'est avérée être la plus fiable. Concernant la microstructure, un raffinement maximal de la connectivité des pores est observé après seulement 3 jours d'hydratation pour les LC³-50 contenant des argiles calcinées de haute qualité. Une fois cette limite atteinte, la réaction du clinker s'arrête, tout comme la formation d'hydrates cristallins. La réaction continue du métakaolin entraîne une augmentation de la quantité d'aluminium incorporée dans le C-A-S-H. La morphologie du C-A-S-H observée par microscope électronique à transmission est très similaire pour tous les systèmes étudiés, tout comme la densité mesurée par ¹H résonance magnétique nucléaire. En combinant toutes ces informations, le rapport quantité de gel par espace disponible a pu être calculé et corrélé aux résistances à la compression pour les systèmes LC³-50 et le PC.

Enfin, la résistance aux chlorures a été étudiée, et les résultats des tests de mise en solution saline montrent également que l'utilisation d'argile avec seulement 40% of kaolinite est particulièrement adaptée. Une meilleure résistance que le PC est obtenue pour tous les LC³-50 avec 40% ou plus de kaolinite calcinée. Ces résultats sont expliqués principalement par le raffinement de la porosité des LC³-50 par rapport au PC. Par ailleurs, la capacité de capture des chlorures est maximale pour les systèmes LC³-50 avec 40-50% de kaolinite calcinée.

Mots-clés

Ciment calcaire argiles calcinées, hydratation, microstructure

Contents

Acknowledgements	iii
Abstract	v
Résumé	vi
Chapter 1 - Introduction	1
1.1 Context.....	1
1.2 From kaolinitic clays to calcined kaolinitic clays	1
1.3 Influence of calcined clay and limestone on hydration	3
1.4 Limestone Calcined Clay Cements (LC ³)	4
1.5 Objective of the thesis	5
Chapter 2 - Development of a new rapid, relevant and reliable (R³) test method to evaluate the pozzolanic reactivity of calcined kaolinitic clays	7
2.1 Introduction	7
2.1.1 Portlandite consumption	7
2.1.2 Degree of reaction of SCMs	8
2.1.3 SCM physical properties	9
2.1.4 Compressive strength on simplified systems.....	9
2.1.5 Objectives	10
2.2 Materials and Methods	10
2.2.1 Material characterization	10
2.2.2 Mortar strength tests	11
2.2.3 Mix design of the R ³ test	12
2.2.4 Methods	13
2.3 Results	14
2.3.1 Mortar compressive strength	14
2.3.2 Optimisation of parameters for R ³ pozzolanic activity tests	16
2.3.3 Application of the R ³ test to calcined clays: heat flow measurements	19
2.3.4 Bound water determination.....	24
2.3.5 Comparison with the modified Chapelle test.....	26
2.4 Conclusion.....	29
Chapter 3 - Determination of the amount of reacted metakaolin in calcined clay blends	31

3.1	Introduction	31
3.2	Methods	32
	3.2.1 Mass balance.....	32
	3.2.2 Thermodynamic modelling.....	33
	3.2.3 PONKCS method	33
3.3	Materials	34
	3.3.1 Characterization of raw and calcined materials.....	34
3.4	Analytical details	35
	3.4.1 Paste sample preparation	35
	3.4.2 Mass balance and thermodynamic modelling.....	36
	3.4.3 PONKCS	37
3.5	Results	39
	3.5.1 Mass balance and thermodynamic modelling.....	39
	3.5.2 Sensitivity analysis for mass balance and thermodynamic modelling	44
	3.5.3 Output reliability.....	45
	3.5.4 PONKCS method	46
3.6	Conclusion.....	48
Chapter 4 - Investigation of the calcined kaolinite content on the hydration of Limestone Calcined Clay Cement (LC³)		
49		
4.1	Introduction	49
4.2	Materials and methods.....	50
	4.2.1 Kaolinitic clays	50
	4.2.2 Microstructure study on pastes	51
4.3	Results	53
	4.3.1 Kinetics of hydration	53
	4.3.2 Determination of clinker hydration degree.....	54
	4.3.3 Characterization of metakaolin reaction.....	55
	4.3.4 Determination of the amount of reacted metakaolin	56
	4.3.5 Porosity characterization	57
4.4	Discussion.....	62
	4.4.1 Slowing down of clinker hydration	62
	4.4.2 Hydration product formation	65
	4.4.3 Correlation with compressive strength results.....	67

4.5	Conclusion.....	67
Chapter 5 - Investigation of C-A-S-H composition, morphology and density in Limestone Calcined Clay Cement (LC³)		
69		
5.1	Introduction	69
5.2	Materials characteristics and mix design.....	70
5.3	Analytical details.....	72
5.3.1	C-A-S-H morphology and composition	72
5.3.2	C-A-S-H density	73
5.3.3	Porosity.....	74
5.4	Results	74
5.4.1	Comparison of hydration between grey and white cement	74
5.4.2	C-A-S-H composition.....	76
5.4.3	C-A-S-H morphology	78
5.4.4	Density of C-A-S-H.....	79
5.4.5	Discussion.....	85
5.5	Conclusion.....	90
Chapter 6 - Relationship between compressive strength and phase assemblage for Limestone Calcined Clay Cement (LC³)		
92		
6.1	Introduction	92
6.2	Results	93
6.2.1	Strength and porosity.....	93
6.2.2	Gel Space Ratio	95
6.3	Conclusion.....	100
Chapter 7 - Chloride resistance of Limestone Calcined Clay Cement (LC³) using various grades of calcined kaolinitic clays		
102		
7.1	Introduction	102
7.2	Materials	103
7.3	Analytical details.....	105
7.3.1	Ponding test	105
7.3.2	Binding isotherm	106
7.4	Results and Discussions.....	107
7.4.1	Ponding test profiles	107
7.4.2	Binding capacity of LC ³ -50 blends.....	109

7.4.3 Porosity results	116
7.5 Conclusion	117
Chapter 8 - Conclusion & perspectives.....	119
8.1 Final summary	119
8.1.1 Understanding of factors controlling reactivity	119
8.1.2 Phase assemblage study	120
8.1.3 Evaluation of chloride resistance.....	121
8.2 Perspectives	121
8.2.1 Strength development	121
8.2.2 Microstructure development.....	122
8.2.3 Durability.....	122
Appendix	123
9.1 Appendix 1 : Cements and sulfate adjustment	123
9.1.1 Grey cement.....	123
9.1.2 Sulfate adjustment for grey and white cement	123
9.2 Appendix 2 - Characterization of raw and calcined clays	126
9.2.1 Kaolinite content, calcined kaolinite content and metakaolin content	126
9.2.2 Influence of other clays on kaolinite quantification by TGA	128
9.2.3 Comparison of kaolinite quantification between XRD-Rietveld and TGA131	
9.2.4 Calcination protocol.....	132
9.2.5 Physical properties and XRF chemical composition of calcined clays	132
9.3 Appendix 3. Application of R^3 test to different calcination temperature and various SCMs.....	135
9.3.1 Optimization of the calcination temperature of calcined clay	135
9.3.2 Application to other Supplementary Cementitious Materials	139
9.3.3 Conclusion	142
9.4 Appendix 4 – Workability of LC ³ -50 blends.....	143
9.4.1 Mortar	143
9.4.2 Paste.....	144
9.5 Appendix 5 – Determination of the density of C-A-S-H by ¹ H-NMR.....	146
9.6 Appendix 6 – XRD patterns of PC and LC ³ -50 blends in binding isotherms	148
References	151
Curriculum Vitae	157

Chapter 1 - Introduction

1.1 Context

Concrete is the most produced material in the world. About 4200 Mt of cement are made per year and its production keeps increasing [1, 2]. Cement is an excellent material, cheap, available and easy to use, and the production of 1 kg of concrete is much less emissive than most of construction materials, such as steel and ceramics for instance [3, 4]. However, due to its massive scale of production, cement is responsible for 5-8% of the anthropogenic CO₂ emissions and about 35% of industrial CO₂ emissions [5, 6]. The most emissive (and the most expensive) step of cement production is the clinker production. To reduce these environmental and economic impacts, the use of Supplementary Cementitious Materials (SCMs) has been the common approach in the recent years to reduce the clinker content of cement. Among the traditional SCMs, glass granulated blast furnace slag (GGBFS) reserves are already almost fully used in cement [7]. Larger amounts of fly ash are available but part of it shows too-low reactivity. This lack of good quality SCMs has led to a stabilization of the clinker to cement ratio in the cement industry over the past years [8]. Two SCMs which are not fully exploited and are widely available are calcined kaolinitic clays and limestone [9]. These could allow significant further savings in clinker costs and use. Limestone Calcined Clay Cements (LC³) exploits the synergy of the combination of cement with calcined kaolinitic clays and limestone.

1.2 From kaolinitic clays to calcined kaolinitic clays

Calcined kaolinitic clays are obtained from the calcination of raw kaolinitic clays. Kaolinitic clays are mainly present in tropical and subtropical climates, in soils formed by chemical weathering under hot and moist conditions. Figure 1.1 shows the wide distribution across the globe of kaolinite, present mainly in oxisols, ultisols and alfisols (in pink, yellow and pale green on the map) [10]. Interestingly, kaolinitic clays are present in areas where the increase for cement demand will be the highest during the next decades.

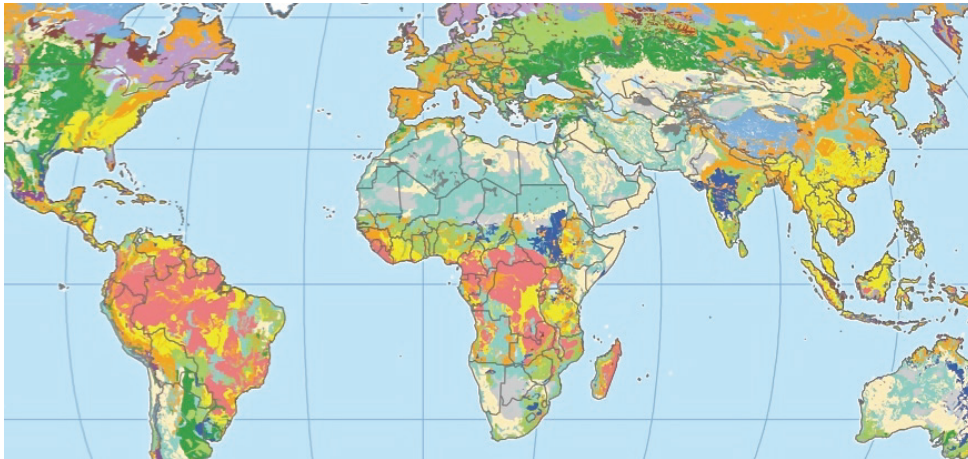


Figure 1.1. Presence of kaolinite in oxisols (pink), ultisols (yellow) and alfisols (pale green) [10].

Kaolinite differs from the other types of clays, such as illite or smectite, by its layer structure, only composed of one octahedral aluminate sheet and one tetrahedral silicate sheet, as presented in Figure 1.2. Hydrogen bonds between siloxane group and aluminol group link consecutive layers of kaolinite and prevent any water to penetrate the interlayer space, characterizing kaolinite as non-swelling clay. Some isomorphous substitution may occur of Al by Fe and of Si by Al, but in a much lower extent than for smectite or illite structures [11, 12].

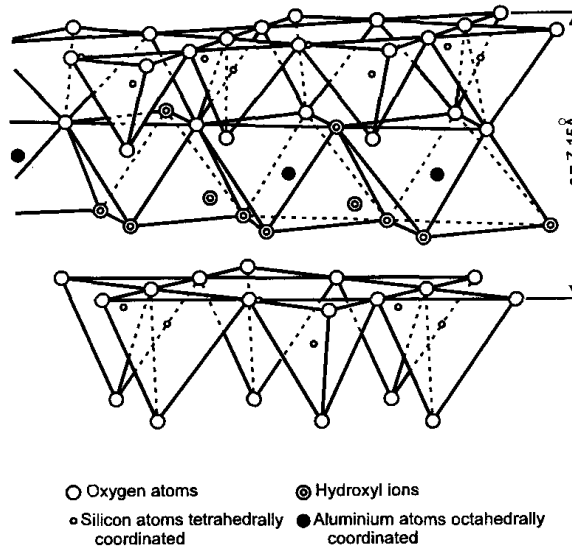
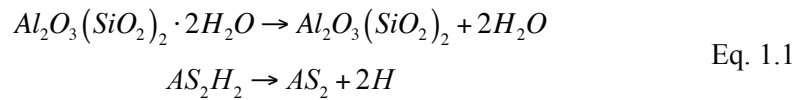


Figure 1.2. Kaolinite structure [13], adapted from [14].

Kaolinite does not show any reactivity in cement. It needs to be calcined to be reactive. During the calcination, the dehydroxylation of kaolinite occurs from 450°C to 600°C [15-19]. Kaolinite transforms into an amorphous metastable phase called metakaolin, according to Equation 1.1. Cement oxide notations are used here: A = Al_2O_3 , S = SiO_2 , etc.



The understanding of dehydroxylation was shown by several authors using ^{27}Al -Nuclear Magnetic Resonance [20-23]. This technique indicates the number of close neighbours Al atoms have. During dehydroxylation, a change of the coordination number of Al occurs from octahedral Al^{VI} to Al^{IV} and especially Al^V , leading to structural change shown in Figure 1.3 [22]. This structural disorder is responsible for the increase of reactivity [24]. Compared with illite or smectite structures, hydroxyl and aluminate groups are at the surface of kaolinite structure. The Al^V groups are thus directly exposed to the environment around metakaolin particles and can easily react. This explains why kaolinite shows the highest pozzolanic potential among the different kinds of clays [25, 26]. Fernandez made the comparison between kaolinite, illite and montmorillonite and he obtained higher mortar compressive strength than reference plain Portland cement (PC) for a blend with 30% of clinker substitution by pure metakaolin from 7 days onwards [22]. Illite and montmorillonite blends showed similar strength to a system containing inert quartz. Similar reactivity results were obtained by Hollanders [27].

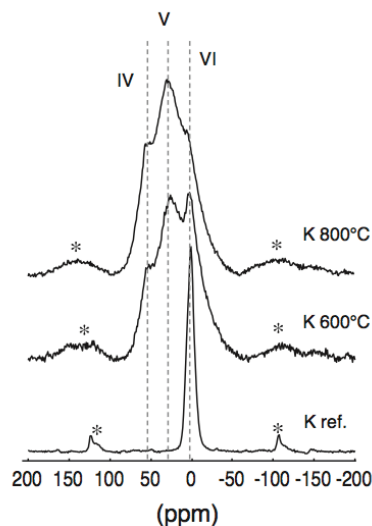
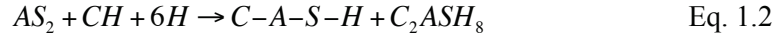


Figure 1.3. ^{27}Al NMR spectra of raw kaolinite and kaolinite calcined at 600°C and 800°C.

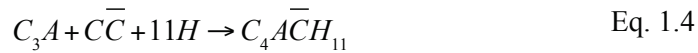
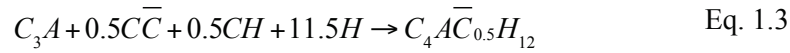
1.3 Influence of calcined clay and limestone on hydration

Both metakaolin and limestone have a physical influence on cement hydration. They provide nucleation sites permitting hydrate formation [28]. Moreover, their substitution for clinker at the same water to binder ratio, effectively increases the water to cement ratio. Thus, hydrates have more space to grow. Last but not least, Berodier showed that hydration was enhanced in presence of fine SCMs thanks to the increase of the shearing between particles. The shearing increase is related to the decrease of the distance between particles when fine SCMs are added [29]. As a consequence, clinker hydration is enhanced [30].

In addition to physical effect, metakaolin and limestone also chemically react during hydration. It is well-known that metakaolin reacts as pozzolan during cement hydration. Its reaction with portlandite CH and water mainly leads to the formation of C-A-S-H, and also strätlingite C_2ASH_8 after portlandite depletion [31-33]. This reaction is summarized in Equation 1.2.



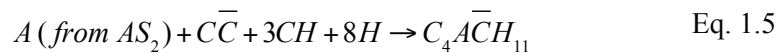
Limestone influences the products of the hydration of the aluminate phase. For reference PC without limestone, C_3A reacts with gypsum $C\bar{S}H_2$ to form ettringite AFt, and after complete consumption of gypsum, some of the ettringite reacts with remaining C_3A to form monosulfoaluminate phase Ms [34]. In presence of limestone, C_3A reacts with calcium carbonate to form carboaluminate hydrates, respectively hemi- and monocarboaluminate phases, Hc and Mc [35-37] according to Equations 1.3 and 1.4. Moreover, ettringite is retained and is not converted into Ms in systems containing limestone [38, 39].



Only 2-5% of limestone reacts during hydration of typical Portland cements [40, 41]. The limiting factor for limestone reaction is the aluminate from C_3A . The amounts of Hc and Mc are related to the initial C_3A content of clinker [42] and the initial aluminate to sulfate ratio [36] of the system.

1.4 Limestone Calcined Clay Cements (LC³)

In LC³, calcined clay and limestone are combined in order to further reduce the clinker content of cement. Antoni et al. showed that in addition to the reactions previously mentioned, metakaolin also provides some aluminate which reacts with calcium carbonate to form carboaluminate hydrates according to Equation 1.5 [43].



Antoni showed that the best compressive strengths were obtained using a calcined clay to limestone ratio of 2:1 [44]. Following this mix design, 45 parts of clinker were substituted by 30 parts of metakaolin and 15 parts of limestone in LC³-50, where 50 refers to the clinker content. The remaining 5 parts approximately corresponds to the gypsum content. Results in Figure 1.4 indicate that despite such low clinker content, higher strength than PC is obtained from 7 days onwards, demonstrating the feasibility of using this combination of metakaolin and limestone as clinker substitute.

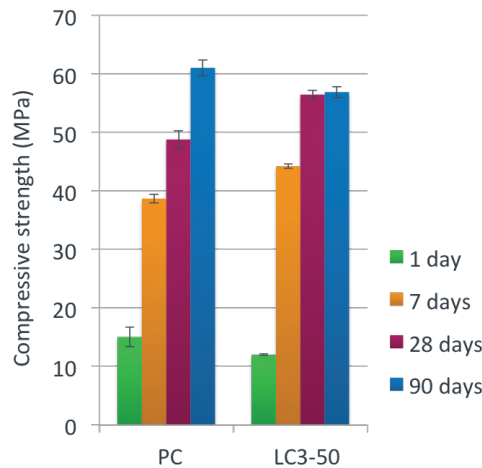


Figure 1.4. Compressive strength of reference PC and LC³-50 blends. Adapted from [43].

Concerning the porosity measured by Mercury Intrusion Porosimetry (MIP), Antoni also showed that LC³-50 blend has a higher total porosity compared to reference PC but a significant refinement of pore connectivity is observed for the blend.

This study from Antoni used pure metakaolin, which is around 3 times the price of Portland cement because it is already used by other industries such as ceramics, paper, etc [13]. Promising results were obtained using “lower” grade calcined kaolinitic clays which have a much higher potential as clinker substitutes [16, 31, 44, 45]. However, no systematic study was carried out to investigate the influence of the grade of calcined clay on the strength of calcined clay blends, or LC³-50 systems. More generally, information is missing concerning the influence of the grade of calcined clay on the hydration of calcined clay blends and their durability properties.

1.5 Objective of the thesis

The primary objective of this thesis is to investigate the influence of the grade of calcined clays on the strength and the chloride resistance of LC³-50 blends. The understanding of the results obtained is provided through the investigation of the microstructure development of the LC³-50 blends.

The first step in Chapter 2 was to understand factors controlling the reactivity of blends containing calcined clays. This was done by launching a benchmark test of mortar strength with various calcined clays from different places around the world. Blends with calcined clays and LC³-50 blends were tested. The goal was to see if criteria of feasibility could be established for a further use of these calcined clays in cement. In parallel to this benchmark test, a new Rapid, Relevant and Reliable (R³) pozzolanic test was developed in order to get a quicker indication on the reactivity of calcined clays. To be meaningful, correlations must be found with mortar strength. This chapter is updated from the paper published in *Cement and Concrete Research* 85 (2016) 1–11.

In order to understand the strength results obtained, a hydration study was carried out. The complete characterization of the hydration of calcined clay blends requires a method to determine the degree

of reaction of metakaolin. There is currently no suitable and reliable method available for any grade of calcined kaolinitic clays. The goal of the work in Chapter 3 was to find the best approach to determine this parameter. Three methods were investigated and compared.

Chapter 4 presents the investigation of the hydration of LC³-50 in pastes. The goal was to determine the influence of the grade of calcined clays on the microstructure development of LC³-50 blends. The work focused on the changes in phase assemblage and kinetics of hydration. The porosity was also characterized. This Chapter has been submitted to Cement and Concrete Research with Chapter 3 as two complementary journal papers.

Chapter 5 presents the full characterization of the C-A-S-H of calcined clay blends in terms of composition, morphology and density. This was to see if a different C-A-S-H forms in the LC³-50 blends.

The relationship between strength and phase assemblage is investigated in Chapter 6. Porosity and gel space ratio are used to try and explain the strength results obtained.

The chloride resistance of LC³ blends was tested and presented in Chapter 7 where it is compared with PC in order to investigate the feasibility of using LC³ in aggressive environment (sea shore, roads with de-icing salts etc.). The microstructure study allowed determination of the chloride distribution in the samples, and which grade of calcined clays is the most suitable for such applications.

Overall this thesis shows that clays containing a kaolinite content as low as 40-50% can be used as clinker substitute in LC³, with excellent strength and chloride resistance.

Chapter 2 - Development of a new rapid, relevant and reliable (R^3) test method to evaluate the pozzolanic reactivity of calcined kaolinitic clays

This Chapter is updated from a paper published in Cement and Concrete Research 85 (2016) 1-11.

François Avet^{1*}, Ruben Snellings^{1,2}, Adrian Alujas Diaz³, Mohsen Ben Haha⁴, Karen Scrivener¹

¹ Laboratory of Construction Materials, IMX, EPFL, 1015 Lausanne, Switzerland

² Sustainable Materials Management, VITO, 2400 Mol, Belgium

³ Centro de Estudios de Química Aplicada, Universidad Central de Las Villas, 54830 Santa Clara, Cuba

⁴ Heidelberg Technology Center GmbH, Rohrbacher Str. 95, 69181 Leimen, Germany

*Corresponding author: Tel.: +41 21 6932821

E-mail address: francois.avet@epfl.ch

2.1 Introduction

Modern day cements are largely composed of blended cements, containing Supplementary Cementitious Materials (SCMs). The reactivity of these blended cements is traditionally measured by testing the compressive strength at 7 days or 28 days of hydration. In order to predict in a faster way the pozzolanic reactivity of SCMs, several rapid test methods have been developed. These methods aim to predict the strength development as accurately as possible and in a reproducible way. Moreover, they should ideally be simple and widely accessible. The different methods have been reviewed by Snellings et al. [46]. The pozzolanic reactivity can be either obtained by:

- measuring the portlandite consumption related with the pozzolanic reaction of the SCM
- monitoring the reaction of the SCM itself
- investigating the SCM composition and physical properties
- measuring the compressive strength on simplified blends which are influenced by the reaction of the SCM.

2.1.1 Portlandite consumption

The first category of test method uses the portlandite consumption as criterion for the reactivity of SCMs. Vicat first described the concentration in a lime-saturated solution due to the pozzolanic reaction of SCMs [47]. The lime concentration was deduced from the alkalinity measurement of the solution by chemical titration. The main drawback of this test is its duration, since the final results can be obtained only at 90 days. Poor correlations with strength were obtained. In order to reduce

this experiment time, Chapelle increased the temperature of the test to 90°C [48]. In this test, 1 g of free lime (CaO) is mixed with 1 g of SCM and 200 g of water. The mix is boiled for 16 h. After cooling, sucrose is added to dissolve the unreacted portlandite. The alkalinity of the solution is used to measure the portlandite concentration by titration with hydrochloric acid (HCl). However, Chapelle noticed that poor correlations were obtained between the output of the test and strength results. A modified version of the Chapelle test was defined with an initial free lime content of 2 g to make sure not to run out of lime during the pozzolanic reaction. This version is used in the French standard NF P18-513 [49].

Another test developed based on the study of Frattini [50] is currently part of the European standard EN 196-5 [51]. The main novelty compared with Vicat or Chapelle test is the that in addition to the alkalinity measurement, the lime concentration is also measured by titration using EDTA as a complexing agent and murexide as indicator. In this test, the concentration of a lime solution in contact with a blended cement is compared with the concentration of a saturated lime solution with similar pH. If the solution containing the blended cement is undersaturated in lime at 7 or 14 days, the test is positive, i.e. the SCM shows a pozzolanic reactivity. The water to binder ratio used is 5, and the temperature of the test is 40 °C. The results of this test are qualitative, and the comparison between different SCMs is not straightforward [52]. Moreover, some segregation in the solid is often observed, influencing the results with different lime concentration between the top and the bottom parts of the beaker [53]. Good correlation with strength results was obtained for calcined clay samples [31], but this is not the case when applied to different SCMs [46] because the pozzolanic behaviour of SCMs significantly varies with the type of SCMs.

Other methods can be used to quantify the portlandite consumption in a blended cement or in a model system, such as X-Ray Diffraction (XRD) with the Rietveld method and Thermogravimetric Analysis (TGA). For XRD, it is not necessary to dry the sample, but the sample preparation and the operator skills can significantly influence the results. For TGA, the main drawback is that the sample needs to be dry. The water should preferentially be removed using solvent exchange method for couple of days.

2.1.2 Degree of reaction of SCMs

The main issue with investigating the portlandite consumption is that a different amount of portlandite will be consumed depending on the type of SCM. Thus, the monitoring of the SCM reaction is a more straightforward way of characterizing its reactivity. Two main methods can be used to follow continuously the reaction of an SCM: the heat release during hydration by isothermal calorimetry and the chemical shrinkage. For both methods, the main issue if blended cements are studied is the difference of clinker hydration degree. A filler can be used to simulate the physical effect of the SCM, and the comparison between the blend containing the SCM and the blend with the reference can give an indication of the reactivity of the SCM only.

Selective dissolution techniques have also been used. They allow the dissolution of unreacted clinker phases and the hydrated phases and to keep only the unreacted SCM. Two main drawbacks can

occur with such methods. First, a too strong acid can partially dissolve the SCM, leading to an overestimation of its degree of reaction. Second, the removal of hydration products and unreacted clinker phases can be incomplete.

Other techniques requiring much more advanced equipment could also be used, such as Nuclear Magnetic Resonance (NMR) mainly used for metakaolin or Scanning Electron Microscopy (SEM) for slag and fly ash. Since these equipments are not widely available, they can not be universally used. Recent development of XRD-Rietveld using the Partial Or Not Known Crystalline Phases method (PONKCS) showed the possibility of quantifying the degree of reaction of SCMs, especially metakaolin and slag, but to date, this method is too complicated to be widely applied.

2.1.3 SCM physical properties

The first approach consisted of correlating the reactivity of SCMs to their initial compositions obtained by X-Ray Fluorescence. In the ASTM C618 standard, an SCM must have a minimal content of $\Sigma(\text{SiO}_2 + \text{Al}_2\text{O}_3 + \text{Fe}_2\text{O}_3)$ of 70 % [54]. For monophasic materials, this could work but this is rarely the case for SCMs. Calcined clays for instance contain most of the time quartz as secondary phase. Moreover, there is no evidence for the reactivity of iron oxide in calcined clay. Thus, considering this parameter as an indicator for the reactivity of calcined clay is meaningless.

Instead of considering the whole composition of an SCM, the content and chemistry of the active phases was then determined. For this method, the active part of the SCM is dissolved using an acid and/or a base. Compared with the selective dissolution discussed before, the acids and bases used here are usually stronger. Poor correlations were generally observed with compressive strength results [46].

2.1.4 Compressive strength on simplified systems

Another approach used in Indian standard IS 1727 and Brazilian standard NBR 5751 to assess the reactivity of SCMs is to run compressive strength tests on mortars composed of lime and SCMs [55, 56]. In the IS 1727 standard, 1 part of lime is mixed with 2 volume parts of SCM and 9 parts of sand. This test is carried out with a constant flow of 70 ± 5 %. After a 2 day cure at room temperature, the samples are then stored at 50 °C for 8 days before being mechanically tested. The SCM passes the test if the strength reached 3 MPa. For the Brazilian NBR 5751 standard, the mortar flow required is 225 mm. The samples are kept in moulds for 24 h, and they are then cured at 55 °C for 6 days before being tested. The standard is satisfied if the strength reaches 6 MPa. The first drawback of this test is the constant flow or consistency used for different SCMs. The impact of SCMs on the rheological properties is much more significant for these simplified systems than for cementitious blends where the SCM content is lower and the rheological properties are also controlled by the clinker. Moreover, the curing temperature potentially changes the hydration products formed during hydration. Finally, for highly reactive SCMs, the system is likely to run out of lime due to its low initial content.

2.1.5 Objectives

To summarize the state of the art of the different pozzolanic tests, each of them shows some drawbacks (lack of correlation with strength tests, requirement of an equipment not widely available or high skills needed and not easy to disseminate). The main purpose of this study is the development of an easy and meaningful test method to evaluate widely available kaolinitic clays. Due to the wide number of clays potentially usable for calcined clays worldwide, it is necessary to develop a new test able to predict the strength development of LC³ systems in a much faster way than waiting for 28 days to get the compressive strength results.

Therefore, this study introduces a novel rapid, relevant and reliable (R³) testing approach for assessing calcined clay reactivity. Two ways were studied to assess reactivity. The first is by measuring the heat release of the exothermal hydration reactions by isothermal calorimetry. Alternatively, since such equipment is not available in all laboratories, a simple thermogravimetric method can be used to determine the bound water content in the range 110 °C to 400 °C with an oven.

The basis of the test is a paste of calcined clay (and limestone) with portlandite and water, with sulfate and alkali levels adjusted to simulate the chemical environment of a hydrating blend. For a wide range of calcined kaolinitic clays, the R³ test results were compared to standard compressive strength on mortar bars. The modified Chapelle test was run in order to compare the R³ test to a commonly used existing testing method.

2.2 Materials and Methods

2.2.1 Material characterization

Forty-six different clays of varying kaolinite contents sourced from around the world were used in this study. Most of the clays were prepared and calcined at 800 °C for 1 h in a high-temperature furnace in our laboratory, according to the protocol described in Appendix 2. The kaolinite content wt%_{kaolinite} was determined according to Equation 2.1 by Thermogravimetric Analysis (TGA), from the water loss over the kaolinite dehydroxylation interval wt%_{kaol-OH}. M_{kaolinite} and M_{water} refer to the molecular weights of kaolinite and water, respectively.

$$wt\%_{kaolinite} = wt\%_{kaol-OH} \times \frac{M_{kaolinite}}{2M_{water}} \quad \text{Eq. 2.1}$$

Some clays from external suppliers were not completely calcined, i.e. some kaolinite was still found in the calcined clay. Thus, the calcined kaolinite content in Equation 2.2 was used to consider the reactive part of the material, as explained in Appendix 2. wt%_{kaol-OH, calcined} refers to the remaining water loss in calcined clay.

$$wt\%_{\text{calcined kaolinite}} = wt\%_{\text{kaolinite}} - wt\%_{\text{kaol-OH, calcined}} \times \frac{M_{\text{kaolinite}}}{2M_{\text{water}}} \times \left(\frac{100 - wt\%_{\text{kaol-OH, calcined}}}{100} \right) \quad \text{Eq. 2.2}$$

The physico-chemical properties of the Portland cement used for the compressive strength tests and the limestone are shown in Table 2.1. The $D_{v,50}$ was measured by Malvern laser diffraction and the specific surface measured by BET nitrogen adsorption. The limestone used was Durcal 5 from Omya Company. The Portland cement was a commercial clinker specially ground with anhydrite from Heidelberg Cement, classified as CEMI 42.5R. The calcined kaolinite content and the physico-chemical properties of the 46 calcined clays are all given in Appendix 2. A wide range of calcined kaolinite content from 95.0 % to 7.4 % was characterized. Quartz (B250, Sibelco) was also used instead of calcined clay as inert filler.

Table 2.1. XRF composition and physical properties of PC and limestone.

	PC	Limestone
$D_{v,50}$ (μm)	8.4	7.2
BET Specific surface (m^2/g)	0.9	1.8
	XRF composition (wt.%)	
SiO ₂	19.3	0.1
Al ₂ O ₃	5.7	0.0
Fe ₂ O ₃	3.6	0.0
CaO	63.6	55.0
MgO	1.6	0.2
SO ₃	3.2	0.0
Na ₂ O	0.2	0.1
K ₂ O	1.2	0.0
TiO ₂	0.3	0.0
P ₂ O ₅	0.2	0.0
MnO	0.1	0.0
Others	0.3	0.0
LOI	0.8	42.6

2.2.2 Mortar strength tests

Standard mortars were cast in order to determine the strength development of the blends. Two substitution levels of Portland cement were studied. The PPC30 system refers to systems with 30 parts of cement substitution by calcined clays. The LC³-50 system refers to cements with 45 parts of substitution of Portland cement by 30 parts of calcined clay and 15 parts of limestone. Previous work demonstrated that a calcined clay to limestone ratio of 2:1 gave the best compressive strength development [44]. The cement used in this study contains a proper sulfate content for a plain cement hydration. However, the addition of gypsum was chosen in order to prevent the system being under-sulfated for the blends and to optimise early-age strengths. This gypsum adjustment was determined

by isothermal calorimetry as shown in Appendix 1. Gypsum was added until the separation of silicate and aluminate peaks could be distinguished on heat flow curves. In general the optimal addition was found to be 2 % gypsum in addition to that already added during grinding of the clinker. Thus, the total amount of gypsum present in PPC30 and LC³-50 blends corresponds to the sum of the initial sulfate from cement and this addition of 2 %. A 98 %+ grade gypsum from Acros company was used for all blends. The exact composition of the different systems is summarized in Table 2.2.

Table 2.2. System compositions.

wt.%	Clinker	Anhydrite	Calcined clay	Limestone	Gypsum
PC	93.2	5.9	-	-	-
PPC30	64.5	4.1	29.4	-	2.0
LC ³ -50	50.6	3.3	29.4	14.7	2.0

Mortar bars were cast using a water to cement ratio of 0.5 according to EN-196-1 [57]. Polycarboxylate superplasticizer (Mapei Dynamon SP914, max. 0.6 wt% of the total solid excluding sand) was used to ensure comparable workability with PC, as shown in Appendix 4. The mortar bars were unmoulded after 1 day and cured in a fog room until tested. The compressive strength measurements were carried out on mortar cubes of 40x40x40 mm at 1, 3, 7, 28 and 90 days after casting.

2.2.3 Mix design of the R³ test

The basis of the R³ test is to use a simplified system to isolate the reaction of the calcined clay from that of the clinker. The three main components of the simplified system are calcined clay, portlandite and, in the LC³-50 system, limestone. In the LC³-50 pastes an identical ratio of calcined clay to limestone of 2:1 was used. A water to solid ratio of 1.2 was used for all systems in order to provide excess water for the hydration reactions and to obtain a fluid homogeneous paste. The aim of the simulated systems was to reproduce the reaction environment of the calcined clay in a real blended cement as closely as possible, without actually incorporating hydrating clinker phases as this would introduce variability according to the clinker used. Therefore, soluble alkalis and sulfate were added 1) to reproduce the cement pore solution pH and accelerate the pozzolanic reaction and 2) to lead to the formation of similar reaction products as in real blended cements, such as C-A-S-H gel, ettringite and AFm phases.

In a first step in the development of the R³ test mix design the effect of alkali and sulfate additions was evaluated. Four different addition levels were investigated for both alkalis and sulfate. Potassium hydroxide and potassium sulfate were added to deionized water to adjust these parameters, varying the pH of the mix solution from 13.3 to 13.7. To evaluate the effect of the portlandite to calcined clay ratio five different mass ratios were selected. The mix design adjustment is summarized in Table 2.3. Pure potassium sulfate and potassium hydroxide were supplied by Reactolab and

Fischer Scientific, respectively. Portlandite was provided by Roth company, with a grade of 96 % min.

Table 2.3. Variations in mix design for sulfate, alkali and portlandite to calcined clay mass ratios.

K ₂ O / Calcined clay SO ₃ / Calcined clay = 0.06	0.06	0.08	0.10	0.12	
SO ₃ / Calcined clay K ₂ O / Calcined clay = 0.08	0.02	0.04	0.06	0.08	
Portlandite / Calcined clay	0.33	0.5	1	2	3

The variations in mix design were tested at 20 °C on two calcined clays of differing calcined clay content, i.e. clays with 95.0 % and 50.3 % of calcined kaolinite. Only results of clay with 95.0 % of calcined kaolinite are shown, the results of clay with 50.3% showed identical trends.

Once the optimal mix design had been chosen, the pozzolanic reactivity test was applied to the whole set of calcined clays. Tests were carried out in systems without and with limestone for correlation to the compressive strength results of the PPC30 and LC³-50 systems, respectively.

2.2.4 Methods

2.2.4.1 Heat flow measurements using isothermal calorimetry

The cumulative heat of reaction was measured in an isothermal calorimeter (TAM Air) both over 7 days at 20 °C and 40 °C. The increase in temperature speeds up the pozzolanic reaction, but maintains the same hydrate assemblage [58-60]. All the paste ingredients, including the mixing solutions were stored overnight at the same temperature as the test. About 110 g of paste was then mixed at 1600 rpm for 2 minutes, 15 g of paste was poured into a glass ampoule, which was closed and placed inside the calorimeter. Accompanying samples from the same batch were cast for XRD and cured at 20°C and 40°C.

X-Ray Diffraction (XRD) was used to characterize the crystalline phases formed and to follow the portlandite consumption. Measurements were carried out on freshly cut paste slices at 1, 4 and 7 days. The slices were mounted on a XRD sample holder and measured in Bragg-Brentano mode using a X'Pert PANalytical diffractometer with CuK α source operated at 45 kV and 40 mA. Samples were scanned from 7 to 70 °2 θ with a step size of 0.0167 °2 θ using a X'Celerator detector, resulting in an equivalent time per step of 30 s.

2.2.4.2 Bound water determination using oven thermal treatment

Since not all laboratories are equipped with an isothermal calorimeter, an alternative technique based on bound water determination is developed to assess the calcined clay reactivity. After mixing the paste samples are cast in plastic containers and sealed at 40 °C for 1 day to reproduce the same conditions as the tests carried out at 40 °C using isothermal calorimetry. Then, three 4 mm-

thick slices were cut for each system using a diamond saw. The slices were dried at 110 °C in an oven from Salvis company. Samples were considered dry when the mass change within 1 day did not exceed 0.5 %, according to ASTM C642, this condition was fulfilled after 2 days of drying. Finally, the bound water was determined according to Equation 2.3 by calculating the mass change after heating the samples at 400 °C for 2 h and cooling it down to 100 °C. The thermal treatment was limited to 400 °C since higher temperatures would lead to portlandite dehydroxylation, which is not desired in this case.

$$\text{Bound water (\%)} = \frac{m_{110^{\circ}\text{C}, \text{stabilized}} - m_{\text{cooled}, 100^{\circ}\text{C}}}{m_{110^{\circ}\text{C}, \text{stabilized}}} \quad \text{Eq. 2.3}$$

2.2.4.3 Modified Chapelle test

To compare the new test to existing method, the modified Chapelle test was run on the different calcined clays according to NF P18-513 [49]. This test was chosen due to the fact that is claimed to give a quick indication of pozzolanic reactivity (within a day) compared to Frattini test. For this test, 1 g of calcined clay was mixed with 2 g of calcium oxide and 250 mL of deionized water. Blank samples were also prepared without calcined clay and run in parallel to the calcined clay samples. The mix was heated at 90 °C for 16 h. Water loss was prevented by a reflux condenser. After cooling down to 20 °C, a solution of 60 g of sucrose in 250 mL of deionized water was added to complex the calcium ions in solution and to dissolve the unreacted portlandite. The suspension was filtered through a Büchner filter and the liquid was titrated with a 0.1 M solution of HCl using phenolphthalein as pH indicator. From the volume of HCl solution added, the amount of bound portlandite was determined according to Equation 2.4, where V_1 and V_2 are the volume of HCl added for the titration of the blank sample and the sample with calcined clay, respectively.

$$\text{mg CH / g calcined clay} = 2 \frac{V_1 - V_2}{V_1} \times \frac{74}{56} \times 1000 \quad \text{Eq. 2.4}$$

2.3 Results

2.3.1 Mortar compressive strength

In Figures 2.1 and 2.2, the compressive strengths of the PPC30 and LC³-50 mortars are shown as a function of the calcined kaolinite content of the calcined clays. The plain PC strengths are indicated by dotted lines. Already, after 3 days the blend containing the calcined clay with the very high calcined kaolinite content (95 %) is equivalent to the reference plain Portland cement. For the other ages (7 days and later), 100 % of the reference strength is obtained for blends containing calcined clay with calcined kaolinite content of around 40 %.

Moreover, strengths of both PPC30 and LC³-50 systems are linearly correlated with the calcined kaolinite content of calcined clays up to 7 days. This shows that for different clays from various

areas with different compositions, secondary phases, fineness and specific surfaces, the strength results are almost exclusively dependent on one parameter only: the calcined kaolinite content. From 28 days onwards, the strength gain for blends containing calcined clay with more than about 45% of calcined kaolinite becomes less significant. Furthermore, the LC³-50 systems have strengths close to those of the PPC30 systems in spite of their higher replacement ratio (lower clinker content). The LC³-50 blends benefit from the synergetic addition of calcined clay together with limestone, leading to the formation of more hydrates from the SCMs.

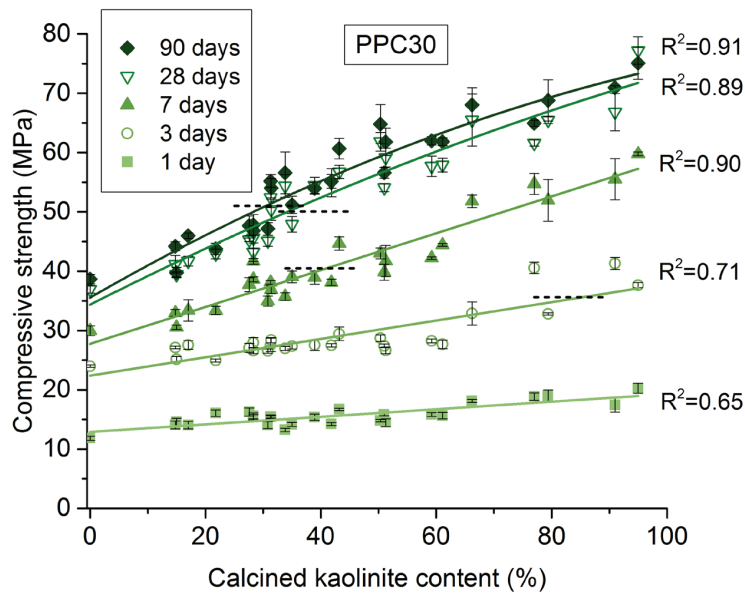


Figure 2.1. Correlation of compressive strengths of PPC30 with the calcined kaolinite content of calcined clays. Dotted lines indicate PC strengths.

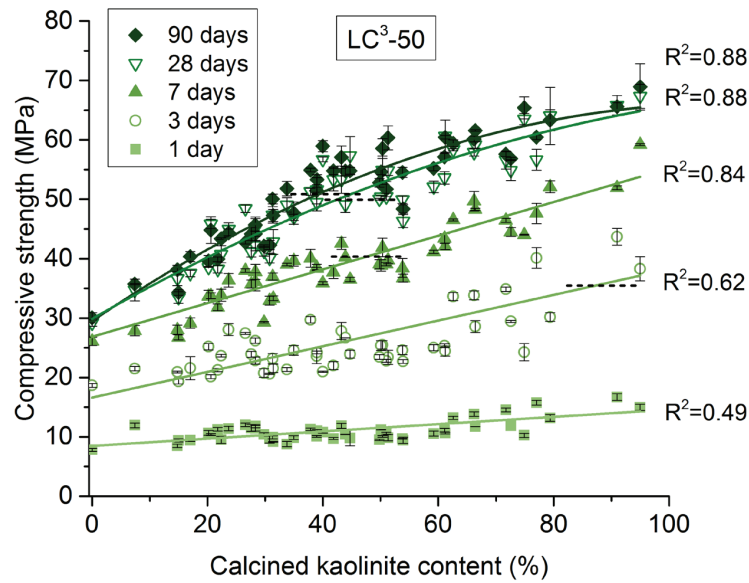


Figure 2.2. Correlation of compressive strengths of LC³-50 with the calcined kaolinite content of calcined clays. Dotted lines indicate PC strengths.

2.3.2 Optimisation of parameters for R³ pozzolanic activity tests

2.3.2.1 Sulfate to calcined clay ratio

Figure 2.3 (a) shows the heat released per gram of solid by isothermal calorimetry for calcined clay with 95.0% of calcined kaolinite for the four sulfate to calcined clay mass ratios (cf. Table 2.3). For systems with higher sulfate content, i.e. 0.06 and 0.08 sulfate to calcined clay ratios, an early heat flow peak appears before 15 h of reaction. XRD patterns at 1 day of hydration in Figure 2.3 (b) indicate that ettringite was formed in these systems. In the low sulfate systems, no early heat flow peak was observed and XRD results did not show the formation of ettringite. In the systems with low sulfate content the sulfate is rapidly depleted by the calcined kaolinite pozzolanic reaction, consuming Al to form AFm phases (mainly Hc) rather than ettringite. The second peak in the calorimetry curves is related to C-A-S-H and AFm formation.

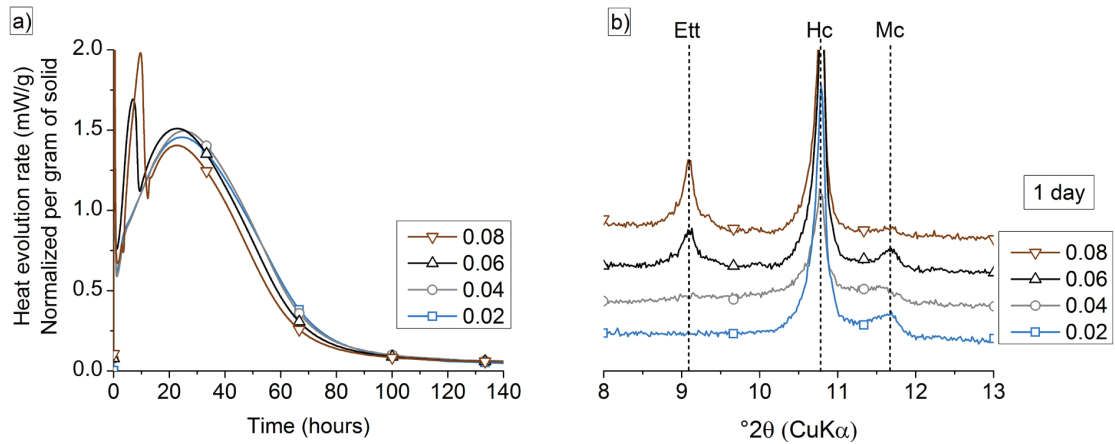


Figure 2.3. Influence of SO_3 to calcined clay ratio on the heat released (a) and on the phase assemblage (b) for calcined clay 1. On XRD patterns at 1 day of hydration, Ett = Ettringite, Hc = Hemicarboaluminate, Mc = Monocarboaluminate.

Figure 2.4 shows the cumulative heat released at 1 day, 2 days and 6 days for the different sulfate to calcined clay ratios for the calcined clays with 95.0 % of calcined kaolinite and with 50.3 % of calcined kaolinite. The cumulative heat does not significantly change with the sulfate content. The highest heat release is reached for the system with 0.06 sulfate to calcined clay ratio.

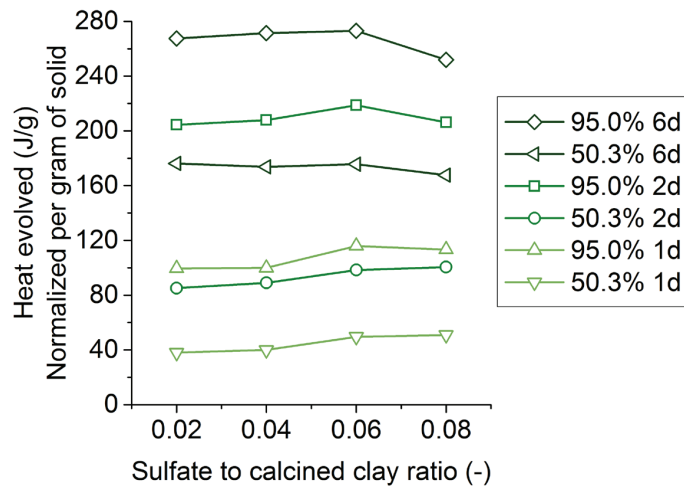


Figure 2.4. Cumulative heat release at 1 day, 2 days and 6 days as a function of SO_3 to calcined clay ratio for calcined clay with 95.0 % and 50.3 % of calcined kaolinite.

Thus, the final sulfate to calcined clay ratio for the pozzolanic reactivity test chosen was 0.06. This ratio was selected because 1) early ettringite formation is a general and desirable feature of cement hydration, and 2) the highest heat release is obtained for this ratio, indicating that higher sulfate levels slow down the pozzolanic reaction.

2.3.2.2 Alkali to calcined clay ratio

The heat released per gram of solid for the four different alkali to calcined clay mass ratios (cf. Table 2.3) is shown in Figure 2.5 (a) for the calcined clay with 95.0 % of calcined kaolinite. An early heat flow peak related to ettringite formation was observed only for the two lowest alkali to calcined clay ratios, i.e. 0.06 and 0.08. This was confirmed by XRD in Figure 2.5 (b). As expected the pozzolanic reaction of calcined kaolinite is enhanced in more alkaline solutions as seen from the increasing height of the main calorimetry peak [61, 62]. AFm phases form rather than ettringite for high alkaline solutions due to the decrease of the ion activity product for ettringite with increasing pH [63]. The alkali U-phase is not observed because this phase only occurs for pH higher than 14 [64].

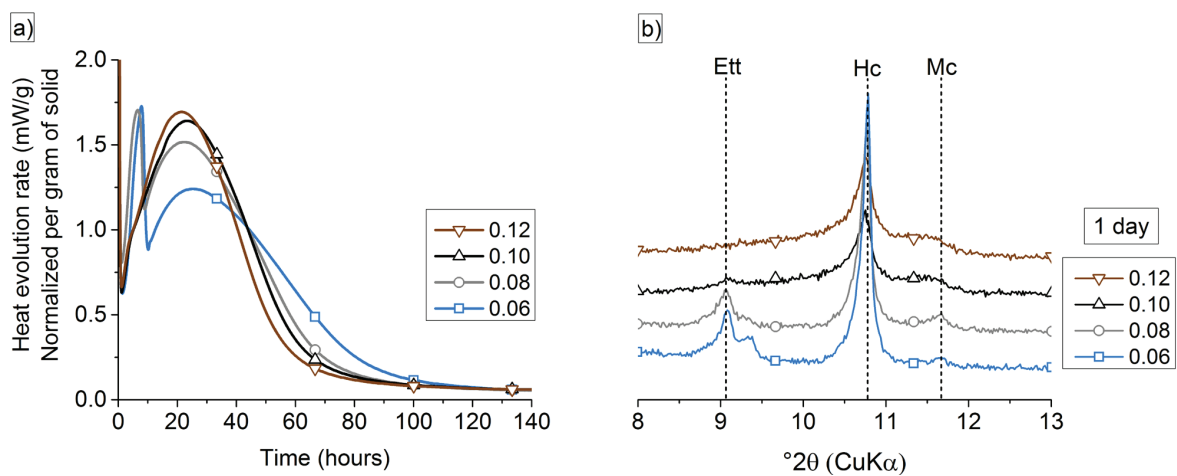


Figure 2.5. Influence of K₂O to calcined clay ratio on the heat released (a) and on the phase assemblage (b) for calcined clay 1 (SO₃/calcined clay ratio of 0.06). On XRD patterns at 1 day of hydration, Ett = Ettringite, Hc = Hemicarboaluminate, Mc = Monocarboaluminate.

The final alkali to calcined clay ratio was chosen at 0.08 to enable both ettringite formation and high calcined clay reactivity.

2.3.2.3 Portlandite to calcined clay ratio

The effect of changing the portlandite to calcined clay ratio was investigated using the sulfate and alkali ratios previously determined (0.06 and 0.08, respectively). Calorimetry curves are shown in Figure 2.6 (a) for calcined clay with 95.0 % of calcined kaolinite. The results show that the cumulative heat release reaches a plateau for systems having portlandite to calcined clay mass ratios of 1/1, 1/2 and 1/3. The plateau is reached sooner and at a lower cumulative heat release for mixes with lower portlandite contents. The XRD patterns at 4 days in Figure 2.6 (b) demonstrate the absence of portlandite in all mixes that reached the plateau. The extent of reaction of the calcined clay depends on the amount of portlandite available as reactant. As soon as portlandite is completely consumed, a plateau is reached and overall reaction rates are reduced.

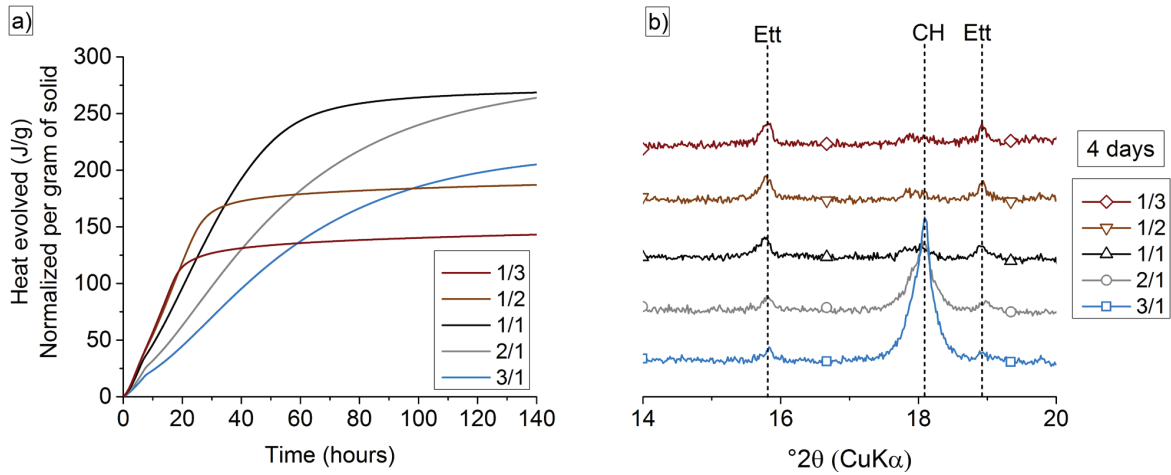


Figure 2.6. Cumulative heat released for the five portlandite to calcined clay ratios for calcined clay 1 (a), the reaching of the plateaus being related to the complete CH consumption as observed by XRD at 4 days of hydration (b). Ett = Ettringite, CH = Portlandite.

In order to assess the intrinsic reactivity of the calcined clays, it was decided to use a 3/1 ratio for the mix design. This way the portlandite reactant will always be in excess and the main factor controlling the reaction kinetics is the calcined clay. The resulting optimal mix design developed for the new pozzolanic reactivity test is presented in Table 2.4. A much lower amount of material is needed compared to mortar test.

Table 2.4 Final mix design of pozzolanic test.

System	Calcined Clay (g)	Portlandite (g)	Calcium carbonate (g)	K ₂ SO ₄ (g)	KOH (g)	H ₂ O (g)
Simulating PPC30 system	12.50	37.50	0	1.47	0.32	60
Simulating LC ³ -50 system	11.11	33.33	5.56	1.31	0.28	60

2.3.3 Application of the R³ test to calcined clays: heat flow measurements

2.3.3.1 Tests carried out at 20 °C

The heat released per gram of solid during hydration of all the calcined clays studied is presented in Figures 2.7 (a) and 2.8 (a) for systems without and with limestone, respectively. In both cases, the calcined clay with 95 % of calcined kaolinite content reacts the most, whereas the quartz system is the least reactive. These results are in agreement with the compressive strength results. For systems without limestone, XRD patterns in Figure 2.7 (b) clearly show the formation of monosulfoaluminate phase for all systems at 7 days, due to the absence of calcite. An AFm solid solution sulfate, carbonate and hydroxide together (discussed by Pöllmann [65]) also forms as seen by the peak at 10.5 °2 θ (CuK α). Ettringite forms at earlier ages, but with the continuing dissolution of the calcined

clay, the aluminate to sulfate ratio increases, leading to the consumption of ettringite and the formation of monosulfoaluminate phase. For systems with limestone, carboaluminates form and ettringite remains present in the systems, as shown in Figure 2.8 (b). Moreover, the height of the peaks of the carboaluminates increase with the calcined kaolinite content of calcined clays.

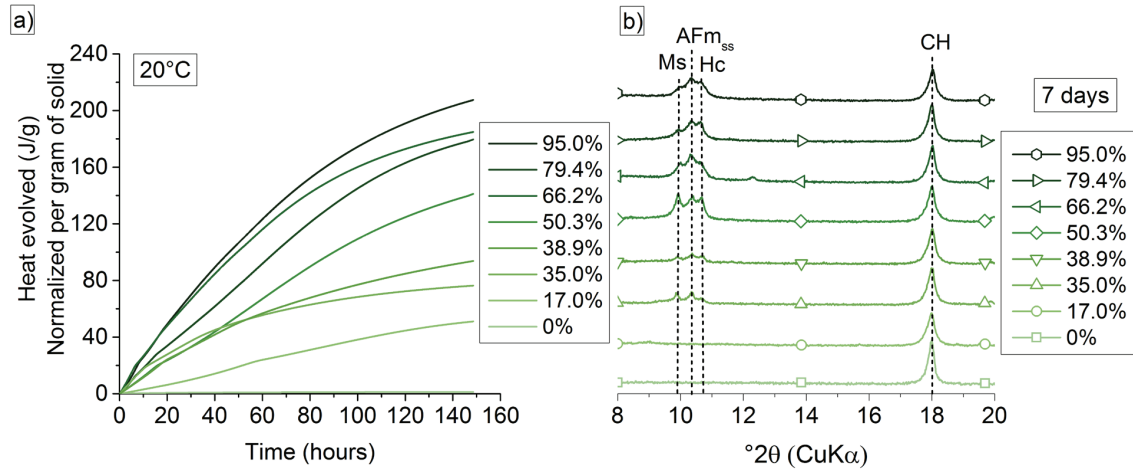


Figure 2.7. (a) Heat released for calcined clay-portlandite blends without limestone at 20 °C. (b) XRD patterns at 7 days, Ms = Monosulfoaluminate, Hc = Hemicarboaluminate, CH = Portlandite, AFm_{ss} = solid solution containing sulfate, carbonate and hydroxyl.

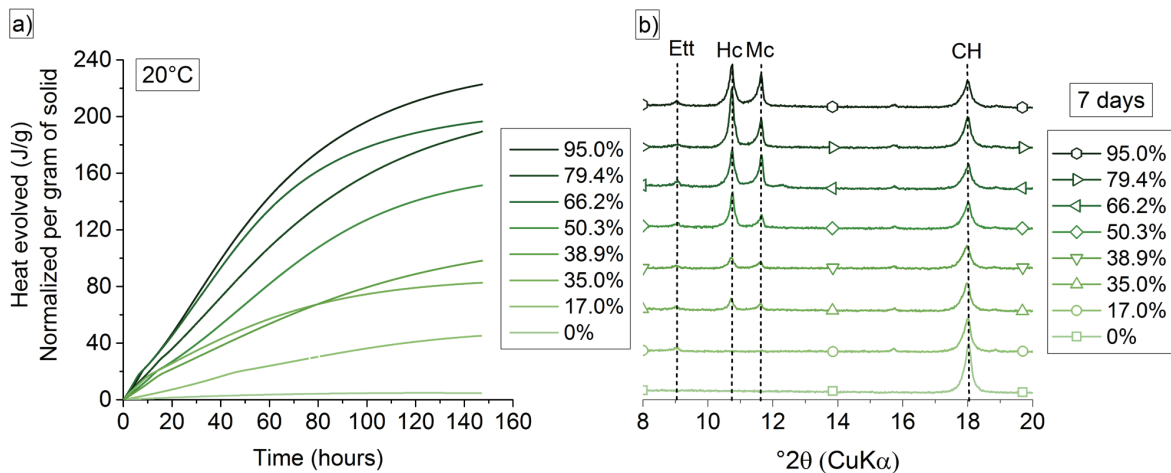


Figure 2.8. (a) Heat released for calcined clay-portlandite-limestone blends at 20 °C. (b) XRD patterns at 7 days of hydration, Ett = Ettringite, Hc = Hemicarboaluminate, Mc = Monocarboaluminate, CH = Portlandite.

To compare with the compressive strength results from 1 to 90 days, cumulative heat values were taken at 6 days of reaction because the reaction significantly slows down at this age. Figures 2.9 and 2.10 show that good linear correlations are obtained at all ages between the heat released for the calcined clay-portlandite and calcined clay-portlandite-limestone model systems and the strengths for PPC30 and LC³-50 systems, respectively.

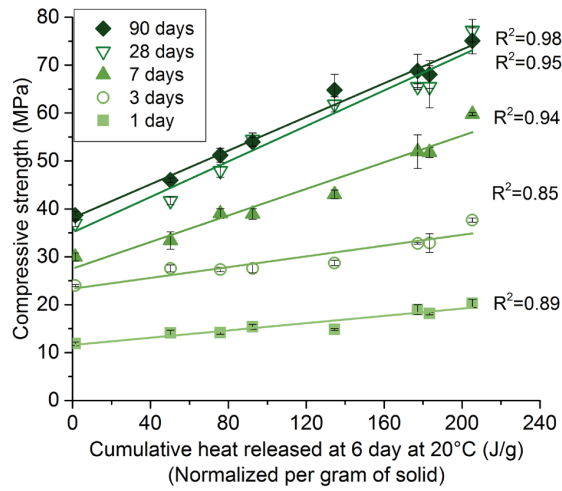


Figure 2.9. Correlation between PPC30 mortar strength (20°C) and cumulative heat released at 6 days of hydration for isothermal calorimetry run at 20 °C for calcined clay-portlandite model systems.

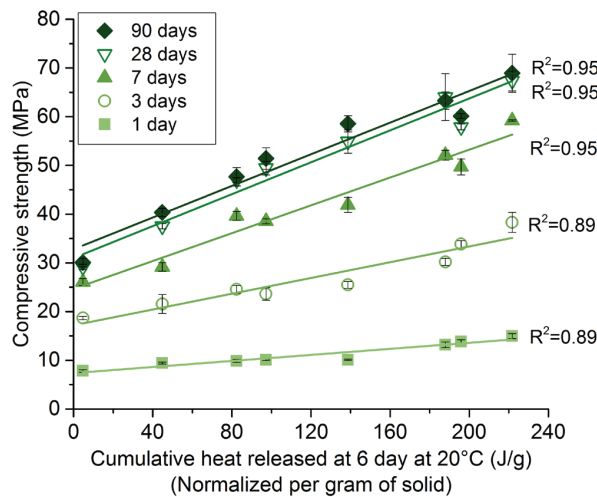


Figure 2.10. Correlation between LC³-50 mortar strength (20°C) and cumulative heat released at 6 days of hydration for isothermal calorimetry run at 20 °C for calcined clay-portlandite-limestone model systems.

2.3.3.2 Impact of temperature

Figures 2.11 (a) and 2.12 (a) show that increasing the temperature for the isothermal calorimetry from 20 to 40 °C accelerates the pozzolanic reaction. No major change in phase assemblage is observed at 1 day in Figures 2.11 (b) and 2.12 (b), except for the ettringite peaks which are lower or absent for systems with limestone. This is likely due to the acceleration of the pozzolanic reaction of metakaolin and the increase of ettringite solubility with temperature [63]. The heat released after only 1 day at 40 °C is globally similar to the heat released at 6 days at 20 °C and the heat evolution

also slows down at this time. Thus, the correlations to strengths are based on the 1 day heat values. In addition to the clays tested at 20 °C, most-recently received clays were also tested at 40 °C and all correlations to strength results are shown in Figures 2.13 and 2.14. Due to the higher number of calcined clays tested, the correlation coefficients are slightly lower to the coefficients obtained at 20 °C. Still very good correlations are obtained.

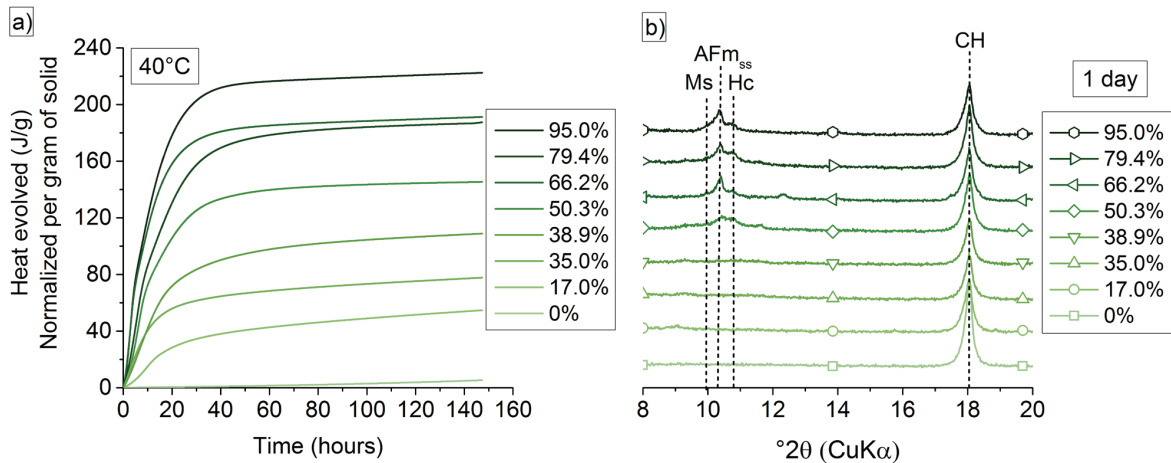


Figure 2.11. (a) Heat released for calcined clay-portlandite blends without limestone at 40 °C. (b) XRD patterns at 1 day of hydration at 40 °C. Ms = Monosulfoaluminate Hc = Hemicarboaluminate, CH = Portlandite, AFm_{ss} = solid solution containing sulfate, carbonate and hydroxyl.

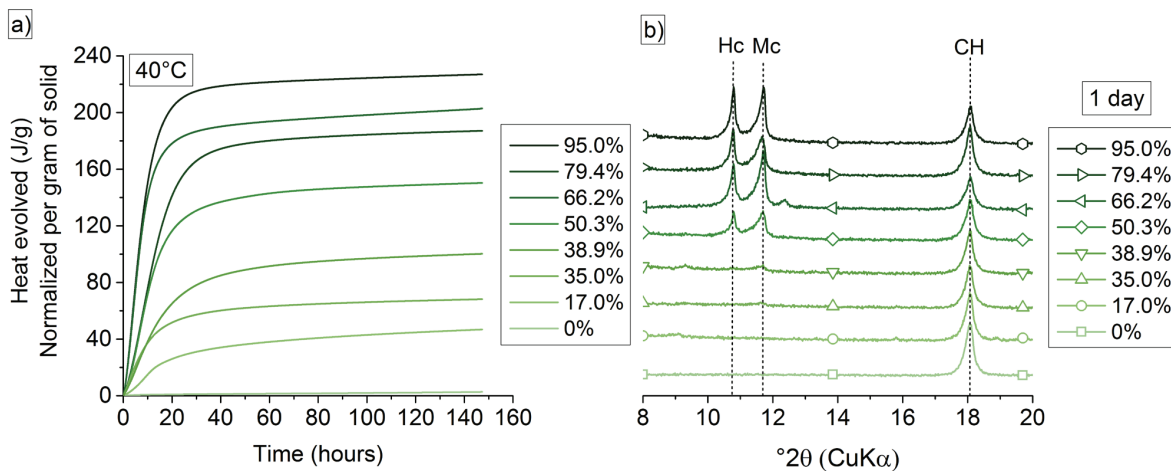


Figure 2.12. (a) Heat released for calcined clay-portlandite-limestone blends at 40 °C. (b) XRD patterns at 1 day of hydration at 40 °C. Hc = Hemicarboaluminate, Mc = Monocarboaluminate, CH = Portlandite.

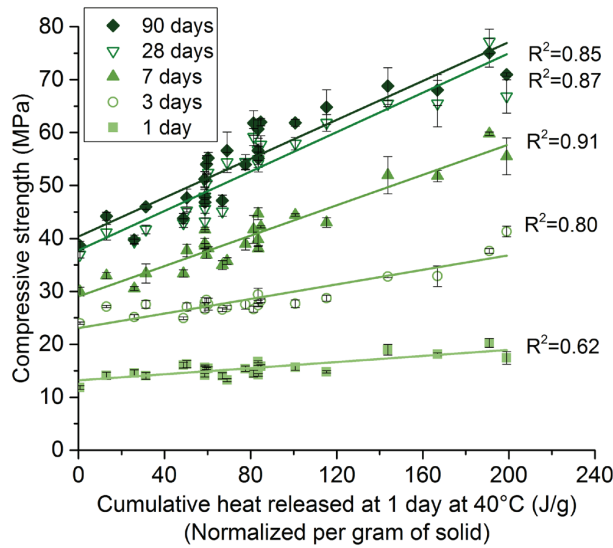


Figure 2.13. Correlation between PPC30 mortar strength (20°C) and cumulative heat released at 1 day of hydration for isothermal calorimetry run at 40 °C for calcined clay-portlandite model systems.

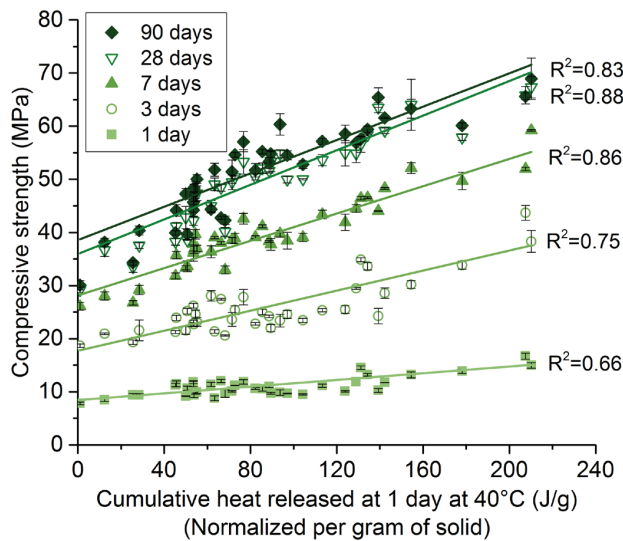


Figure 2.14. Correlation between LC³-50 mortar strength (20°C) and cumulative heat released at 1 day of hydration for isothermal calorimetry run at 40 °C for calcined clay-portlandite-limestone model systems.

2.3.3.3 Repeatability

To control the repeatability of the R³ test, three independent tests were carried out on clay with 50.3% of calcined kaolinite, with and without limestone, as shown in Figure 2.15 (a) and (b), respectively. The standard deviations were calculated based on the heat values at 6 days and 1 day for

tests run at 20 °C and 40 °C, respectively. Their values are shown in Table 2.5. The standard deviations are very small.

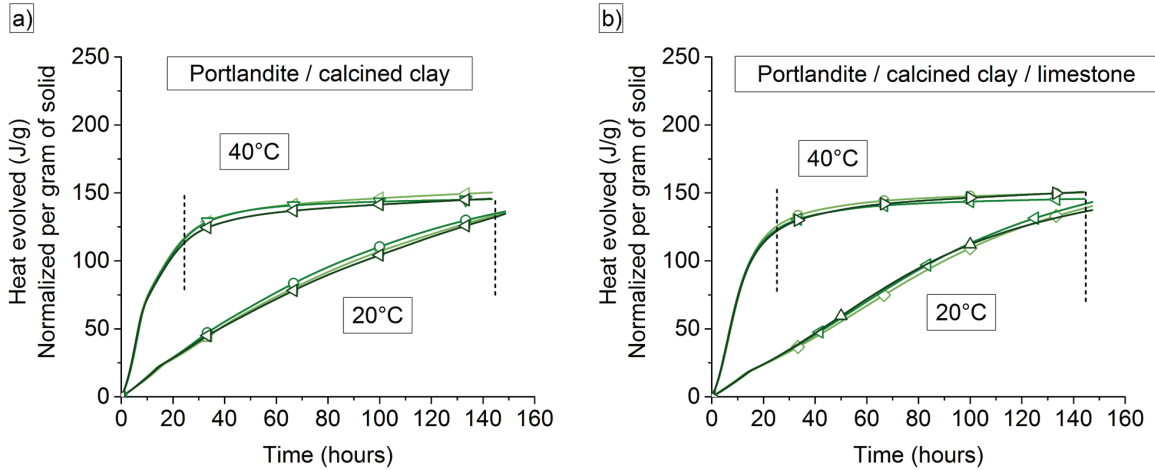


Figure 2.15. Reproducibility tests on blends containing calcined clay with 50.3% of calcined kaolinite at 20 °C and 40 °C without (a) and with limestone (b). Heat values at 6 days and 1 day (dotted lines) are used to calculate the standard deviations.

Table 2.5. Standard deviation values for blends containing calcined clay with 50.3% of calcined kaolinite.

Testing temperature	Model system	Standard deviation	
		(J/g)	(%)
20 °C	Calcined clay-portlandite	1.34	1.01
	Calcined clay-portlandite-limestone	2.80	2.02
40 °C	Calcined clay-portlandite	1.86	1.61
	Calcined clay-portlandite-limestone	1.79	1.46

2.3.4 Bound water determination

Figures 2.16 and 2.17 show that linear correlations are obtained between strength and bound water for systems without and with limestone, similar to the correlations with the heat released at 1 day. Therefore, the bound water indicator is also a relevant method to predict the strength development of blends.

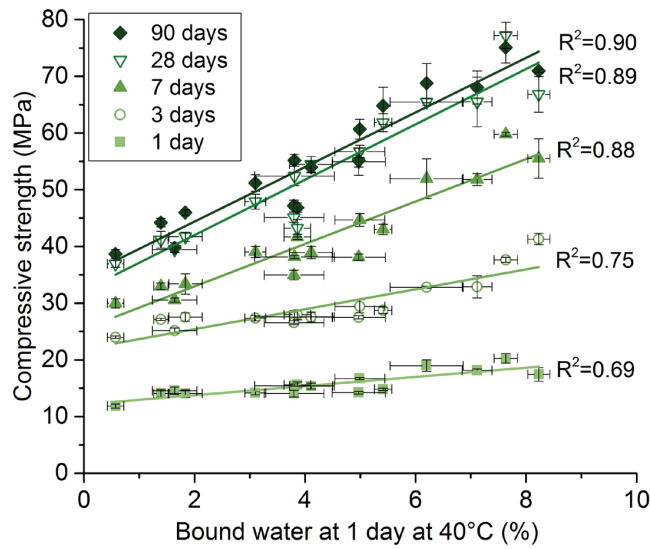


Figure 2.16. Correlation of PPC30 mortar strength (20°C) with bound water after 1 day of hydration at 40°C for calcined clay-portlandite model systems.

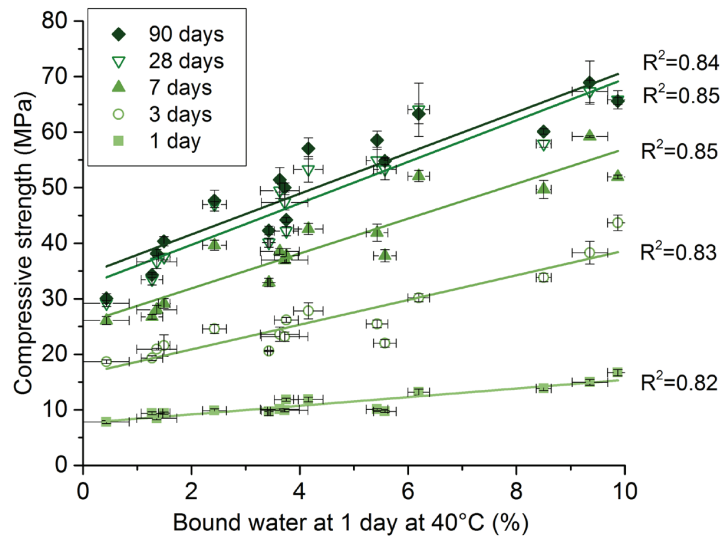


Figure 2.17. Correlation of LC³-50 mortar strength (20°C) with bound water after 1 day of hydration at 40°C for calcined clay-portlandite-limestone model systems.

Moreover, the correlation with the heat release values at 1 day for systems without and with limestone in Figures 2.18 and 2.19 clearly shows the reliability of the R³ test using the bound water determination.

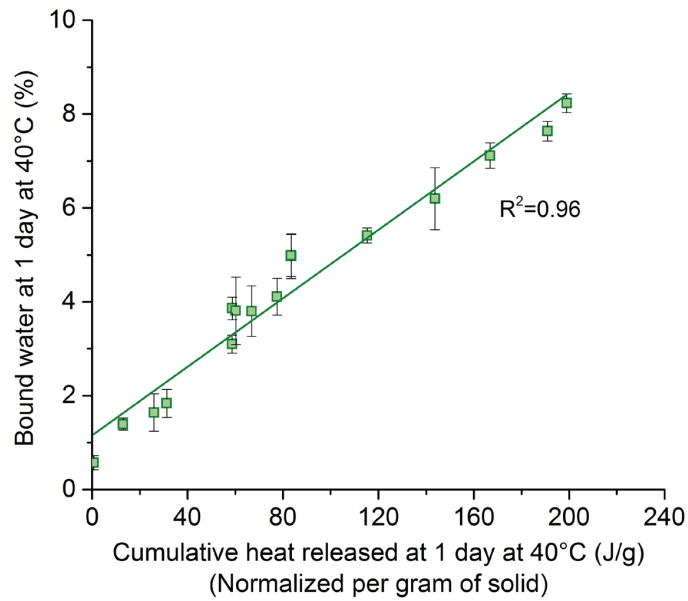


Figure 2.18. Correlation of bound water and cumulative heat released after 1 day of hydration at 40°C for calcined clay-portlandite model systems.

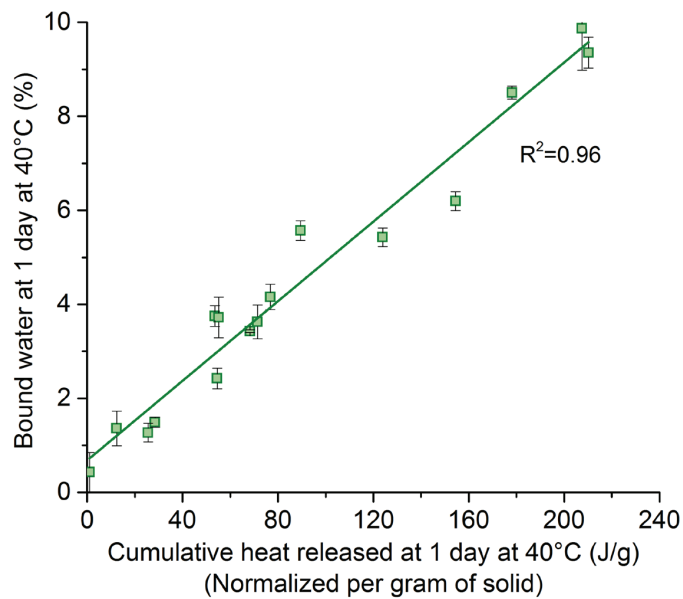


Figure 2.19. Correlation of bound water and cumulative heat released after 1 day of hydration at 40°C for calcined clay-portlandite-limestone model systems.

2.3.5 Comparison with the modified Chapelle test

Figure 2.20 shows the portlandite consumption for the calcined clays ranked in order of their calcined kaolinite content. The consumption of portlandite globally increases with the calcined kaolinite content. Also the quartz system shows some portlandite consumption, this is due to the elevated

temperature of the test. This pozzolanic reactivity of quartz has already been observed for blends at 80 °C [66].

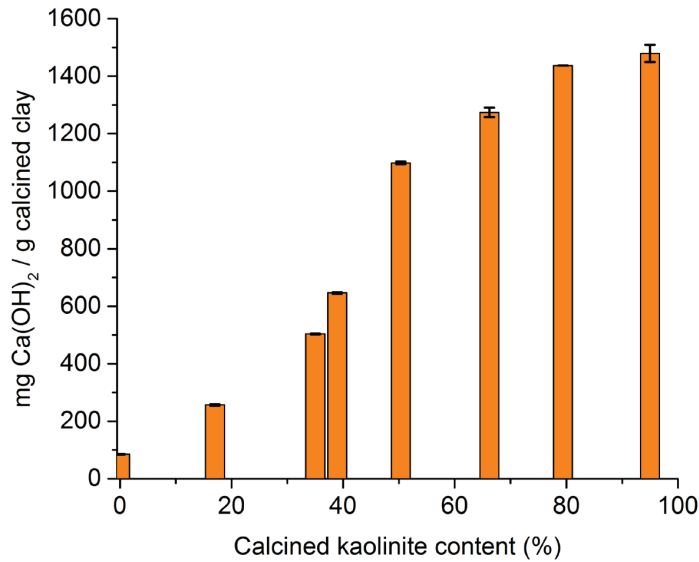


Figure 2.20. Portlandite consumption from Chapelle test for the different calcined clays.

The prediction of strengths based on the modified Chapelle test is also good, somewhat more scatter is observed for higher calcined kaolinite contents, as shown in Figures 2.21 and 2.22 for PPC30 and LC³-50 blends, respectively.

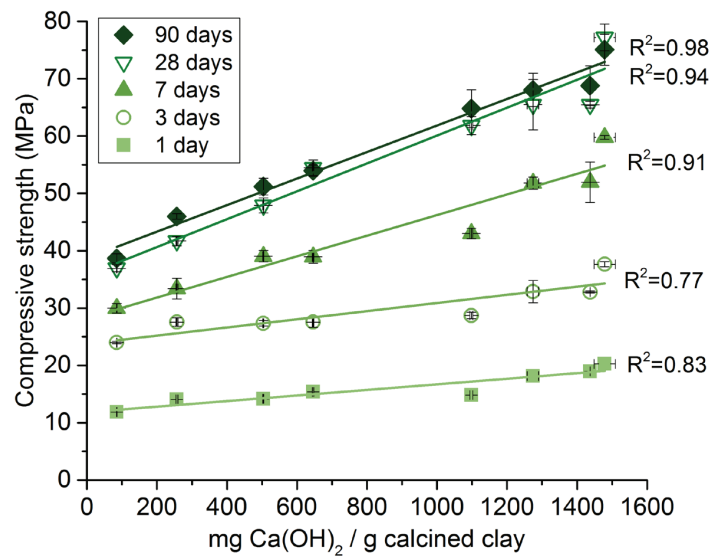


Figure 2.21. Correlation of PPC30 mortar strength (20°C) with the portlandite consumption in the modified Chapelle test.

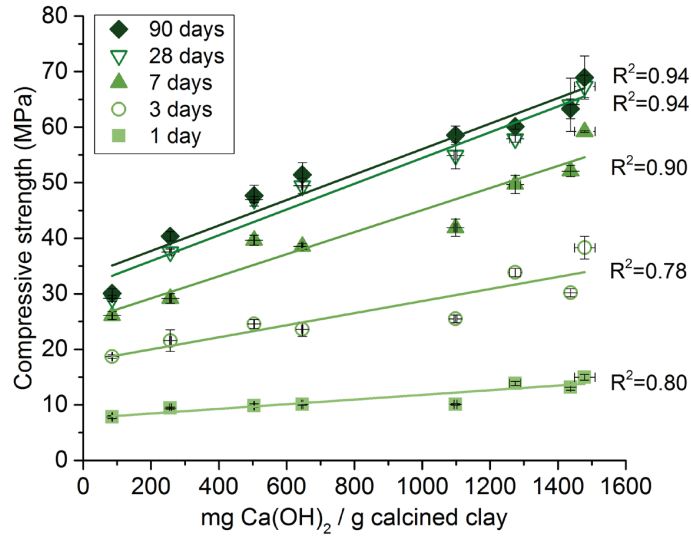


Figure 2.22. Correlation of LC³-50 mortar strength (20°C) with the portlandite consumption in the modified Chapelle test.

Finally, the comparison with the heat released at 1 day and the bound water from the R³ test in Figures 2.23 and 2.24 shows that the portlandite consumption is well correlated with the outputs of the R³ test.

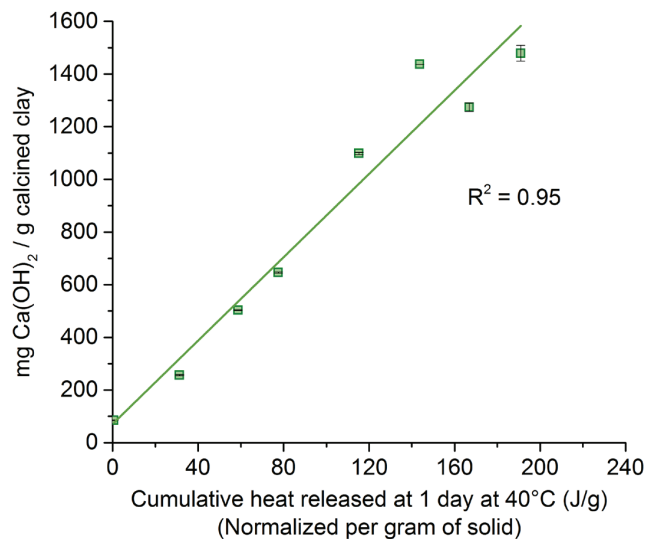


Figure 2.23. Correlation of portlandite consumption in the modified Chapelle test and cumulative heat released at 1d at 40°C for calcined clay-portlandite model systems.

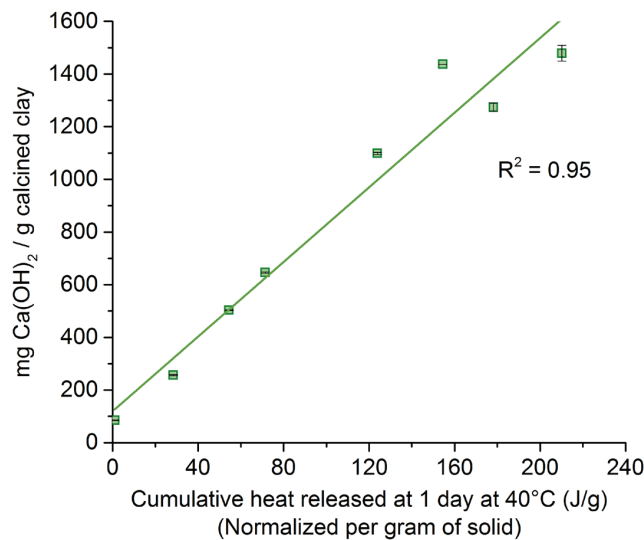


Figure 2.24. Correlation of portlandite consumption in the modified Chapelle test and cumulative heat released at 1d at 40°C for calcined clay-portlandite-limestone model systems.

Thus, the new R³ test provides at least similarly reliable indications of the reactivity of calcined kaolinitic clays as the modified Chapelle test. In comparison to the modified Chapelle test which is performed at 90 °C and without addition of alkali or sulfate the proposed R³ tests are closer to the reaction environment in Portland cement system.

2.4 Conclusion

This study shows that similar compressive strengths to plain PC are obtained for calcined clays with a calcined kaolinite content $\geq 40\%$ from 7 days onwards, demonstrating the feasibility of using low-grade kaolinitic calcined clays as a cement substitute, even for LC³-50 blends containing only 50 % of clinker. The strengths of PPC30 and LC³-50 blends linearly increase with the calcined kaolinite content of calcined clays from 1 to 7 days. The calcined kaolinite content parameter is the overwhelming factor determining strength development accounting for more than 85 % of the variation from 7 days onwards. Other factors, such as the secondary phases present, fineness and method of calcination do not account for more than 15 % of the variability. At 28 days and 90 days, the increase of strength with the calcined kaolinite content becomes less significant for clays with more than 45% of calcined kaolinite. Thus, there is only a little additional benefit of using calcined clays in LC³-50 with more than 50-60% of calcined kaolinite.

For the development of the new R³ test, the mix design was adjusted in order to reproduce typical conditions for cement systems. The optimal mix design was 0.06 SO₃/Calcined clay and 0.08 K₂O/Calcined clay mass ratios in order to get ettringite formation and to ensure high pozzolanic reactivity. Portlandite to calcined clay mass ratio was fixed to 3 so as not to run out of portlandite. The R³ test using isothermal calorimetry gives a rapid indication of calcined clay reactivity, after 6 days for tests carried out at 20 °C and 1 day at 40 °C, using significantly lower amount of material

compared to mortar test. Linear correlations with compressive strengths are obtained for all ages, proving the relevance of this test. Increasing the testing temperature to 40 °C does not affect the correlations and it is therefore considered to be a valid way of reducing the test duration from 6 days to 1 day. Small variability ensures good reliability for this test.

The R³ test using bound water determination after heating to 400 °C shows very closely-related results to the heat released at 1 day. Bound water values are linearly correlated to strength results. The bound water determination method does not require any specific equipment except an oven able to reach 400 °C. Despite its slightly longer experiment time (2.5-3 days instead of 1 day for the calorimetry experiment), this method can be applied in nearly all laboratories with basic equipment. Similar correlations to the existing modified Chapelle test are obtained for the R³ test, bringing the R³ test as an alternative testing method which is more practical and closer to reaction conditions in real Portland cement systems.

Thus, the R³ test outputs are found to be well correlated with the compressive strength, supporting the use of the new test as a predictive tool for compressive strength at both the short and the long term. This test can also be applied for optimizing the calcination temperature of a clay, as shown in Appendix 3. Other SCMs are also tested to demonstrate the reliability of the R³ test at least for slags and fly ashes.

Chapter 3 - Determination of the amount of reacted metakaolin in calcined clay blends

This Chapter has been submitted as journal paper to Cement and Concrete Research. This paper is the precursor to another (Chapter 4) detailing the microstructural evolution in LC³-50 systems, which discusses in more detail the evolution of all the hydrates phases and the porosity.

François Avet^{1*}, Xuerun Li¹, Karen Scrivener¹

¹ Laboratory of Construction Materials, IMX, EPFL, 1015 Lausanne, Switzerland

Corresponding author: Tel.: +41 21 6932821

E-mail address: francois.ayet@epfl.ch

3.1 Introduction

Calcined clays are receiving increasing attention as supplementary cementitious materials (SCMs). The supplies of traditional SCMs (fly ash and slag) are limited compared to the amount of clinker produced. The only widely available materials able to meet the increasing demand of cement production are calcined kaolinitic clays [9]. Calcined kaolinitic clays show the highest pozzolanic potential among the different kinds of clays, thanks to the formation during calcination of the highly reactive amorphous metakaolin phase [22]. There have been numerous previous studies on the use of pure metakaolin, but clays with a lower kaolinite content are much more promising for a massive use in cement due to their wide availability, and low cost, as in Limestone Calcined Clay Cements (LC³) [67]. The measurement of the degree of reaction of metakaolin for these various grades of calcined clays is a key step to better understand the influence of the grade of clay on the properties of cementitious blends containing calcined clays.

Methods for the determination of the reaction degree of SCMs were reviewed by Scrivener and al. [68].

- Nuclear Magnetic Resonance (²⁷Al and ²⁹Si) can be used with a good accuracy [69-71]. However, this technique is not readily available, it is expensive and a major issue is the presence of paramagnetic iron ions (Fe³⁺) [72] coming from cement and in impure calcined clays, where iron oxide is frequently found as a secondary phase. These ions are responsible for decreasing the magnetization during the experiment, influencing the reliability of the results.
- Image analysis cannot be used to accurately quantify the amount of reacted metakaolin due to the fine nature of calcined clay particles.
- Calorimetry was thought to be a promising method, but Berodier [29] showed that the long term reaction of the clinker is affected by reactive SCMs so errors are produced when the

output is compared to that of an inert material. Moreover, the specific heat of hydration of metakaolin reaction is unknown.

- Antoni and al. [43] estimated the degree of reaction of metakaolin from the portlandite consumption. However, his method underestimates the real reaction degree of metakaolin, because it is assumed that the C-A-S-H composition measured is only related to the reaction of metakaolin. This method does not take into account the change in composition of the C-A-S-H coming from the reaction of clinker [73].

In this study, three methods are compared to determine the amount of reacted metakaolin. First, a global mass balance is investigated considering all the phases involved during hydration, as proposed by Durdzinski et al. [74], but with a fitting for the reaction degree of metakaolin. Using the same inputs as mass balance, a thermodynamic modelling approach is used with the Gibbs Free Energy Minimization Software (GEMS). Finally, the Partial Or Not Known Crystalline Structure method (PONKCS) based on XRD Rietveld analysis is used, which has shown previously promising results on high-grade metakaolin [62].

3.2 Methods

3.2.1 Mass balance

“Mass balance” is a method for calculating the hydrated phase assemblage. The amounts of each oxide coming from the reacted anhydrous phases are redistributed between the hydrate phases known to form [75]. The amount of reacted components coming from clinker phases, limestone and gypsum was considered. Since the degree of reaction of metakaolin is unknown, its amount is the free variable of the system. It is determined from the best agreement of the mass balance outputs with experimental data.

The sum of the different oxides coming from all the reacting phases are considered: CaO, SiO₂, Al₂O₃, Fe₂O₃, SO₃, CO₂ and MgO. Then a series of steps are used to calculate the amounts of the different phases formed, analogous to the Bogue calculation for the anhydrous phases in Portland cement. The sequence of steps is as follows:

- All MgO is considered to form hydrotalcite like phase M₄AH₁₀, subtracting the Al₂O₃ contribution from the initial Al₂O₃ amount available for the formation of hydration products.
- All Fe₂O₃ is then considered to form Fe-siliceous hydrogarnet C₃FS_{0.84}H_{4.32}, which is more stable than Fe-ettringite and Fe-AFm phases [76]. The required amounts of silicon and calcium oxides used for hydrogarnet formation are subtracted from their initial available content.
- All the remaining SiO₂ is then considered to be in C-A-S-H. Knowing the Al/Ca, Si/Ca ratios for the different systems at all ages by Scanning Electron Microscopy in Energy Dispersive X-Ray Spectroscopy mode (SEM-EDX), the aluminium and calcium contributions are subtracted.
- The quantity of ettringite C₃A.3(C\$)H₃₂ is taken as that measured by X-Ray Diffraction - Rietveld method and from this the amounts of SO₃ CaO and Al₂O₃ are subtracted. Another strategy would consist of consuming all SO₃ for the formation of ettringite. But this leads to errors due to the sulfate adsorption in C-A-S-H.

- The remaining Al_2O_3 is used for the formation of monocarboaluminate $\text{C}_4\text{ACH}_{11}$, consuming the available CO_2 . Al_2O_3 was used as the limiting factor of the reaction rather than CO_2 because of the relative difficulty for the quantification of calcite by XRD-Rietveld.
- The amount of remaining CaO is used to form portlandite CH.

With the increase of the metakaolin reaction, extra SiO_2 and Al_2O_3 are provided to the system. To determine the amount of reacted metakaolin, calculations are made at steps of 1% metakaolin reactions and then plotted against the amount of portlandite. The real amount of metakaolin reactions can then be estimated from the portlandite content measured by XRD-Rietveld results.

3.2.2 Thermodynamic modelling

For thermodynamic modelling, the same oxide contributions as mass balance are used as an input. The Gibbs Free Energy Minimization Software (GEMS) is used [77], with the Cemdata14 database [78] and the CSHQ model from Kulik for C-S-H [79]. Al-incorporation in C-A-S-H was fixed for each system based the Al/Si ratio obtained by SEM-EDX point analysis. According to recent results by $^1\text{H-NMR}$ from Müller [80], the density of C-S-H used is $2.00 \text{ g}\cdot\text{cm}^{-3}$. Moreover, 4 water molecules per silicate ion were considered. Thus, the amount of C-A-S-H and water given by thermodynamic modelling are corrected to include the same water content as the C-A-S-H used by mass balance. As for mass balance, the amount of reacted metakaolin was determined when the same portlandite content as experimental XRD-Rietveld was obtained.

3.2.3 PONKCS method

The traditional use of XRD-Rietveld analysis is limited to the quantification of crystalline phases and the total amorphous content. For hydrated calcined clay blended cement, the amorphous part is mainly composed of C-A-S-H and unreacted metakaolin. The quantification of the distinct amorphous humps from these two phases is made possible by the PONKCS method [62, 73, 75].

Using Rietveld analysis, the weight content of a phase α can be obtained according to Equation 3.1, by comparing the scale factor S_α to the scale factor of the external standard S_{std} measured under the same conditions. The differences of phase density ρ and volume V between the phase α and rutile are considered, as well as the different mass absorption coefficients μ .

$$w_\alpha = \frac{S_\alpha \left(\rho V^2 \right)_\alpha \mu_{\text{mix}} w_{\text{std}}}{S_{\text{std}} \left(\rho V^2 \right)_{\text{std}} \mu_{\text{std}}} \quad \text{Eq. 3.1}$$

For amorphous materials, the phase constants are unknown. The phase constants can be calibrated according to Equation 3.2, where a sample composed of a known quantity of amorphous material is analysed. The phase volume is set to 1 to simplify the calculation, leaving ρ_{Ponkcs} as the only unknown of the system.

$$\rho_{\text{Ponkcs}} V^2 = \frac{K_{\text{std}} w_{\text{Ponkcs}}}{S_{\text{Ponkcs}} \mu_{\text{mix}}} \quad \text{Eq. 3.2}$$

Once ρ_{Ponkes} is determined, the amount of each amorphous phase can be found from Equation 3.1. The determined ρ_{Ponkes} has no physical meaning but it can be used in Rietveld analysis to obtain the content of the amorphous phases.

3.3 Materials

3.3.1 Characterization of raw and calcined materials

The number of calcined clays tested was reduced compared with Chapter 2. Six different clays were used, still covering a wide range of composition. The clay calcination was either carried out at EPFL at 800 °C for 1 h in a high-temperature oven or by external companies using flash or furnace calcination. Thermogravimetric Analysis (TGA) using the tangent method [81] was used on raw and calcined materials to determine the metakaolin content of calcined clays. The calculation to get the metakaolin content $\text{wt}\%_{\text{metakaolin}}$ is detailed in Appendix 2, and is obtained according to Equation 3.3, where $\text{wt}\%_{\text{kaol-OH, raw}}$ is the water loss during the dehydroxylation step of kaolinite from approx. 400°C to 600°C leading to the formation of metakaolin [15, 18, 22]. $M_{\text{kaolinite}}$ (258.16 $\text{g}\cdot\text{mol}^{-1}$) and M_{water} (18.02 $\text{g}\cdot\text{mol}^{-1}$) refer to the molecular weights of kaolinite and water, respectively. This metakaolin value obtained has to be normalized to the final weight of the calcined clay since the sample mass does not remain constant during the calcination process. TGA was also run on calcined clays to assess the efficiency of calcination. In case of incomplete calcination, the amount of uncalcined material was subtracted based on the remaining water loss corresponding to kaolinite dehydroxylation $\text{wt}\%_{\text{kaol-OH, calcined}}$.

$$\text{wt}\%_{\text{metakaolin}} = \text{wt}\%_{\text{kaol-OH, raw}} \times \frac{M_{\text{metakaolin}}}{2M_{\text{water}}} \times \left(\frac{100}{100 - \text{wt}\%_{\text{kaol-OH, raw}}} \right) - \text{wt}\%_{\text{kaol-OH, calcined}} \times \frac{M_{\text{metakaolin}}}{2M_{\text{water}}} \quad \text{Eq. 3.3}$$

For all calcined clays, the metakaolin content is indicated in Table 3.1. The secondary phases were quantified by XRD-Rietveld analysis. The X-Ray Fluorescence chemical composition, the $D_{V,50}$ and the specific surface are shown in Appendix 2. The significant amorphous content observed by XRD-Rietveld for calcined clays 18 and 29 is mainly composed of SiO_2 as well as Al_2O_3 and Fe_2O_3 , as calculated by the difference between XRF chemical composition and the phase composition by XRD-Rietveld. Limestone Durcal 5 from Omya company is used, and the Portland cement (PC) is a commercial CEM I 42.5R from Heidelberg Cement. The cement phase composition is shown in Table 3.2.

Table 3.1. Phase composition of calcined clays.

Calcined clay	1	3	9	18	29	43
Origin of clay	North America	South Asia	South America	South-east Asia	South America	South Asia
Calcination	Flash	Furnace	Flash	Furnace	Furnace	Furnace
Phase composition (wt.%)						
Metakaolin	94.2	76.8	64.4	46.5	31.7	15.0
Anatase	1.2	1.9	1.1	0.6	0.7	0.2
Hematite	-	0.2	-	10.0	1.7	3.9
Illite	-	-	1.7	-	-	36.2
Kaolinite	-	-	11.6	-	3.7	-
Mullite	4.6	-	-	1.2	-	-
Quartz	-	0.4	0.6	0.8	24.5	32.2
Rutile	-	-	-	-	4.3	1.5
Amorphous	0	20.7	20.6	40.9	33.4	11.0

Table 3.2. Cement phase composition.

Clinker	Content (wt.%)	Clinker	Content (wt.%)
Alite	65.1	Periclase	0.8
Belite	5.3	Arcanite	1.7
Aluminate	7.2	Anhydrite	5.9
Ferrite	13.9		

3.4 Analytical details

3.4.1 Paste sample preparation

LC³-50 pastes were cast using 55 parts of cement, and a combination of 30 parts of calcined clay and 15 parts of limestone. The cement used in this study contains an adequate sulfate content for a plain Portland cement hydration. For LC³-50 blends, the addition of 2% extra gypsum (Acros, 98+ grade) was needed to avoid undersulfation, as detailed in Appendix 1. Thus, the LC³-50 blends were composed of 53.9% of cement (50.6% of clinker and 3.3% of anhydrite), 29.4% of calcined clay, 14.7% of limestone and 2% of gypsum addition.

A water to binder ratio of 0.4 was used for the paste casting. Pastes were mixed at 1600 rpm for 2 min. Similar workability between the different LC³-50 blends was obtained using polycarboxylate superplasticizer (Mapei Dynamon SP914). The amount of superplasticizer required increases with the metakaolin content, up to 1.4% of total solid mass, as described in Appendix 4. Pastes were sealed cured at 20°C. 3 mm-thick slices for X-Ray Diffraction (XRD) and Scanning Electron Microscopy (SEM) were cut at 1, 3, 7, 28 and 90 days of hydration. Fresh slices were used to carry out XRD measurements combined with the Rietveld refinement method. For SEM and XRD/PONKCS samples, isopropanol was used to stop hydration. The solvent was changed after 1 h, 1 day and 3 days. Samples were then stored in a desiccator under vacuum for at least 3 days. For SEM, samples were then impregnated in epoxy resin and polished using sprays of diamond particles of 9, 3 and 1

μm for 20 min, 2 h and 3 h, respectively. A 15-nm carbon coating was finally applied to prevent charging effect.

3.4.2 Mass balance and thermodynamic modelling

3.4.2.1 Consumption of anhydrous phases

XRD-Rietveld analysis was used to quantify the amount of unreacted clinker phases, limestone and gypsum at 1, 3, 7, 28 and 90 days. The consumption of these phases is used as input for mass balance and thermodynamic modelling. XRD also permitted us to quantify the ettringite content used for mass balance. Hemi- and monocarbonate phases were also measured to be compared with the outputs of mass balance and thermodynamic modelling. Fresh samples were used for the phase quantification by XRD-Rietveld analysis to make sure that hydrated phases did not undergo any partial dehydration due to the hydration stopping method (isopropanol and vacuum drying) [81]. XRD patterns were acquired with Bragg-Brentano mode with a X'Pert PANalytical diffractometer with $\text{CuK}\alpha$ radiation operated at 45 kV and 40 mA. Samples were scanned from 5 to 70 $^{\circ}2\theta$ with a step size of 0.0167 $^{\circ}2\theta$ using a X'Celerator detector. The equivalent time per step was 30 s, resulting in a total measurement time of 15 min per scan. Rutile was used as external standard.

3.4.2.2 Composition of clinker phases

Since clinker phases do not exactly have their stoichiometric compositions, a SEM/EDX point analysis was carried out to more precisely determine the contribution of each main oxide to the hydration reactions. The compositions of the clinker phases are shown in Table 3.3 and are very close to the typical values given by Taylor [82].

Table 3.3. Clinker phase composition determined by SEM/EDX point analysis.

wt%.	Alite	Belite	Aluminate	Ferrite
CaO	70.68	62.07	56.68	48.50
SiO ₂	24.81	31.28	4.74	4.85
Al ₂ O ₃	1.14	1.43	28.02	18.79
Fe ₂ O ₃	0.74	1.11	5.11	21.07
MgO	1.03	0.62	0.91	3.55
Na ₂ O	0.29	0.47	1.38	0.59
K ₂ O	0.88	1.75	2.97	0.91
SO ₃	0.08	0.18	0.13	0.15
TiO ₂	0.13	0.22	0.01	1.39
P ₂ O ₅	0.22	0.87	0.05	0.22

3.4.2.3 C-A-S-H composition

To determine the C-A-S-H composition used for mass balance and thermodynamic modelling calculations, a FEI Quanta 200 SEM was used with an accelerating voltage of 15 kV on polished

cross-sections, with a working distance of 12.5 mm, and a spot size adjusted to get a current of approx. 0.8 nA. The determination of C-A-S-H composition was obtained by Energy Dispersive X-Ray Spectroscopy (EDX) on 200 points per sample per age according to the method of Rossen [83]. In order to get a more accurate composition of C-A-S-H, the inner product was selected for analysis to minimise the intermixing with other phases present in the microstructure. The composition of inner and outer C-A-S-H is very similar if the intermixing is carefully taken into account for outer C-A-S-H [84]. Figure 3.1 shows an example of the significant differences in terms of Al/Ca and Si/Ca ratios for C-A-S-H for PC and LC³-50 (46.5%) at 28 days of hydration. The small coloured symbols represent all the points analysed for each system, and the large symbols show the composition of the “pure” C-A-S-H (the least intermixed).

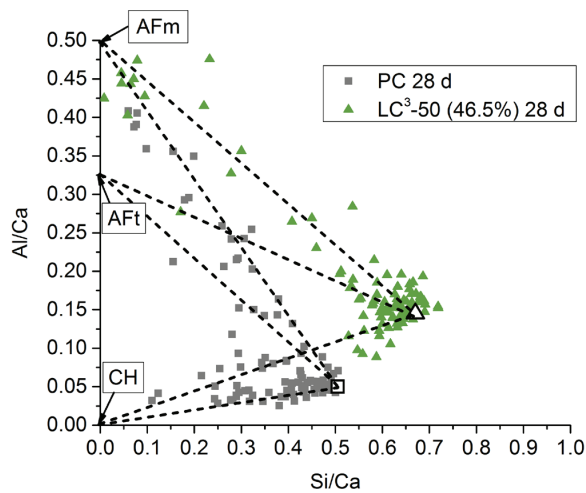


Figure 3.1. Al/Ca versus Si/Ca ratio of C-A-S-H for PC and LC³-50 (46.5%) at 28 days of hydration.

3.4.3 PONKCS

3.4.3.1 XRD data collection

For the PONKCS method, the protocol described in [62] was used. Similar parameters as Rietveld measurements were used, except the equivalent time per step which was increased to 60 s to get a better signal to noise ratio, increasing the total measurement time to 30 min per scan. Dried samples were used to get a similar background for all samples. 2 g of sample were ground for 5 min in a ceramic mortar to make sure that the particle size of the powder is similar for each test. This amount of sample was chosen to ensure a short grinding time in order to limit the potential carbonation of the hydration products. The samples were back-loaded to minimize preferred orientation. Topas-Academic v6.0 software was used to perform the Rietveld analysis.

For all tested samples, a zero-order Chebyshev polynomial accompanied by $1/x$ term was used to fit the background. The hump of C-A-S-H was defined from using sets of pseudo Voigt peaks on a 7-year old hydrated white cement, and the metakaolin hump was defined using one asymmetric split pseudo Voigt peak (as shown in Figure 3.3 (b)) [62]. The amorphous hump for metakaolin was de-

fined on the purest metakaolin sample, specifically the calcined clay containing 94.2% of metakaolin. This metakaolin hump was then applied to the other calcined clays, after making sure that the position of the amorphous hump is similar for all calcined clays samples, as shown in Figure 3.2. ρ_{Ponkes} was then determined, using w_{Ponkes} as the metakaolin content of each calcined clay (cf. Table 1). For a metakaolin content lower than 75% in calcined clay, amorphous impurities do not permit to get a good fit using the metakaolin hump only. Thus, a second hump (namely the impurity hump) was introduced to model the global amorphous hump of the calcined clay, as well as some short-term ordering of metakaolin structure [85, 86]. Figure 3.3 (a) shows the two humps used to fit the calcined clay containing 64.4% of metakaolin. For hydrated blends, the parameters of these amorphous humps were kept fixed except the scale factor. The contribution of the C-A-S-H and the calcined clay humps to the calculated pattern for LC³-50 (64.4%) at 28 days of hydration is shown in Figure 3.3 (b).

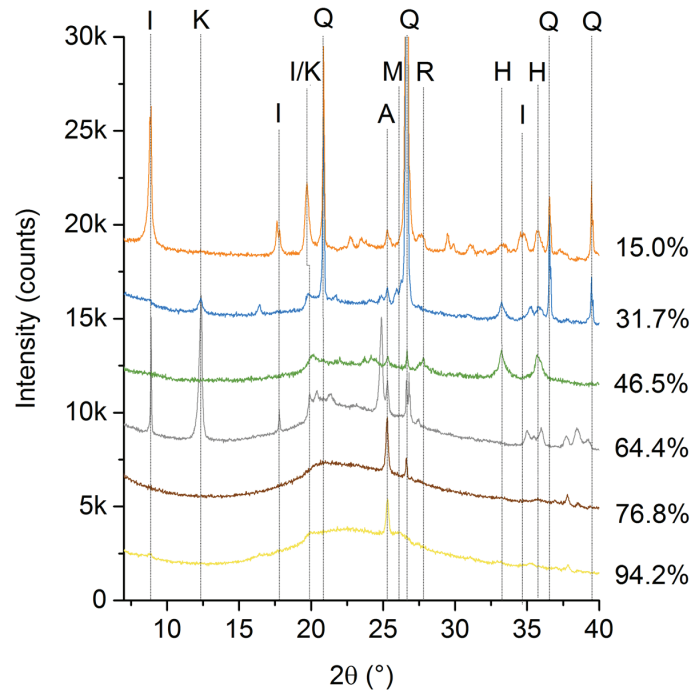


Figure 3.2. XRD patterns of calcined clays. The main peaks of illite (I), uncalcined kaolinite (K), quartz (Q), mullite (M), rutile (R) and hematite (H) are indicated.

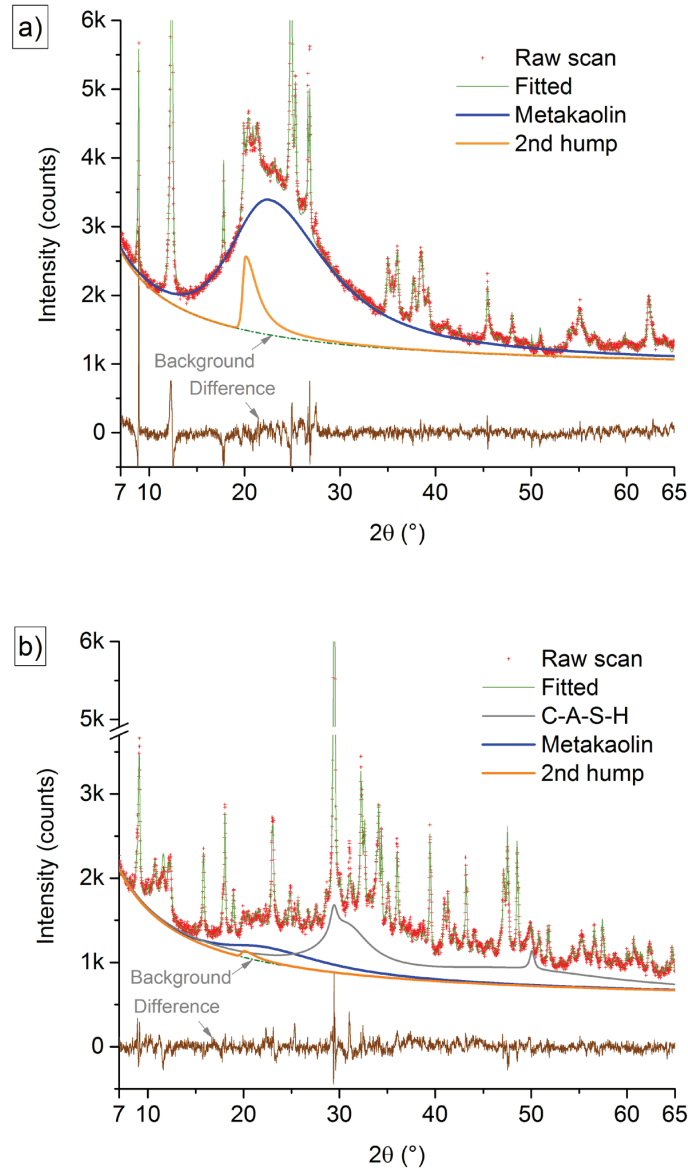


Figure 3.3. Decomposition of the XRD pattern of the calcined clay containing 64.4% of metakaolin (a) and of the LC³-50 (64.4%) at 28 days of hydration (b) with the contributions of C-A-S-H, metakaolin and the secondary hump of calcined clay.

3.5 Results

3.5.1 Mass balance and thermodynamic modelling

An example of mass balance procedure and thermodynamic modelling applied to LC³-50 (94.2%) at 28 days of hydration is shown in Figure 3.4 (a) and (b), respectively. The amount of reacted metakaolin in the calcined clay is shown up to 45% in order to focus on the range of interest (until the end of portlandite consumption). The phase assemblage predicted by both methods is very close,

especially in the range from 20 to 40% of reacted metakaolin. With the increase of the amount of reacted metakaolin, portlandite gets consumed, leading to the formation of C-A-S-H and monocarboaluminate. Below 15% of reacted metakaolin, the mass balance method does not predict any formation of carboaluminate hydrates because the input of aluminium is all used to form hydrotalcite, C-A-S-H and ettringite. Hydrotalcite, hydrogarnet and ettringite contents are independent of the amount of reacted metakaolin, since their amount is limited by the availability of MgO, Fe₂O₃ and SO₃. Below 10% of reaction, thermodynamic modelling predicts a lower amount of ettringite and no carboaluminate hydrates. This is also due to the lack of aluminium in the system. Most of aluminium is used for C-A-S-H formation, based on a constant Al/Si ratio independent of the amount of reacted metakaolin. Thermodynamic modelling starts predicting strätlingite in LC³-50 systems after complete reaction of portlandite (from 35% of reacted metakaolin onwards).

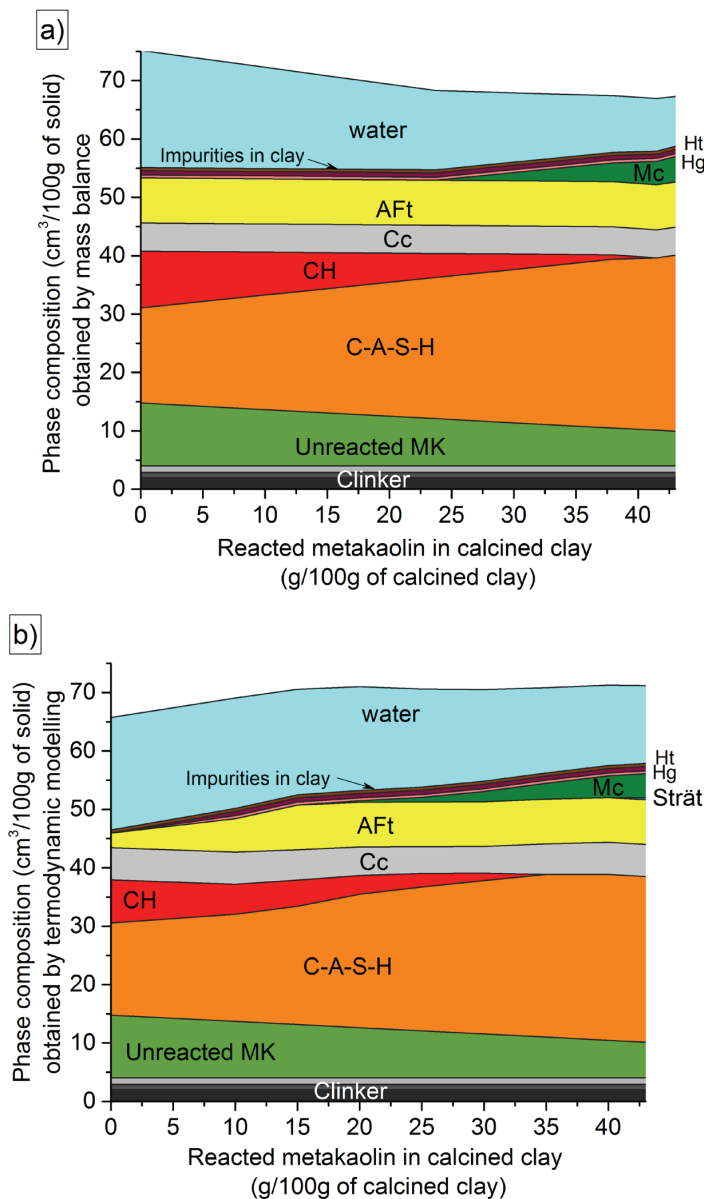


Figure 3.4. Phase assemblage of LC³-50 (94.2%) at 28 days of hydration using mass balance (a) and thermodynamic modelling (b).

The determination of the reacted metakaolin is shown in Figure 3.5 for the same system. Portlandite gets consumed as the amount of reacted metakaolin increases. The amount of reacted metakaolin is estimated from the actual portlandite content from experimental XRD-Rietveld data (horizontal line). The grey and blue solid lines show the portlandite as a function of reacted metakaolin from mass balance and thermodynamic modelling, respectively. The dashed lines represent the experimental error of portlandite quantification by XRD-Rietveld analysis. This gives the errors on the determination of the amount of reacted metakaolin.

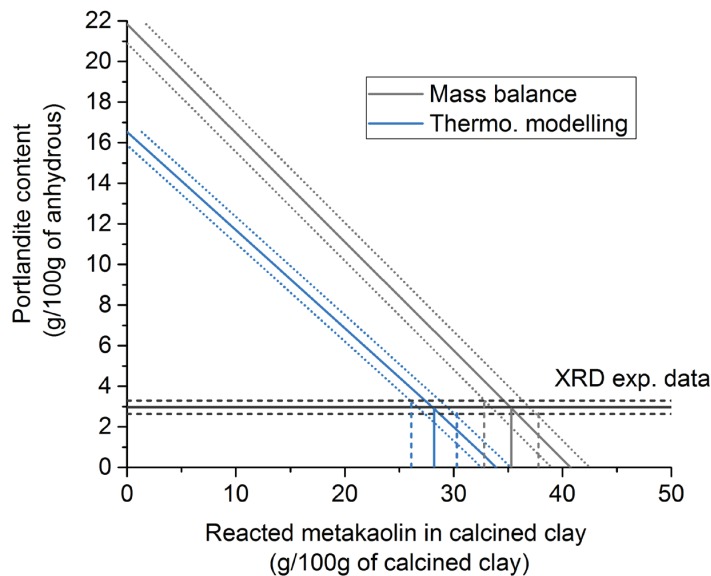


Figure 3.5. Determination of the degree of reaction of metakaolin for mass balance and thermodynamic modelling for LC³-50 (94.2%) at 28 days of hydration.

Mass balance and thermodynamic modelling were applied to the different LC³-50 systems, and the results obtained at 1, 3, 7, 28 and 90 days of hydration are shown in Figure 3.6 (a) and (b), respectively. It shows that at 1 and 3 days, the amount of reacted metakaolin is globally similar for all systems except for the LC³-50 (15.0%) which is lower. From 7 days onwards, the amount of reacted metakaolin globally increases with the metakaolin content by mass balance. However, the amplitude of the increase decreases with the metakaolin content. The amount of reacted metakaolin by thermodynamic modelling is quite similar for calcined clays containing more than 50% of metakaolin.

The correlation of the amount of reacted metakaolin by mass balance and by thermodynamic modelling is shown in Figure 3.7. The results obtained until 7 days are very similar between both methods. At 28 and 90 days, thermodynamic modelling predicts a slightly lower amount of reacted metakaolin. This difference could be explained by the C-S-H model used in this method. The Ca/Si ratio of C-S-H model is 1.63 (C_{1.63}SH_{2.9}), whereas the measured Ca/Si ratios by SEM-EDX are lower (1.49 to 1.58). Thus, more calcium is used in thermodynamic modelling for the formation of C-S-H. As a consequence, the amount of portlandite left is lower, leading to a slight decrease of the amount of reacted metakaolin.

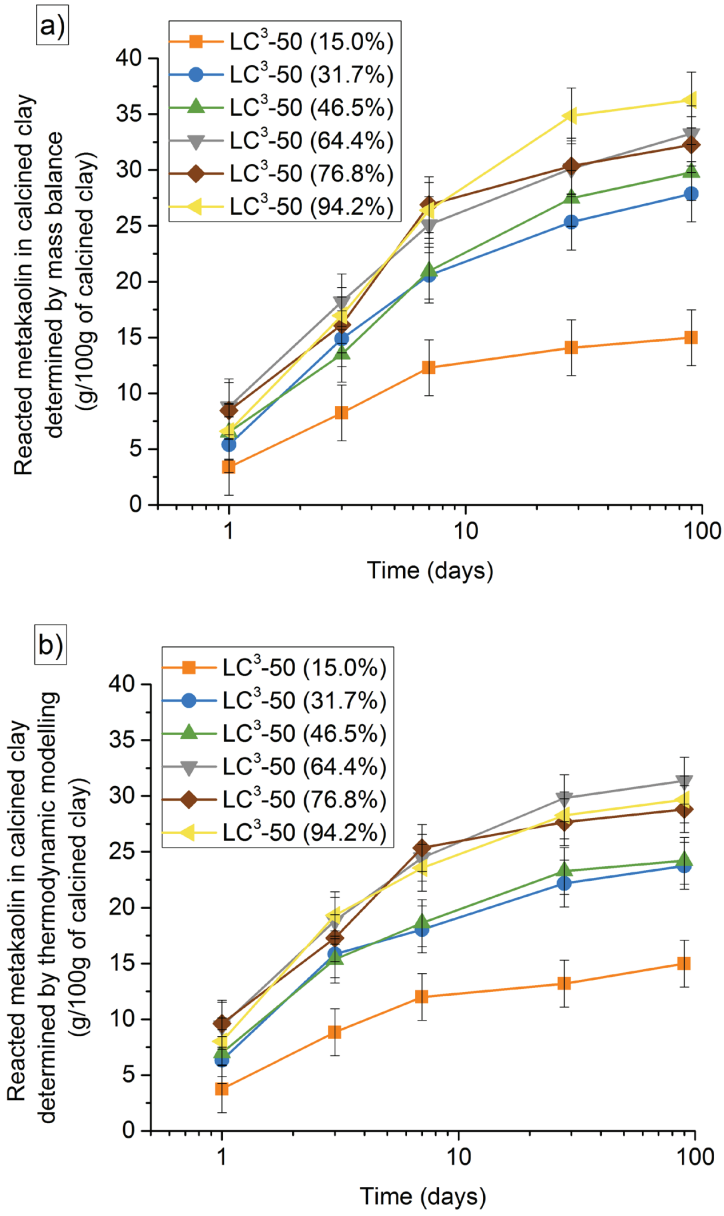


Figure 3.6. Amount of reacted metakaolin for the different LC³-50 blends at 1, 3, 7, 28 and 90 days determined by mass balance (a) and thermodynamic modelling (b).

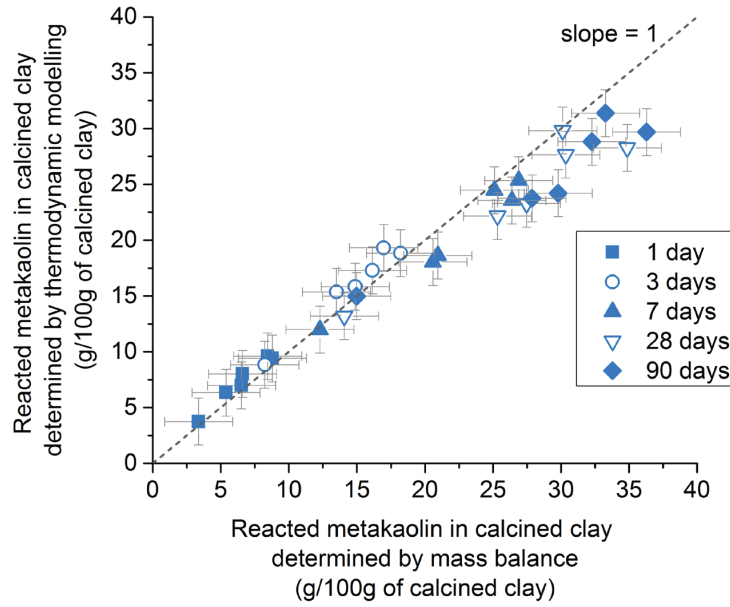


Figure 3.7. Correlation between the amount of reacted metakaolin obtained by mass balance and by thermodynamic modelling.

The reaction degree of metakaolin is then calculated according to Equation 3.4. It is shown in Figure 3.8 (a) and (b) for mass balance and thermodynamic modelling, respectively. It shows that for both methods, the reaction degree of metakaolin decreases with the metakaolin content of the calcined clay. For the calcined clay containing 15.0% of metakaolin, all metakaolin has reacted at 90 days of hydration.

$$\text{Reaction degree metakaolin} = \frac{\text{Reacted metakaolin} \times 100}{\text{wt}\%_{\text{metakaolin}}} \quad \text{Eq. 3.4}$$

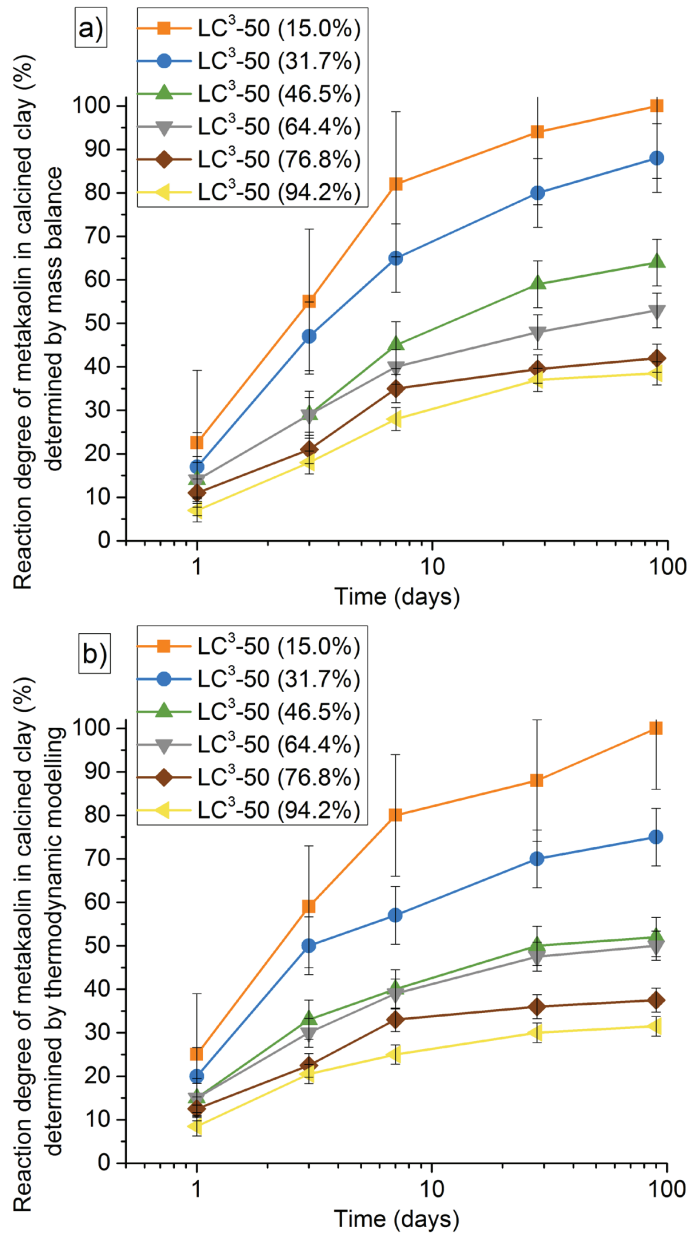


Figure 3.8. Reaction degree of metakaolin for the different LC³-50 blends at 1, 3, 7, 28 and 90 days determined by mass balance (a) and thermodynamic modelling (b).

3.5.2 Sensitivity analysis for mass balance and thermodynamic modelling

In order to estimate the influence of the errors of measurements of the input data on the determination of the amount of reacted metakaolin for mass balance and thermodynamic modelling, a sensitivity analysis was carried out. Table 4 shows the error values considered for the determination of the clinker phase content, the ettringite quantification, the C-A-S-H composition and the portlandite quantification. Based on these errors, the maximum variations are applied to study their impact on the final amount of reacted metakaolin. The maximum deviation obtained for the amount of reacted metakaolin by mass balance is ± 2.5 g/100g of calcined clay. For thermodynamic modelling, a

slightly smaller deviation is obtained, ± 2.1 g/100g of calcined clay, since ettringite content and Si/Ca ratio are not experimentally measured.

Table 3.4. Error of measurement of clinker phases, C-A-S-H composition, ettringite and portlandite.

Phase	Error (g/100g of anhydrous)
Clinker (XRD-Rietveld)	± 1.0
C-A-S-H composition (SEM-EDX)	
Al/Ca	± 0.015
Si/Ca	± 0.015
Ettringite (XRD-Rietveld)	± 1.1
Portlandite (XRD-Rietveld)	± 0.4

3.5.3 Output reliability

Since metakaolin provides SiO_2 and Al_2O_3 to the system, C-A-S-H and carboaluminate formation are mainly affected, because their formation is limited by the complete consumption of the remaining SiO_2 and Al_2O_3 . For C-A-S-H formation, we do not have any precise independent method for measuring the amount. But the amount of carboaluminates formed during hydration can be compared between mass balance, thermodynamic modelling and experimental XRD-Rietveld data. For mass balance, the formation of carboaluminate hydrates corresponds to the complete consumption of the remaining aluminium after the formation of hydrotalcite, C-A-S-H and ettringite. Both hemi- and monocarboaluminate phases are identified for the different blends by XRD-Rietveld method. Figure 3.9 shows the comparison of the sum of hemi- and monocarboaluminate hydrates between mass balance, thermodynamic modelling and XRD-Rietveld results. A good agreement is found for all calcined clay blends. The relative low content as well as the poor crystallinity of hemicarboaluminate phase is the main source of the observed differences for XRD-Rietveld results.

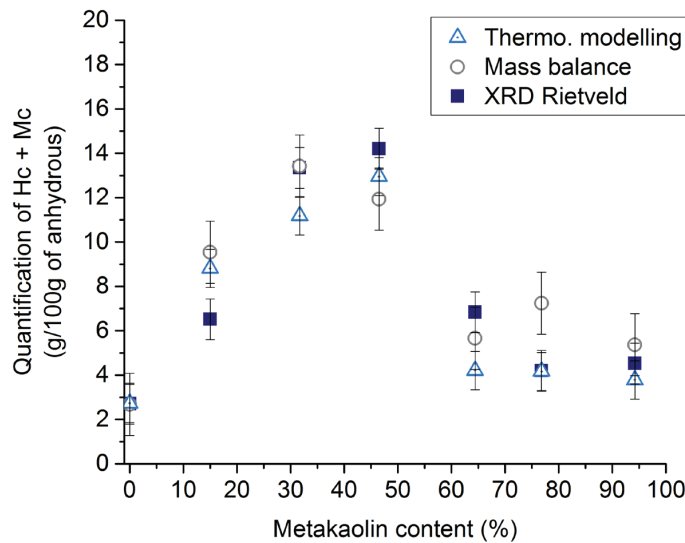


Figure 3.9. Amount of carboaluminate hydrates obtained at 28 days of hydration by thermodynamic modelling, mass balance and XRD/Rietveld.

3.5.4 PONKCS method

The results obtained using PONKCS method are shown in Figure 3.10 for the different LC³-50 systems. The error of measurement was determined based on three series of measurements. It shows that the amount of reacted metakaolin increases with time, but the trends are not as clear as mass balance and thermodynamic modelling. The results obtained are more spread, with higher deviations, especially for the LC³-50 systems containing <50% of metakaolin.

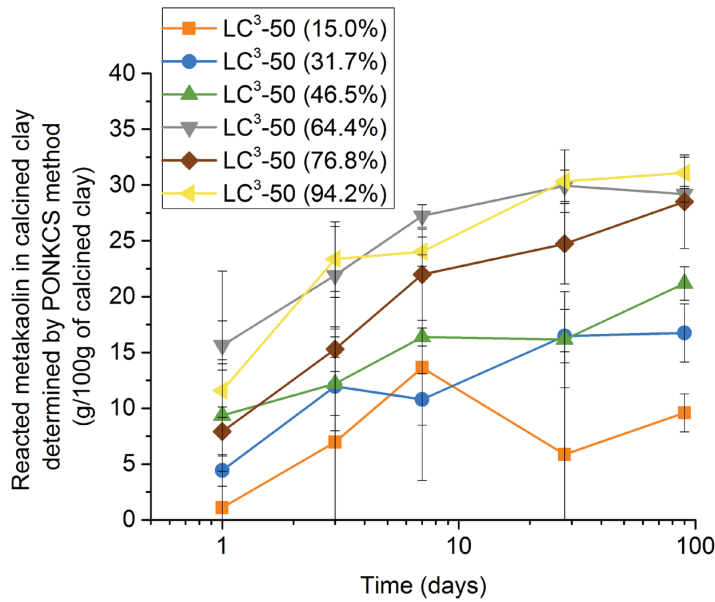


Figure 3.10. Amount of reacted metakaolin at 1, 3, 7, 28 and 90 days determined by PONKCS method.

The reaction degree of metakaolin at 1, 3, 7, 28 and 90 days is shown in Figure 3.11 for the different LC³-50 systems. Due to the high scatter of the data, clear trends cannot be obtained. As observed for mass balance and thermodynamic modelling, the reaction degree of metakaolin globally decreases with the metakaolin content of the calcined clay.

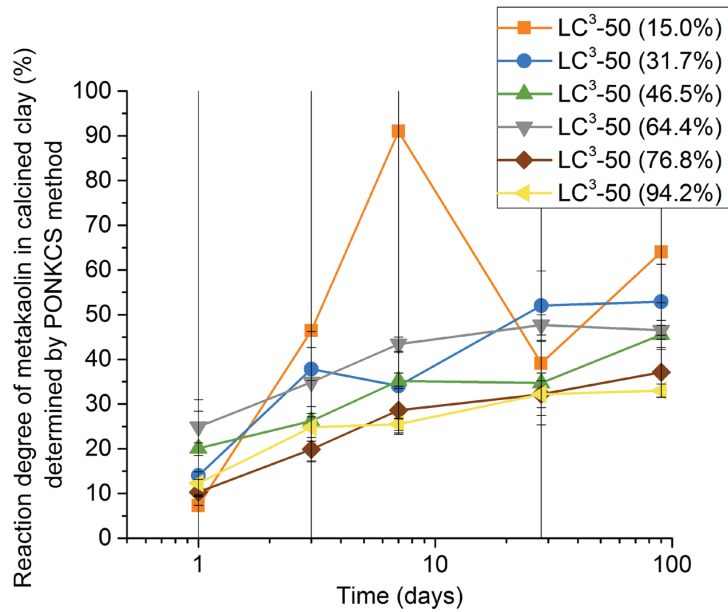


Figure 3.11. Reaction degree of metakaolin at 1, 3, 7, 28 and 90 days determined by PONKCS method.

A comparison with mass balance is shown in Figure 3.12. Similar values to mass balance are reached for LC³-50 systems with a metakaolin content higher than 60% in calcined clay, as shown by the hollow symbols. The plain symbols show the correlation for the blends containing less than 60% of metakaolin in the calcined clay. The amount of reacted metakaolin obtained for blends with less than 60% of metakaolin in calcined clay is lower than the values obtained by mass balance. Moreover, the deviations globally increase with the decrease of the metakaolin content of the calcined clay. With the decrease of the metakaolin content in the calcined clay, the measurement of the amount of reacted metakaolin becomes more challenging due to the detection limit for the PONKCS method. As example, in LC³-50 (15.0%), the initial amount of metakaolin in the system is 4.5 g per 100 g of anhydrous binder only. During hydration, the residues of unreacted metakaolin are not easy to identify and quantify, leading to significant errors of measurement. Besides, the impurity hump increases with the decrease of the metakaolin content of the calcined clay. The complexity of the amorphous humps also decreases the reliability of the results even if the overall fitting is improved.

Thus, the PONKCS method gives a quite reliable indication of the amount of reacted metakaolin for blends containing more than 60% of metakaolin in calcined clay, i.e. with more than 14 g of unreacted metakaolin left per 100 g of binder. Below this value, the precision of PONKCS method becomes poor.

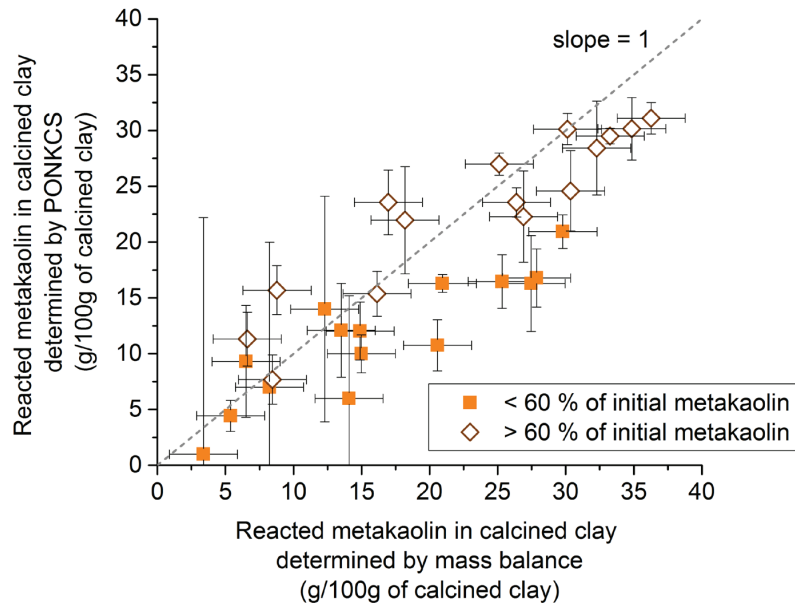


Figure 3.12. Correlation between the amount of reacted metakaolin obtained by mass balance and by PONKCS.

3.6 Conclusion

Among the three methods used in this study, the mass balance approach shows the most reliable results to determine the amount of reacted metakaolin. Thermodynamic modelling is less time-consuming than mass balance since it does not necessarily require any SEM-EDX measurement and it can be run simply based on XRD-Rietveld outputs. However, despite very similar results to mass balance until 7 days of hydration, thermodynamic modelling underestimates the amount of reacted metakaolin for later ages due to the fixed Ca/Si ratio used in the model of C-S-H.

PONKCS method gives close results to mass balance and thermodynamic modelling for LC³-50 blends containing more than 60% of metakaolin in the calcined clay. However, this method gives higher deviations in the results, especially for blends containing calcined clays with less than 60% of metakaolin. Below 60% of metakaolin, the quantification becomes very complex due to the small amount left of unreacted metakaolin.

Chapter 4 - Investigation of the calcined kaolinite content on the hydration of Limestone Calcined Clay Cement (LC³)

This Chapter has been submitted to Cement and Concrete Research, together with the detailed comparison of different methods to quantify the amount of calcined clay reacted (Chapter 3).

François Avet^{1*}, Karen Scrivener¹

¹ Laboratory of Construction Materials, IMX, EPFL, 1015 Lausanne, Switzerland

* Corresponding author: Tel.: +41 21 6932821

E-mail address: francois.avet@epfl.ch

4.1 Introduction

Limestone calcined clay cements (LC³)¹ are a promising approach to producing cement with lower environmental impact [87-89]. The amounts of traditional SCMs such as fly ash or slag are limited compared to the amount of cement produced and most suitable materials are already used in composite cements or concrete [9]. LC³ combines two widely available materials to substitute clinker: calcined kaolinitic clays (which show the highest pozzolanic potential among the different classes of clays [22, 25, 26]), and limestone. Clinker content can be reduced to 50% in LC³-50, while maintaining mechanical properties comparable to plain Portland cement (OPC) [43]. A linear correlation is found between strength and calcined kaolinite content for LC³-50 blends [90]. From 40% of calcined kaolinite, higher strengths than reference Portland cement can be obtained from 7 days onwards, independent of calcined clay fineness, specific surface or secondary phases.

The reactivity of calcined kaolinitic clays comes from the formation of metakaolin during the thermal activation of raw clays [18, 21, 22, 91]. Metakaolin reacts as pozzolanic material with portlandite, water and sulfate to form C-A-S-H, ettringite, AFm phases and/or strätlingite [31, 32]. When limestone is added to Portland cement, calcite reacts with C₃A from clinker to form hemi- and monocarboaluminate phases [37, 38, 41]. In LC³, aluminate from the metakaolin also reacts with calcite and enhances the formation of carboaluminate phases [43].

Most previous studies on the impact of metakaolin on hydration have used fairly pure metakaolin [69, 70, 92], but such materials are not very interesting from an economic point of view as they typically cost around 3 times the price of Portland cement. There is little information available about calcined clays with lower calcined kaolinite content, which have a much higher potential as clinker substitutes. Thus, the goal of this study is to investigate the influence of the calcined kaolinite content of calcined clay on the hydration of LC³ blends in terms of kinetics of hydration and microstructural development.

¹ LC³: Limestone Calcined Clay Cement: <http://www.lc3.ch>

4.2 Materials and methods

4.2.1 Kaolinitic clays

In this study, seven kaolinitic clays with various compositions were used. Same clays as Chapter 3 are investigated. As detailed in Appendix 2 and previously in Chapter 2, the calcined kaolinite content in Equation 4.1 was determined by TGA to consider the reactive part of the material only. $wt\%_{kaol-OH, calcined}$ refers to the remaining water loss in calcined clay, $M_{kaolinite}$ and M_{water} correspond to the molecular weights of kaolinite and water, respectively.

$$wt\%_{calcined\ kaolinite} = wt\%_{kaolinite} - wt\%_{kaol-OH, calcined} \times \frac{M_{kaolinite}}{2M_{water}} \times \left(\frac{100 - wt\%_{kaol-OH, calcined}}{100} \right) \quad \text{Eq. 4.1}$$

For all the calcined clays, the calcined kaolinite content is indicated in Table 4.1, as well as the XRF chemical composition, the $D_{v,50}$ measured by Malvern laser diffraction and the specific surface measured by nitrogen adsorption using the BET model. Quartz was used as inert material to simulate a calcined clay with 0 % of calcined kaolinite. Characteristics of cement and limestone used in this study are also shown in Table 4.1. The Portland cement (PC) used was a commercial CEM I 42.5 R from Heidelberg Cement, the limestone used was Durcal 5, from Omya Company.

Table 4.1. XRF Compositions and main characteristics of calcined clays, cement and limestone.

Calcined clay	1	3	9	18	27	29	43	Quartz	Cement	Lime-stone
Origin of clay	North America	South Asia	South America	South-east Asia	North America	South America	South Asia			
Calcination	Flash	Furnace	Flash	Furnace	Furnace	Furnace	Furnace			
Calcined kaolinite content (wt.%)	95.0	79.4	66.2	50.3	38.9	35.0	17.0	0	-	-
D _{v,50} (µm)	5.1	5.3	4.0	10.9	8.5	23.5	5.9	11.2	8.4	7.2
BET Specific surface (m ² /g)	9.6	15.3	12.9	45.7	23.1	18.5	18.7	1.2	0.9	1.8
XRF composition (wt.%)										
SiO ₂	52.0	51.8	50.3	44.9	54.7	67.6	68.4	99.8	19.3	0.1
Al ₂ O ₃	43.8	42.4	42.7	32.3	26.8	22.6	17.5	-	5.7	-
Fe ₂ O ₃	0.3	1.9	0.6	15.4	13.6	6.1	8.9	-	3.6	-
CaO	-	0.1	-	1.3	0.3	0.5	0.6	-	63.6	55.0
MgO	-	0.1	-	0.8	1.0	-	0.7	-	1.6	0.2
SO ₃	0.1	-	-	0.1	-	-	-	-	3.2	-
Na ₂ O	0.3	0.1	-	0.4	-	-	0.1	-	0.2	0.1
K ₂ O	0.1	0.1	0.1	0.2	0.4	0.3	2.3	0.1	1.2	-
TiO ₂	1.5	2.4	1.8	2.4	1.1	1.5	0.8	-	0.3	-
P ₂ O ₅	0.2	0.1	0.1	0.4	-	-	0.1	-	0.2	-
MnO	-	-	-	0.1	-	-	0.1	-	0.1	-
Others	0.1	0.2	0.2	0.2	-	-	0.2	-	0.3	-
LOI	1.5	1.0	3.6	1.7	1.9	1.4	0.5	0.1	0.8	42.6

4.2.2 Microstructure study on pastes

Pastes were made of the reference PC alone and LC³-50 pastes in which 45 parts of the materials is made up by 30 parts of calcined clay and 15 parts of limestone. The cement used in this study contains an optimized sulfate content for a plain Portland cement hydration. For LC³-50 blends, the addition of 2% extra gypsum (Acros, 98+ grade) was needed to avoid undersulfation, as detailed in [43]. The mix composition of the LC³-50 blends is shown in Table 4.2.

Table 4.2. Mix composition of PC and LC³-50 blends.

Composition (wt.%)	Cement		Calcined clay	Limestone	Gypsum addition
	Clinker	Anhydrite			
PC	94.1	5.9	-	-	-
LC ³ -50	50.6	3.3	29.4	14.7	2.0

Pastes were cast using a water to binder ratio of 0.4. To ensure comparable workability to PC, polycarboxylate superplasticizer was used in LC³-50 pastes (Mapei Dynamon SP914, max 1.4 wt% of total solid mass, as described in Appendix 4). The pastes were mixed for 2 min at 1600 rpm, and then sealed cured at 20°C until tested.

The heat release during hydration was measured in an isothermal calorimeter (TAM Air) for 28 days. 10 g of paste was poured in a glass ampoule, which was then sealed and put in the calorimeter. X-Ray Diffraction (XRD) measurements combined with the Rietveld refinement method were carried out on freshly cut slices at 1, 3, 7, 14, 28 and 90 days to quantify the main crystalline phases present and to determine the degree of hydration of clinker in the different systems. The slices were analysed in Bragg-Brentano mode with a X'Pert PANalytical diffractometer with CuK α source operated at 45 kV and 40 mA. Samples were scanned from 5 to 70 °2 θ with a step size of 0.0167 °2 θ using a X'Celerator detector, resulting in an equivalent time per step of 30 s. Rutile was used as external standard.

For TGA, Mercury Intrusion Porosimetry (MIP) and Scanning Electron Microcopy (SEM), isopropanol was used to stop hydration. The solvent was changed after 1 h, 1 day and 3 days. Samples were then stored in a desiccator under vacuum for at least 3 days. TGA was used to quantify the portlandite content using the tangent method [81]. 50 mg of powdered sample was analysed using Mettler Toledo TGA/SDTA 851 balance with a heating rate of 10 °C/min from 30 °C to 1000 °C under constant nitrogen flow of 30 mL/min. To compare XRD on fresh slices and TGA on dried samples, data are normalized per 100 g of anhydrous in Equations 4.2 and 4.3, as reported in [81], using the water to cement ratio w/c and the amount of bound water H₂O_{bound}.

$$\text{Fresh slice XRD} \quad \text{wt}\%_{\text{rescaled}} = \text{wt}\%_{\text{Rietveld}} \left(1 + \frac{w}{c} \right) \quad \text{Eq. 4.2}$$

$$\text{Dried powder TGA} \quad \text{wt}\%_{\text{rescaled}} = \frac{\text{wt}\%_{\text{TGA}}}{1 - H_2O_{\text{bound}}} \quad \text{Eq. 4.3}$$

To characterize the porosity, MIP was used. MIP gives reliable information concerning the capillary porosity if the samples are prepared by solvent exchange with isopropanol. A contact angle of 120° was used between mercury and paste. Müller showed that 120° gives better agreement with pore sizes calculated by ¹H-NMR than 140° [93]. Paste pieces were cut to get 0.7 g for MIP experiments carried out with Porotec Pascal 140 and 440 devices.

To observe the microstructure, FEI Quanta 200 SEM was used with an accelerating voltage of 15 kV on polished cross-sections, with a working distance of 12.5 mm, and a spot size adjusted to get a current of approx. 0.8 nA. The determination of C-A-S-H composition was obtained by Energy Dispersive X-Ray Spectroscopy (EDX) on 200 points per sample per age according to the method of Rossen [83]. In order to get a more accurate composition of C-A-S-H, inner products were sampled to minimise intermixing with other phases present in the microstructure.

The pore solution was obtained by mechanical squeezing at 800 kN for samples cured for 28 days of hydration. The solution was then filtered using 0.45 μ m filter. To limit precipitation, the extracted liquid was then diluted in a HNO₃ solution with a 1:9 ratio. The ionic concentrations were obtained using inductively coupled plasma optical emission spectroscopy (ICP-OES, Shimadzu ICPE 9000).

Relative humidity measurements were carried out using Rotronic chambers equipped with high-precision relative humidity sensors. Sensors were calibrated before and after testing with salt solutions of known relative humidity from 97.6% to 75.5% (using K_2SO_4 , KNO_3 , KCl and $NaCl$). Circulating water around the sample holder ensured constant temperature of $20^\circ C$. Sample pieces of 4-8 mm were cut at 0.6 day of hydration and sealed in the RH chambers. The RH was continuously monitored for 28 days.

4.3 Results

4.3.1 Kinetics of hydration

The heat release during the first days of hydration is shown in Figure 4.1 per gram of solid (a) and per gram of clinker (b) for PC and LC³-50 (0%), (50.3%) and (95.0%). Not all the clay systems are shown for better clarity but the range of calcined kaolinite contents is covered. The hydration of C_3S is enhanced for LC³-50 blends due to the filler effect of calcined clay (quartz for LC³-50 (0%)) and limestone, as shown by the higher slope and intensity of the silicate peak. Moreover, calcined clay significantly affects the intensity of the aluminate peak. The intensity of the peak increases with the calcined kaolinite content. In addition to the filler effect, this heat increase can be explained by the beginning of the metakaolin reaction with portlandite.

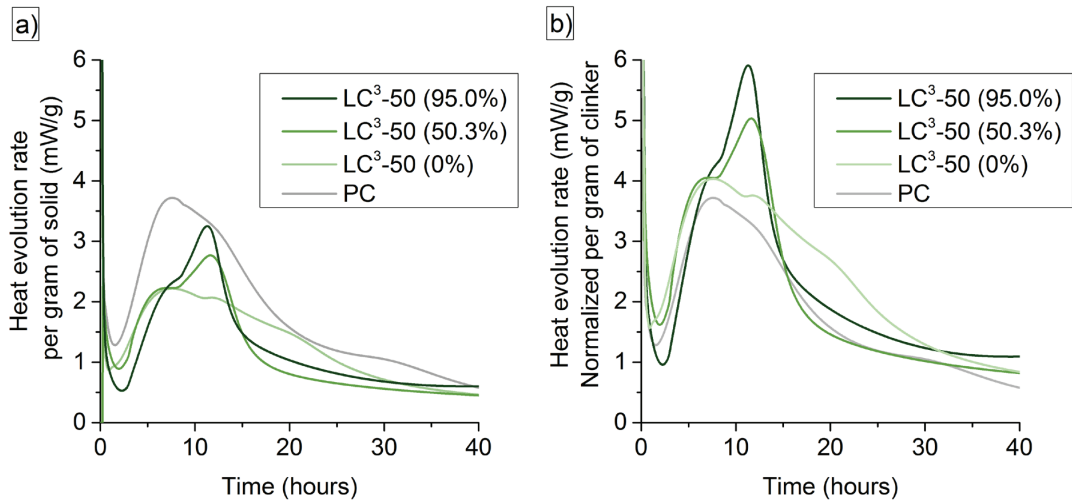


Figure 4.1. Heat release per gram of solid (a) and normalized per gram of clinker (b) for PC, LC³-50 (0%), (50.3%) and (95.0%).

The cumulative heat released is shown in Figure 4.2 per gram of solid (a) and per gram of clinker (b). For the LC³-50 blends, the difference of heat release between LC³-50 (0%) blend and the two other LC³-50 blends can be attributed to the reaction of metakaolin. The highest heat is released by the blend with the highest calcined kaolinite content at early ages (<~150 hrs). However, after approximately 3 days, the rate of heat increase significantly slows down for this system, and from 5 days onwards, the cumulative heat is lower than for the blend with 50.3% of calcined kaolinite in the calcined clay.

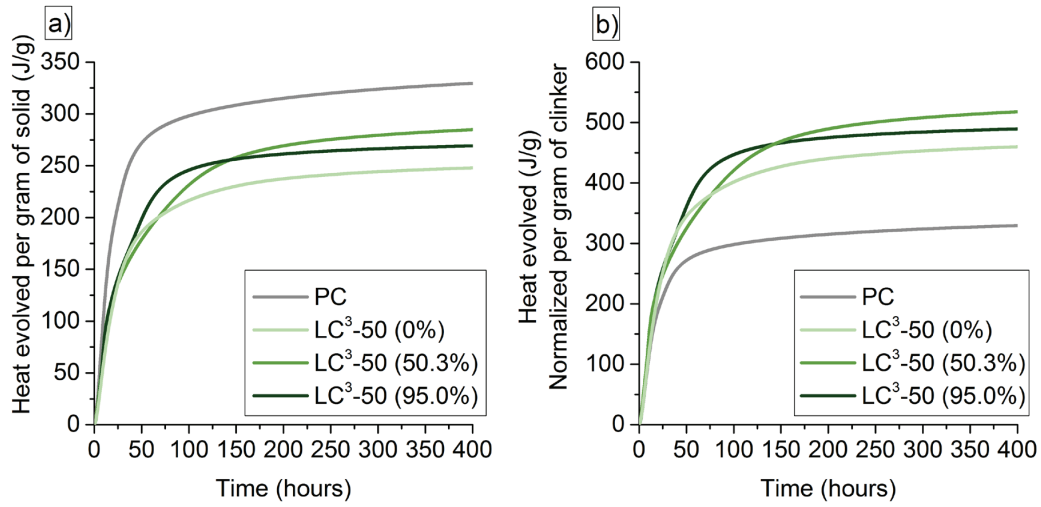


Figure 4.2. Cumulative heat released per gram of solid (a) and normalized per gram of clinker (b) for PC, LC³-50 (50.3%) and (95.0%).

4.3.2 Determination of clinker hydration degree

The degree of hydration (DoH) of clinker is determined by XRD-Rietveld according to Equation 4.4:

$$\text{Hydration degree}_t = \frac{\sum(C_3S + C_2S + C_3A + C_4AF)_i - \sum(C_3S + C_2S + C_3A + C_4AF)_t}{\sum(C_3S + C_2S + C_3A + C_4AF)_i} \quad \text{Eq. 4.4}$$

The DoH is higher for LC³-50 (0%) and (50.3%) than the PC reference, as shown in Figure 4.3 (a), due to the filler effect of calcined clay and limestone. For LC³-50 (95.0%), the hydration degree of clinker is also higher than PC at early age. However, it becomes almost constant from 3 days onwards, whereas the hydration degree of PC, LC³-50 (0%) and (50.3%) blends keeps increasing with time. This indicates a significant slowing down of clinker hydration.

To extend these results to all calcined clays, the DoH is plotted as a function of the calcined kaolinite content at 1, 3 and 28 days of hydration in Figure 4.3 (b). At 28 days, the clinker DoH decreases with the calcined kaolinite content of calcined clays. Above a calcined kaolinite content of about 65% there is almost no increase in the clinker DoH between 3 days and 28 days. For blends with $\leq 65\%$ of calcined kaolinite, hydration continues and the clinker DoH keeps increasing with time.

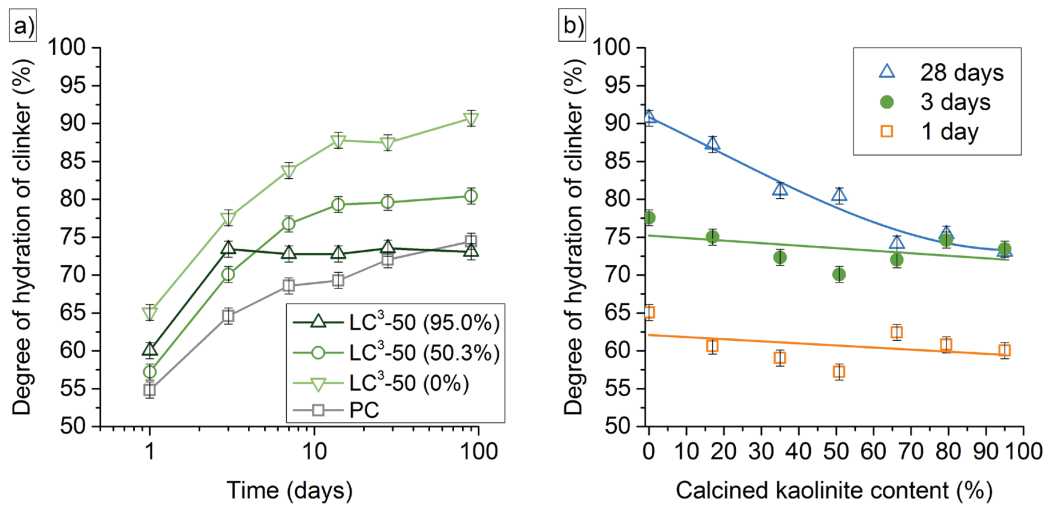


Figure 4.3. Degree of Hydration (DoH) of clinker determined by Rietveld analysis as a function of time (a) and of the calcined kaolinite content (b).

4.3.3 Characterization of metakaolin reaction

Figure 4.4 (a) shows the portlandite content normalized per gram of clinker. The results for LC³-50 (0%) demonstrate the filler effect whereby the clinker reaction is enhanced. By comparison, it is evident that a significant amount of portlandite has already been consumed at 24 hours of hydration for LC³-50 (50.3%) and (95.0%). Figure 4.4 (b) shows this portlandite consumption per gram of solid by TGA at 1, 3 and 28 days for the different LC³-50 blends. For all ages, the portlandite content decreases with the calcined kaolinite content. However, above a calcined kaolinite content of about 65% the differences are not significant.

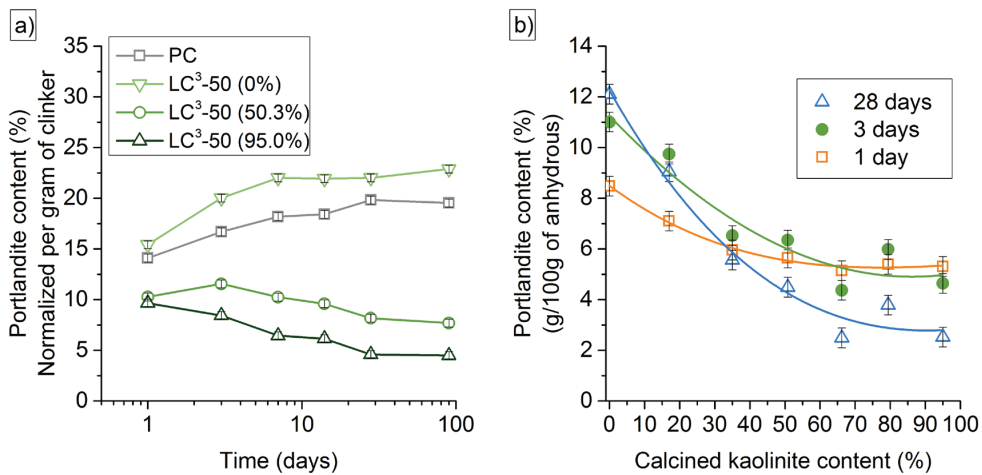


Figure 4.4 Portlandite quantification by TGA as a function of time (a) and of the calcined kaolinite content (b).

Table 4.3 shows the incorporation of silicon and aluminium in C-A-S-H due to metakaolin reaction at 3 and 28 days for LC³-50 (17.0%), (50.3%) and (95.0%) compared with PC. The aluminium incorporation in C-A-S-H increases with the calcined kaolinite content whereas silicon incorporation

is similar, but higher than PC. The increase of the aluminium incorporation is quite small for the LC³-50 (50.3%) compared with the LC³-50 (17.0%) and PC but a larger increase is observed for the LC³-50 (95.0%) system. Moreover, the increase of the Al/Ca ratio from 3 to 28 days is also the highest for the LC³-50 (95.0%) system. Figure 4.5 shows the change in C-A-S-H composition at 28 days. The small coloured symbols represent all the points analysed for each system, and the large symbols show the composition of the “pure” C-A-S-H (least intermixed). More intermixing with Ca bearing hydration products and metakaolin is observed for LC³-50 (95.0%).

Table 4.3. Al/Ca and Si/Ca atomic ratios of C-A-S-H at 3 and 28 days.

± 0.015	3 days		28 days	
	Al/Ca	Si/Ca	Al/Ca	Si/Ca
PC	0.06	0.52	0.06	0.51
LC ³ -50 (17.0%)	0.06	0.56	0.07	0.62
LC ³ -50 (50.3%)	0.08	0.56	0.13	0.67
LC ³ -50 (95.0%)	0.16	0.57	0.26	0.67

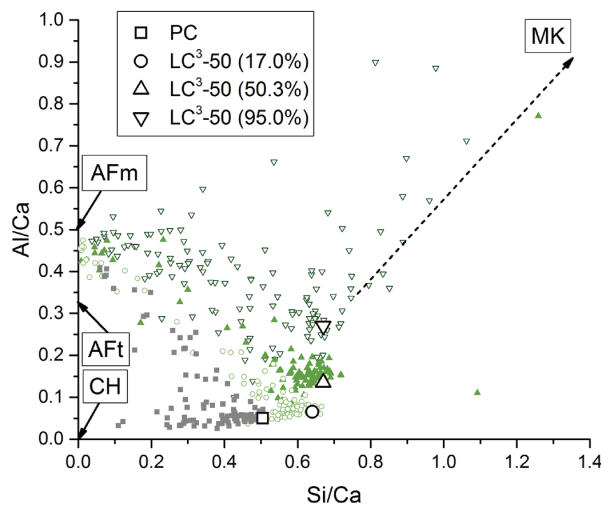


Figure 4.5. SEM-EDX of Al/Ca as a function of Si/Ca at 28 days of hydration for PC and LC³-50 (17.0%), (50.3%) and (95.0%).

4.3.4 Determination of the amount of reacted metakaolin

The amount of reacted metakaolin is estimated by mass balance, adapted from Durdzinski [74] and detailed in Chapter 3. The consumption of clinker phases, limestone and gypsum is used as input to predict the phase assemblage. The amount of reacted metakaolin is determined by iterations, by comparing for each metakaolin increment the predicted portlandite content with experimental XRD/TGA results.

The amount of reacted metakaolin is shown as a function of time in Figure 4.6 (a) for the LC³-50 (17.0%), (50.3%) and (95.0%). The amount of reacted metakaolin increases with time. There is no

slowing down of reaction from 3 days onwards for the LC³-50 (95.0%) blend, as previously observed for the hydration of clinker. The amount of reacted metakaolin as a function of the calcined kaolinite content in Figure 4.6 (b) increases with the calcined kaolinite content of calcined clays until 65% of calcined kaolinite. Above this content, the amount of reacted metakaolin is very similar for LC³-50 blends at 1 and 3 days, with a slightly higher amount for the LC³-50 (95.0%) at 28 days.

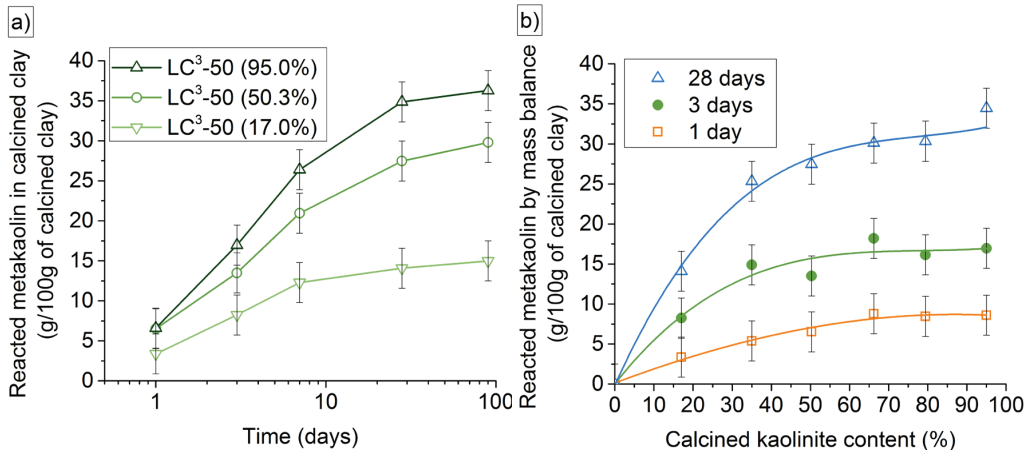


Figure 4.6. Amount of reacted metakaolin as a function of time (a) and of the calcined kaolinite content (b).

4.3.5 Porosity characterization

Figure 4.7 shows MIP results at 3 days (a) and 28 days (b) of hydration. At 3 days of hydration, the connectivity of porosity for LC³-50 blends containing calcined clay with more than 65% of calcined kaolinite is significantly refined compared with PC. SEM pictures of the microstructure at 3 days in Figure 4.8 also show a much denser microstructure for LC³-50 (95.0%), whereas more porosity can be seen for PC and LC³-50 (50.3%). At 28 days, MIP results show that all LC³-50 blends except quartz blend have a finer pore connectivity than PC as indicated by the smaller breakthrough pore entry radius where the intrusion of mercury starts to increase significantly. SEM pictures in Figure 4.9 show a much denser microstructure for LC³-50 (50.3%) and (95.0%) than PC.

There is a difference in the kinetics of pore refinement depending on the calcined kaolinite content: the porosity is already well-refined for blends containing > 65% of calcined kaolinite in calcined clay at 3 days, and no major further refinement occurs later on, whereas LC³-50 blends with ≤ 50% of calcined kaolinite show significant refinement between 3 and 28 days.

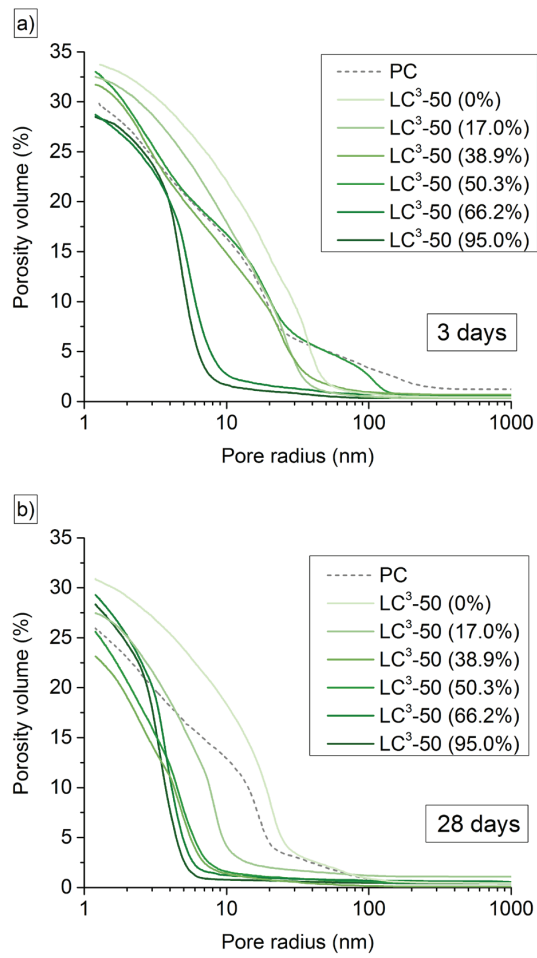


Figure 4.7. Porosity observed by MIP for PC and LC³-50 blends at 3 days (a) and 28 days (b).

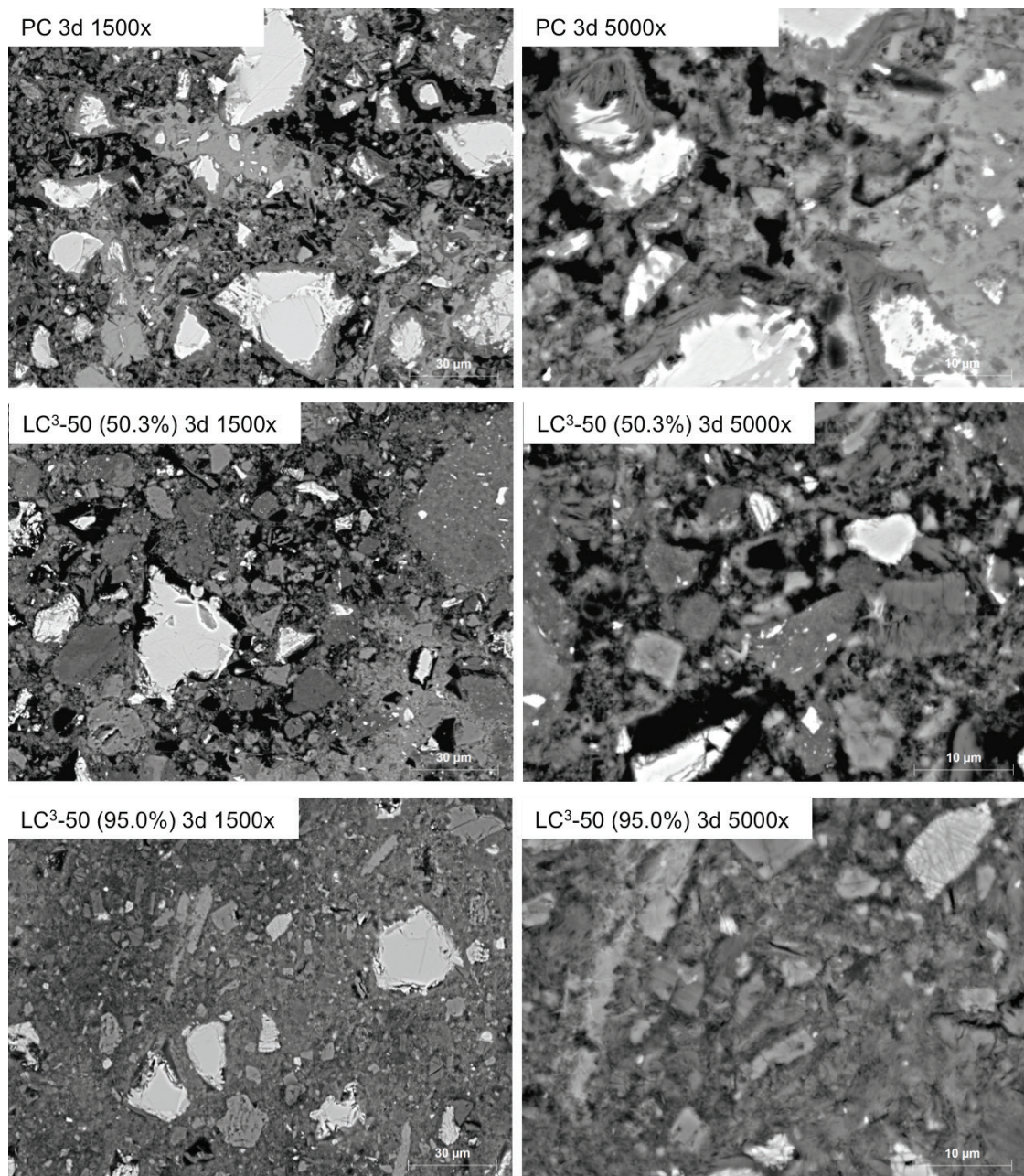


Figure 4.8. SEM pictures of PC, LC³-50 (50.3%) and (95.0%) at 3 days of hydration for 1500x and 5000x magnifications.

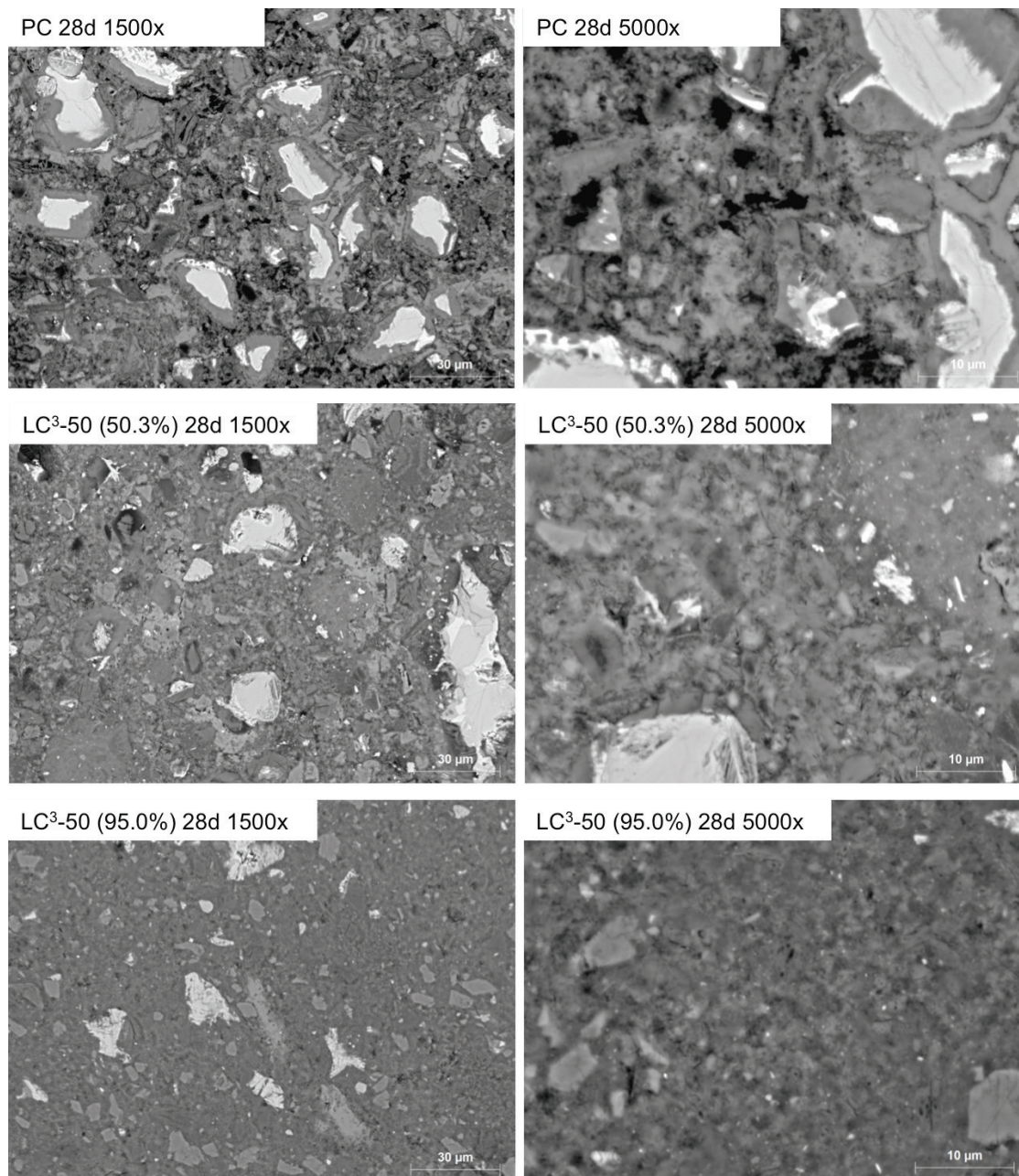


Figure 4.9. SEM pictures of PC, LC³-50 (50.3%) and (95.0%) at 28 days of hydration for 1500x and 5000x magnifications.

4.3.5.1 Hydration products

XRD patterns at 1 day and 28 days of hydration for PC and LC³-50 blends are shown in Figure 4.10 (a) and (b), respectively. At 1 day of hydration, a similar amount of ettringite is observed for the reference PC and for the blends. At 28 days, a slightly higher AFt content is observed for LC³-50 blends compared with the PC, because limestone reacts with the additional alumina and avoids dissolution of ettringite to give the monosulfate phase [37, 94]. Thus, despite the slightly higher initial

sulfate content for PC compared with LC³ blends, the ettringite content is slightly higher for LC³-50 blends than for PC at late ages.

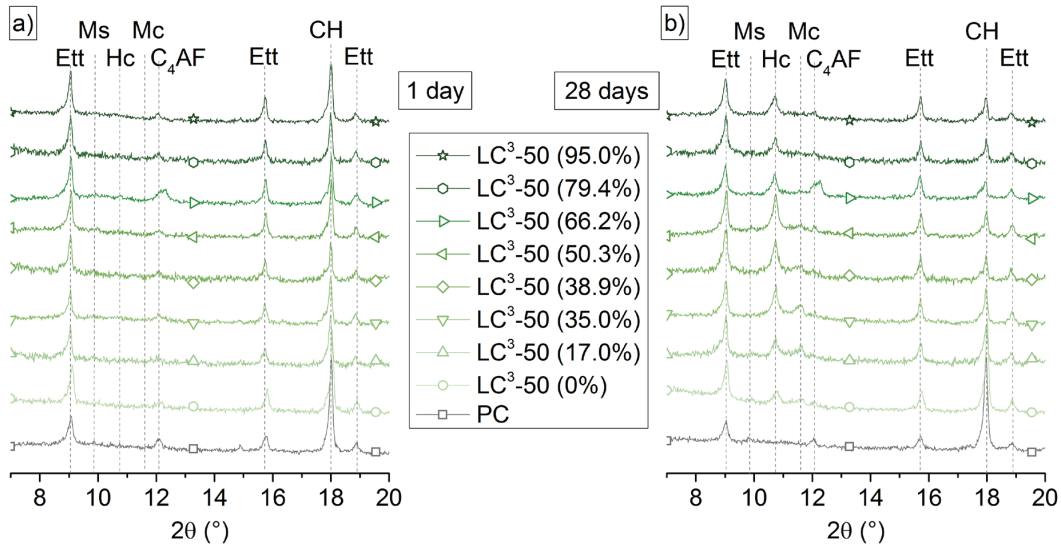


Figure 4.10. XRD patterns at 1 day (a) and 28 days (b) of hydration for reference PC and LC³-50 blends.

The quantitative analyses of ettringite are shown in Figure 4.11 at 1, 3 and 28 days of hydration. The ettringite content does not significantly vary with the calcined kaolinite content as it is related to the initial sulfate content which is constant.

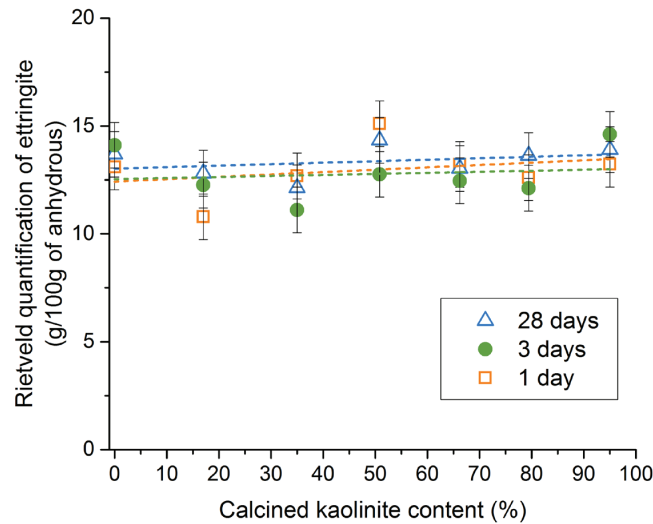


Figure 4.11. Ettringite Rietveld quantification at 1, 3 and 28 days as a function of calcined kaolinite content.

The presence of limestone contributes to the formation of hemicarboaluminate and monocarboaluminate phases, as shown at 28 days in Figure 4.12. In contrast to the study of Antoni and al. [43],

none or small traces of carboaluminate phases are observed at 1 day of hydration, because of the higher $\text{SO}_3 / \text{Al}_2\text{O}_3$ ratio in this study, due to the gypsum optimisation. The formation of carboaluminate hydrates starts after sulfate depletion, as shown in [36, 41]. At 28 days, hemicarboaluminate and monocarboaluminate coexist for LC³-50 containing $\leq 50\%$ of calcined kaolinite in the calcined clay. Even if monocarboaluminate is slightly more stable thermodynamically, the kinetics of formation are faster for hemicarboaluminate [36]. However, with the increase of calcined kaolinite content, the amount of available aluminate increases, which seems to favour the formation of hemicarboaluminate rather than monocarboaluminate [40].

The quantitative analysis of the sum of these phases is shown by volume in Figure 15 in order to look at the influence of the calcined kaolinite content on the space occupied by the carboaluminate phases. The content of these phases increase until 50% of calcined kaolinite. The enhancement of carboaluminate formation is made possible by the extra aluminate provided by the metakaolin in calcined clay. However, their content decreases for LC³-50 blends containing more than 50% of calcined kaolinite in calcined clay.

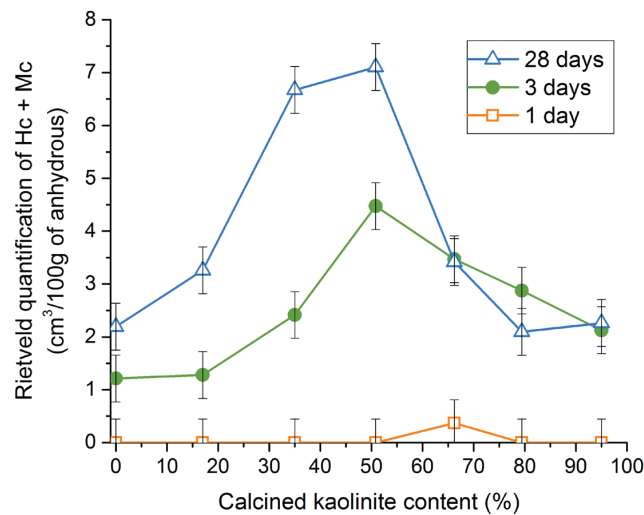


Figure 4.12. Hemicarboaluminate and monocarboaluminate vol.% Rietveld quantification at 1, 3 and 28 days of hydration as a function of calcined kaolinite content.

4.4 Discussion

4.4.1 Slowing down of clinker hydration

4.4.1.1 Relative humidity measurements

The measurements of relative humidity were carried out in order to investigate if the slowing down of clinker hydration for LC³-50 containing more than 65% of calcined kaolinite could be due a stronger decrease in relative humidity due to reaction of metakaolin. Relative humidity results are shown in Figure 4.13 for PC, and LC³-50 (50.3%) and LC³-50 (95.0%). LC³-50 (95.0%) shows that the decrease of relative humidity is in fact LESS in the systems containing metakaolin and does not

decrease much after 5 days. The relative humidity value at 28 days is 96.6%. For LC³-50 (50.3%), the relative humidity keeps decreasing until 28 days of hydration, reaching a value of 91.8% at 28 days. These results indicate that the lack of available water is not the reason for the slowing down of clinker hydration for LC³-50 systems with > 65% of calcined kaolinite.

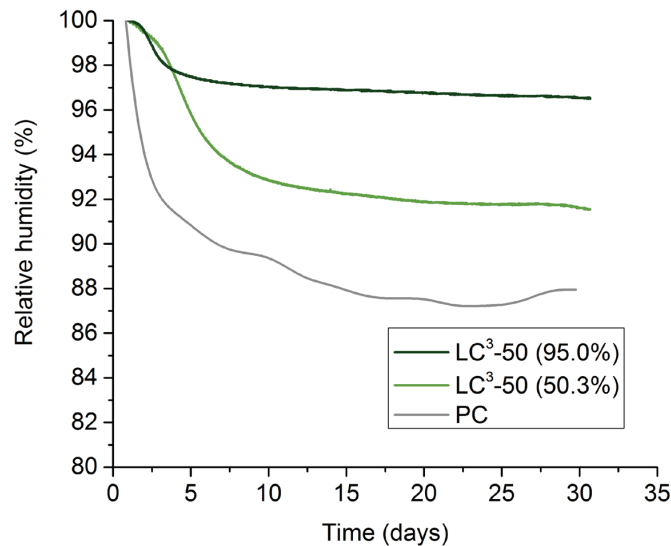


Figure 4.13. Relative humidity measurements for PC, LC³-50 (50.3%) and (95.0%).

4.4.1.2 Pore solution extraction

The concentrations of calcium, silicon and aluminium and the pH of the pore solution at 28 days are shown in Figure 4.14. Calcium concentration globally decreases with the calcined kaolinite content due to the pozzolanic reaction involving the consumption of portlandite and change in composition of the C-A-S-H. The silicon concentration remains constant for all the blends. It shows that the aluminium concentration increases with the calcined kaolinite content. Snellings showed that the presence of aluminium in the pore solution slows down the dissolution of anhydrous phases [95]. This would explain the slowing down of clinker hydration for LC³-50 containing more than 65% of calcined kaolinite. However, this does not explain why the reaction of metakaolin keeps occurring after 3 days of hydration. The values of pH slightly decrease with the calcined kaolinite content, due to the alkali incorporation in hydration products of metakaolin reaction.

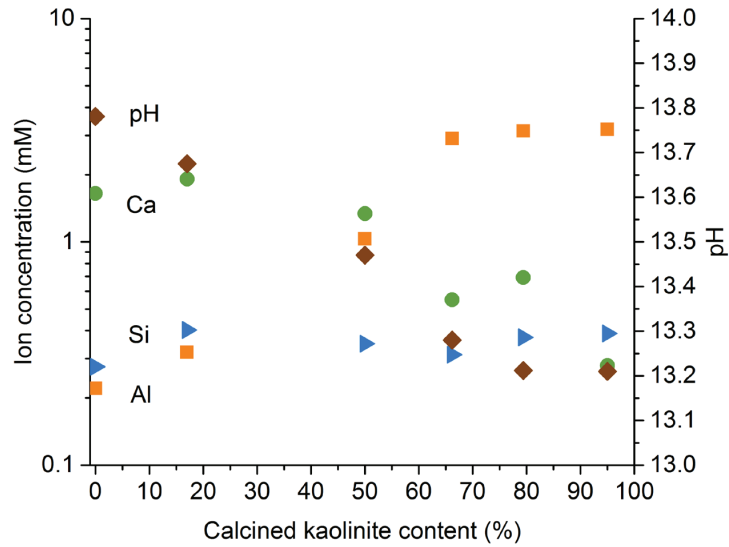


Figure 4.14. Influence of the calcined kaolinite content on the Ca, Si, Al concentration in the pore solution and the pH at 28 days of hydration.

4.4.1.3 Porosity refinement

From results in Figure 4.7, the determination of the critical pore entry radius allows better visualisation of the refinement of pore connectivity, as shown in Figure 4.15. The critical pore entry radius is defined as the inflexion point of the cumulative curve (or the maximum of the capillary peak of the derivative curve). It confirms the different kinetics of refinement between LC³-50 blends containing \leq and $>$ than 65% of calcined kaolinite in calcined clay. Moreover, at 28 days of hydration, all the LC³-50 blends containing at least 40% of calcined kaolinite show a similar critical pore entry radius of approximately 3 to 5 nm. There is no further refinement of the porosity. This limit of refinement is slightly lower than the results of Berodier [96], due to the different contact angles used between mercury and cement paste (140° versus 120° in this study).

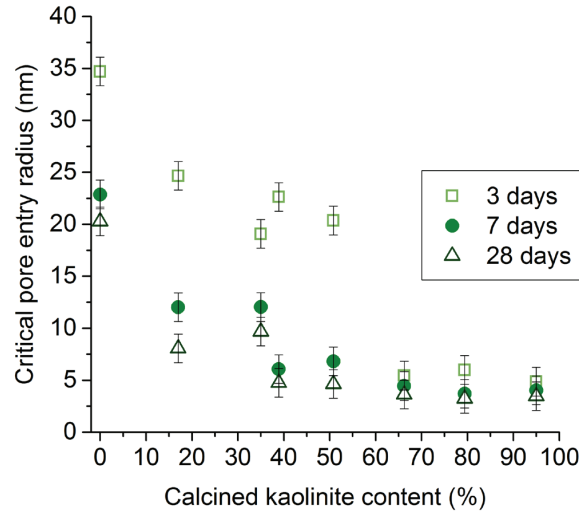


Figure 4.15. Critical pore entry radius for LC³-50 blends at 3, 7 and 28 days.

The reason for such a limiting critical pore entry radius could be the increase of supersaturation level needed for further hydrate growth to occur with the decrease of pore size, as already observed in our previous studies of cementitious materials [96, 97]. Equation 4.5 shows that as the pore size, r , goes down, the curvature at the solid/liquid interface increases, and the saturation index SI must increase as well for further hydrate growth [98, 99]. K refers the ion activity product, K_{sp} is the solubility product of the hydrate growing in the pore. R refers to the gas constant, T is the temperature, V_m is the molar volume of the hydration product growing in the pore. γ is the interfacial energy between the hydration product and the solution.

$$\frac{RT}{V_m} \ln(10^{SI}) = \frac{RT}{V_m} \ln\left(\frac{K}{K_{sp}}\right) = \frac{2\gamma}{r} \quad \text{Eq. 4.5}$$

As a consequence, the driving force for the further growth of hydration products, i.e. the supersaturation, needs to be higher to oppose the increase of the curvature at the liquid solid interface. Thus, the classical growth of hydration products can be limited due to the lack of large pores in the microstructure.

The time at which the limiting pore entry radius is reached seems to correspond well with the slowing down of hydration observed in Figure 2 and 3, especially for the LC³-50 (95.0%) blend.

4.4.2 Hydration product formation

Even if clinker hydration in Figure 4.3 is significantly slowed down from 3 days onwards for the LC³-50 blends containing calcined clay with more than 65% of calcined kaolinite, the reaction of metakaolin continues after 3 days as observed in Figure 4.6. The formation of carboaluminate hydrates is limited from 3 days onwards for these blends, as shown in Figure 4.12.

Based on the pore solution concentration shown in Figure 4.14, the saturation index of monocarboaluminate phase (more thermodynamically-stable than hemicarboaluminate phase) was calculated using the Gibbs Free Energy Minimization Software (GEMS) [77], with the Cemdata14 database [78]. For the LC³-50 (95.0%) at 28 days of hydration, a saturation index of 0.65 is obtained, indicating that the pore solution is oversaturated with respect to monocarboaluminate phase. Thus, according to the pore solution, monocarboaluminate growth could keep occurring in this system.

The limited amount of carboaluminate is likely to be due to the lack of pores large enough for their growth. The level of supersaturation is not high enough to enable the growth in such fine pores. Thus, the reaction of metakaolin no longer forms AFm phases for these systems once the limiting critical pore entry radius is reached.

Figure 4.16 shows the correlation between the amount of carboaluminate hydrates formed, the aluminium concentration of the pore solution and the aluminium incorporation in the C-A-S-H. For LC³-50 blends containing more than 65% of calcined kaolinite, the aluminium concentration in the pore solution as well as the aluminium incorporation in the C-A-S-H significantly increases compared with blends with lower calcined kaolinite content. The on-going reaction of metakaolin provides more aluminium to the system, which is not used for the formation of the carboaluminate hydrates due to the lack of large pores. As a consequence, the on-going metakaolin reaction leads to the increase of the aluminium concentration of the pore solution. Since there is more aluminium in the pore solution, the incorporation of aluminium in the C-A-S-H also significantly increases [100, 101].

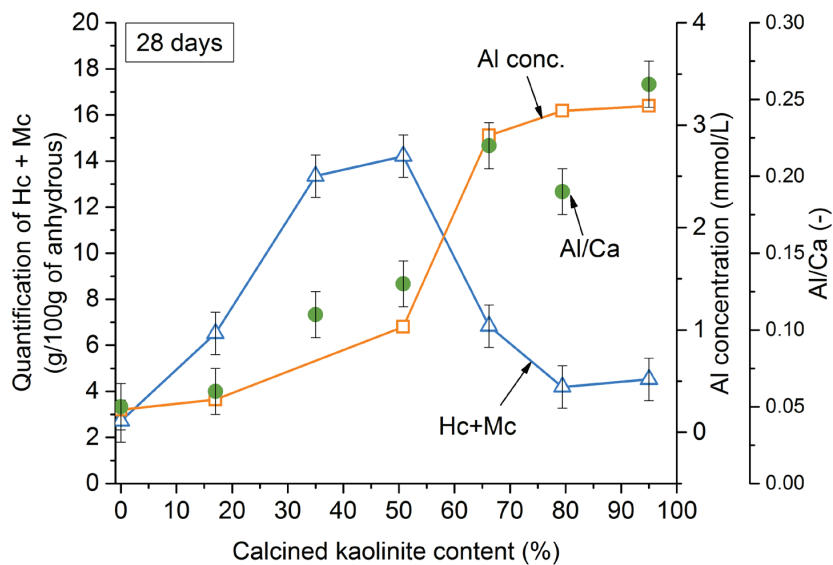


Figure 4.16. Amount of carboaluminate hydrates, aluminium concentration of the pore solution and Al/Ca of the C-A-S-H for the different LC³-50 systems at 28 days of hydration.

Since the reaction of metakaolin mainly impacts the C-A-S-H phase for the blends containing calcined clay with more than 65% of calcined kaolinite, it is likely that the gel pores (intrinsic pores of

C-A-S-H of nanometer size) would mainly be affected by this reaction. This could explain why the pore size distribution by MIP is very similar for these blends at 3 and 28 days of hydration, since gel pores are mostly not reached by MIP technique [80].

4.4.3 Correlation with compressive strength results

Compressive strength tests in Chapter 2 showed that up to 7 days of hydration, strength is linearly correlated with the calcined kaolinite content. This parameter overwhelms the strength development. After 7 days, the strength gain for LC³-50 blends with calcined clay containing more than about 45% of calcined kaolinite becomes less significant.

This lower gain of strength at late ages for the LC³-50 blends with more than 45% can be explained by:

- the decrease of the clinker hydration degree with the increase of the calcined kaolinite content (cf. Figure 4.3) due to the reaching of the maximal refinement of the critical pore entry in Figure 4.15
- the quite similar amount of reacted metakaolin for calcined clays with more than 50% of calcined kaolinite as shown in Figure 4.6
- the limited formation of carboaluminate hydrates observed in Figure 4.12

4.5 Conclusion

Metakaolin reaction starts before 1 day, independent of the calcined kaolinite content of calcined clay. At later ages, the degree of reaction of the clinker is influenced by the calcined kaolinite content. For LC³-50 blends containing > 65% of calcined kaolinite in calcined clay, clinker hydration is significantly slowed down from 3 days onwards. The reason for such slowing down is likely to be due to the lack of capillary pores above a critical size. A critical pore entry size of 3-5 nm is reached at 3 days for these blends and the growth of hydrates becomes more difficult after this point due to the supersaturation level required. The highest relative humidity is measured for the LC³-50 blend with the highest calcined kaolinite content. Thus, the slowing down of clinker hydration cannot be explained by a lack of water.

The amount of reacted metakaolin increases with the calcined kaolinite content and that metakaolin keeps reacting after 3 days for all LC³-50 blends. For LC³-50 blends containing calcined clay with less than 65% of calcined kaolinite, the amount of carboaluminate hydrates increases with the calcined kaolinite content thanks to the alumina provided by metakaolin. For blends with more than 65% of calcined kaolinite, the formation of carboaluminate hydrates is likely to be limited by the lack of pores above a critical size. As a consequence, the aluminium provided by the on-going metakaolin reaction goes into the C-A-S-H, as evidenced by the increase of the aluminium concentration of the pore solution, which leads to a higher incorporation of aluminium in the C-A-S-H measured by SEM-EDX.

Ettringite formation does not depend on the calcined kaolinite content. Similar amount is quantified for all LC³-50 blends, showing that ettringite content depends more on the initial sulfate content

(also constant). After sulfate depletion, aluminates react with carbonates to form carboaluminate hydrates.

Chapter 5 - Investigation of C-A-S-H composition, morphology and density in Limestone Calcined Clay Cement (LC³)

5.1 Introduction

C-S-H is the main hydrated phase present in cementitious materials. The solid structure of C-S-H, based on tobermorite, is shown in Figure 5.1 [101]. It is composed of calcium oxide layers in contact on both sides with silica chains. The silica chains show a dreierketten arrangement with two silica tetrahedra pairing the calcium oxide layers and a third bridging to the next pair of silicates. The space between the layers of calcium oxide and silicate chains is the interlayer space which is mainly composed of water and calcium ions. C-S-H has a variable stoichiometric depending of the pore solution concentration, which is in turn affected by factors such as the water to binder ratio [102], clinker composition [83] and mix composition [35, 69, 74, 103-105]. C-S-Hs found in cementitious materials have higher calcium to silicon ratios than tobermorite in the range of about 1.3-2. Three kinds of defect allow for the variation in calcium to silica ratio: missing bridging silicate tetrahedra; substitution of two protons terminating unlinked silicate tetrahedra by calcium ions; and calcium ions in the interlayer. Other ions than silicon and calcium can be found in C-S-H. The most commonly found one is aluminium which can be incorporated in a bridging site of the C-S-H structure [101, 106-108]. Aluminium mostly occupies bridging sites linking dimers of silicate tetrahedra, which may lead to an increase of the average chain length of C-S-H [109]. The term C-A-S-H is often used rather than C-S-H to take into account the aluminium incorporation. Higher aluminium contents in C-A-S-H are usually observed with alumino-silicate SCMs: slags, fly ashes and especially calcined clays [43, 74, 83, 103].

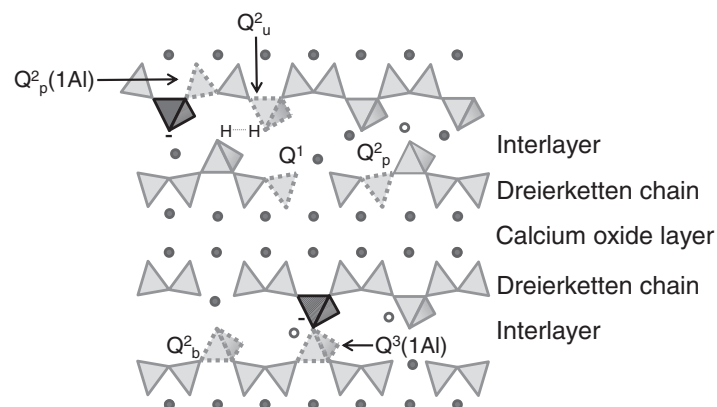


Figure 5.1. Schematic structure of C-A-S-H [101]. Full and empty circles correspond to calcium ion and water/alkali, respectively. Dark grey tetrahedra: AlO₄. Light grey tetrahedral: SiO₄⁻. Qⁿ: n indicates the number of Si neighbours. Q²_b and Q²_p refer to bridging and pairing positions.

The measurements of the C-A-S-H composition by SEM-EDX is challenging for blends containing fine particles such as metakaolin or silica fume due to the volume of interaction which can include C-A-S-H and also other phases. Transmission Electron Microscopy in scanning mode (STEM) provides a complementary tool to estimate the C-A-S-H composition, with the main benefit of determining it without any interaction with other phase [84]. TEM also permits a better understanding of the C-A-S-H formation by providing information on its morphology. Richardson [110] observed either fibrillar-like or foil-like morphologies for outer C-A-S-H, with a foil-like morphology only observed for a Ca/Si atomic ratio close to 1.5. A more compact uniform morphology was observed for inner products.

New insights on C-A-S-H are provided by the use of ^1H Nuclear Magnetic Resonance ($^1\text{H-NMR}$) relaxometry. This method allows measurement of the water in the interlayer and gel pores of the C-A-S-H, as shown by Müller et al. [80, 111]. This technique is non-destructive and does not require any drying prior to analysis. Continuous measurements can be carried out to track the evolution of the different water populations with time. Müller used these data for a mass and volume balance to determine the density of both solid (excluding gel water) and bulk (including gel water) C-A-S-H [80].

In this study, the C-A-S-H for Limestone Calcined Clay Cements (LC^3) is characterized. We previously showed that for LC^3 -50 systems with a clinker content reduced to 50 %, similar strength to reference PC is obtained from 7 days onwards even using clays with a calcined kaolinite content as low as 40% [90]. A better understanding of the strength results requires a better characterization of the C-A-S-H for these blends. Thus, the composition, the morphology and the density of C-A-S-H have been studied for LC^3 -50 blends using a wide range of calcined kaolinitic clays and the results are compared with plain PC. The chemical composition of the C-A-S-H was determined using both SEM-EDX and STEM-EDX techniques. STEM was also used to investigate the influence of the calcined kaolinite content on the morphology of C-A-S-H. The density of C-A-S-H was obtained based on $^1\text{H-NMR}$ results. Moreover, thanks to the valuable information provided by $^1\text{H-NMR}$, especially concerning the amount of gel and capillary water, a precise characterization of the porosity of cementitious materials can be obtained [112]. Müller et al. found an average pore size of 2.5 nm and 8.0 nm for gel and capillary pores, respectively [80]. The porosity of LC^3 -50 was investigated and the results compared with reference cement to give a better understanding of the results obtained with the widely-used Mercury Intrusion Porosimetry (MIP) technique.

5.2 Materials characteristics and mix design

The same CEMI 42.5R grey cement from Heidelberg cement was used for the study of the morphology and the composition of the C-A-S-H. In addition to reference PC, LC^3 -50 systems were studied, in which 45 parts of cement are substituted by 30 parts of calcined clays and 15 parts of limestone. 2% of gypsum was added to prevent undersulfation for LC^3 -50 blends, as detailed in Appendix 1.

Due to the complexity of preparing the samples for TEM, only three calcined clays were used as LC³-50 blends, in addition to plain PC, with 17.0%, 50.3% and 95.0% of calcined kaolinite. The final mix design is shown in Table 5.1.

Table 5.1. Mix composition of PC and LC³-50 blends.

The brackets indicate the calcined kaolinite content of the calcined clay for LC³-50 blends.

Composition (wt.%)	Cement		Calcined clay	Limestone	Gypsum addition
	Clinker	Anhydrite			
PC	94.1	5.9	-	-	-
LC ³ -50 (17.0%)	50.6	3.3	29.4 (17.0%)	14.7	2.0
LC ³ -50 (50.3%)	50.6	3.3	29.4 (50.3%)	14.7	2.0
LC ³ -50 (95.0%)	50.6	3.3	29.4 (95.0%)	14.7	2.0

For the study on the determination of the C-A-S-H density, the use of this grey cement was not compatible with ¹H-NMR measurements. The iron content (3.6% Fe₂O₃) is too-high decreasing the magnetization and degrading the accuracy of the results [72]. Thus, a white cement from Aalborg Cement was used for all ¹H-NMR experiments. Plain white cement (WPC) and LC³ blends (WLC³-50) were cast.

The alkali level of the white cement was adjusted in order to get similar Na₂O_{eq} to the grey cement used in the previous studies. Potassium hydroxide (Acros) was used for the alkali adjustment. The sulfate level was then also adjusted based on heat flow curves by isothermal calorimetry. 2% of gypsum was added for WPC and 3% for WLC³-50 blends (shown in Appendix 1).

Since most of kaolinitic clays contain significant amount of iron oxide, some simulated mixes of fairly pure kaolinitic clay with quartz were used. In addition to WLC³-50 with 95.0% of calcined kaolinite, two mixes were prepared by replacing 50% and 75% of calcined clay by quartz to model calcined clays with 23.8% and 47.5% of calcined kaolinite, respectively. A fourth blend consisted of using a clay with a low iron oxide content (1.0%) and 39.0% of calcined kaolinite. The final mix design used for the determination of the density of C-A-S-H is shown in Table 5.2.

Table 5.2. Mix composition of WPC and WLC³-50 blends.

The brackets indicate the calcined kaolinite content of the calcined clay for each WLC³-50 mix.

wt.%	Cement		Calcined clay	Quartz	Limestone	Alkali addition	Gypsum addition
	Clinker	Gypsum					
WPC	92.7	4.2	-	-	-	1.2	2.0
WLC ³ -50 (95.0%)	50.7	2.3	28.9 (95.0%)	-	14.5	0.6	3.0
WLC ³ -50 (47.5%)	50.7	2.3	14.5 (95.0%)	14.5	14.5	0.6	3.0
WLC ³ -50 (39.0%)	50.7	2.3	28.9 (39.0%)	-	14.5	0.6	3.0
WLC ³ -50 (23.8%)	50.7	2.3	7.2 (95.0%)	21.7	14.5	0.6	3.0

The XRF and the physical characteristics of the grey and white cements, the limestone, and the different calcined clays are shown in Table 5.3.

Table 5.3. XRF composition of white cement, calcined clays and limestone.

Clay number	Calcined Clays				Quartz	Grey cement	White Cement	Limestone
	43	18	1	26				
Calcined kaolinite content (%)	17.0	50.3	95.0	39.0	0	-	-	-
$D_{v,50}$ (μm)	5.9	10.9	5.1	10.8	11.2	8.4	7.4	7.2
BET Specific surface (m^2/g)	18.7	45.7	9.6	10.7	1.2	0.9	1.3	1.8
XRF composition (wt.%)								
SiO ₂	68.4	44.9	52.0	71.0	99.8	19.3	24.2	0.1
Al ₂ O ₃	17.5	32.3	43.8	23.4	-	5.7	1.9	-
Fe ₂ O ₃	8.9	15.4	0.3	1.0	-	3.6	0.3	-
CaO	0.6	1.3	-	0.3	-	63.6	69.2	55.0
MgO	0.7	0.8	-	0.4	-	1.6	0.7	0.2
SO ₃	-	0.1	0.1	-	-	3.2	2.0	-
Na ₂ O	0.1	0.4	0.3	0.2	-	0.2	0.2	0.1
K ₂ O	2.3	0.2	0.1	1.4	0.1	1.2	0.1	-
TiO ₂	0.8	2.4	1.5	1.2	-	0.3	0.1	-
P ₂ O ₅	0.1	0.4	0.2	0.2	-	0.2	0.3	-
MnO	0.1	0.1	-	-	-	0.1	-	-
Others	0.2	0.2	0.1	-	-	0.3	0.3	-
LOI	0.5	1.7	1.5	0.9	0.1	0.8	0.9	42.6

5.3 Analytical details

5.3.1 C-A-S-H morphology and composition

The PC and the LC³-50 (17.0%), (50.3%) and (95.0%) were tested at 28 days of hydration. Similar protocol as detailed in [83] was used for the sample preparation. The paste was mixed for 2 minutes at 1600 rpm. Slices were cut at 28 days of hydration. Hydration was stopped using solvent exchange method (isopropanol). This method is the best for preserving the microstructure [113, 114]. The slices were then stored in desiccator under vacuum. For TEM samples, a small piece of paste was then impregnated in a hard resin (Gatan G2) and the impregnated sample was cut as a 2x2x0.7-mm³-slice using diamond saw. This slice is then polished using diamond-lapping films (Allied) until optical translucency. Due to the brittleness of hydrated cementitious paste, it is not possible to get a uniform thin lamella. Thin areas could be obtained only using the Tripod method at the edge of a bevel. The last step of polishing is done by ion milling (Gatan 691) using Precision Ion Polishing System (PIPS) until reaching electron transparency (thickness of about 100-150 nm). Low voltages of 1-2 kV were used in order to avoid ion beam damage. The detection of fringes of equal thickness by optical microscopy is a good clue to ensure the presence of areas transparent to electrons.

For the SEM sample preparation, a quarter of a slice was impregnated in epoxy resin (Epotek-301) and the impregnated sample was then polished with diamond particles of 9 μm , 3 μm and 1 μm for 30 min, 2 h and 3 h, respectively.

For the TEM observations, a FEI Tecnai Osiris was used (CIME, EPFL) with a XFEG source. Two Super-X Windowless SDD EDS detectors were used. Both the bright field (BF) and the high angle annular dark field (HAADF) detectors were used in scanning mode (STEM). An acceleration voltage as low as 80 kV (combined with low spot size) was used in order to avoid beam damage. A magnification of 56000x for imaging was used. Once the images were taken, several zones of interest were delimited and analysed to get their global EDX spectrum. Between 5 and 15 areas were analysed to get the C-A-S-H composition.

The C-A-S-H composition obtained by STEM-EDX was compared with results obtained by SEM-EDX. The determination of the C-A-S-H composition was done according to the method of Rossen [83]. An FEI Quanta 200 SEM was used with an accelerating voltage of 15 kV, with a working distance of 12.5 mm, and a spot size adjusted to get a current of approximately 0.8 nA. The determination of C-A-S-H composition was obtained from 200 points per sample. In order to get a more accurate composition of C-A-S-H, inner product areas were sampled to minimise intermixing with other phases present in the microstructure.

5.3.2 C-A-S-H density

Immediately after mixing for 2 minutes at 1600 rpm, about 0.5 g of fresh paste was injected in the tube for NMR experiments. The tube was then sealed with parafilm and directly inserted in the NMR device to be continuously tested. A Bruker Minispec NMR spectrometer was used for all experiments. The temperature of the device was kept constant at 20 °C. Both Carr-Purcell-Meiboom-Gill (CPMG) and Quadrature-Echo (QE) pulse sequences were carried out in order to cover the whole range of T_2 relaxation times. The CPMG and QE pulse sequences were alternatively used in a 3 hour / 1 hour arrangement. For QE sequences, the pulse gap τ varies from 15 μs to 45 μs . The signal was decomposed in the Gaussian solid part and the exponential liquid part. The solid intensity was then extrapolated to zero pulse using a Gaussian fit. Concerning the liquid part, the CPMG sequence was composed of 256 echoes recorded from 50 μs to 12 ms in a logarithmic spacing to cover five ranges of relaxation times. From the echo decays, the Inverse Laplace Transform (ILT) was applied to extract the relaxation times. The regularization factor which sets the sensitivity of the ILT is set to 1.5×10^{-6} .

The methodology for the determination of the C-A-S-H density by ^1H -NMR is detailed in Appendix 5. Mass and volume balance are applied, and in addition to ^1H -NMR outputs, other data are required, such as the clinker, limestone and metakaolin reaction degree, as well as the chemical shrinkage data.

For the XRD data collection needed for the mass and volume balance, the tests were carried out on fresh slices at 1, 3, 7, 28 and 90 days of hydration. XRD patterns were acquired with Bragg-Brentano mode with a X'Pert PANalytical diffractometer with $\text{CuK}\alpha$ radiation operated at 45 kV

and 40 mA. Samples were scanned from 5 to 70 °2θ with a step size of 0.0167 °2θ using a X'Celerator detector. The equivalent time per step was 30 s, resulting in a total measurement time of 15 min per scan. Rutile was used as external standard.

The chemical shrinkage was measured by continuously monitoring the position of an oil drop in a capillary on top of a sealed container of 7 g of cement paste (6-mm height) covered by water. The experiments were carried out in a bath at a constant temperature of 20 °C. The experiments were repeated 3 times for each sample. A blank sample filled with quartz and water was used to isolate the shrinkage of the cementitious blends only. The signal of the quartz system was subtracted to the signal of the systems.

5.3.3 Porosity

For MIP measurements, dried samples were tested. All experiments were carried out using Porotec 140 and 440 devices. 0.7 g (2 pieces) of paste was used for each experiment. A contact angle of 120° was used since a better agreement was found with the pore size obtained by ¹H-NMR using this value [93].

5.4 Results

5.4.1 Comparison of hydration between grey and white cement

The hydration study was carried out on white cement to show that similar hydration process takes place compared to grey cement. Figure 5.2 shows the microstructure observed by SEM of PC and LC³-50 (95.0%) blend using grey cement and WPC and WLC³-50 (95.0%) with white cement at 3 days of hydration. No significant differences are observed, except the absence of iron-bearing phase in the microstructure of white cement systems. A much denser microstructure is observed for the blends compared with plain cement.

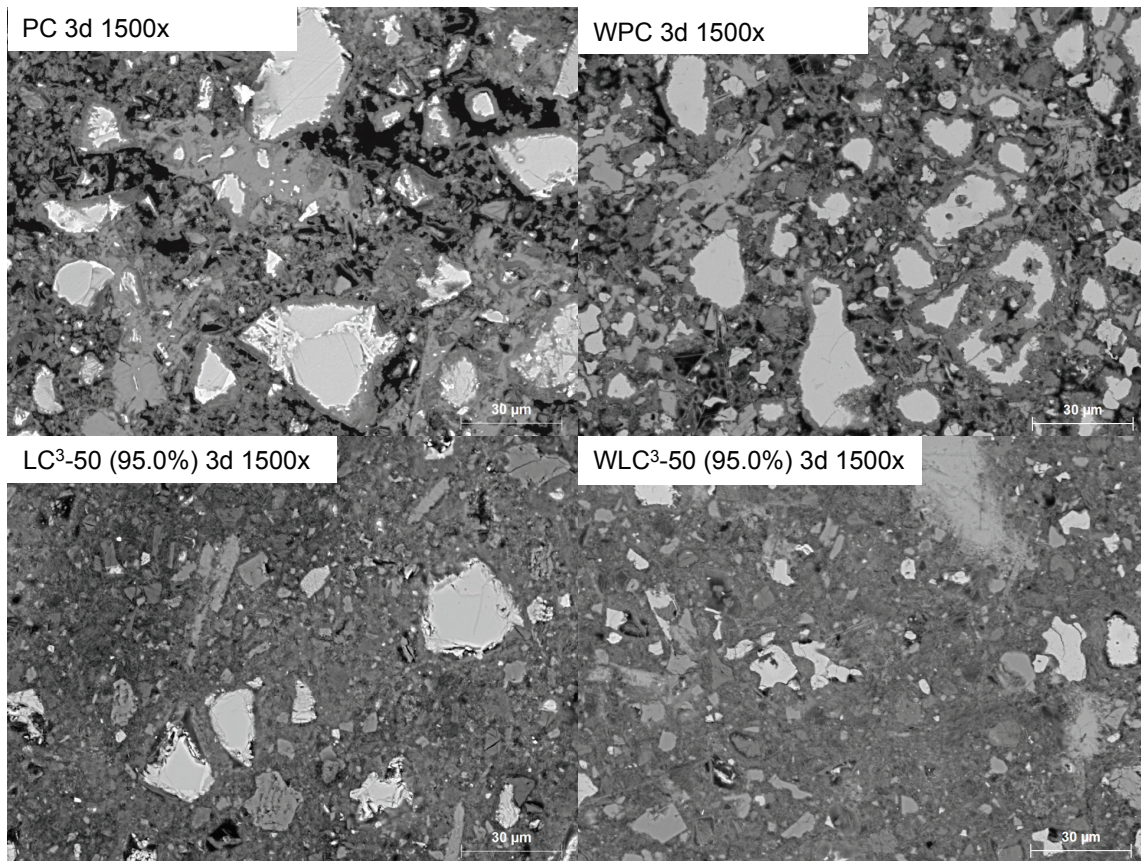


Figure 5.2. Microstructure of PC and LC³-50 (95.0%) blend using grey cement and WPC and WLC³-50 (95.0%) with white cement at 3 days of hydration.

As example of the similarities of hydration observed between white and grey cement, the degree of hydration of clinker is shown in Figure 5.3. The WPC system has a slightly higher DoH at late ages, which can be due to the absence of the low-reactive ferrite phase in the clinker. Moreover, the slowing down of clinker hydration from 3 days onwards observed for the LC³-50 (95.0%) is also measured using white cement in the WLC³-50 (95.0%) blend. Portlandite content is also shown in Figure 5.3. The portlandite consumption for the pozzolanic reaction is slightly delayed for the WLC³-50 (95.0%).

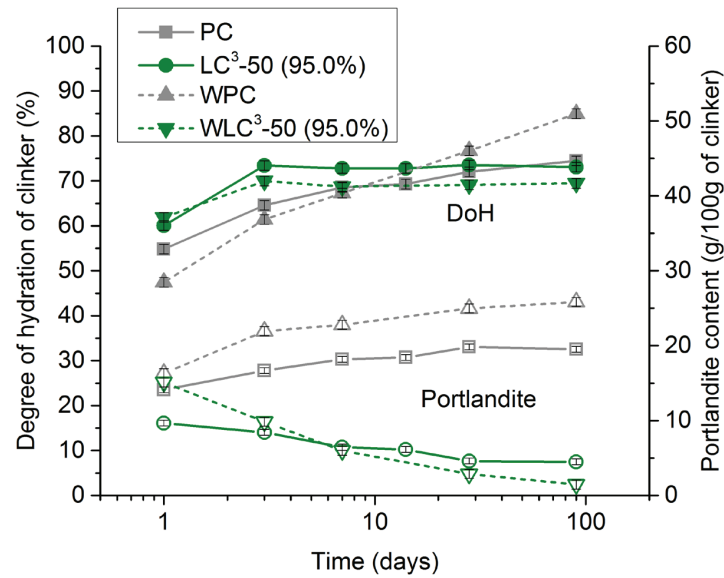


Figure 5.3. Clinker hydration degree and portlandite content for PC and LC³-50 (95.0%) blend using grey cement and WPC and WLC³-50 (95.0%) with white cement.

5.4.2 C-A-S-H composition

Figure 5.4 shows the comparison of SEM-EDX and STEM-EDX results for the PC and the LC³-50 systems. The Al/Ca and Si/Ca atomic ratios are plotted to better identify the C-A-S-H composition and to exclude the phases intermixed with C-A-S-H. A global good agreement is found between the two techniques, considering the error of measurements. The deviations observed for STEM-EDX can be explained by the absence of a standard database for the measurements, as well as the inhomogeneities of the sample thickness. For SEM-EDX, the intermixing with other phases is the main reason for the error in the determination of the C-A-S-H composition, especially for the LC³-50 (95.0%) system.

Table 5.4 summarizes the Al/Ca and Si/Ca atomic ratios obtained for the different systems using both SEM-EDX and STEM-EDX techniques. Similar aluminium incorporation is observed for the reference PC and the LC³-50 (17.0%). The aluminium incorporation in C-A-S-H significantly increases with the calcined kaolinite content of the calcined clay. This increase of aluminium incorporation is due to the increase of the aluminium concentration of the pore solution with the increase of the calcined kaolinite content, as described in Chapter 4. The Si/Ca ratio is higher for the LC³-50 blends than for PC. This can be explained by the pozzolanic reaction of the metakaolin in the calcined clay, providing aluminium and silicon to the system. This leads to the consumption of portlandite and a decrease of the calcium concentration in the pore solution [28]. It seems that the Si/Ca ratio also increases with the calcined kaolinite content for STEM-EDX results. However, this is not really observed by SEM-EDX.

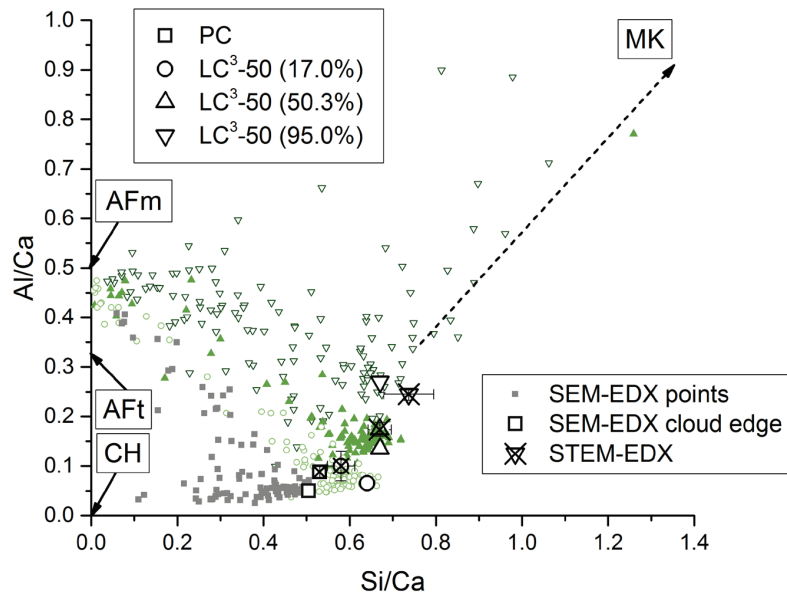


Figure 5.4. C-A-S-H composition for PC and LC³-50 (17.0%), (50.3%) and (95.0%) at 28 days of hydration obtained by SEM-EDX and STEM-EDX.

Table 5.4. Al/Ca and Si/Ca atomic ratios of C-A-S-H obtained by SEM-EDX and STEM-EDX.

	SEM-EDX		STEM-EDX	
	Al/Ca	Si/Ca	Al/Ca	Si/Ca
PC	0.06 ± 0.01	0.51 ± 0.02	0.08 ± 0.01	0.53 ± 0.03
LC ³ -50 (17.0%)	0.07 ± 0.02	0.62 ± 0.02	0.08 ± 0.03	0.57 ± 0.03
LC ³ -50 (50.3%)	0.13 ± 0.02	0.67 ± 0.02	0.16 ± 0.01	0.65 ± 0.03
LC ³ -50 (95.0%)	0.26 ± 0.03	0.67 ± 0.04	0.24 ± 0.01	0.73 ± 0.06

As comparison, the C-A-S-H composition of the white cement systems is given in Table 5.5. Similar results are obtained between PC and WPC systems, and between LC³-50 and WLC³-50 blends, for a similar calcined kaolinite content.

Table 5.5. Al/Ca and Si/Ca atomic ratios of C-A-S-H by SEM-EDX for WPC and WLC³-50 blends at 28 days of hydration.

SEM-EDX		
	Al/Ca	Si/Ca
WPC	0.05 ± 0.01	0.54 ± 0.02
WLC ³ -50 (23.8%)	0.12 ± 0.01	0.62 ± 0.01
WLC ³ -50 (39.0%)	0.17 ± 0.02	0.62 ± 0.02
WLC ³ -50 (47.5%)	0.19 ± 0.04	0.64 ± 0.05
WLC ³ -50 (95.0%)	0.28 ± 0.02	0.64 ± 0.03

5.4.3 C-A-S-H morphology

The microstructure of PC and the LC³-50 (17.0%), (50.3%) and (95.0%) blends is shown in Bright Field (BF) mode and in High Angle Annular Dark Field (HAADF) mode in Figure 5.5 (PC and LC³-50 (17.0%)) and in Figure 5.6 (LC³-50 (50.3%) and LC³-50 (95.0%)). In all systems, a fibrillar C-A-S-H morphology is observed. Thus, neither the reaction of the calcined clay nor the calcined kaolinite content of the calcined clay influence the morphology of C-A-S-H. In addition to C-A-S-H, ettringite (AFt) is also observed in the LC³-50 (17.0%), as well as unreacted metakaolin in LC³-50 (95.0%).

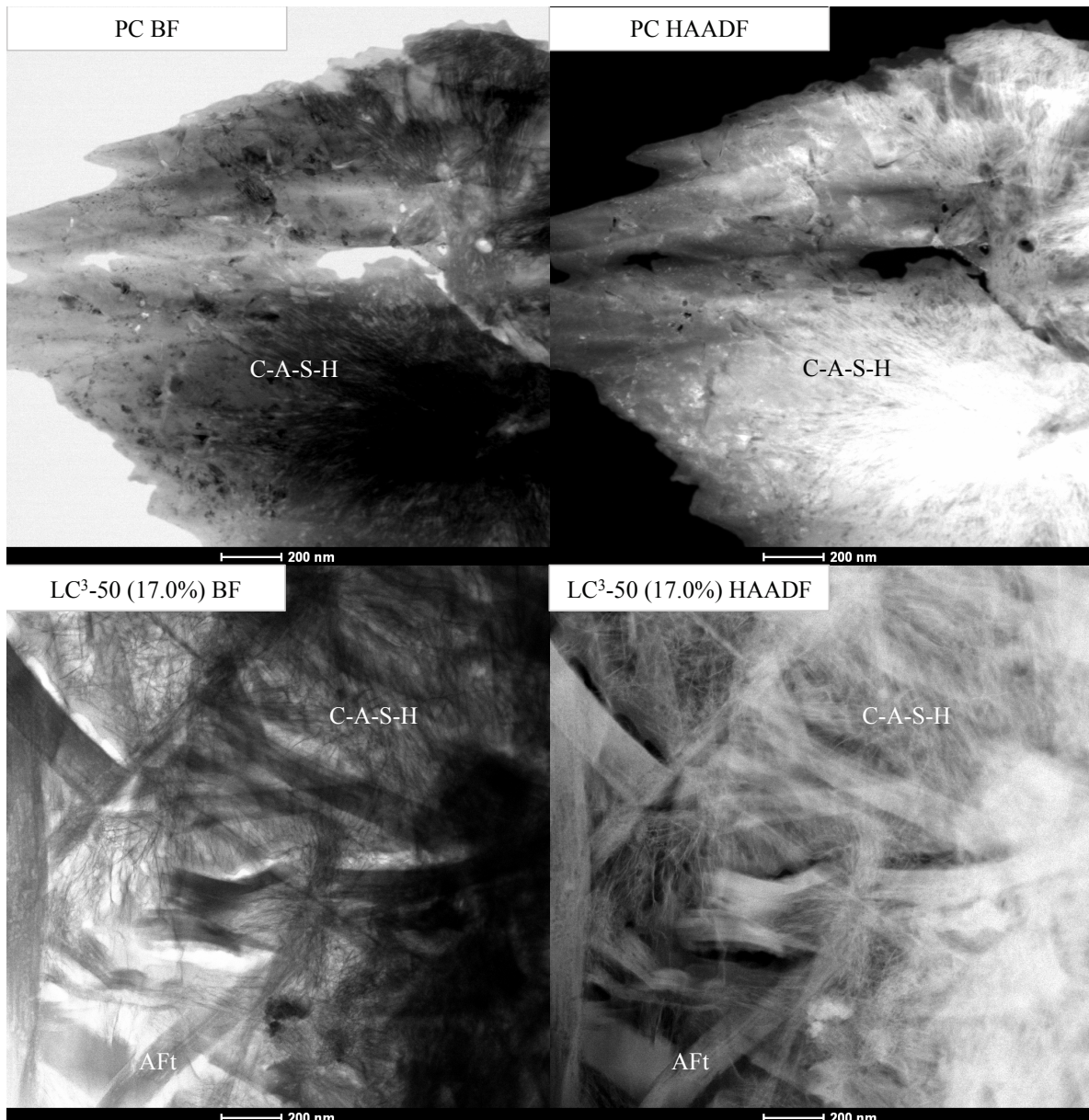


Figure 5.5. Microstructure of PC and LC³-50 (17.0%) at 28 days of hydration in Bright Field (BF) and High Angle Annular Dark Field (HAADF) modes. AFt refers to ettringite.

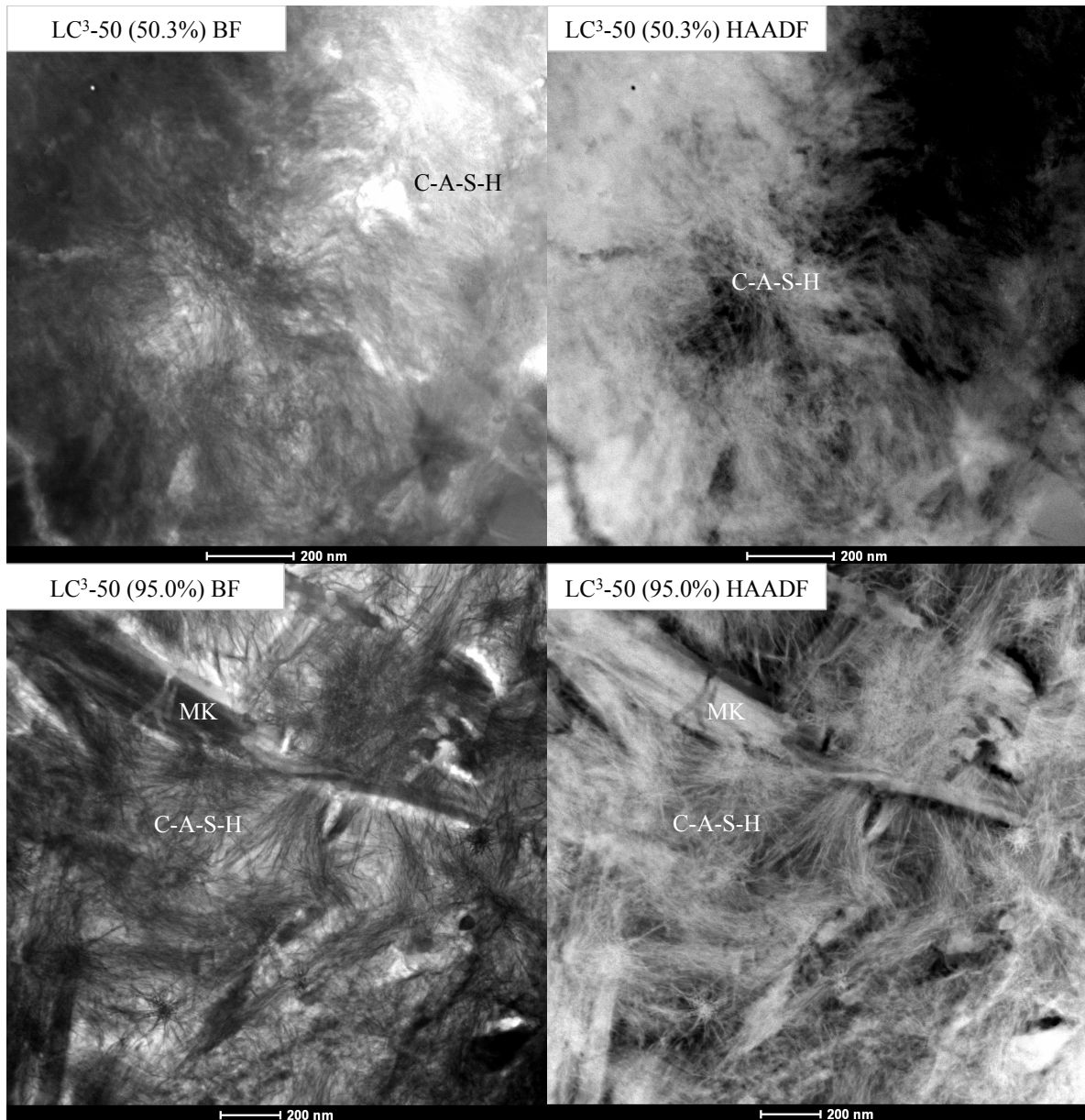


Figure 5.6. Microstructure of LC³-50 (50.3%) and (95.0%) at 28 days of hydration in Bright Field (BF) and High Angle Annular Dark Field (HAADF) modes.

MK refers to unreacted metakaolin particle.

5.4.4 Density of C-A-S-H

5.4.4.1 Adsorption of water on metakaolin particles

A preliminary test was carried out to investigate the influence of the water adsorption on metakaolin particles. A mix of calcined clay with 95.0% of calcined kaolinite and water with the same water to calcined clay ratio as for the WLC³-50 blend was studied. Figure 5.7 shows the CPMG signal for this sample. It shows that 97.5 % of water is present as free water in pores as large as capillary

pores detected 30 minutes after casting for WPC and WLC³-50 blends. Only a minor part of the signal is detected in pores showing similar relaxation time as spins in gel and interlayer water of C-A-S-H, with respectively 0.7 % and 1.8 % of the signal. No solid signal was detected using QE pulse sequence. In Figure 5.7 is also shown the signal of the clay stored at 100 % relative humidity, until reaching stable mass of the wet powder. A very small amount of water is adsorbed by the metakaolin particles. A mass increase of 2.8 % was measured, with 76.1 % of this mass increase with similar relaxation time to interlayer water. 12.5 % and 11.3 % are described similar to gel water and capillary water of C-A-S-H, respectively. Thus, the influence of the water adsorption on metakaolin particles plays a negligible role in the ¹H-NMR outputs.

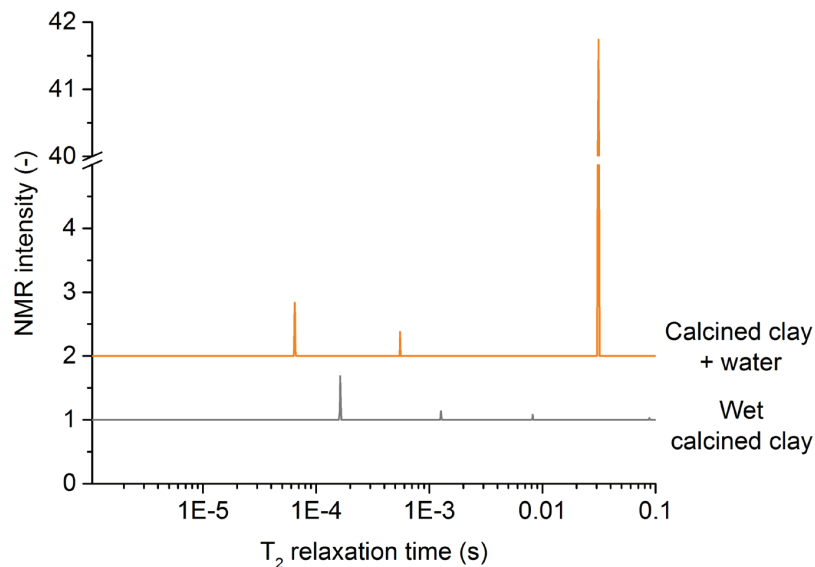


Figure 5.7. T_2 distribution for calcined clay – water mix and calcined clay stored at 100 % of relative humidity.

5.4.4.2 Assignment of ¹H-NMR signals

The evolution of the relaxation times with hydration is shown in Figure 5.8 (a) for WPC from 30 minutes after casting to 160 days. Rectangles indicate the range of relaxation time for the different water populations corresponding to the water present in the capillaries / interhydrate space, in the gel pores, in the interlayer of the C-A-S-H or bound to crystalline phases. The small differences of relaxation times for instance for C-A-S-H interlayer water are due to the error of measurements of the device. The amount of capillary water progressively decreases with time due to its consumption during hydration. The trend towards smaller relaxation time indicates the refinement of the size of the capillary pores. The C-A-S-H formation is observed through the evolution of gel water and interlayer water. Finally, the formation of crystalline phases keeps increasing with time.

Based on the quantification of the different water populations in Figure 8 (a), their evolution is shown in Figure 5.8 (b). The amount of capillary water rapidly decreases to reach 45% of the total water signal at 1 day and 20% at 7 days. This amount keeps decreasing with time to be close to 3%

at 160 days of hydration. The amount of interlayer and gel water keeps increasing with time. The amount of water bound to crystalline phases also continuously increases with time.

As comparison, the results obtained by Müller are indicated by plain lines [80]. Similar white cement was used, except for the alkali and sulfate contents adjusted in this study. The previous results from Müller showed that after 2 days, the gel pore water signal stabilizes [80]. In this study, the ratio of gel to interlayer water decreases with time but no stabilization is observed. This decrease can be explained by the formation of inner (denser) C-A-S-H forming without any gel water. This absence of stabilization of the amount of gel water observed in this study could be due to the sulfate adjustment of the cement, which slows down hydration, as observed by the later decrease of the capillary water in this study. The maximum of gel water might be reached at 60 days.

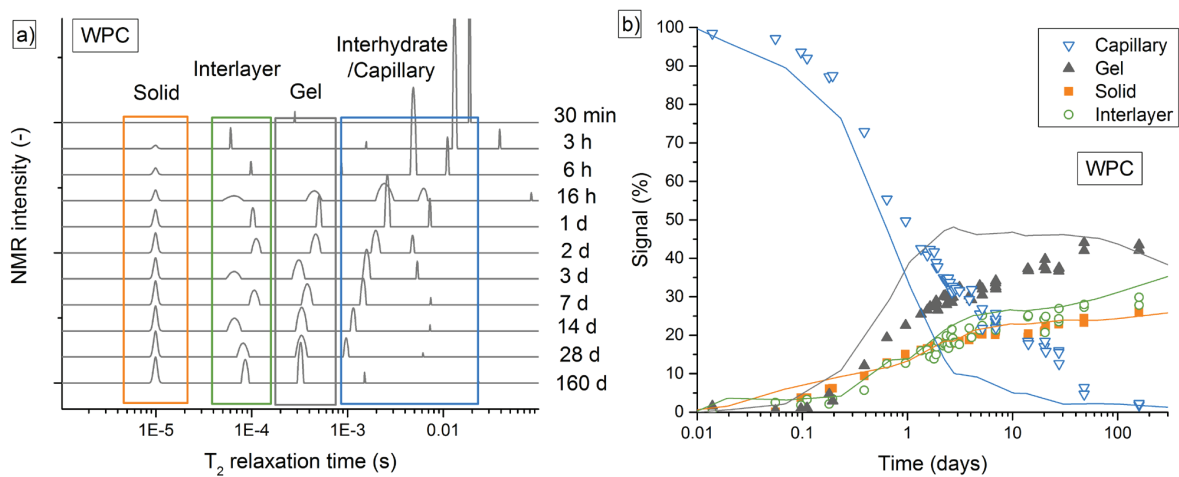


Figure 5.8. Evolution of relaxation time (a) and of the different NMR signal fractions (b) for WPC. Plain lines indicate Müller's data for WPC [80].

For the WLC³-50 (95.0%) in Figure 5.9 (a), the decrease of the amount of capillary water occurs until 1 – 2 days with a shift towards smaller relaxation times, and then the peak intensities and areas remain similar with time. This is confirmed by the quantification of the capillary water in Figure 5.9 (b). The amount of capillary water is constant with time from 1.5 days onwards. About 43% of the total water signal is still present in the capillaries from 1 day onwards and the average capillary water left after 1.5 days is about 33%.

For the C-A-S-H formation, the main difference observed compared with WPC is the higher relaxation time of the hydrogen spins of the water in the gel pores (about 5.0×10^{-4} s for WLC³-50 (95.0%)) compared with 3.2×10^{-4} s for WPC). This tends to indicate that the gel pores are slightly bigger for WLC³-50 (95.0%) blend. Moreover, the amount of water present in the gel pores reaches a maximum of about 36% of the total water signal at approximately 1.5 days of hydration. This amount slightly decreases then to 26% after 200 days of hydration. After 1.5 days, the interlayer water signal keeps increasing. The increasing formation of C-A-S-H can be the reason for the decrease of the gel water. First, the decrease of the gel to interlayer water ratio from 1.5 days onwards is thought of being due to the formation of inner “denser” C-A-S-H, without gel pores. Moreover, the slight de-

crease of the gel water signal can be due to a progressive consumption of this gel water to form C-A-S-H solid layers and this water is then present in the C-A-S-H interlayer.

Concerning the signal fraction of the water bound to crystalline phases, a decrease could have been expected with time due to the pozzolanic reaction of the metakaolin from calcined clay with portlandite. However, this decrease is not observed even if the intensity of the peak is slightly lower than for WPC at late ages. This is explained first by the formation of carboaluminate hydrates in WLC³-50 blends, and also because the fraction of water bound in portlandite (0.24 g of water per g of portlandite) is lower than ettringite (0.45 g of water per gram of ettringite). Thus, the amount of ettringite plays a bigger role in the peak intensity than portlandite.

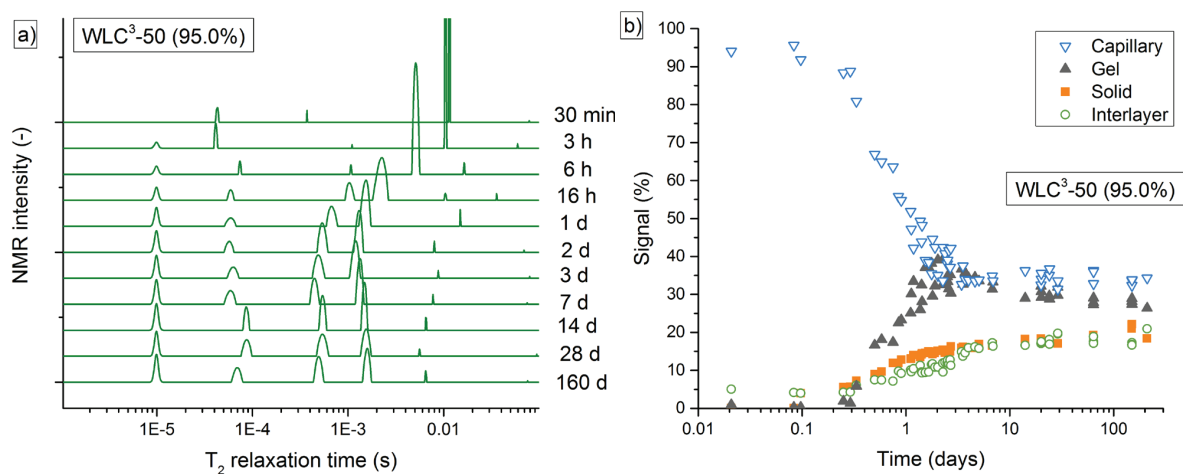


Figure 5.9. Evolution of relaxation time (a) and of the different NMR signal fractions (b) for WLC³-50 (95.0%).

The influence of the calcined kaolinite content is shown for the WLC³-50 (39.0%) blend in Figure 5.10. The relaxation time for the capillary water in Figure 5.10 (a) decreases until 1 day and is then constant with time. The main difference with the WLC³-50 (95.0%) is that the stabilization of the capillary water content occurs at around 7 days and its amount is lower (27% of the total water signal), as shown in Figure 5.10 (b). Thus, less water is present in the capillaries.

The maximal amount of gel water is measured at around 5 days of hydration and decreases then, whereas the amount of interlayer water keeps increasing with time. The signal of the water bound to crystalline phases keeps slightly increasing with time.

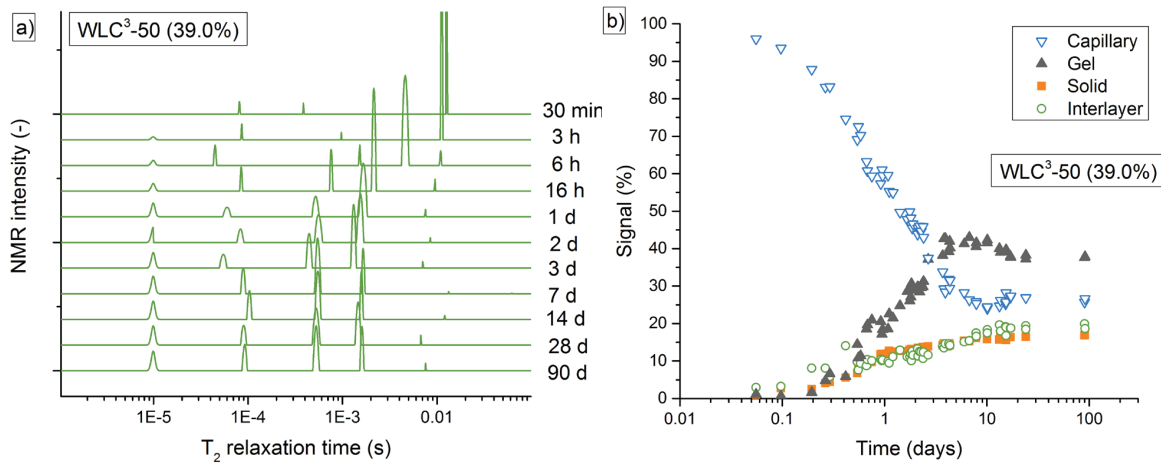


Figure 5.10. Evolution of relaxation time (a) and of the different NMR signal fractions (b) for WLC³-50 (39.0%).

5.4.4.3 Chemical shrinkage

The chemical shrinkage results are shown in Figure 5.11. The WLC³-50 (95.0%) shows the highest shrinkage at early age with a significant increase until 5 days of hydration and the shrinkage is almost constant later on. The shrinkage is quite similar for the other blends, including the reference WPC system. There is no direct correlation between the calcined kaolinite content of the calcined clay and the chemical shrinkage. The main difference between the plain WPC and the blends is the slope of the shrinkage at late ages. Whereas the shrinkage does not significantly change with time for the WLC³-50 blends, the shrinkage keeps occurring for the plain WPC system.

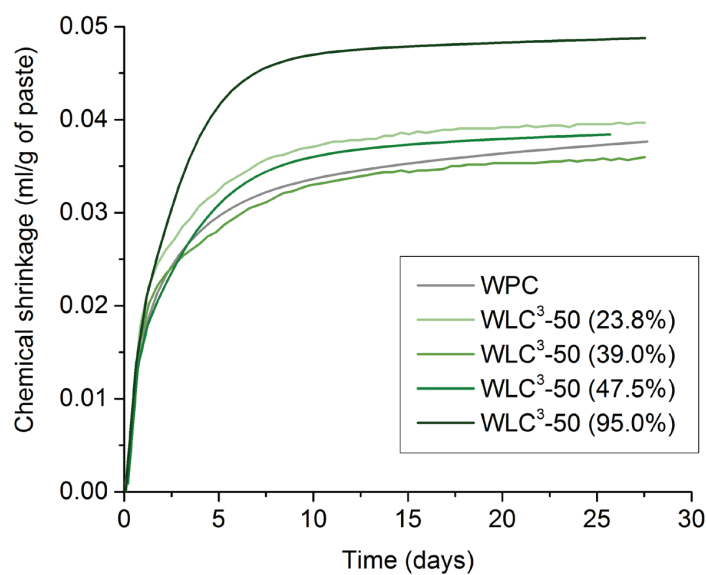


Figure 5.11. Chemical shrinkage measured for WPC and WLC³-50 blends.

5.4.4.4 Bulk and solid density of C-A-S-H

The values of solid and bulk density of C-A-S-H were determined according to the method described in Appendix 5. The values are shown in Figure 5.12 for WPC and for the different WLC³-50 blends. The solid density of C-A-S-H (excluding gel water) globally slightly decreases from about 2.9 g.cm⁻³ to 2.7 g.cm⁻³ from 1 to 28 days of hydration. There is a spread between the different systems but the variations are in the range of error. Thus, there is no major change in C-A-S-H solid density for reference WPC and for the WLC³-50 blends. The slight decrease of the solid density observed with time for all systems can be explained by the increase of the C-A-S-H layers with time. The water present at the surface of the C-A-S-H surface is in direct contact with the gel water and shows a longer relaxation time than the interlayer water. For a number l of calcium silicate layers, $l-1$ interlayers of water are detected by ¹H-NMR. Thus, with the increase of the number of layers l of the C-A-S-H, the average solid density slightly decreases since the ratio $l / l-1$ decreases with l .

The determination of the bulk density of C-A-S-H (including gel water) also shows very similar results for WPC and for WLC³-50 blends. The values globally slightly increase from 1.85 g.cm⁻³ at 1 day to 1.92 g.cm⁻³ at 28 days of hydration. Once again, the small variations observed between the different systems are in the range of error. Thus, neither the calcined clay nor the calcined kaolinite content in the calcined clay actually impact the density of C-A-S-H. The slight increase with time observed for all systems corresponds to the densification of the C-A-S-H, with the slowing down / stopping of gel pore formation from 1 to 7 days depending on the system. Similar results were found by Müller [112] for a blend with 10% of silica fume.

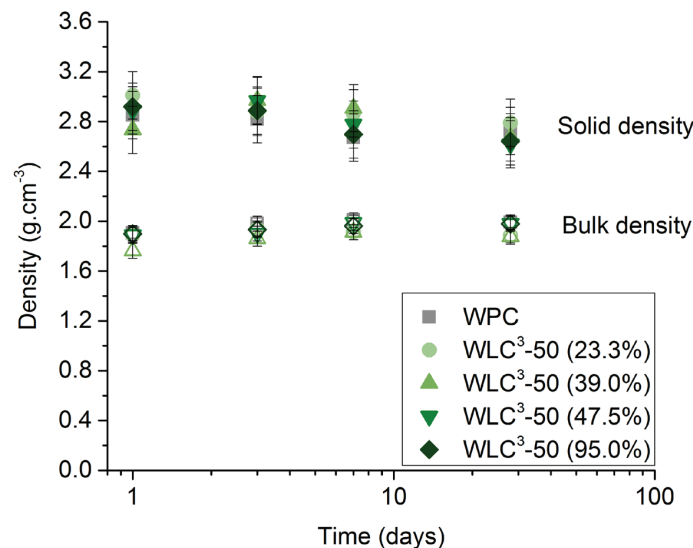


Figure 5.12. C-A-S-H density for WPC and WLC³-50 blends. Plain and hollow symbols represent the solid and bulk densities, respectively.

5.4.5 Discussion

5.4.5.1 Porosity investigation: Comparison between MIP and NMR data

The MIP results obtained at 3 days and 28 days of hydration for WPC and the different WLC³-50 blends are shown in Figures 5.13 and 5.14. At 3 days of hydration, a significant refinement of pore connectivity is observed for the WLC³-50 (47.5%) and (95.0%) blends compared with PC, with a lower pore threshold radius. However, these three systems show the same total porosity value. At 28 days of hydration, the reference WPC has the lowest total porosity. All blends however present a refinement of pore connectivity compared with PC, this refinement increasing with the calcined kaolinite content of the calcined clay. Figures 5.15 and 5.16 show the derivative of the MIP cumulative curves. The peak corresponding to capillary peaks can be observed for each sample. However, contrary to the study of Müller [112], it is not possible here to clearly distinguish a second peak corresponding to the gel porosity of C-A-S-H. For WPC, a clear peak for capillary pores is observed, but the gel pore peak is hard to identify. For the WLC³-50 blends, the capillary peak is shifted towards lower pore entry radius, which might cause an overlapping with the measurement of the gel pores.

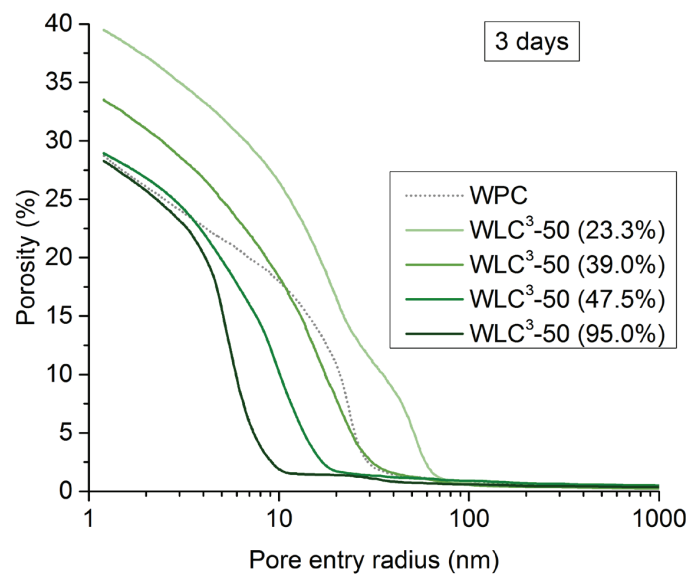


Figure 5.13. MIP results at 3 days of hydration for WPC and WLC³-50 blends.

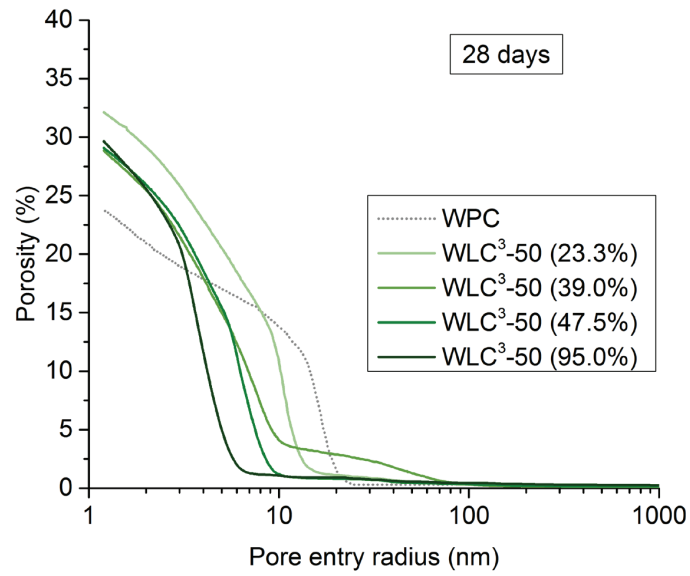


Figure 5.14. MIP results at 28 days of hydration for WPC and WLC³-50 blends.

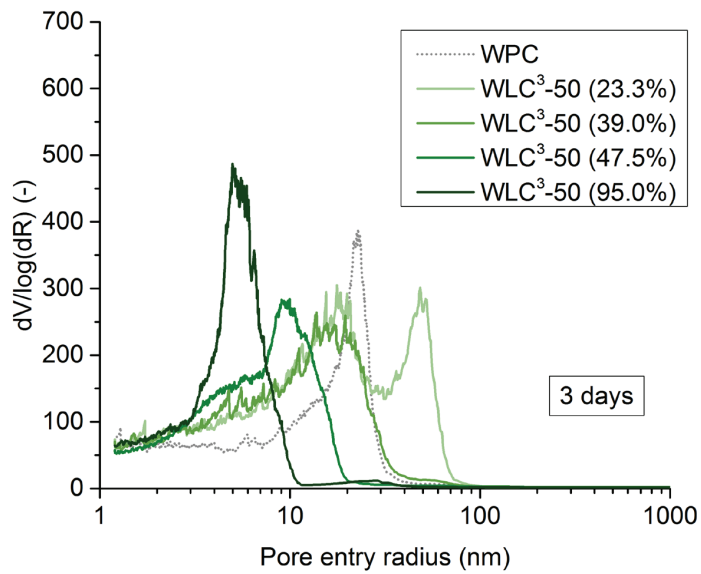


Figure 5.15. MIP derivative curves at 3 days of hydration for WPC and WLC³-50 blends.

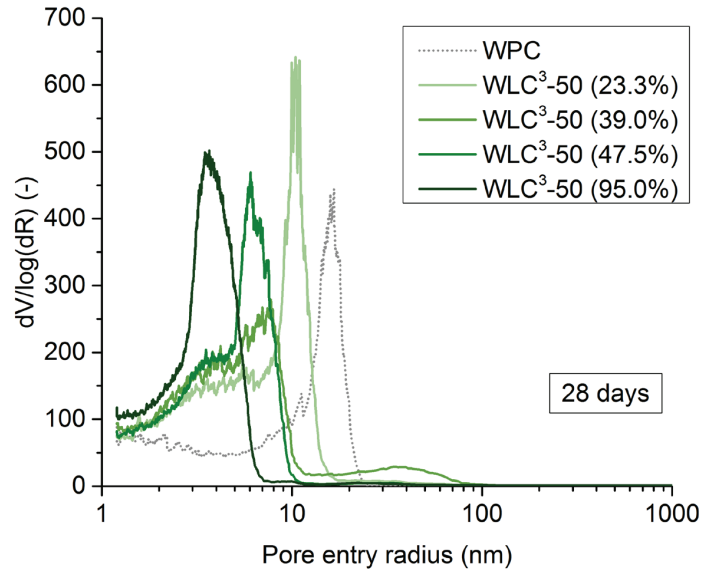


Figure 5.16. MIP derivative curves at 28 days of hydration for WPC and WLC³-50 blends.

In his work, Müller got excellent correlation between MIP and ¹H-NMR capillary porosity [112]. In this study, since it is not possible to distinguish the capillary from the gel pore peak, the approach consists of determining the capillary pore volume based on ¹H-NMR measurements to better understand which kind of information is obtained by MIP for the WLC³-50 blends. From the results obtained by ¹H-NMR in Figures 5.8-5.10, the volume of capillary and gel porosity can be measured according to Equations 5.1-5.3, considering the gel water I_{gel} , the water-filled capillaries I_{cap} and the capillary voids formed due to chemical shrinkage and self-desiccation I_{void} . w/b refers to the water to binder ratio and V_{paste} is the volume of paste per gram of anhydrous binder.

$$V_{capillary\ voids} = I_{void} \times \frac{w/b}{V_{paste}} \quad \text{Eq. 5.1}$$

$$V_{capillary\ water} = I_{cap} \times \frac{w/b}{V_{paste}} \quad \text{Eq. 5.2}$$

$$V_{gel\ pores} = I_{gel} \times \frac{w/b}{V_{paste}} \quad \text{Eq. 5.3}$$

Figures 5.17 and 5.18 show the volume occupied by the capillary and gel pores in the WPC and the different WLC³-50 blends at 3 days and 28 days of hydration, respectively. The total porosity obtained by MIP is also shown and compared to the results obtained by ¹H-NMR. For all systems, all capillary pores are reached by MIP. For WPC, 33% of gel pores are reached by MIP at 3 days of hydration, and approximately 47% are reached at 28 days of hydration. For WLC³-50 blends, the fraction of gel pores measurable by MIP is globally smaller, and this fraction decreases with the

increase of the calcined kaolinite content. For the WLC³-50 (23.8%) blend, 62% and 36% of gel pores are reached by MIP at 3 days and 28 days of hydration, respectively. For the WLC³-50 (95.0%) blend, MIP permits the measurement of only 10% of gel pores at 3 days and 11% at 28 days of hydration. As observed by MIP in Figures 5.13-5.16, a significant refinement of pore connectivity is observed for the blends, this refinement increasing with the calcined kaolinite content of the calcined clay. If the connectivity is finer, it might become harder for the mercury to intrude the C-A-S-H gel pores. This could explain why the fraction of gel pores intruded by mercury decreases with the increase of the calcined kaolinite content.

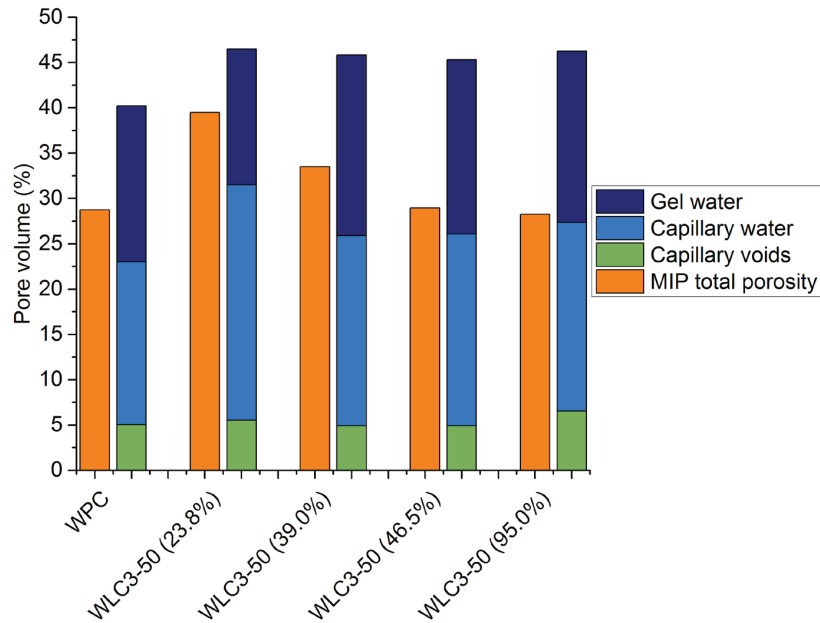


Figure 5.17. Comparison between MIP porosity and ¹H-NMR combined with chemical shrinkage outputs at 3 days of hydration.

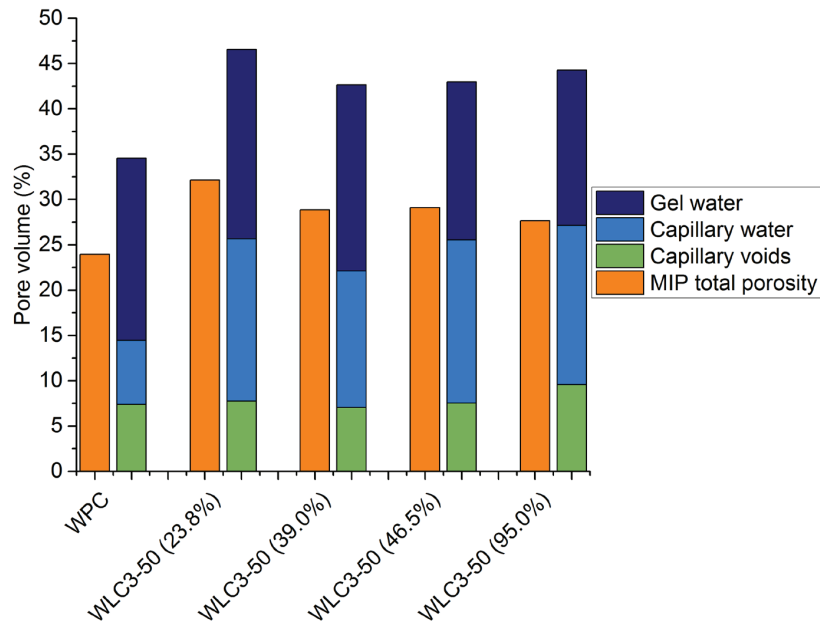


Figure 5.18. Comparison between MIP porosity and $^1\text{H-NMR}$ combined with chemical shrinkage outputs at 28 days of hydration.

Using the fast exchange model of relaxation, the pore size can be estimated from $^1\text{H-NMR}$ results [115, 116]. The size of capillary / interhydrate and gel pores is shown in Tables 5.6 and 5.7. The deviation for the capillary / interhydrate and the gel pore sizes is ± 1.6 nm and ± 1.2 nm, respectively. As comparison, the pore diameter obtained by MIP is also shown at 3 and 28 days of hydration in Table 5.6, with a deviation of ± 2.7 nm. The size of capillary pores is underestimated by $^1\text{H-NMR}$ compared to MIP for all samples at 3 days and at 28 days, except for the WLC³-50 (95.0%) blend. This underestimation by $^1\text{H-NMR}$ can be explained by the non-water saturation for most of pores. Empty pores are not detected by $^1\text{H-NMR}$ and partially water-filled are “seen” finer (thin layers of water on the pore wall). This means that only the finest fraction of the pores is measured. The only acceptable correlation for the interhydrate pore size is obtained for the WLC³-50 (95.0%) blend. This could be explained by the higher relative humidity measured in Chapter 4 for the LC³-50 (95.0%) compared to the PC and the other calcined clay blends.

Concerning gel pore size, it is not possible to really distinguish by MIP a clear peak, contrary to the study of Müller [112]. $^1\text{H-NMR}$ shows that the pore size is just at the limit of detection by MIP or slightly below.

Table 5.6. Estimation of pore size for capillary/interhydrate pores.

Capillary / Interhydrate pore (nm)	WPC	WLC ³ -50 (23.8%)	WLC ³ -50 (39.0%)	WLC ³ -50 (47.5%)	WLC ³ -50 (95.0%)
1 day	19.1	14.1	14.1	12.3	11.5
3 days	11.7	12.5	9.6	11.3	9.0
7 days	10.7	10.6	12.3	11.7	9.8
28 days	7.1	10.8	10.8	14.3	11.5
3 days MIP	45.7	96.8	39.1	20.0	10.0
28 days MIP	33.2	20.9	15.5	12.1	7.3

Table 5.7. Estimation of pore size for gel pores.

Gel pore (nm)	WPC	WLC ³ -50 (23.8%)	WLC ³ -50 (39.0%)	WLC ³ -50 (47.5%)	WLC ³ -50 (95.0%)
1 day	3.7	5.1	5.1	3.6	4.9
3 days	2.3	3.8	3.2	4.3	3.5
7 days	2.8	4.3	4.0	4.1	3.2
28 days	2.4	3.9	3.8	4.7	4.0

5.4.5.2 Microstructure development

It is observed in Figure 5.9 that a significant amount of capillary water is still present by ¹H-NMR from 3 days onwards in WLC³50 (95.0%) system. MIP results also show that the total porosity value is very similar at 3 and 28 days for this system in Figures 5.13 and 5.14. At the same time, very fine capillary pores are measured (size of 6-8 nm). Since the formation of hydration products becomes harder and harder with the decrease of the capillary pore size, the amount of capillary water does not significantly decrease with time. As a consequence of the slowing down of hydration, the water present in the capillaries stays in the very fine water-saturated capillaries.

Despite the slowing down of clinker hydration, the metakaolin reaction keeps occurring. First, the portlandite keeps being consumed from 3 days onwards (Figure 5.3). Moreover, the aluminium incorporation in C-A-S-H keeps increasing from 3 to 28 days, cf. Table 5.5. Finally, the amount of interlayer water keeps increasing, as shown in Figure 5.9. It increases from 12 % of the total signal at 3 days of hydration to 20 % at 28 days. At the same time, the amount of gel water decreases from 38 % to 32 %.

5.5 Conclusion

The C-A-S-H of LC³-50 systems shows significant changes in terms of composition. The aluminium incorporation increases with the calcined kaolinite content of the calcined clay. The silicon to calcium ratio is quite similar for all blends, but higher than plain cement. A good agreement was found between SEM-EDX and STEM-EDX. STEM permits to overcome the interaction volume issue occurring with SEM. However, larger deviations were obtained using STEM. Due to its much

easier sample preparation, SEM-EDX is much more practical and more accessible way to obtain the composition of the C-A-S-H.

In terms of morphology, STEM provides unique information on the morphology of the C-A-S-H, where a fibrillar morphology is observed for all systems. There is no influence of the calcined clay or of the calcined kaolinite of the calcined clay on the C-A-S-H morphology.

The density of C-A-S-H investigated by $^1\text{H-NMR}$ also shows that there is no significant influence of the calcined kaolinite content of the density of C-A-S-H. A solid density of around 2.8 g.cm^{-3} is found, and a bulk density of 1.95 g.cm^{-3} is determined for all systems at 28 days of hydration.

In parallel to the determination of the C-A-S-H density, $^1\text{H-NMR}$ reveals that a much higher amount of capillary water is measured for the blends than for the plain cement. Considering the amount of capillary voids by chemical shrinkage, the comparison with MIP results shows that for blends, mostly capillary pores are characterized by MIP. The fraction of gel pores reached by MIP decreases with the increase of the calcined kaolinite content of the calcined clay. About half of gel pores are reached by MIP for the plain cement system at 28 days of hydration.

Chapter 6 - Relationship between compressive strength and phase assemblage for Limestone Calcined Clay Cement (LC³)

6.1 Introduction

The characterisation of the microstructure is a key step to understand the mechanical properties of cementitious systems. Several authors attempted to correlate strength results with porosity [35, 43, 66, 92, 117-123], with for most of cases a linear decrease of strength with the increase of porosity. However, this relationship cannot be universally applied for instance with a change of mix composition [118] or of temperature [60]. For calcined clay blends, Fernandez observed a linear trend between strength and porosity for plain PC and blends with 30% of illite or montmorillonite. However, some shift was observed for a blend containing 30% of metakaolin [22].

Another approach to explain the strength consists of considering the total volume of hydration products formed. To keep this approach consistent independent of the water to binder ratio for example, the space available for the formation of hydration products needs to be taken into account. The gel to space ratio approach suggests that the strength is dependent of the volume of hydrates per space available for hydration. Powers used this approach to correlate strength and phase assemblage [124]. In his study, the best correlation with strength was obtained assuming that the gel was including all hydrates except portlandite [125]. Powers found a cubic relationship between strength and gel space ratio. There is no clear evidence why a cubic fit was used rather than a linear fit. However, this is probably because it forces the correlation to cross the origin. Lam and al. also used the gel space ratio and used an exponential fit for plain PC and fly ash blends [126]. The gel was considered as the volume of hydrated cement based on the hydration degree of clinker and fly ash, and the space was defined as the initial water content and the volume of reacted binder. More recently, Termkhajornkit et al. [127] used the gel space ratio approach to claim that hydration products do not have the same contribution to strength development and that C-S-H phase plays a critical role. This is explained by the fact that during a compressive strength test, failure occurs through the weakest point of the microstructure, which would be a “foam” composed of C-S-H intermixed with porosity. Durdzinski et al. [74] considered for the gel space ratio calculation the exact amount of each hydration products obtained by mass balance and thermodynamic modeling. In his study, the gel was defined as the sum of hydration products. He found a bi-linear fit between mortar strength and the gel space ratio on pastes. This would indicate that contrary to the study of Termkhajornkit et al. [127], all hydrates contribute equally to the strength development. Two main linear regimes were obtained, and a third one for very early-age hydration could also be assumed:

- the first regime would go from setting time until reaching a connected network of hydration products
- the second regime corresponds to the space filling by hydration products

- the third regime is claimed to be due to a densification of C-S-H, as observed by $^1\text{H-NMR}$ [80]

In this study, the use of Limestone Calcined Clay Cement (LC³-50) is investigated using various grades of calcined kaolinitic clays. Strength results in [90] showed a linear correlation with the calcined kaolinite content of the calcined clays, and similar strength to PC was obtained from 7 days onwards for LC³-50 blends containing calcined clays with about 40% of calcined kaolinite. In order to understand such strength results, a study of the microstructure development of LC³-50 was carried out in Chapter 4. The porosity was characterized, as well as the phase assemblage. In this chapter, the correlations between strength results and both approaches, i.e. porosity and gel space ratio, are applied to try to understand the compressive strength results obtained for LC³-50 blends.

6.2 Results

6.2.1 Strength and porosity

Figure 6.1 shows the correlation between the compressive strength at 3, 7 and 28 days and the total porosity values. At 3 days of hydration, a linear correlation is observed, i.e. higher porosity leads to lower strength. However, from 3 days onwards, the total porosity values remain very similar for the LC³-50 blends with calcined clay containing more than 65% of calcined kaolinite, while strength values keep increasing. The blends with a lower calcined kaolinite content progressively reach the limit of refinement of pore connectivity, as shown in Chapter 4. When this limit is reached, the correlation between strength and total porosity starts deviating from the linear trends to a near vertical relationship.

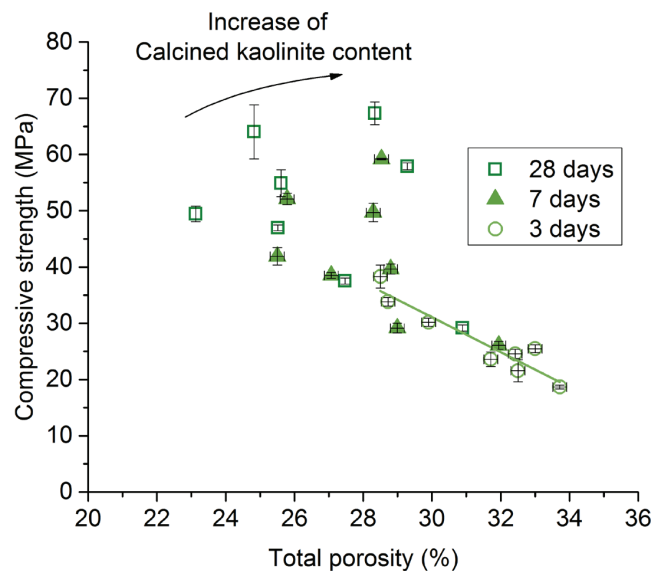


Figure 6.1. Correlation between mortar compressive strength and total porosity for LC³-50 blends.

In addition to the total porosity, the critical pore entry radius is another output obtained by MIP which permits to characterize the size of pore connected through the sample. The correlation between the compressive strength and the critical pore entry radius is shown in Figure 6.2. As observed with total porosity, two regimes are observed, for LC³-50 with more or less than 65% of calcined kaolinite in calcined clay.

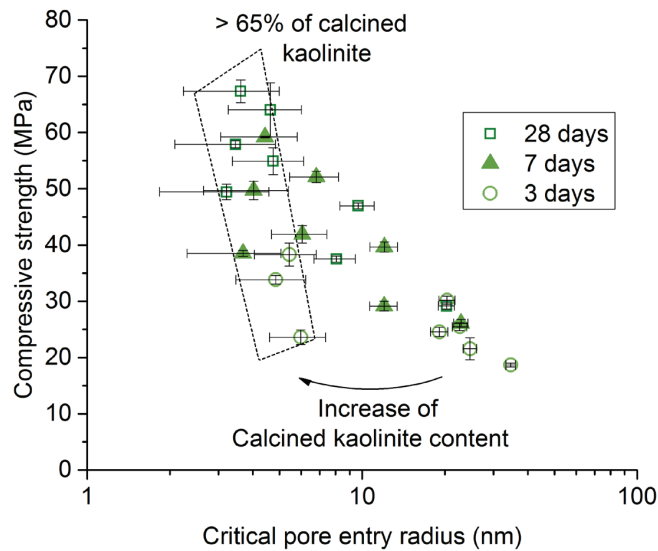


Figure 6.2. Correlation between mortar compressive strength and critical pore entry radius for LC³-50 blends.

The mortar strength tests were carried out using samples with a water to binder ratio of 0.5 stored in a moist room. However, 0.4 sealed-cured samples were tested for pastes. In order to make sure that neither the curing condition nor the water to binder ratio play a role in these results, MIP results were also carried out on mortars at 28 days of hydration, for samples cured in the same conditions as mortar cubes used for compressive strength tests. The correlation between compressive strength and total porosity is shown in Figure 6.3. Lower total porosity values are obtained due to the presence of sand grains in the samples. The LC³-50 (95.0%) is clearly out of the trend since a higher total porosity is obtained for this system. The correlation between the mortar compressive strength and the critical pore entry radius in Figure 6.4 also shows similar results to MIP on paste. Even for mortars stored in moist room using a water to binder ratio of 0.5, a similar limit of pore connectivity refinement is reached at around 3-5 nm. Thus, the strength development of LC³-50 blends cannot be well explained by characteristics of the overall porosity.

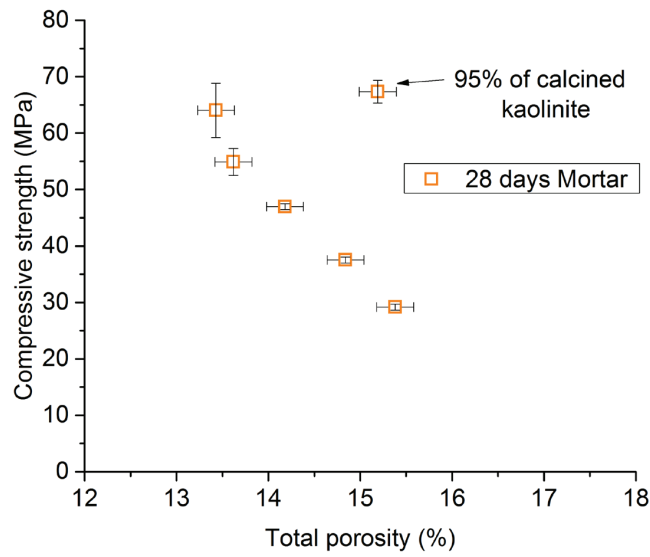


Figure 6.3. Correlation of compressive strength and total porosity on LC³-50 mortar samples at 28 days of hydration.

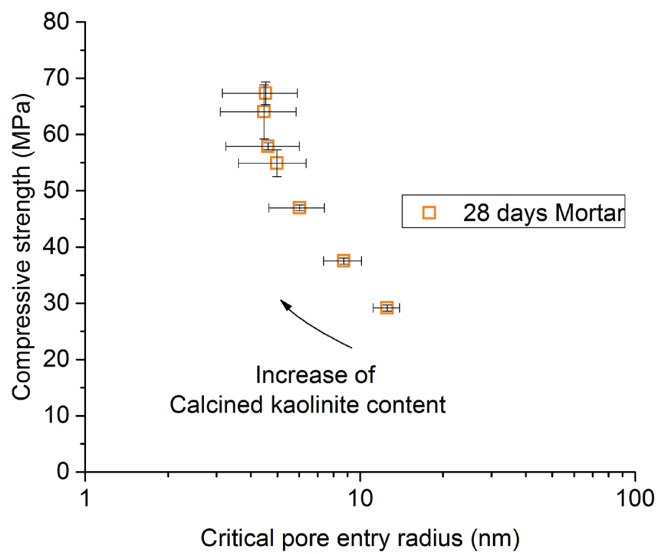


Figure 6.4. Correlation of compressive strength and critical pore entry radius on LC³-50 mortar samples at 28 days of hydration.

6.2.2 Gel Space Ratio

In order to determine the gel space ratio, the phase assemblage in cm³/100g is shown for PC and the different LC³-50 blends at 3 days of hydration in Figure 6.5 and at 28 days of hydration in Figure 6.6. Mass balance was used to determine the amount of reacted metakaolin and the amount of C-A-S-H formed, as detailed in Chapter 3. The bulk density value of C-A-S-H similar for all systems

was obtained from Chapter 5. The density of the other phases (anhydrous or hydrate) was taken from [128]. The highest volume of C-A-S-H is obtained for reference PC system at 3 days and at 28 days. The total volume of hydration products is also the highest for PC. Moreover, at 3 days of hydration, a similar volume of hydrates is obtained for LC³-50 blends containing calcined clay with more than 65% of calcined kaolinite. At 28 days of hydration, LC³-50 with at least 35% of calcined kaolinite show a similar total hydrate volume.

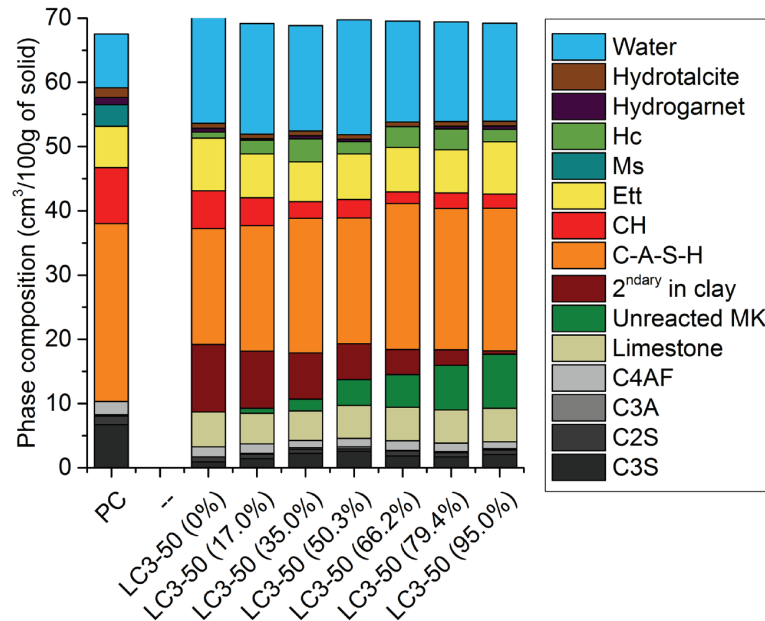


Figure 6.5. Phase assemblage at 3 days of hydration for PC and LC³-50 systems. Hc = hemicarboaluminate, Ms = monosulfoaluminate, Ett = ettringite, CH = portlandite, Unreacted MK = unreacted metakaolin in the calcined clay, 2^{ndary} in clay = other phases in calcined clay.

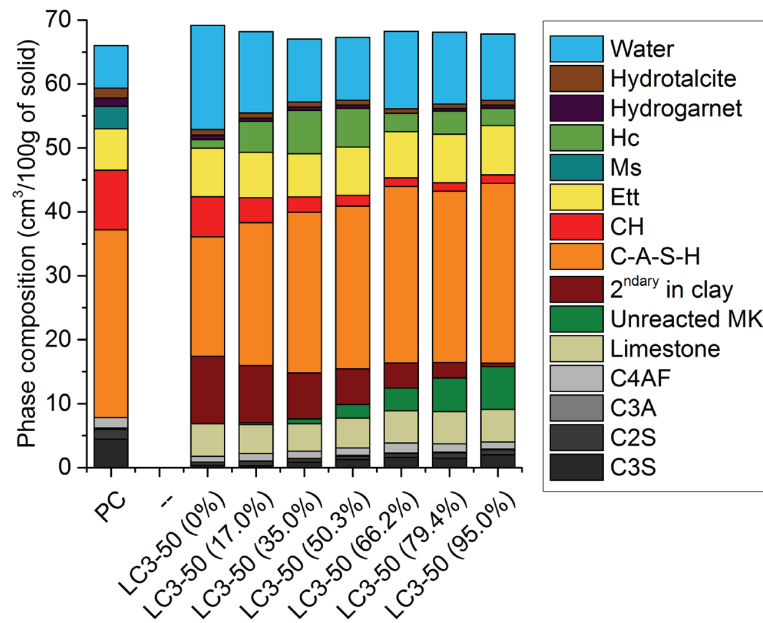


Figure 6.6. Phase assemblage at 28 days of hydration for PC and LC³-50 systems. Hc = hemicarboaluminate, Ms = monosulfoaluminate, Ett = ettringite, CH = portlandite, Unreacted MK = unreacted metakaolin in the calcined clay, 2^{ndary} in clay = other phases in calcined clay.

The gel space ratio as proposed by Termkhajornkit was first applied in this study [127], according to Equation 6.1. The gel was only composed of the volume occupied by C-A-S-H, $V_{C-A-S-H}$. The space was defined as the sum of the initial water volume, $V_{water,i}$, and the volume of reacted binder $V_{reacted\ binder}$ (sum of the volume of reacted clinker, metakaolin, limestone and gypsum determined by XRD-Rietveld and mass balance). Figure 6.7 shows that considering only C-A-S-H as gel, a clear linear correlation is obtained for PC and for all LC³-50 blends. This could mean that the volume occupied by C-A-S-H plays a dominant role in the strength development, as claimed by Termkhajornkit et al. [127]. The dashed lines indicate the deviations based on sensitivity analysis for all phases for LC³-50 blends.

$$GSR_{C-A-S-H} = \frac{V_{C-A-S-H}}{V_{water,i} + V_{reacted\ binder}} \quad \text{Eq. 6.1}$$

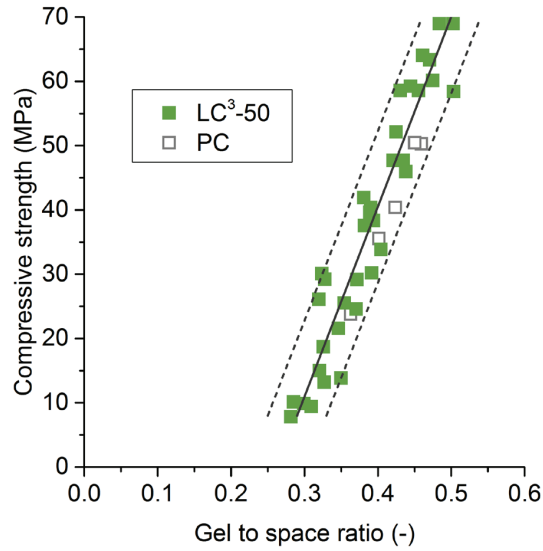


Figure 6.7. Correlation between compressive strength and gel space ratio considering only C-A-S-H as gel.

The approach based on the study of Durdzinski et al [74] was then studied. The gel was defined as the sum of the volume occupied by the hydration products $\Sigma V_{\text{hydration products}}$ (sum of the volume of C-A-S-H, CH, E_{tt}, M_s, H_c, hydrogarnet and hydrotalcite), and the space was still defined as the sum of the initial water volume and the volume left by the reacted binder, as detailed in Equation 6.2. Figure 6.8 shows that some shift is observed between PC and LC³-50 blends. For the same strength, higher gel space ratio is determined for plain PC. The amount of gel is higher for PC due to the higher formation of hydration products, as observed in Figures 6.5 and 6.6. This higher gel is not compensated by a slightly higher available space.

$$GSR_{\Sigma \text{hydrates}} = \frac{\Sigma V_{\text{hydration products}}}{V_{\text{water},i} + V_{\text{reacted binder}}} \quad \text{Eq. 6.2}$$

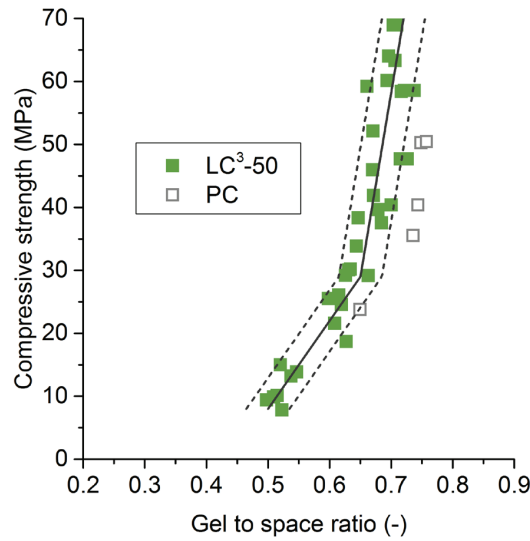


Figure 6.8. Correlation between compressive strength and gel space ratio considering the sum of hydration products as gel.

The role of soft SCMs was then considered. Table 6.1 shows the elastic modulus measured by nanoindentation for most of phases involved in the LC³-50 blends. Metakaolin and limestone elastic modulus values are close to cement hydration products. As comparison, clinker phases or impurities in the calcined clay (mainly quartz) show a much stiffer behaviour. These fine inclusions of metakaolin and limestone in the hydration product matrix with similar elastic properties could behave similarly to C-A-S-H. They could take part of the load applied and strengthen the material. Moreover, these soft inclusions could also decrease stress concentrations in the material due to the decrease of the interfaces between the hydration product matrix and the sand / unreacted clinker particles.

Table 6.1. Elastic modulus for the main cement phases and for minerals involved in LC³-50 blends.

Phase	Elastic modulus (GPa)
Low density C-S-H (outer C-S-H)	21.7 ± 2.2 [129]
High density C-S-H (inner C-S-H)	29.4 ± 2.4 [129]
Portlandite	38 ± 5 [129]
Metakaolin	40.1 ± 7.2 [130]
Limestone	38.5 ± 2.5 [131]
C ₃ S	135 ± 7 [132]
C ₂ S	130 ± 20 [132]
C ₃ A	145 ± 10 [132]
C ₄ AF	125 ± 25 [132]
Quartz	104.2 ± 5.9 [133]

To consider this assumption in the gel space ratio calculation, a modified version includes the volume of the soft inclusions $V_{\text{unreacted metakaolin}} + V_{\text{unreacted limestone}}$ (unreacted metakaolin and limestone particles) as part of the gel according to Equation 6.3. The space calculation then includes the volume occupied by these unreacted soft inclusions.

$$GSR_{\Sigma \text{hydrates+soft inclusions}} = \frac{\sum(V_{\text{hydration products}}) + V_{\text{unreacted metakaolin}} + V_{\text{unreacted limestone}}}{V_{\text{water, i}} + V_{\text{reacted binder}} + V_{\text{unreacted metakaolin}} + V_{\text{unreacted limestone}}} \quad \text{Eq. 6.3}$$

Figure 6.9 shows that considering this assumption, less scatter is observed and the data of PC and the different LC³-50 blends fall on the same trend, with the two regimes observed by Durdzinski et al. [74]. The reason for the shift observed in Figure 6.8 could thus be the presence of the inclusions of soft SCMs in the microstructure.

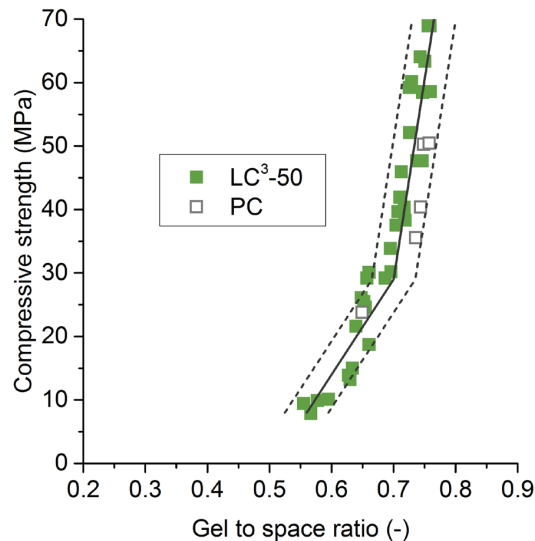


Figure 6.9. Correlation between compressive strength and gel space ratio considering the sum of hydration products and the unreacted limestone and metakaolin particles as part of the gel.

6.3 Conclusion

Due to the limited refinement of pore connectivity observed on paste and mortar for LC³-50 blends, it is not possible to get a good correlation between porosity measured by MIP and compressive strength. Neither the total porosity nor the critical pore entry radius permit to understand the strength results.

In the case of considering only C-A-S-H phase as gel, a clear linear correlation between compressive strength and gel space ratio is obtained for PC and for LC³-50 blends for all ages.

When all hydration products were included in the gel, a shift is observed between PC and LC³-50 blends. This shift could be due to the influence of the fine inclusions of soft SCMs in the matrix. By correcting the gel space ratio, a clear bi-linear regime is observed for all systems.

Thus, two possible interpretations are possible to explain strength results, either that the C-A-S-H is the critical phase for strength development (C-A-S-H intermixed with porosity as weakest point of the microstructure) or that the fine unreacted soft SCM inclusions play a role.

Chapter 7 - Chloride resistance of Limestone Calcined Clay Cement (LC³) using various grades of calcined kaolinitic clays

The experiments of this Chapter were carried out by François Avet and Dr. Hamed Maraghechi. Dr. Hamed Maraghechi specially helped in μ XRF and chloride ponding measurements.

7.1 Introduction

One of the most important durability concerns for concrete infrastructure is corrosion of steel reinforcement as a consequence of the transport of chloride ions (e.g., from sea water or de-icing salts) through concrete. The rate and extent of ion transport in concrete is influenced by both the physical pore structure of concrete at nano and micro scales, and the physical or chemical binding of chlorides into some hydrates, specifically C-A-S-H and Al- or Fe-AFm phases. While the un-bound or free chlorides ions are considered to be responsible for corrosion of reinforcement, research on whether some of the bound chloride ions are perhaps contributing to corrosion or not is still ongoing. Therefore, understanding and quantifying physical and chemical characteristics of concrete with new cementitious components is essential for more accurate service-life prediction of concrete.

Generally, it is known that the use of SCMs improves the resistance of concrete to ion transport. This is mainly attributed to the refinement of porosity observed for blended cements [44, 134]. In addition, the phase assemblage of hydrates is altered by addition of SCMs, with consequent changes (usually improvement) to chloride binding capacity of concrete [135-139].

The binding of chloride can be first chemical. The presence of chloride mainly affects the AFm phases. For PC system, and after exposure to low Cl concentrations ($< \approx 0.2$ M), formation of only Kuzel's salt was thermodynamically predicted, and by increasing Cl concentration, Friedel's salt formation occurs [140]. In presence of limestone, chloride ions progressively substitute carbonate ions in the AFm structure, leading to the conversion of hemi- and monocarboaluminate phases to Friedel's salt. Kuzel's salt does not form in presence of monocarbonate and Friedel's salt [141]. Thomas et al. found an almost linear relationship between the bound chloride and the amount of Friedel's salt formed [142].

In addition to the chemical binding, some chloride ions can also be adsorbed on C-A-S-H [44, 143]. The physical adsorption of chloride on C-A-S-H depends on the C-A-S-H composition: the higher the Ca/Si, the higher the chloride adsorption [144, 145]. The type of salt and the cation used also influences the binding on C-A-S-H. Exposure of well-hydrated cement paste to CaCl_2 was observed to result in more bound chloride compared to NaCl solution of the same Cl concentration [140, 144]. As explained by Shi [71], the amount of chloride ions adsorbed in the diffuse layer of C-A-S-H is due to the adsorption of positively-charged calcium ions on the negatively-charged C-A-S-H

surface. Chloride ions would then be adsorbed to compensate the positive charge of calcium. As a consequence, the pH drops using CaCl_2 salt. This pH decrease is not observed for NaCl salt [71, 140].

There have been several studies on the durability of concrete containing calcined kaolinite clay, either as binary (PPC) or ternary (LC^3) blends [137, 142, 146-149]. One main phase modification with the use of calcined clay is the uptake of Al in C-(A)-S-H structure, proven through ^{29}Si MAS NMR analysis of hydrated LC^3 pastes [69] or by SEM-EDX [150]. Limestone in LC^3 cements, due to the availability of reactive aluminate from the clay, contributes to formation of further AFm phases of calcium monocarboaluminate (Mc) and calcium hemicarboaluminate (Hc) [43], which is expected to increase binding capacity of the concrete, while retaining ettringite against decomposition to monosulfoaluminate [37, 38].

Shi et al [71, 151] used pure metakaolin in preparation of binary PC-calcined clay or ternary LC^3 blends with 35% replacement level, with the clay/limestone ratio of 4. Significant improvement against chloride transport resistance of mortars was reported. It was observed that monocarboaluminate and stratlingite transform into Friedel's salt, and the NaCl exposed zones are leached with portlandite, along with destabilization of limestone. Exchange of chloride ions with carbonates from monocarbonate is expected to increase calcite content, and reduce portlandite. Using TGA and XRD Rietveld analysis to quantify Friedel's salt in blends containing pure metakaolin, it was concluded that from the total chloride diffused into mortars, less than 5-10 % is bound into Friedel's salt [151]. Moreover, chloride binding in LC^3 and PPC paste mixtures was analyzed, using both NaCl and CaCl_2 . The distribution of chloride between Friedel's salt, C-A-S-H and free chloride was quantified, and it was concluded that in PC-metakaolin blends, almost all bound chloride is chemically bound to Friedel's salt and not physically adsorbed on C-A-S-H [71].

This Chapter is focused on evaluating the chloride resistance characteristics of cementitious materials composed of ternary mixtures of LC^3 -50 and also binary blends PPC30. While most past research was focused on the use of fairly pure metakaolin, which is not viable as clinker substitute due to its high cost, we studied properties of mortar and paste mixtures with various grades of kaolinite content, as they have larger global availability with lower cost. In addition to the rate of chloride transport, binding characteristics of PPC30 and LC^3 -50 binders are also studied.

7.2 Materials

The cementitious materials of this study include a CEM-I 42.5R from Heidelberg cement, Durcal 5 limestone from Omya and five kaolinitic clays obtained from different sources worldwide. The clays were either calcined at around 800 °C for 1 h in a high temperature furnace in our laboratory, or received as calcined. The calcined kaolinite content $\text{wt}\%_{\text{calcined kaolinite}}$ was calculated by TGA according to Equation 7.1, and detailed in Appendix 2, where $\text{wt}\%_{\text{kaol-OH, calcined}}$ corresponds to the water loss of the remaining kaolinite in the calcined clay. $M_{\text{kaolinite}}$ and M_{water} refer to the molecular weights of kaolinite and water, respectively. As it can be seen in Table 7.1, a wide range of clay composition and of calcined kaolinite content is used in this study. Quartz was used to simulate a clay material with 0% kaolinite content. The values of d_{v50} were obtained using laser diffractometer

(Malvern) analysis, and the specific surface was measured by nitrogen adsorption using BET model.

$$wt\%_{\text{calcined kaolinite}} = wt\%_{\text{kaolinite}} - wt\%_{\text{kaol-OH, calcined}} \times \frac{M_{\text{kaolinite}}}{2M_{\text{water}}} \times \left(\frac{100 - wt\%_{\text{kaol-OH, calcined}}}{100} \right) \quad \text{Eq. 7.1}$$

Table 7.1 Properties of the cementitious components used in this study.

	Cement	Limestone	Quartz	Clay 1	Clay 3	Clay 18	Clay 16	Clay 43
Calcined kaolinite content (wt. %)	–	–	–	95.0	79.4	50.3	41.9	17.0
D _{v,50} (µm)	8.4	7.2	11.2	5.1	5.3	10.9	7.8	5.8
BET surface (m ² /g)	0.9	1.8	1.2	9.6	15.3	45.7	9.2	18.7
	XRF composition (wt.%)							
SiO ₂	19.3	0.1	99.8	52.0	51.8	44.9	53.5	68.4
Al ₂ O ₃	5.7	–	–	43.8	42.4	32.3	34.8	17.5
Fe ₂ O ₃	3.6	–	–	0.3	1.9	15.4	3.3	8.9
CaO	63.6	55	–	–	0.1	1.3	0.1	0.6
MgO	1.6	0.2	–	–	0.1	0.8	0.1	0.7
SO ₃	3.2	–	–	0.1	–	0.1	0.03	–
Na ₂ O	0.2	0.1	–	0.3	0.1	0.4	0.2	0.1
K ₂ O	1.2	–	0.1	0.1	0.1	0.2	0.2	2.3
TiO ₂	0.3	–	–	1.5	2.4	2.4	2.3	0.8
P ₂ O ₅	0.2	–	–	0.2	0.1	0.4	0.2	0.1
MnO	0.1	–	–	–	–	0.1	0.01	–
Others	0.3	–	–	0.1	0.2	0.2	0.02	0.2
LOI	0.8	42.6	0.1	1.5	1.0	1.7	4.7	0.5

In addition to a reference PC system, two series of blends, including PPC30 and LC³-50 were prepared. All the calcined clays were used in the LC³-50 blends. Only clays 1 and 16 of Table 7.1 were used in PPC30 blends. As detailed in the previous Chapters and in Appendix 1, 2% of gypsum was added to the PPC30 and LC³-50 blends to avoid undersulfation. The final composition of the plain PC and the blends is shown in Table 7.2.

Table 7.2. Mix composition (wt.%) of PC, PPC30 and LC³-50 blends.

	Clinker	Anhydrite	Calcined clay	Limestone	Gypsum
PC	94.1	5.9	-	-	-
PPC30	64.5	4.1	29.4	-	2.0
LC ³ -50	50.6	3.3	29.4	14.7	2.0

7.3 Analytical details

7.3.1 Ponding test

Both mortar and paste samples were prepared using a water to binder ratio of 0.5. This water to binder ratio was also used on paste to accelerate the chloride penetration in the samples. To ensure similar workability to plain cement, a polycarboxylate superplasticizer was used (Mapei Dynamon SP914). The amount of superplasticizer added to the water increases with the calcined kaolinite content of the calcined clay, as detailed in Appendix 4. Mortar mixtures were cast in cylindrical (11 cm diameter - 30 cm height) molds. After 24 h of curing in sealed conditions, specimens were demolded and stored in a fog room (RH>95%). After 28 days of curing, the mortar cylinders were saw cut into two halves, epoxy coated on all surfaces except the saw cut face and submerged in 3 wt. % NaCl solution. Chloride profiles were obtained in accordance with ASTM-C1152 procedure after 1 and 2 years of exposure. This ponding experiment excludes the PPC-30 and LC³-50 mixtures with quartz system and 41.9 % of kaolinite content.

Paste samples were prepared by initially blending the powders and mixing with distilled water for 2 minutes at 1600 rpm. Fresh paste mixtures were cast in small plastic containers (3 cm diameter - 5 cm height), cured for 24 h in sealed conditions, and followed by a curing under saturated lime water for 28 days. In a similar approach to mortar ponding experiment, after cutting away 1 cm from the surface of the paste cylinders, the side surface was coated with epoxy and exposed to 3 wt% NaCl solution. After 6 months of exposure, the paste samples were removed from the solutions, and dry saw cut to have a surface with chloride gradient being exposed. The paste samples were then ground using a sand paper for 2 minutes, while attention was made to ensure grinding was executed in a direction perpendicular to the diffusion direction (Figure 7.1). The samples were then dried using freeze-drying method. This method was used to prevent any loss of free or bound chloride. The exposed surface was analyzed using a μ -XRF technique (Orbis micro EDXRF). Multiple points were selected at each depth and the average values of EDX counts were calculated and reported. The analysis settings are provided in Table 7.3. Further information on the use of μ -XRF to analyze chloride transport in cementitious materials can be found in [152].

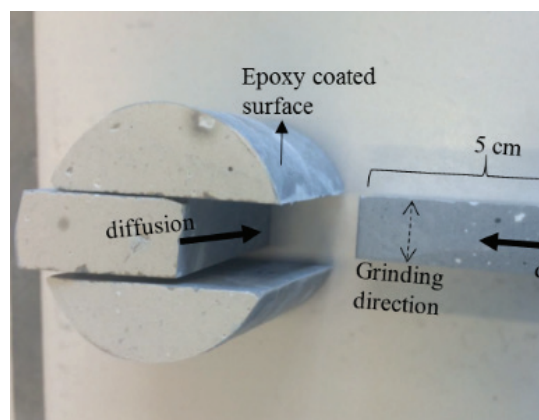


Figure 7.1 μ -XRF sample preparation.

Table 7.3 μ -XRF settings used in this study.

Operating condition	Details
Beam voltage (kV)	25
Dead time (%)	30 (beam current was automatically adjusted)
Chamber	Vacuum
Filter	25 μ m aluminum
Acquisition time (s Live)	300
Beam spot size (μ m)	30
Time constant (μ s)	12.8

7.3.2 Binding isotherm

To measure the chloride binding capacity and study the interactions of NaCl solution with LC³-50 and PPC-30 mixtures, 28 day cured paste samples were dried. Small pieces (0.5-1.0 mm) of dried paste, as well as one 1.0 mm thin paste slice (3 cm diameter) were submerged in NaCl solutions of 0.1, 0.3, 0.5, 1.0 to 2.0 mol/L (M), and a reference deionized water. The slice in each container was used for characterization purposes, as explained below. After 4 months of exposure, when the stabilization of NaCl concentration was achieved, the concentration of the solutions was measured using AgNO₃ potentiometric titration method to measure the amount of bound and free chloride. No further adjustment was made to analyze the isotherms at higher pH and the findings of this study are valid only for the conditions explained here. The solution volume to dried paste ratio was kept at 4 cm³/g.

X-ray powder diffraction (XRD), with Rietveld refinement, was employed to quantify phase assemblage in paste samples after exposure to NaCl solutions or water on the thin slice in the solution. A PANalytical X'Pert Pro MPD diffractometer using Cu-K α source ($\lambda=1.54$ Å) with a fixed divergence slit size of 0.5° was employed. To get a better identification and quantification of Friedel's salt, an equivalent step size of 1 min was used, with a step size of 0.0167 °2 θ . To keep the test duration close to 15 minutes, the samples were scanned from 5° to 40° only. XRD results were coupled with mass balance approach to determine the reaction degree of metakaolin as well as for quantifying the amount of C-A-S-H formed.

To investigate the chloride adsorption on C-A-S-H, the elemental composition of C-A-S-H was determined by SEM-EDX. Paste samples that were exposed to either water or 2 M NaCl solution were dried using solvent exchange method and impregnated in a low viscosity epoxy resin. This drying method is assumed to removing only the free chloride, but not the chemically and physically bound chloride. Through successive grinding and polishing, using diamond abrasives down to 1 μ m size, a flat surface was exposed for the analysis. The carbon-coated polished sections were studied using a FEI quanta 200 scanning electron microscope, equipped with a W-filament operated at an accelerating voltage of 15 kV. Over 200 points per sample were measured to find the average composition of C-A-S-H, and the amount of chloride in C-A-S-H.

Mercury intrusion porosimetry (MIP) (Porotec Pascal 140-440 instruments) up to a maximum pressure of 400 MPa was employed. As before, the solvent exchange drying method was employed. In

addition to the water cured paste sample, selected mixtures were analyzed after exposure to 2 M NaCl solution to investigate if interaction of the binders with chloride ions may affect the porosity of the binders or not. Those mixtures include PC as well as LC³ prepared using clays with 17.0%, 50.3% and 95.0% of calcined kaolinite.

7.4 Results and Discussions

7.4.1 Ponding test profiles

The extent of chloride diffusion in mortar samples after 1 and 2 years of exposure to 3 wt.% NaCl solution is shown in Figure 7.2. It shows that the chloride content is the highest for PC at the surface at the sample but also in depth. All LC³-50 blends show a better chloride resistance to PC, even for the LC³-50 (17.0%) containing 17.0% of calcined kaolinite. The depth of chloride diffused in LC³-50 mortars made using calcined clays with more than 50% of calcined kaolinite content are much lower than that of PC. After 2 years of exposure, chloride ions have reached down to approximately 5 cm in PC mortars, while in LC³-50 mixtures (of 50% and higher kaolinite content), it is only about 1 cm. It is interesting to notice that the chloride content measured at the top surface of the samples is also much higher for PC, which would mean that PC has a higher binder capacity than the LC³-50 blends. However, it is likely that the lack of detailed information at the top surface does not permit to claim such statement. Shi managed to quantify the chloride content at 0.5 mm and 1.5 mm deep [151], and he found that the chloride content was significantly increasing for a ternary blend of calcined clay and limestone and it was reaching values close to the reference PC blend.

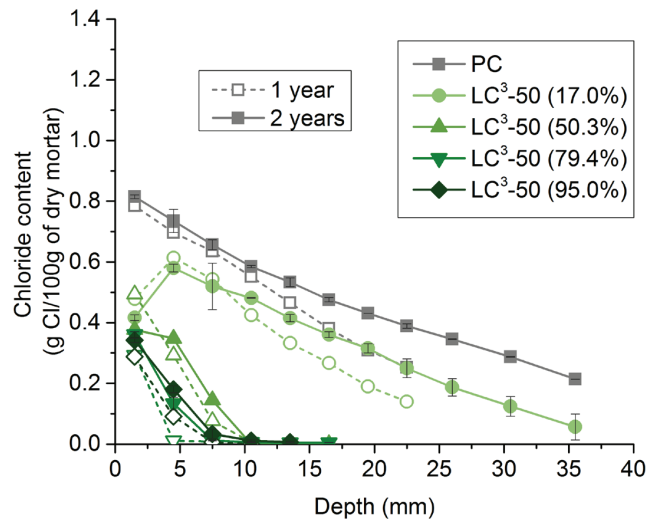


Figure 7.2 Total chloride profiles for PC and LC³-50 mortars after 1 and 2 years of exposure to 3 wt.% NaCl ponding solution.

Profiles of total chloride are plotted in Figure 7.3 on paste samples that were exposed to 3 wt.% NaCl solution for 6 months. The measurements were carried out using μ -XRF method. These re-

sults are globally in agreement with the mortar results in Figure 7.2. In Figure 7.3 (a), the LC³-50 (17.0%) shows a very similar behavior to PC. Only the system with quartz (LC³-50 (0%)) has a worse resistance to chloride than PC. The improvement of the chloride resistance is related to the calcined kaolinite content. The chloride penetration depth decreases faster with increasing the calcined kaolinite content. However, there is no significant gain of using calcined clay with 79.4% and 95.0% of calcined kaolinite compared with LC³-50 (50.3%) and LC³-50 (41.9%).

A better spatial resolution is obtained by μ -XRF compared with chloride titration. The difference at the top surface is slightly lower between PC and the LC³-50 blend (50.3%) for instance compared with mortar samples.

Figure 7.3 (b) shows the comparison between LC³-50 and PPC30 blends. LC³-50 and PPC-30 paste mixtures show comparable resistance against diffusion of chloride ions. Chloride seems to penetrate slightly deeper for the PPC30 (41.9%), whereas a lower chloride content is measured at the surface of the PPC30 (95.0%). Globally the results are similar between PPC30 and LC³-50 blends.

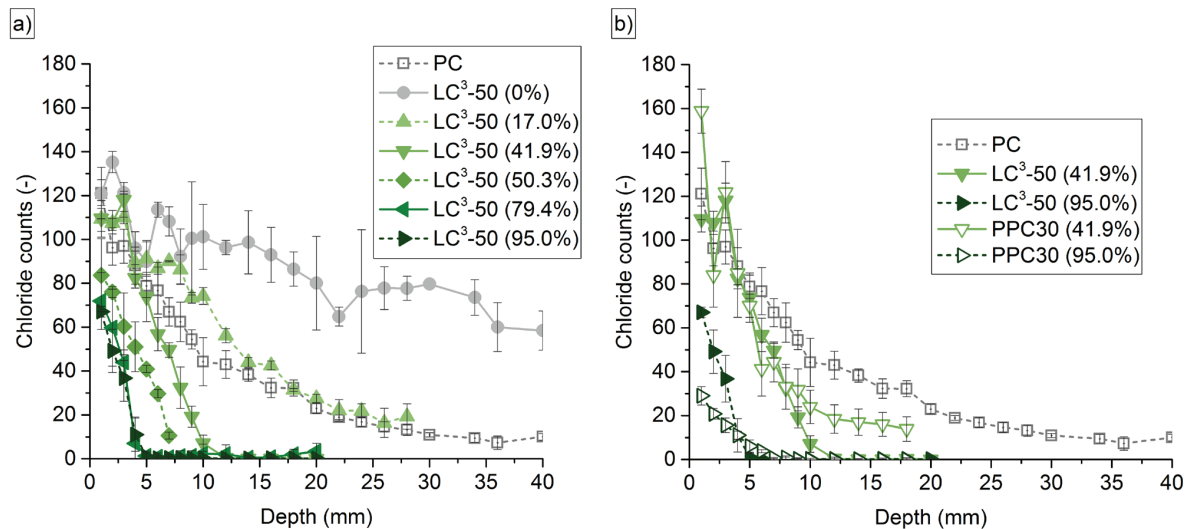


Figure 7.3 Profile of chloride measured using u-XRF method after 6 months of exposure to 3 wt.% NaCl ponding solution for PC and LC³-50 pastes (a), and compared with PPC30 (b).

The apparent diffusion coefficient values corresponding to the ponding test on mortar and on paste are calculated based on total chloride content, using Fick's 2nd law of diffusion according to ASTM C1556. The values are reported in Figure 7.4. The apparent diffusion coefficient decreases with the increase of the calcined kaolinite content of the calcined clay. It is about two orders of magnitude lower for LC³-50 (95.0%) compared with LC³-50 (0%) containing quartz.

Similar trends are obtained for the mortar and the paste samples. However, the apparent diffusion coefficient is about twice higher for paste samples. This could be due to the slightly more advanced hydration for mortar samples (1 year and 2 years). It might also be explained by the higher resolution for μ -XRF samples. The apparent diffusion coefficient is determined from the slope of the chloride profiles. Since μ -XRF gives more points, especially at very low depth, the slope is better captured and is slightly higher compared with profile titration [152].

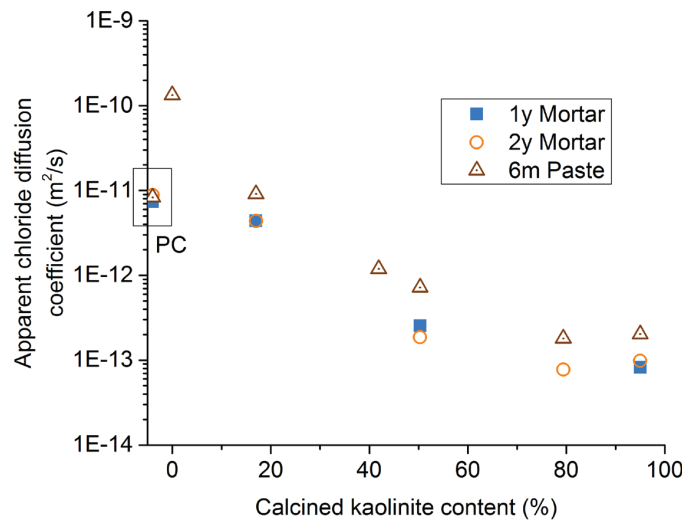


Figure 7.4 Apparent diffusion coefficients for PC and LC³-50 mortar and paste samples, calculated using ASTM C1556 method.

7.4.2 Binding capacity of LC³-50 blends

7.4.2.1 Binding isotherms

Binding of chloride ions to different hydrates, specifically C-A-S-H and AFm phases may also mitigate the rate and extent of chloride diffusion through concrete and ultimately the time of reinforcement corrosion in concrete structures. Binding isotherm curves of the LC³-50 and PPC-30 pastes are plotted in Figure 7.5. As comparison with the ponding test, a line at 0.51 M (3 wt.%) indicates the NaCl concentration used for the ponding test. Figure 7.5 (a) shows that at 0.1 M and 0.3 M NaCl, the total binding in PC is very similar to all LC³-50 blends. At 0.5 M and 1M, LC³-50 (0%), (17.0%) and (95.0%) show a lower binding than the other systems. At 1 M and 2 M, higher binding than PC is measured for LC³-50 blends (41.9%), (50.3%) and (79.4%). Thus, the binding is the highest for calcined clays with 40-80% of calcined kaolinite.

At the concentration of the ponding test (0.51 M), the chloride binding is very similar for PC and the LC³-50 blends with 40%-80% of calcined kaolinite. Thus, the difference observed for these systems in the ponding test may not be explained by a different binding capacity.

The comparison of PPC30 with LC³-50 in Figure 7.5 (b) shows that for the LC³-50 (95.0%), less chloride is bound for the PPC30 (95.0%), whereas the PPC30 (41.9%) seems to have a higher binding capacity than the corresponding LC³-50 (41.9%).

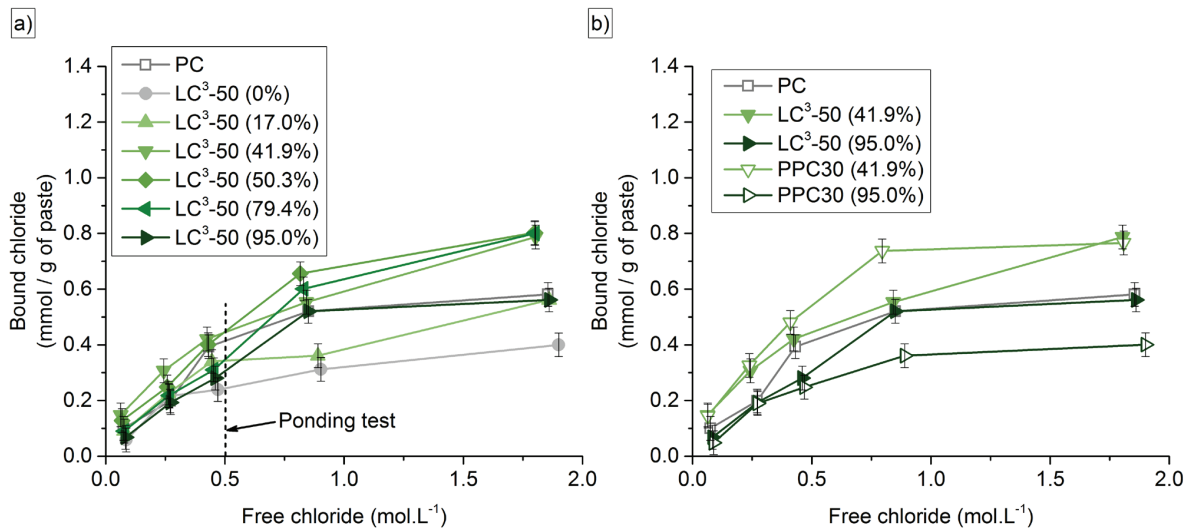


Figure 7.5 Binding isotherm curves for PC and LC³-50 pastes (a), compared with PPC30 (b).

In order to better observe the influence of the grade of calcined clay on the chloride binding, Figure 7.6 shows the bound chloride as a function of the calcined kaolinite content for the different NaCl concentrations. It can be observed that from 0.3 M onwards, the chloride binding is the highest for the calcined clays containing 40%-50% of calcined kaolinite, range which can be extended to 40%-80% at 1 M and 2 M.

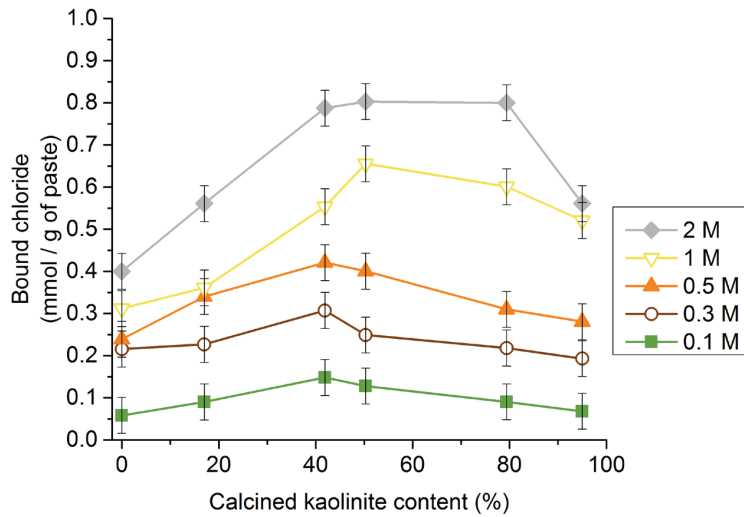


Figure 7.6 Total chloride binding as function of the calcined kaolinite content.

7.4.2.2 Distribution of the bound chloride in the hydrated phases

To understand these binding isotherms results, the phase assemblage study was carried out to determine in which phase the chloride plays a role. The degree of hydration is shown in Figure 7.7, as

well as the amount of reacted metakaolin determined by mass balance. The degree of hydration of clinker decreases with the calcined kaolinite content, whereas the amount reacted metakaolin increases. Concerning the formation of hydration products in Figure 7.8, the amount of C-A-S-H globally increases with the calcined kaolinite content, whereas the amount of carboaluminate hydrates increases up to 41.9% of calcined kaolinite, it is similar up to 79.4% of calcined kaolinite and decreases then. The explanation for this limited formation of carboaluminate hydrates is likely to be the lack of large pores in the microstructure, as discussed in Chapter 4. The same minimum critical pore entry radius of about 2-5 nm is reached for the LC³-50 (50.3%) and (95.0%), as shown in Figure 7.9. In this study, pastes were cast using a water to binder ratio of 0.5. Thus, more space is provided compared to the pastes cast at 0.4 in Chapter 4. Still this lack of big pores is faced at least for the LC³-50 (95.0%) where the formation of carboaluminate hydrates is limited.

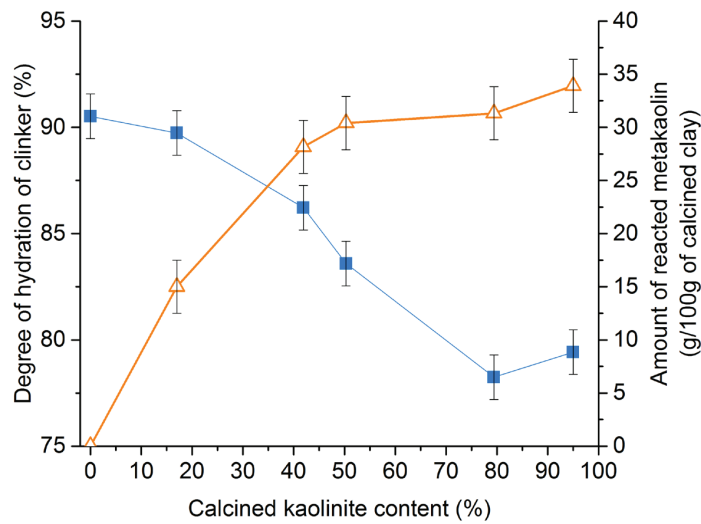


Figure 7.7 Degree of hydration of clinker and amount of reacted metakaolin for the different LC³-50 blends.

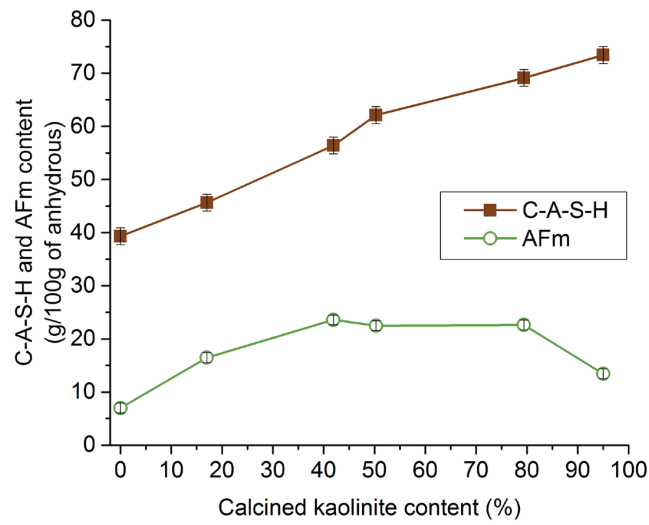


Figure 7.8 Amount of C-A-S-H and carboaluminate hydrates for the different LC³-50 blends.

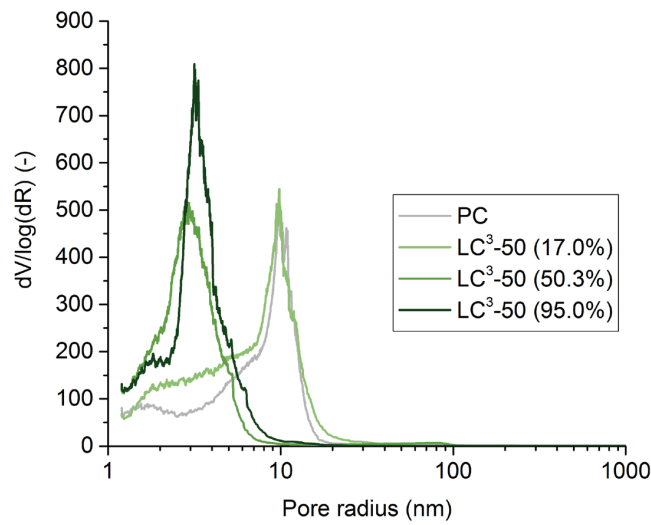


Figure 7.9 MIP results for PC and LC³-50 (17.0%), (50.3%) and (95.0%).

The amount of Friedel's salt shown in Figure 7.10 (a) for the different NaCl concentrations, in parallel to the amount of carboaluminate phases in Figure 7.10 (b). Significant amount of Friedel's salt already form in 0.1 M NaCl solution, consuming most of the amount of carboaluminate hydrates. The amount of Friedel's salt is higher in LC³-50 containing calcined clays with 40%-50% of calcined kaolinite, which originates from the higher amount of carboaluminate phases in these systems.

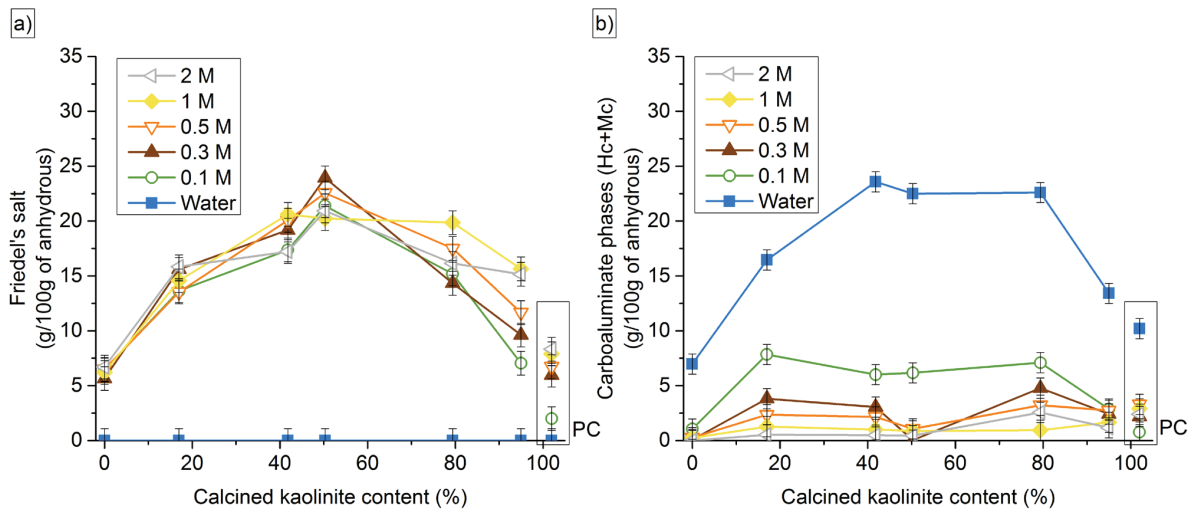


Figure 7.10 Amount of Friedel's salt (a) and carboaluminate phases (b) in PC and LC³-50 pastes.

It should be noted that in this study, the binding experiment was carried out on paste samples with a water to binder ratio of 0.5, unlike other studies where a higher water content was used. The use of w/b of 0.5 limits hydration of the solids, yet has the advantage of better representing the real microstructure that develops in concrete. If higher w/b was allowed, perhaps the degree of hydration of clinker and the amount of reacted metakaolin would become higher, which could have resulted in higher binding capacity of the pastes.

In order to get the complete distribution of the bound chloride in the different samples, the amount of chloride adsorbed on C-A-S-H can be obtained as the difference between the total bound chloride in Figure 7.5 and the amount of Friedel's salt in Figure 7.10. This distribution is shown for PC and the different LC³-50 blends in Figure 7.11 at 1 M and 2 M. The determination of the chloride content in Friedel's salt at low NaCl concentrations (0.1 M, 0.3 M and 0.5 M) is challenging due to the coexistence of solid solutions of Mc (or Hc) and Friedel's salt [141]. This is shown on XRD patterns of the pastes, presented in Appendix 6. The peak around 11.7 2 θ° corresponds to Mc phase, which after exposure to NaCl of low concentration shifts towards lower angle, and by increasing the NaCl concentration shifts back to the theoretical position of pure Friedel's salt, when Friedel's salt is completely replacing Mc. The LC³-50 (17.0%) even shows at 0.1 M and 0.3 M two peaks within 10.5-11.5 2 θ° , indicating the coexistence of two phases, most probably Friedel's salt and a solid solution of Mc and Friedel's salt. Thus, the accurate amount of chloride bound to Friedel's salt is not straightforward to obtain at low NaCl concentrations.

In Figure 7.11, the error for quantification of Friedel's salt in XRD is found to be ± 1.1 g Friedel's salt in 150 g paste (100 g initial solid). The error for total bound chloride, measured using AgNO₃ titration is also found to be 0.05 mmol Cl per g dried paste. These errors affect the bar charts.

The results evidence that the binding of chloride ions occurs in Friedel's salt and in C-A-S-H. In LC³-50 pastes, the binding of chloride is dominated by the chloride bound to Friedel's salt, whereas

the chloride for the reference PC is mainly adsorbed on C-A-S-H. For PC, the lower initial amount of AFm phase is the reason for the lower formation of Friedel's salt.

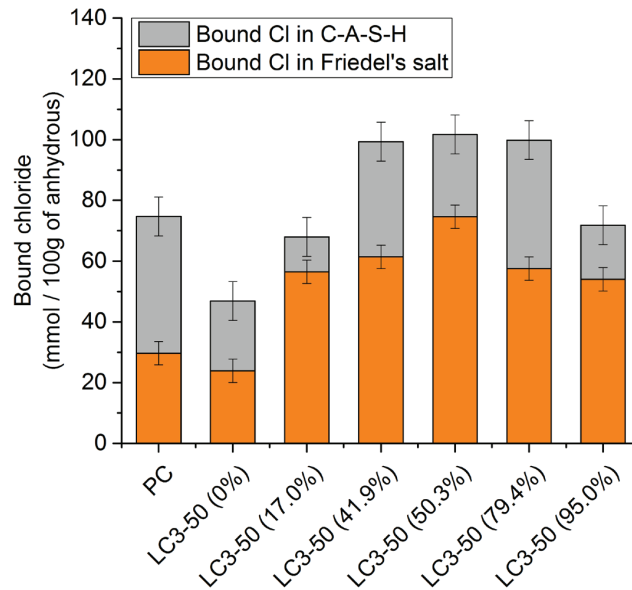


Figure 7.11 Distribution of bound chloride between C-A-S-H and Friedel's salt in PC and in the different LC³-50 pastes.

One way to verify that the chloride content adsorbed on C-A-S-H in Figure 7.11 is correct is to calculate this amount, knowing the total C-A-S-H formed by mass balance, and the Cl/Ca ratio of the C-A-S-H. Figure 7.12 shows the atomic composition of the C-A-S-H for samples stored in water and in 2 M NaCl solution. Al/Ca versus Si/Ca and Al/Ca versus Cl/Ca atomic ratios are shown in Figure 7.12 (a) and (b), respectively, for PC and LC³-50 (17.0%), (50.3%) and (95.0%). The interaction with chloride ions does not change the composition of C-A-S-H, except for the chloride adsorption which is observed for all samples stored in 2 M NaCl solution. A slightly higher Cl/Ca is measured for the LC³-50 (95.0%) and PC.

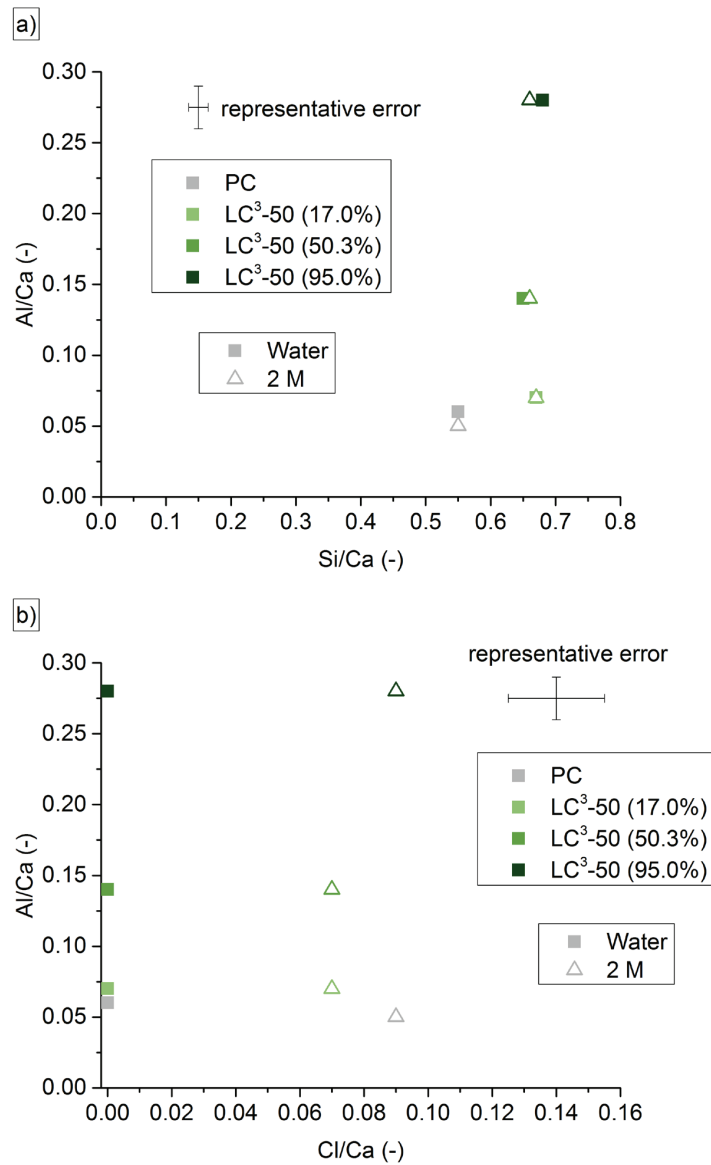


Figure 7.12 (a) Al/Ca versus Si/Ca and (b) Al/Ca versus Cl/Ca atomic ratios of C-A-S-H for PC and LC³-50 pastes stored in water or in 2 M NaCl solution.

The correlation of the amount of adsorbed chloride measured experimentally and calculated as the difference of the total bound chloride and the chloride incorporated in Friedel's salt is shown in Figure 7.13. The dashed line indicates the ideal fit. A good correlation is obtained for PC and the LC³-50 (17.0%) and LC³-50 (50.3%) blends. However, some deviation is observed for LC³-50 (95.0%) sample. This could be due to the difficulty of accurately measuring the Cl/Ca for this system due to the fine intermixing of metakaolin particles with C-A-S-H observed for this system.

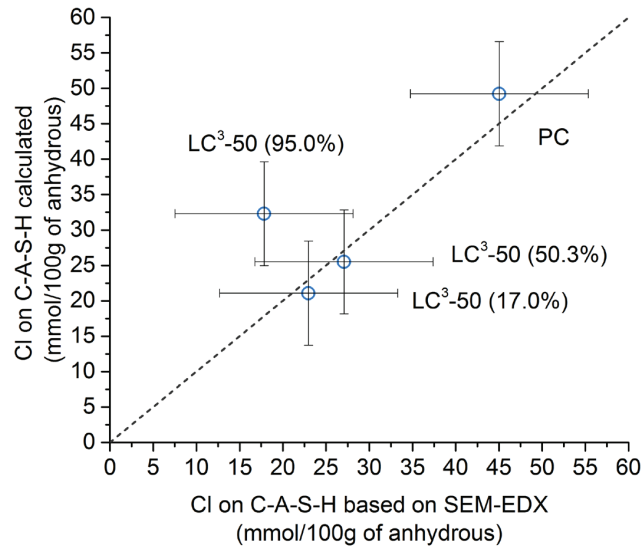


Figure 7.13 Amount of adsorbed chloride on C-A-S-H determined experimentally by SEM-EDX and calculated as the difference of the total bound chloride and the chloride in Friedel's salt.

7.4.3 Porosity results

MIP cumulative and derivative results in Figure 7.14 (a) and (b) show that the interaction of the binders with chloride ions does not significantly affect the porosity. Significant refinement of porosity is observed for LC³-50 (50.3%) and (95.0%) compared to PC for samples stored in water or in the 2 M NaCl solution. The samples stored in the 0.5 M NaCl (concentration of the ponding test) are likely to also show similar porosity distribution. This refinement of pore connectivity is in good agreement with the ponding results obtained in Figure 7.2, i.e. a smaller critical pore entry radius leads to a lower apparent diffusion coefficient. The critical pore entry radius of PC and LC³-50 (17.0%) is very close, as well as their apparent diffusion coefficient. The same observation can be made for the LC³-50 (50.3%) and LC³-50 (95.0%) blends.

Since the binding is quite similar for all systems at 0.5 M NaCl solution, the difference in ponding results can be explained by the significant differences in terms of pore refinement.

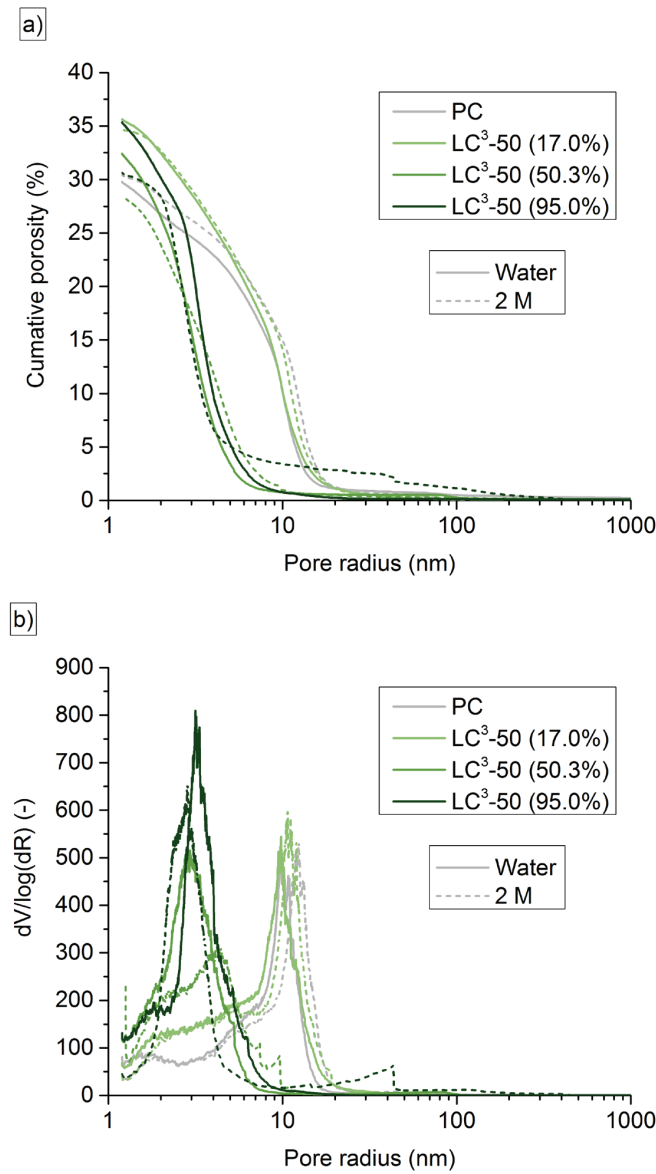


Figure 7.14 Cumulative (a) and derivative (b) pore structure of PC and LC³-50 (17.0%), (50.3%) and (95.0%).

7.5 Conclusion

The chloride resistance of LC³-50 blends with more than 40% of calcined kaolinite is significantly improved compared with PC. The apparent diffusivity values are calculated to be 1-2 order of magnitude lower than PC. This is mainly attributed to the refined porosity of the binders when calcined kaolinitic clays are used.

The binding of chloride ions to monocarboaluminate phase is evident. The amount of Friedel's salt is related to the initial amount of AFm phases present in the samples. Also, some of the bound chloride is physically bound to C-A-S-H.

Thus, this study demonstrated the feasibility of using widely-available calcined kaolinitic clays with a calcined kaolinite content of 40%-50% as clinker substitute. These calcined clays can be found in many locations worldwide, where substantial improvement with regards to chloride penetration can be achieved.

Chapter 8 - Conclusion & perspectives

The thesis aimed to investigate the feasibility of using various grades of calcined kaolinitic clays as clinker substitute in LC³ in terms of strength and chloride resistance.

8.1 Final summary

8.1.1 Understanding of factors controlling reactivity

- 46 clays collected from different places around the world were characterized and their reactivity was assessed through a benchmark test of calcined clay strength. Compressive strengths are linearly correlated with the calcined kaolinite content up to 7 days, showing that the calcined kaolinite content is the overwhelming parameter controlling the strength development of the LC³-50 blends. Other factors such as the fineness, the specific surface, the calcination process or the secondary phases of the calcined clays do not significantly impact the strength development.
- Moreover, similar compressive strength to PC is obtained already at 3 days for LC³-50 containing fairly pure metakaolin. From 7 days onwards, the use of clays with 40% of calcined kaolinite or more reach strengths higher than PC, demonstrating the potential of using these widely-available clays as clinker substitute.
- From 7 days onwards, the strength increase with the calcined kaolinite content becomes less significant for the clays with more than 45% of kaolinite content. Thus, there is no major gain of using fairly pure metakaolin rather than clays of 40-50% of calcined clays.
- In parallel to this benchmark test, a new R³ reactivity test was developed in order to predict in a much faster way the reactivity of calcined clays. To ensure high pozzolanic reactivity and similar environment conditions as a hydrating LC³-50 blend, the optimal mix design by mass was found to be 0.06 SO₃ / calcined clay, 0.08 K₂O / calcined clay with a portlandite to calcined clay ratio of 3. Based on isothermal calorimetry test at 40°C, linear correlations were obtained between compressive strength and the heat release after only 24 h of reaction, showing the relevance of the test. To make this test even more practical and universal without any need of a calorimeter or any other expensive equipment, an alternative way of measuring the reactivity was designed simply using an oven. Good correlations with mortar strength were obtained within 3 days of testing. Thus, instead of waiting for 28 days to get the reference strength of LC³-50 mortar, the R³ permits to get after 24 h by isothermal calorimetry or after 3 days for the oven method a reliable indication on the reactivity of calcined clay.

8.1.2 Phase assemblage study

- To fully characterize the hydration of LC³-50 blends, a reliable method to determine the amount of reacted metakaolin was required. Mass balance permits to get the most reliable results compared with thermodynamic modelling and PONKCS method. Thermodynamic modelling underestimates the amount of reacted metakaolin at late ages because of the model used as C-S-H in GEMS, which fixes the Ca/Si to 1.63. The experimental values obtained for the LC³-50 blends are lower (from 1.49 to 1.58). Despite its very fast experiment time, higher deviations were obtained with PONKCS. Quite similar results of reacted metakaolin were obtained for LC³-50 blends containing more than 60% initially present in the calcined clay. Below this value, the small amount of unreacted metakaolin left in the sample was too small to be accurately quantified.
- The hydration study of LC³ showed that the calcined kaolinite content significantly influences the kinetics and the phase assemblage. The higher the calcined kaolinite content, the faster the refinement of pore connectivity until a maximum refinement of the critical pore entry radius of about 3-5 nm was reached. From this point, the growth of hydration products is limited by the increase of the supersaturation level required. This limit is reached at 3 days of hydration for LC³-50 blends containing calcined clays with more than 65% of calcined kaolinite. From this age, the clinker hydration is significantly slowed down. This lack of large pores also limits the formation of carboaluminate hydrates for these blends. As a consequence, the on-going reaction of metakaolin of the calcined clay leads to the increase of the aluminium in the pore solution. Following the pore solution composition, the aluminium incorporation in the C-A-S-H increases.
- The main difference observed for the C-A-S-H between PC and LC³-50 blends was the significant change of composition, especially concerning the aluminium incorporation increasing with the calcined kaolinite content. The morphology and the density of the C-A-S-H were found to be very similar between PC and the LC³-50 containing different calcined clays.
- Concerning the relationship between strength and phase assemblage, a first attempt using porosity results did not permit to get a clear correlation, due to the limit of refinement of pore connectivity reached already at 3 days for LC³-50 blends with calcined clay with more than 65% of calcined kaolinite. The gel space ratio approach was then used and a good relationship was obtained with compressive strength, considering either C-A-S-H as gel (C-A-S-H intermixed with porosity as weakest point of the microstructure), or considering unreacted metakaolin and limestone particles as part of the gel (fine soft inclusions acting similarly to C-A-S-H due to similar elastic properties).
- The lower increase of mortar strength with the calcined kaolinite content at late ages can be explained by the decrease of the clinker hydration and the quite similar amount of reacted metakaolin with the increase of the calcined kaolinite content of the calcined clay.

8.1.3 Evaluation of chloride resistance

- For ponding test in 2M NaCl, LC³-50 blends with calcined clays with at least 40% of calcined kaolinite show better resistance than plain PC. The diffusivity coefficient calculated from these ponding tests is 1 order of magnitude lower for LC³-50 with 95% of calcined kaolinite compared with PC. These results are in good agreement with porosity results, and especially with the refinement of pore connectivity. The higher the calcined kaolinite content, the higher the porosity refinement, the higher the chloride resistance.
- The influence of the binding does not play a major role in the chloride resistance. The binding is the highest for blends with about 50% of calcined kaolinite, because this system shows the highest formation of carboaluminate hydrates, which is then converted into Friedel's salt. For PC and the blend with the fairly pure metakaolin, the formation of Friedel's salt is limited due to the limited formation of AFm phases (due to the lack big pores for the LC³-50 blend). Chloride adsorption on C-A-S-H is observed for all systems.

8.2 Perspectives

8.2.1 Strength development

- More work is currently underway to enhance the early-age strength of LC³-50. Alkali addition is a way of accelerating clinker and SCM reactions. An optimized alkali adjustment could maybe permit to get higher strength, while maintaining similar strength to PC at later ages.
- Another strategy would consist of improving the initial packing of LC³-50 blends. In this study, the limestone and the clinker used showed similar size distribution, and most of calcined clays were also covering the same range of size. With a better packing working at constant flow, the space filling could be optimized and the porosity could be reduced.
- The enhancement of reactivity could also be promoted using grinding aids. The grinding of LC³ is quite challenging due to the different materials used. Intergrinding is not ideal because the soft SCMs will be ground very fine while the clinker remains coarse. Separate grinding would be more efficient, but it is less economically-viable. Grinding aids would permit us to improve the intergrinding by preventing the agglomeration of fine particles. This would permit to adequately grind the clinker. Some type of grinding aids also seem to accelerate the hydration of specific phases, such as C₄AF of clinker. The influence of the grinding aids on the reactivity of clinker and metakaolin could thus be investigated.
- Since higher strengths than PC are obtained for clays with more than 60% of calcined kaolinite, the clinker content could be further decrease to 45% or even 40% to see if further CO₂ savings could be feasible. The lack of portlandite is likely to limit the reaction of metakaolin of the calcined clay. Moreover, part of the unreacted metakaolin could be replaced by limestone to improve rheology and reduce the cost of the blended cement.

8.2.2 Microstructure development

- The lack of large pores responsible for the slowing down of clinker hydration and the limited formation of carboaluminate hydrates is observed for the sealed samples at a w/b of 0.4. It would be interesting to increase the space available by increasing the water to binder ratio to see until which water to binder ratio the space limits the hydration progress. A first insight is given by the chloride study where 0.5 was used. It showed that the formation of carboaluminate hydrates was still limited for the LC³-50 containing the fairly pure metakaolin, and that the degree of hydration of clinker was decreasing with the calcined kaolinite content of the calcined clay.
- Concerning the porosity investigation, in addition to MIP technique, ¹H-NMR results could also be compared with nitrogen adsorption measurements to investigate if the pore size obtained is in good agreement for both techniques.

8.2.3 Durability

- Concerning the durability, an on-going study is carried out to investigate the influence of the calcined kaolinite content on the carbonation resistance of the LC³-50 blends. Natural carbonation is studied for different curing times, different storage conditions and different climates. Carbonation is expected to be worse than PC for any SCMs for the same curing time and same humidity conditions due to the lower amount of carbonatable phases in blends. However, a comparison with other SCMs will be done to observe the behaviour of LC³-50 blends compared with fly ash or slag.

Appendix

9.1 Appendix 1 : Cements and sulfate adjustment

9.1.1 Grey cement

The cement used in this study is a commercial clinker specially ground with anhydrite from Heidelberg cement, classified as CEMI 42.5R. Several batches were used for the whole study. Each time a new batch was received, the reactivity was compared with the previous ones. Compressive strengths are shown in Figure 9.1. Minor differences were measured between the different batches.

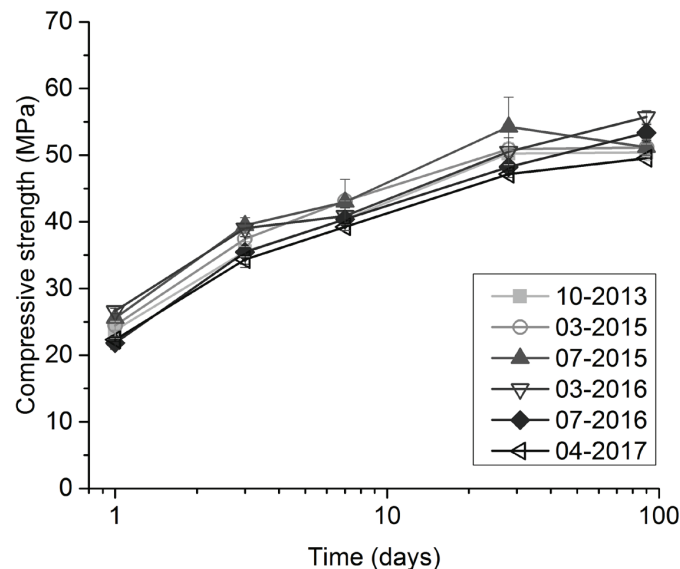


Figure 9.1. Compressive strength of the different batches of reference PC.

9.1.2 Sulfate adjustment for grey and white cement

To prevent undersulfation and to optimize early-age strength, the sulfate content needs to be adjusted in calcined clay blends [43]. The adequate sulfate content was obtained by adding gypsum to the blends. The adjustment was done on both grey and white cements. The gypsum used for this study is a 98 % + grade from Acros company.

9.1.2.1 Grey cement

1 %, 2 % and 3 % were added respectively and Figure 9.2 shows the influence of this gypsum addition on the heat flow curves obtained by isothermal calorimetry for LC³-50 (95.0%). The appropriate gypsum adjustment was defined when it was possible to distinguish the silicate and aluminate peak on heat flow curves. Thus, a 2 % extra addition is found to be required to avoid the undersul-

fation of calcined clay blends. Since this calcined clay has the highest metakaolin content, this system is the upper limit for gypsum addition, i.e. there is no undersulfation using clays with lower metakaolin content. The same gypsum was applied to all calcined clay blends. The final amount of sulfate present in the calcined clay blends correspond to the initial sulfate from the anhydrite of the cement and from this extra-addition of 2 % of gypsum.

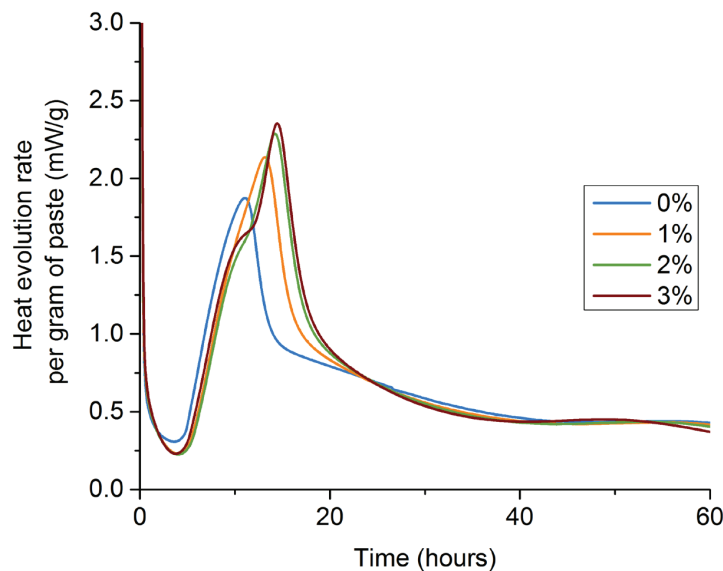


Figure 9.2. Influence of gypsum addition on the heat flow of LC³-50 (95.0%) blend.

9.1.2.2 White cement

For white cement, similar adjustment to grey cement was carried out. However, before adjusting sulfate level, the alkali content was adjusted to reach similar level to the grey cement. The influence of the alkali addition on the heat flow curves is shown in Figure 9.3 (a) for WPC and in Figure 9.3 (b) for WLC³-50 (95.0%). For reference WPC blend, it is not possible anymore to distinguish the silicate from the aluminate peak. The addition of 2% of sulfate permits to separate these two peaks. For WLC³-50 blends, 3% of gypsum was necessary to observe the separation between the two peaks.

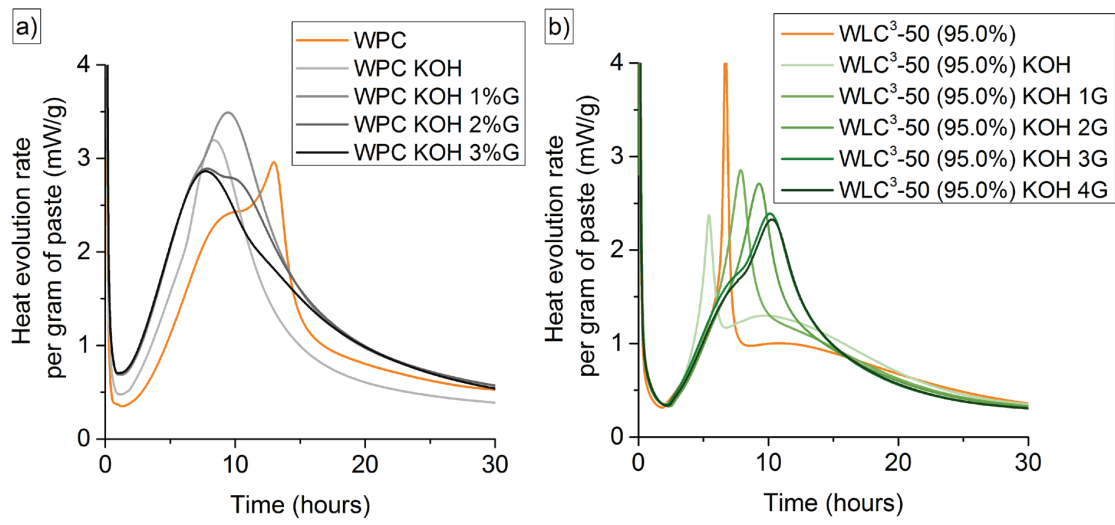


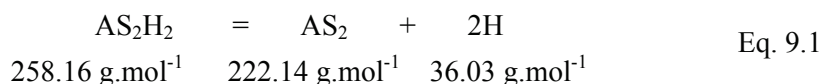
Figure 9.3. Influence of alkali and sulfate addition on the heat flow curves of reference WPC (a) and WLC³-50 (95.0%) blend (b).

9.2 Appendix 2 - Characterization of raw and calcined clays

9.2.1 Kaolinite content, calcined kaolinite content and metakaolin content

9.2.1.1 Kaolinite content in raw clay

The dehydroxylation of kaolinite (AS_2H_2) occurs from 400 °C to 650 °C [15, 16], leading to the formation of the metakaolin phase (AS_2), according to Equation 9.1.



The initial kaolinite content of each raw clay $wt\%_{kaolinite}$ was calculated according to Equation 9.2 by Thermogravimetric Analysis (TGA) using tangent method from the weight loss over the kaolinite dehydroxylation interval, defined as $wt\%_{kaol-OH}$, where $M_{kaolinite}$ and M_{water} stand for the molecular mass of kaolinite and water, respectively. TGA experiments were repeated three times for each clay, with an average deviation of 1.1%.

$$wt\%_{kaolinite} = wt\%_{kaol-OH} \times \frac{M_{kaolinite}}{2M_{water}} \quad \text{Eq. 9.2}$$

9.2.1.2 Calcined kaolinite content

TGA experiments were also run on all calcined clays to assess the calcination efficiency. Some of the clays calcined by the material supplier were found not to be entirely dehydroxylated. Consequently the calcined kaolinite content was defined as the part of kaolinite which was dehydroxylated during the calcination process. This parameter was calculated by taking the difference between the kaolinite content before and after calcination. However, the basis of kaolinite content in calcined clays is not the same as in raw clays, since the sample mass does not remain constant during the calcination process due to the water loss. Figure 9.4 gives an example of this basis change for a pure kaolinitic clay in which only half of kaolinite is dehydroxylated. During calcination, 50 % of kaolinite transforms into 43.4 % of metakaolin and 6.6 % of water. The amount of unreacted kaolinite in the calcined clay given by TGA is not 50 %, but $50/(50+43.4)\%$ because of the water evaporation.

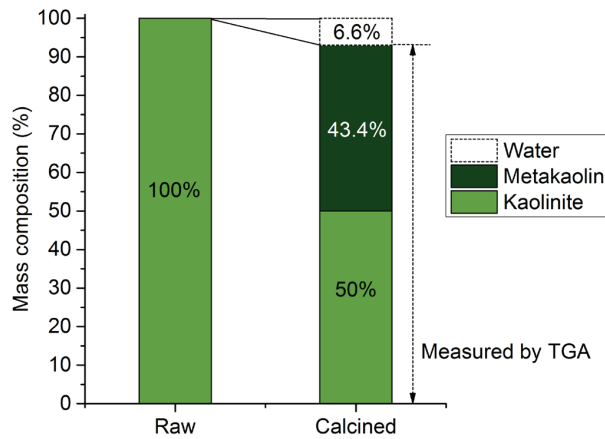


Figure 9.4. Basis change of unreacted kaolinite in calcined clay.

Thus, the amount of unreacted kaolinite in the calcined clay has to be normalized as shown in Equation 9.3, based on the remaining water loss in calcined clay corresponding to kaolinite dehydroxylation $wt\%_{kaol-OH, calcined}$.

$$wt\%_{calcined\ kaolinite} = wt\%_{kaolinite} - wt\%_{kaol-OH, calcined} \times \frac{M_{kaolinite}}{2M_{water}} \times \left(\frac{100 - wt\%_{kaol-OH, calcined}}{100} \right) \quad \text{Eq. 9.3}$$

9.2.1.3 Metakaolin content in calcined clay

The metakaolin content is used in Chapter 3 to consider the reactive phase of calcined kaolinitic clays and it is meaningful for the determination of the reaction degree of metakaolin phase. The metakaolin content in calcined clay $wt\%_{metakaolin}$ is obtained by determining the maximum metakaolin obtainable in the raw clay, similar to Equation 9.2 for kaolinite but considering the molecular mass of metakaolin $M_{metakaolin}$. This metakaolin value calculated from the raw clay has to be normalized on a calcined clay basis, contrary to the calcined kaolinite content. Figure 9.5 shows an example for a pure kaolinitic clay. The estimation of the metakaolin content from the raw clay gives 86.7 %, whereas the calcined clay is composed of 100 % of metakaolin. The reason for this difference comes from the water evaporation which is not taken into account before the normalization.

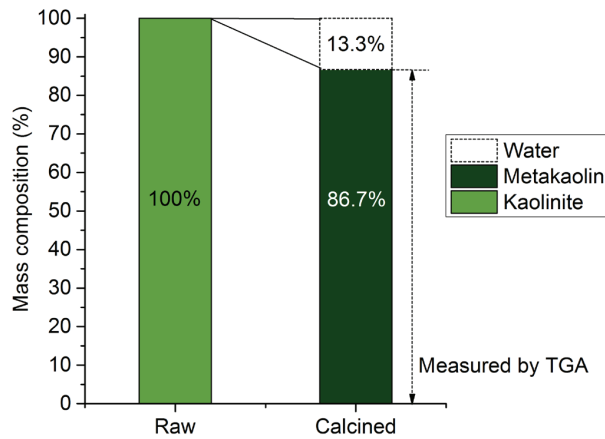


Figure 9.5. Basis change from raw to calcined clay.

In case of incomplete calcination, the amount of uncalcined material was subtracted based on the remaining water loss corresponding to kaolinite dehydroxylation $wt\%_{kaol-OH, calcined}$.

$$wt\%_{metakaolin} = wt\%_{kaol-OH, raw} \times \frac{M_{metakaolin}}{2M_{water}} \times \left(\frac{100}{100 - wt\%_{kaol-OH, raw}} \right) - wt\%_{kaol-OH, calcined} \times \frac{M_{metakaolin}}{2M_{water}} \quad \text{Eq. 9.4}$$

9.2.2 Influence of other clays on kaolinite quantification by TGA

A source of error of the kaolinite content determination by TGA can come from the presence of other types of clays as secondary phases in the clay which also partially dehydroxylate over this temperature range [22]. To investigate the influence of these other clays, high-grade illite, muscovite and montmorillonite were studied. The kaolinitic clay contains 79.4% of kaolinite. An 85%-grade illitic clay and montmorillonitic clay from Wards company are used. The muscovitic clay is provided by ABCR. Figure 9.6 shows the XRD patterns of these clays.

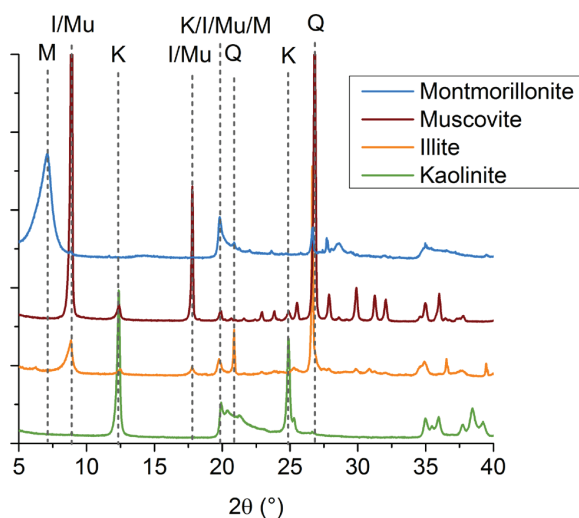


Figure 9.6. XRD patterns of clays rich in kaolinite, illite, muscovite and montmorillonite.

The TGA curves for these clays is shown in Figure 9.7. It shows that with the increase of temperature, montmorillonite first loses the water present in the interlayer space from 30 °C to approximately 150 °C. Then, the four clays lose their structural water from 400 °C to 650 °C for kaolinite, from 450 °C to 700 °C for illite, from 550 °C to 700 °C for montmorillonite and from 650 °C to 900 °C for muscovite. These results are in agreement with Fernandez [45].

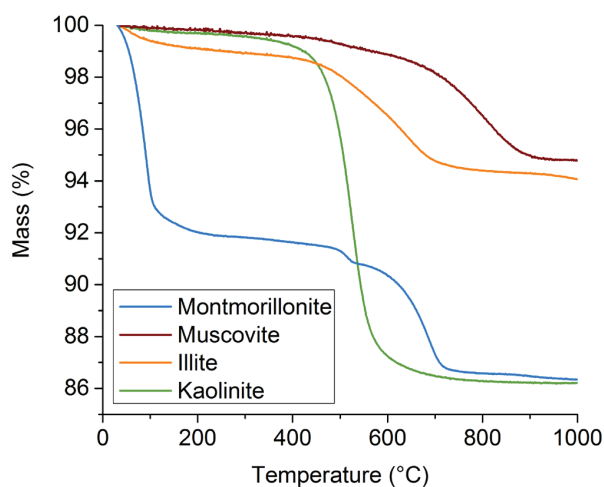


Figure 9.7. TGA of clays rich in kaolinite, illite, muscovite and montmorillonite.

Thus, the main clay interfering with kaolinite dehydroxylation is the illitic clay. Several mixes of this clay with the kaolinitic clay were prepared and analysed by TGA. 25 %, 50 %, 75 % of the kaolinitic clay was substituted by the illitic clay. Figures 9.8 and 9.9 show the TGA and DTG curves for the different mixes. With the increase of the content of the illitic clay, the total water loss decreases.

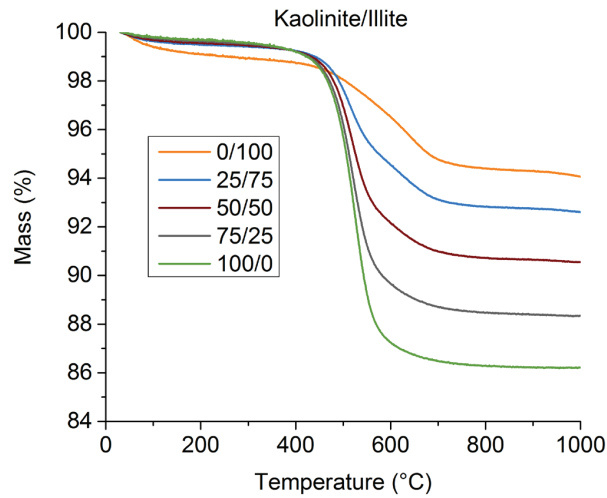


Figure 9.8. TGA curves of the mix kaolinitic clay / illitic clay.

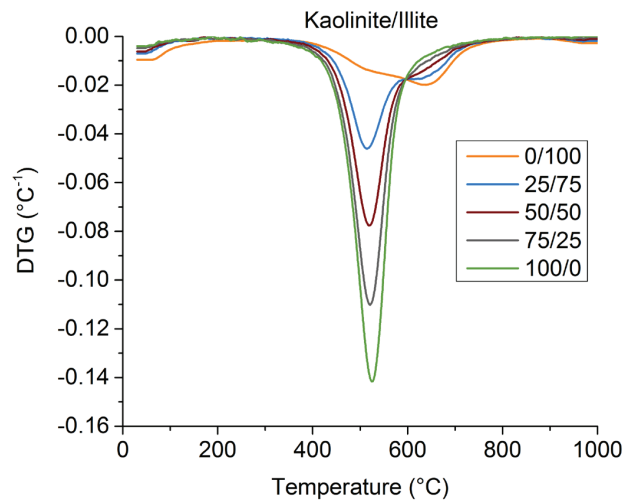


Figure 9.9. DTG curves of the mix kaolinitic clay / illitic clay.

The kaolinite content obtained by TGA is then compared with the theoretical one in Figure 9.10. An excellent correlation is found. The maximum deviation is found for the mix containing 75 % of illitic clay for which the difference of kaolinite content between the measured and the theoretical values is 2.65 %. Thus, the kaolinite content is not significantly impacted by the presence of illite as main secondary phase.

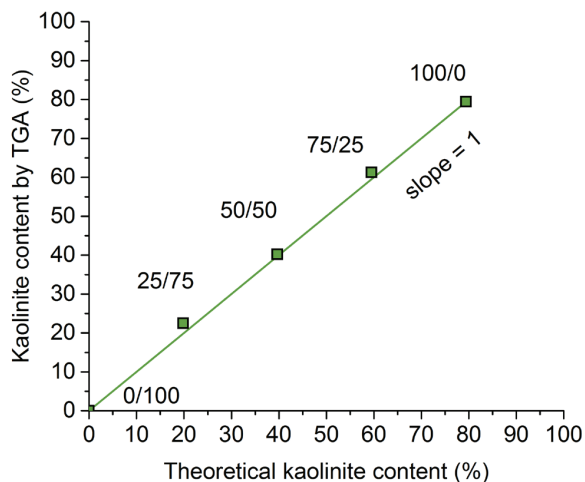


Figure 9.10. Determination of the kaolinite content by TGA in the mixes containing different kaolinitic to illitic fractions.

9.2.3 Comparison of kaolinite quantification between XRD-Rietveld and TGA

X-Ray Diffraction is a more widely used technique than TGA to quantify the kaolinite content of clays. However, the quantification of kaolinite by XRD-Rietveld method is very challenging due to the structure of kaolinite, in which extensive layer-disorder and preferred orientation are observed. For the different clays used in this study, the comparison of kaolinite content between TGA and XRD-Rietveld is shown in Figure 9.11. For most of clays, the kaolinite content obtained by TGA is in agreement with XRD-Rietveld. However, significant differences are also observed (max. 29.8 %). An average absolute difference of 6.1 % is measured.

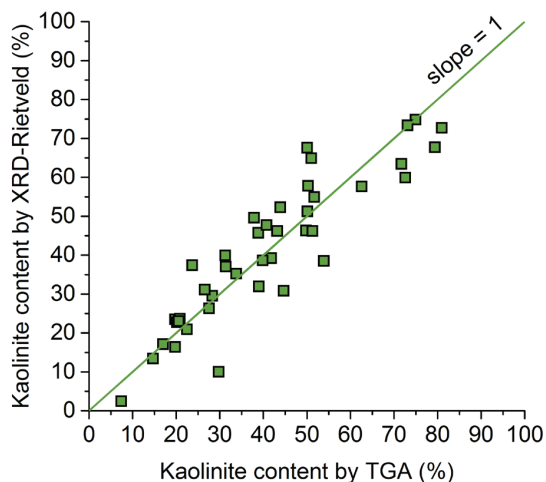


Figure 9.11. Comparison of kaolinite content obtained by XRD-Rietveld and TGA.

9.2.4 Calcination protocol

Most of clays were not ground when received. To remove the moisture from clays to ensure an efficient grinding, the clays were first stored over night in an oven at 90 °C. Clays were then crushed and then ground using a disc mill (Siebtechnik TS250) for 1 minute. Some of the clays were calcined by external companies using flash or static calcination. Most of the clays were calcined in our laboratory, about 1 kg per batch, in alumina crucibles. The crucibles were then heated at 800 °C for 1 h in a high-temperature furnace (Borel FP1100). This calcination temperature was chosen to ensure a complete dehydroxylation of kaolinite and to get the highest pozzolanic potential of calcined clay [16, 22, 153, 154]. The temperature profile of the heating step, the storage at 800 °C and the air quenching is shown in Figure 9.12.

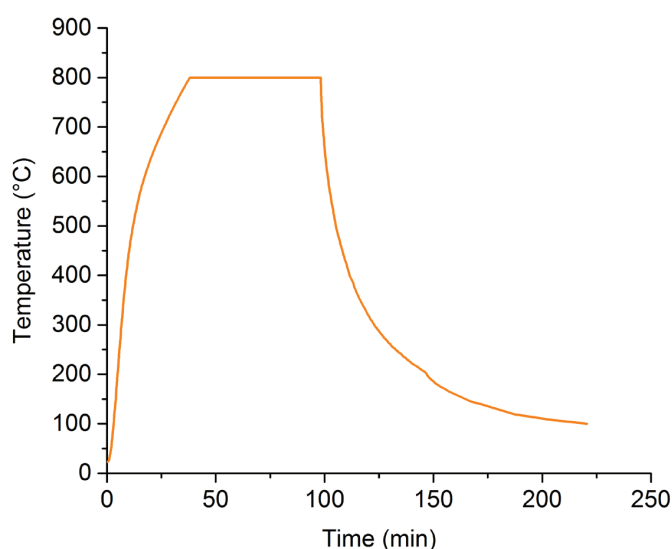


Figure 9.12. Temperature profile during the calcination of clay.

9.2.5 Physical properties and XRF chemical composition of calcined clays

The origin, the calcination process, the calcined kaolinite content, the $D_{v,50}$ measured by laser diffraction, the specific surface area measured by nitrogen adsorption for all calcined clays are shown in Table 9.1. Table 9.2 indicates the chemical composition obtained by XRF.

Table 9.1. Origin, kaolinite content and physical properties of calcined clays.

Calcined clay	Origin of clay	Calcination	Calcined kaolinite content (%)	D _{v,50} (µm)	Span (-)	BET Specific surface (m ² /g)
1	North America	Flash	95.0	5.1	3.8	9.6
2	South America	Flash	91.0	5.9	3.5	15.9
3	South Asia	Furnace	79.4	5.3	5.4	15.3
4	South America	Flash	77.0	5.6	5.7	11.7
5	East Asia	Furnace	74.9	-	-	-
6	South Asia	Furnace	72.6	8.0	7.9	14.4
7	South Asia	Furnace	71.7	27.0	2.7	28.0
8	Central Africa	Furnace	66.4	27.4	6.8	50.1
9	South America	Flash	66.2	4.0	7.4	12.9
10	South Asia	Furnace	62.6	25.3	10.1	15.2
11	South America	Furnace	61.2	7.4	7.6	47.2
12	East Asia	Furnace	61.1	16.6	2.1	-
13	Carribbean	Furnace	59.2	5.7	4.5	33.9
14	South America	Furnace	53.9	7.8	6.2	-
15	East Asia	Furnace	53.8	-	-	-
16	South Asia	Rotary kiln	51.3	7.8	6.2	9.2
17	Carribbean	Furnace	51.0	4.6	4.3	35.7
18	South-east Asia	Furnace	50.3	10.9	3.7	45.7
19	South America	Furnace	50.1	-	-	-
20	South America	Furnace	49.8	-	-	-
21	Western Asia	Furnace	44.7	-	-	-
22	South America	Furnace	43.9	-	-	-
23	South America	Furnace	43.2	13.3	15.0	29.1
24	Europe	Furnace	41.8	9.1	3.1	22.7
25	Western Asia	Furnace	40.0	4.5	1.4	-
26	South Asia	Furnace	39.0	10.8	4.9	11.2
27	Carribbean	Furnace	38.9	8.5	3.1	23.1
28	South America	Furnace	37.9	-	-	-
29	South America	Furnace	35.0	23.5	11.5	18.5
30	North America	Furnace	33.8	20.8	4.1	12.5
31	Carribbean	Furnace	31.4	4.6	5.6	71.7
32	South America	Furnace	31.3	7.5	3.7	12.2
33	Carribbean	Furnace	30.8	3.8	5.5	20.0
34	Europe	Furnace	29.8	-	-	-
35	South America	Furnace	28.3	5.6	5.7	19.3
36	Europe	Furnace	27.6	4.2	6.6	45.8
37	West Africa	Furnace	26.6	15.2	10.7	23.4
38	West Africa	Furnace	23.7	20.5	3.7	21.1
39	Carribbean	Furnace	22.4	8.2	3.1	-
40	East Asia	Furnace	21.8	16.4	3.7	4.4
41	Western Asia	Furnace	20.6	7.7	7.2	-
42	West Africa	Furnace	20.2	29.7	4.7	13.3
43	South Asia	Furnace	17.0	5.9	4.7	18.7
44	Southern Africa	Flash	15.0	8.9	2.6	4.7
45	North America	Furnace	14.8	25.1	7.2	4.7
46	Western Asia	Furnace	7.4	-	-	-
Quartz	-	-	0.0	11.2	2.4	1.2

Appendix

Table 9.2. XRF chemical composition of calcined clays.

Calcined clay	SiO ₂	Al ₂ O ₃	Fe ₂ O ₃	CaO	MgO	SO ₃	Na ₂ O	K ₂ O	TiO ₂	P ₂ O ₅	MnO	Others	LOI
1	52.0	43.8	0.3	-	-	0.1	0.3	0.1	1.5	0.2	-	0.1	1.5
2	51.7	42.9	0.9	0.0	0.0	0.0	0.0	0.1	2.3	0.0	0.0	0.0	2.0
3	51.8	42.4	1.9	0.1	0.1	-	0.1	0.1	2.4	0.1	-	0.2	1.0
4	52.3	43.8	0.6	0.0	0.1	0.0	0.1	0.0	1.8	0.0	0.0	0.1	1.0
5	-	-	-	-	-	-	-	-	-	-	-	-	-
6	54.3	39.0	1.4	0.1	0.4	0.0	0.1	1.5	1.2	0.3	0.0	0.0	1.7
7	53.8	39.3	1.2	0.6	0.7	0.0	0.2	0.8	1.6	0.3	0.0	0.2	1.3
8	57.0	35.1	2.5	0.1	0.3	0.0	0.1	0.7	1.8	0.3	1.0	0.0	2.0
9	50.8	42.7	0.6	-	-	-	-	0.1	1.8	0.1	0.0	0.2	3.6
10	60.9	33.1	0.9	1.6	0.3	0.0	0.2	0.4	1.9	0.2	0.0	0.0	0.5
11	48.1	35.1	9.4	0.8	0.5	0.0	0.2	0.1	2.3	0.3	2.0	0.0	3.0
12	54.7	39.9	0.5	0.1	0.2	0.0	0.1	2.2	0.4	0.6	0.0	0.1	0.8
13	44.8	35.7	14.7	0.1	0.6	0.2	0.0	0.2	0.6	0.1	0.2	0.3	2.2
14	54.9	28.6	9.0	0.9	1.3	0.2	0.2	3.0	1.1	0.5	0.1	0.0	0.2
15	60.7	35.9	0.7	0.1	0.1	0.0	0.1	0.1	1.1	0.1	0.0	0.0	1.1
16	59.2	33.1	4.0	0.1	0.1	0.0	0.2	0.2	2.2	0.0	0.0	0.0	0.6
17	47.3	29.5	19.2	0.1	0.7	0.1	0.5	0.1	0.7	0.3	0.0	0.2	1.4
18	44.9	32.3	15.4	1.3	0.8	0.1	0.4	0.2	2.4	0.4	0.1	0.2	1.7
19	44.9	28.8	20.9	0.0	0.2	0.0	0.0	0.3	3.5	0.2	0.2	0.0	0.8
20	72.3	24.2	2.1	0.0	0.1	0.0	0.0	0.3	0.4	0.0	0.0	0.0	0.6
21	61.3	24.2	6.2	0.7	0.4	0.2	0.2	1.6	2.5	1.0	0.0	0.8	1.0
22	51.8	25.8	15.6	1.8	0.8	0.0	0.1	0.2	1.1	0.3	0.2	0.6	1.6
23	61.0	25.2	9.1	0.1	0.2	0.0	0.1	1.1	1.4	0.2	0.1	0.2	1.1
24	61.8	27.3	3.4	0.2	0.4	0.0	0.2	3.5	0.4	0.1	0.0	0.0	2.6
25	68.6	26.1	0.7	1.1	0.3	0.1	0.1	0.5	0.0	0.3	0.0	0.5	1.6
26	71.3	23.5	1.0	0.3	0.4	0.0	0.2	1.4	1.3	0.2	-	0.1	0.4
27	54.7	26.8	13.6	0.3	1.0	-	-	0.4	1.1	-	-	-	1.9
28	-	-	-	-	-	-	-	-	-	-	-	-	-
29	67.6	22.6	6.1	0.5	-	-	-	0.3	1.5	-	-	-	1.4
30	73.6	21.6	0.5	0.5	0.2	0.3	0.1	0.4	0.8	0.3	0.0	0.2	1.2
31	53.2	21.9	16.2	3.1	0.8	0.1	0.1	0.1	1.3	0.0	0.8	0.1	2.0
32	69.7	21.4	2.2	0.1	0.4	0.1	0.3	2.4	0.3	0.2	0.0	0.1	2.5
33	66.0	19.7	10.9	0.1	0.1	0.0	0.3	1.1	0.7	0.1	0.0	0.0	0.9
34	63.3	18.9	6.8	1.0	2.1	0.2	0.3	3.6	1.0	0.3	0.0	0.6	1.8
35	70.4	18.1	7.4	0.0	0.3	0.0	0.1	1.4	1.1	0.2	0.0	0.2	0.7
36	60.9	22.3	10.3	0.3	0.7	0.0	0.2	2.9	1.3	0.1	0.0	0.2	0.7
37	66.7	19.6	7.3	0.2	0.8	0.0	0.5	2.9	0.7	0.3	0.0	0.1	0.7
38	67.2	16.0	12.1	0.1	0.2	0.0	0.1	0.1	3.0	0.3	-	0.1	0.8
39	-	-	-	-	-	-	-	-	-	-	-	-	-
40	64.2	23.9	1.1	0.1	0.2	0.0	0.2	9.3	0.1	0.1	0.0	0.1	0.6
41	75.5	16.1	0.8	3.5	0.2	0.2	0.1	0.6	0.0	0.3	0.0	0.7	1.9
42	81.6	10.7	4.8	0.2	0.1	0.0	0.1	0.1	0.9	0.3	0.0	0.2	1.0
43	68.4	17.5	8.9	0.6	0.7	-	0.1	2.3	0.8	0.1	0.1	0.2	0.5
44	67.8	20.1	1.7	0.1	1.1	0.0	0.6	3.8	0.9	0.0	0.0	0.0	3.8
45	63.7	15.7	4.5	7.7	2.6	0.6	0.4	2.6	0.6	0.2	0.0	0.2	1.0
46	62.3	19.3	8.7	0.5	0.5	0.2	1.1	3.5	1.7	0.8	0.0	0.8	0.7
Quartz	99.8	-	-	-	-	-	-	0.1	-	-	-	-	0.1

9.3 Appendix 3. Application of R^3 test to different calcination temperature and various SCMs

The R^3 was developed and applied to a wide range of calcined clays in Chapter 2. It was also shown in this chapter that the calcined kaolinite content is a relevant parameter for the strength development of PPC30 and LC³-50 systems. However, this parameter can not be used anymore in two cases. First, if the clay is calcined at too high-temperature. The calcined kaolinite content takes into account an incomplete calcination, but not an “over”-calcination. Second, the calcined kaolinite content can not be used for other SCMs obviously. Thus, in this appendix, the R^3 test is first applied to a clay calcined at different temperatures. Then, the R^3 is applied to a wide range of SCMs.

9.3.1 Optimization of the calcination temperature of calcined clay

The R^3 test was applied to the clay with 50.3% of calcined kaolinite to investigate the influence of the calcination temperature on the reactivity of the calcined clay. Five calcination temperatures were chosen: 600 °C, 700 °C, 750 °C, 800 °C and 850 °C. The raw clay was tested as comparison.

9.3.1.1 Calcination assessment

The calcination was assessed by XRD in Figure 9.13. A partial dehydroxylation of kaolinite is observed at 600 °C and this dehydroxylation is complete from 700°C onwards.

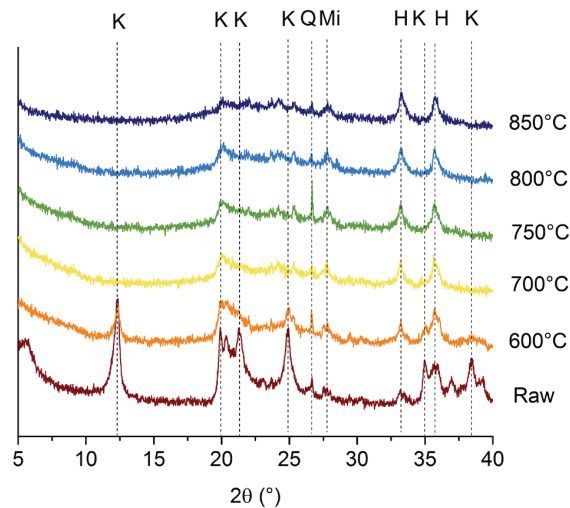


Figure 9.13. XRD patterns of raw clay and clay calcined at 600 °C, 700 °C, 750 °C, 800 °C and 850 °C. H, Mi and Q refers to hematite, microcline and quartz, respectively.

The calcination efficiency was also investigated by TGA. TGA and DTG results are shown in Figure 9.14 (a) and (b), respectively. At 600 °C, the calcination of goethite is complete, since there is no mass loss from 250 °C to 350 °C. but there is still some kaolinite left. A complete calcination is obtained for a minimum calcination temperature of 700°C.

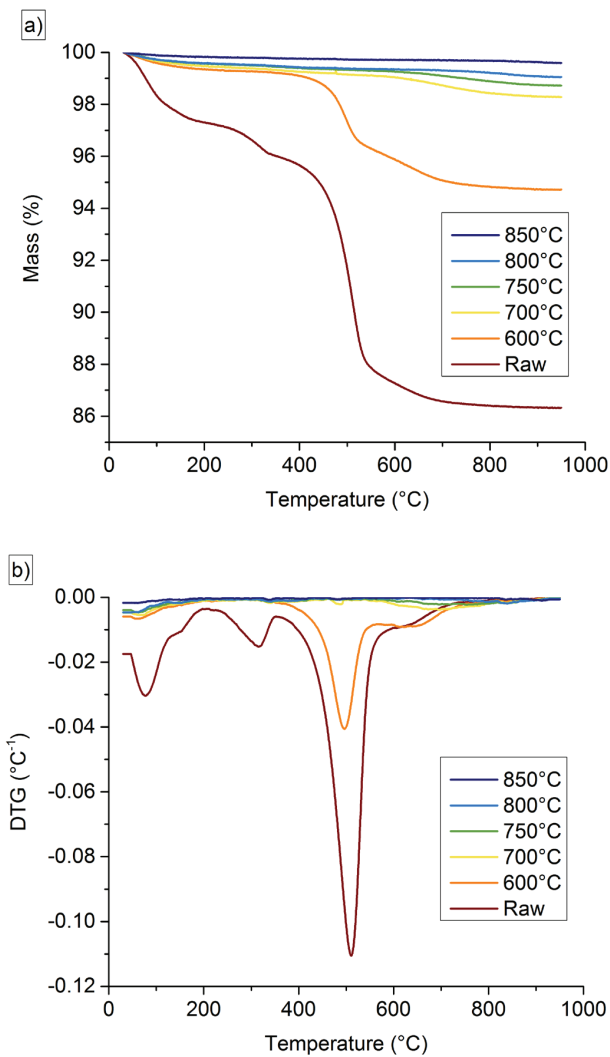


Figure 9.14. TGA (a) and DTG (b) of raw clay and clay calcined at 600 °C, 700 °C, 750 °C, 800 °C and 850 °C.

9.3.1.2 Reactivity of calcined clay

The results of compressive strength tests are shown in Figure 9.15 at 1, 3, 7, 28 and 90 days of hydration. The highest strengths are obtained for a calcination temperature of 750 °C and 800 °C. Even at 600 °C where the calcination of kaolinite is incomplete, higher strength than PC is reached at 90 days of hydration.

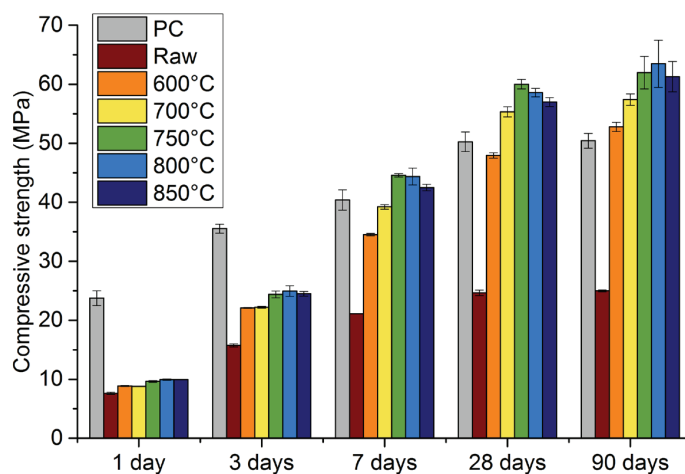


Figure 9.15. Compressive strength at 1, 3, 7, 28 and 90 days of hydration for reference PC and LC³-50 (50.3%) for different calcination temperature.

The R³ test results by isothermal calorimetry at 40 °C in Figure 9.16 show that the highest heat is obtained for the clay calcined at 800 °C, with a slightly lower reactivity for the clay calcined at 700 °C and 750 °C. The reason for the lower reactivity at 600 °C is due to the incomplete dehydroxylation of kaolinite observed in Figures 9.13 and 9.14 by XRD and TGA, respectively.

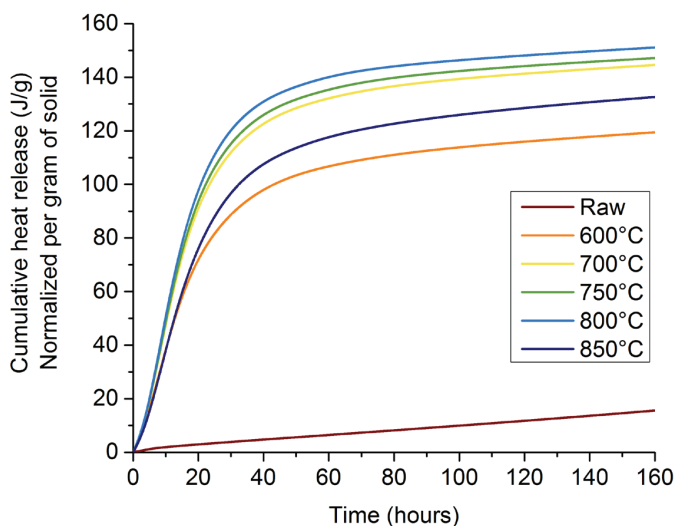


Figure 9.16. Cumulative heat release for the raw clay and the clays calcined at 600 °C, 700 °C, 750 °C, 800 °C and 850 °C.

In order to understand the decrease of reactivity for the clay calcined at 850 °C, the $D_{v,50}$ as well as the specific surface are shown in Figure 9.17 for the different calcination temperatures. It shows the continuous increase of the $D_{v,50}$ and the continuous decrease of the specific surface with the calcina-

tion temperature, with a significant drop of the specific surface from 800 °C to 850 °C. The calcination tends to agglomerate the particles of clay together. Fernandez showed the formation of agglomerates of smaller particles by SEM from 800 °C onwards [45]. Thus, the drop in specific surface due to the agglomeration of calcined clay particles is likely to be responsible for the decrease of reactivity compared with the clay calcined at 800 °C.

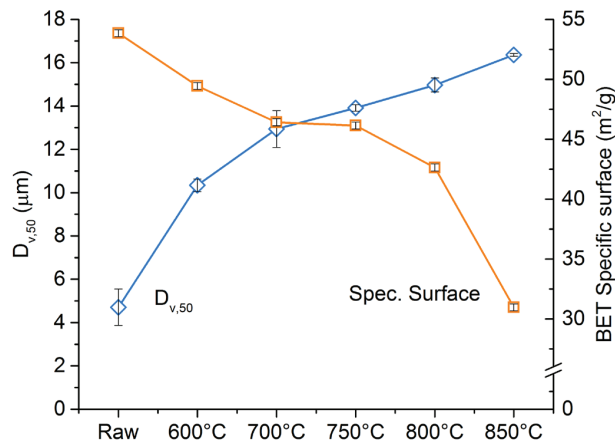


Figure 9.17. Evolution of the $D_{v,50}$ and the specific surface with the calcination temperature.

The correlation of LC^3 -50 mortar strength with the cumulative heat released at 24 h of hydration is shown in Figure 9.18. Good correlations are obtained. The decrease of reactivity for the clay calcined at 850 °C due to the physical rearrangement of clay particles is more clearly observed by the R^3 test than for strength results. The more important shearing force during the mixing of the mortar with the sand particles might break some of the agglomerates formed, improving the reactivity of the calcined clay.

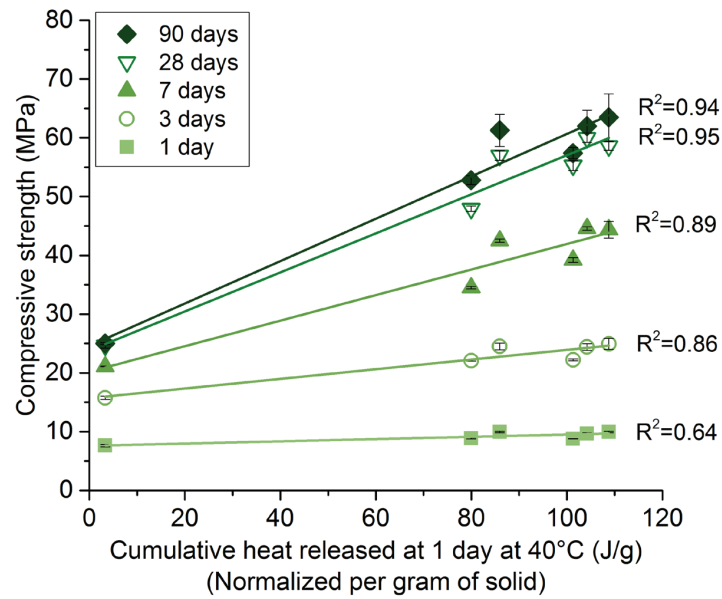


Figure 9.18. Correlation between the mortar strength results of LC³-50 (50.3%) and the heat release after 24 h by isothermal calorimetry.

9.3.2 Application to other Supplementary Cementitious Materials

To extend the scope of the R³ test to other SCMs, two slags (S1 and S8), two fly ashes (FA1 and FA2), a silica fume (SF) and a burnt oil shale (BOS) were tested. Their composition and physical properties are shown in Table 9.3. Two calcined kaolinitic clays with 95.0 % and 50.3 % of calcined kaolinite are also used for comparison. PPC30 systems were studied here, i.e. without limestone. The compressive strength results are shown in Figure 9.19. At 1 day of hydration, all blends show lower strength than plain PC system, except for the burnt oil shale mix. At 3 days of hydration, silica fume and the highest-grade calcined clay reach PC strength. Progressively with time, all SCMs exceed PC strength except quartz. Similar strength to PC is reached for slag systems at 7 days, for fly ash 2 at 28 days. Silica fume shows a significant increase of strength at 28 days and 90 days of hydration.

Table 9.3. XRF composition and physical properties of the different SCMs.

	BOS	S1	S8	SF	FA1	FA2
$D_{v,50}$ (μm)	6.1	19.5	18	0.2	18.3	7.2
BET Specific surface (m^2/g)	6.5	1.2	1.0	21.4	0.7	-
XRF Compositions (%)						
SiO_2	33.5	36.1	34.7	92.5	50.5	33.6
Al_2O_3	10.1	12.1	20.1	2.9	24.7	18.2
Fe_2O_3	6.1	0.8	0.4	0.2	9.3	6.4
CaO	29.7	42.0	33.3	0.0	5.1	26.5
MgO	1.8	7.1	9.4	0.0	2.9	6.4
SO_3	9.7	1.5	0.7	0.0	0.7	2.2
Na_2O	0.3	0.1	0.1	0.2	1.1	1.9
K_2O	2.0	0.3	0.8	0.1	4.1	0.4
TiO_2	0.5	0.5	0.9	0.0	1.0	1.3
P_2O_5	0.3	0.0	0.0	0.5	0.0	0.9
MnO	0.1	0.2	0.1	0.0	0.0	0.0
Others	0.2	0.0	0.0	2.8	0.0	0.0
LOI	5.4	-0.7	-0.5	0.6	0.7	0.9

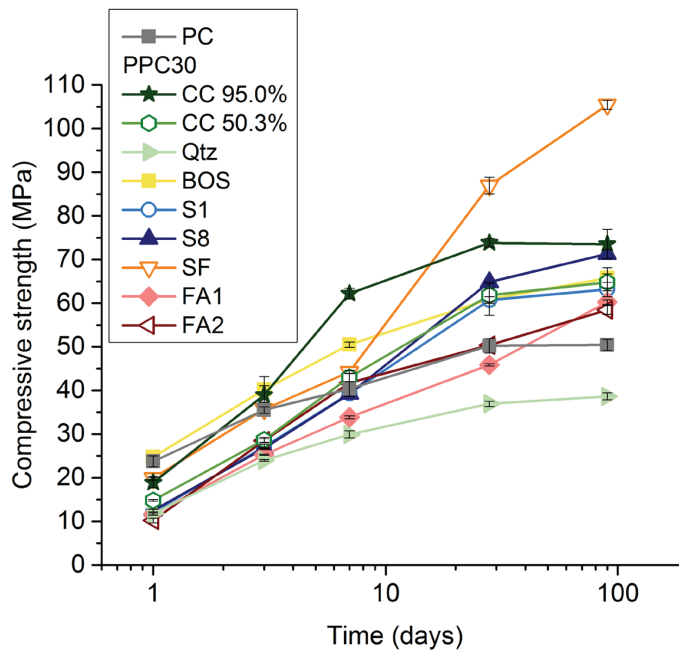


Figure 9.19. Compressive strength tests at 1, 3, 7, 28 and 90 days of hydration for the various SCMs.

For the R^3 test, the mix design was chosen to simulate PPC30 systems, i.e. without limestone. The cumulative heat release at 40 °C is shown in Figure 9.20. Significant differences in kinetics of hydration are observed between the different SCMs. Calcined clays are clearly the most reactive SCMs, reaching a plateau at about 24 h, whereas burnt oil shale and the two slags show a slowing

down of hydration from 3 days onwards. Fly ash 1 and silica fume still react at 7 days. Thus, the heat value at 6 days of hydration is used for the correlation with the compressive strength of PPC30 mortar.

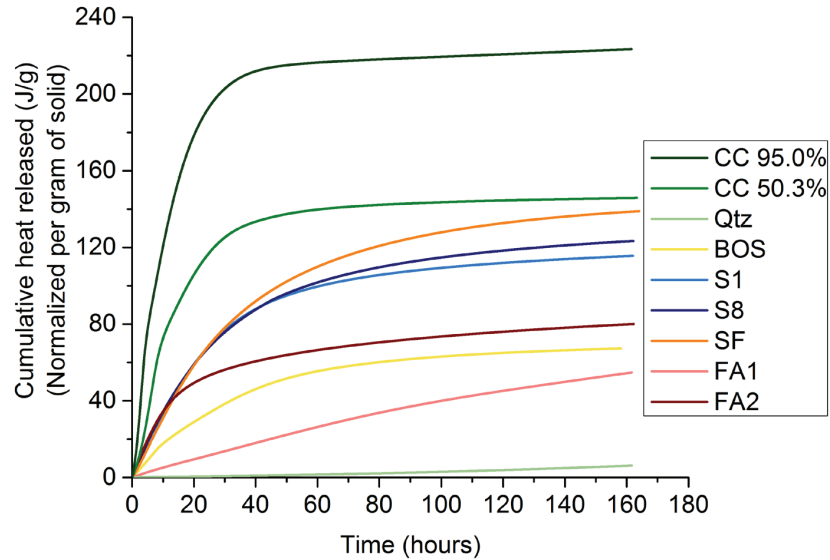


Figure 9.20. Cumulative heat release at 40°C for various SCMs.

Figure 9.21 shows the correlation between the mortar strength results of PPC30 blends with the heat release. It shows that good correlations are obtained for quartz, slags, fly ashes and calcined clays. These results are in agreement with the results obtained by Snellings and al. [46] with a slightly different mix design. However, some deviations are observed for silica fume and burnt oil shale. The reason especially for the deviations at very early age could be the dominance of the filler effect combined with the physical effect of silica fume and burnt oil shale particles which could explain why a low heat value is obtained whereas high strengths are measured.

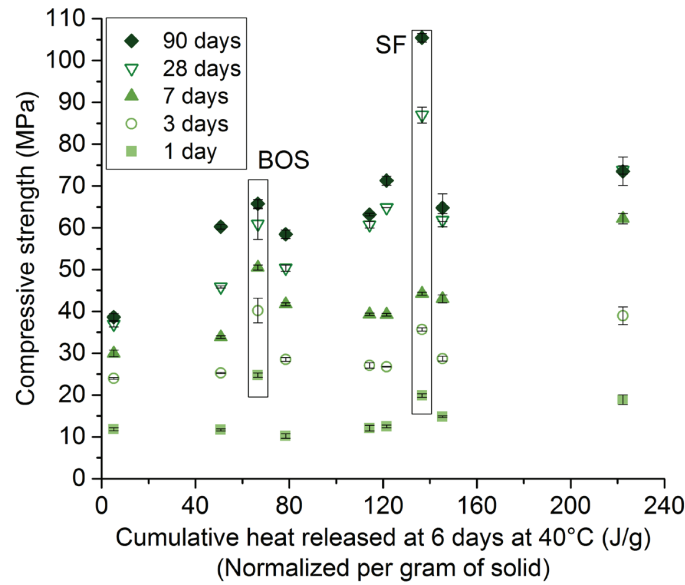


Figure 9.21. Correlation between mortar compressive strength of PPC30 systems and the cumulative heat release at 40 °C at 6 days of hydration for portlandite/SCM model systems.

9.3.3 Conclusion

The R^3 test permits to determine the optimal calcination temperature of a clay, which is around 750 °C to 800 °C. Above this temperature, the reactivity decreases. This calcination at too-high temperature would not be detected by simply considering the calcined kaolinite content as an indicator or reactivity. In addition to calcined clays (and quartz), the R^3 test also reliably predicts the strength development of mortar blend containing fly ashes and slags. However, some discrepancies are observed for burnt oil shale and silica fume, likely due to the physical and/or filler effect of these fine particles.

9.4 Appendix 4 – Workability of LC³-50 blends

Due to water adsorption on metakaolin particles, the workability of LC³-50 blends is worse than plain Portland cement. To get similar workability for all systems, a polycarboxylate superplasticizer from Mapei (SP490) was used for pastes and mortars. For mortars, the superplasticizer was progressively added to the mixer to reach an adequate workability (similar to PC with a flow of 16 ± 2 cm). The mortar casting was carried out according to EN 197-1 using a water to binder ratio of 0.5. The flow was measured on a flow table using a cone of 5 cm-high, and tapping 15 times in 15 seconds the flow table. Two perpendicular diagonals were then measured and the average value gives the flow of the system. For pastes, the superplasticizer was added to reach workability close to PC, i.e. a flow 8.5 ± 2 cm and 13 ± 2 cm for w/b of 0.4 and 0.5, respectively. The mini cone test was used. A cone of 5 cm high was filled with fresh paste, and the cone was removed. No tapping was necessary. Two diagonals were measured and the average indicates the flow value.

9.4.1 Mortar

Figure 9.22 shows the amount of superplasticizer added as a function of the calcined kaolinite content. For high-grade calcined clay, the mix became more plastic and did not show the same viscosity as plain Portland cement. Since the flow obtained was not exactly the same for all systems, the amount of superplasticizer as a function of the calcined kaolinite content is normalized by the flow value in Figure 9.23. It shows a linear correlation between the admixture content and the calcined kaolinite content. The higher the calcined kaolinite content in the calcined clay, the more superplasticizer needs to be added to reach similar workability to PC. Some scatter is observed, especially for calcined clays with a fairly low calcined kaolinite content. With the decrease of the calcined kaolinite content the amount of secondary phases increases, which can improve or worsen the rheological properties. Other factors such as the calcination process, the fineness and the specific surface of the calcined clays can also play a minor role in the workability properties of LC³-50 blends.

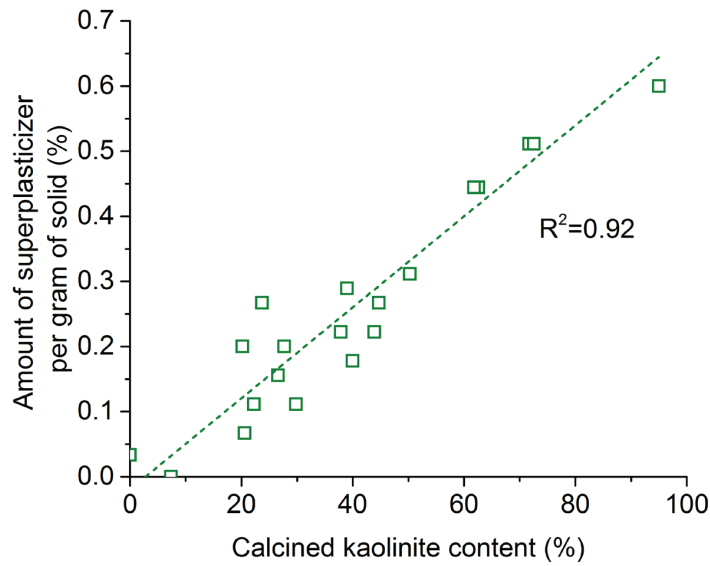


Figure 9.22. Amount of superplasticizer added in LC³-50 mortars.

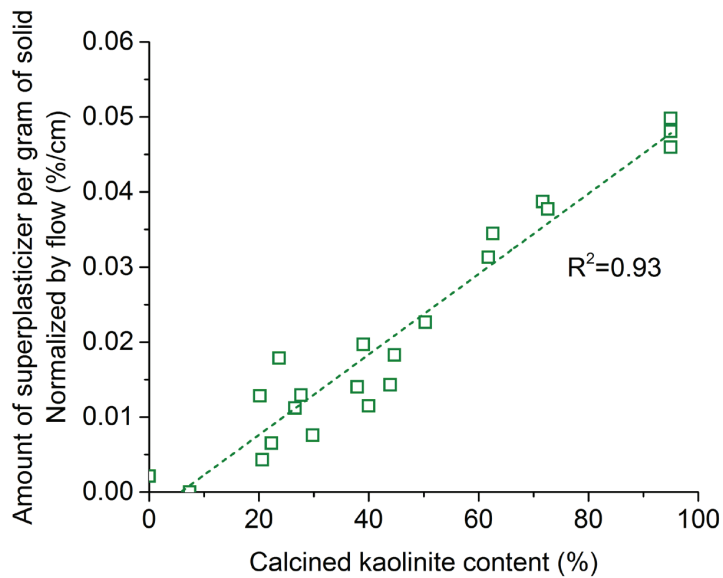


Figure 9.23. Amount of superplasticizer added in LC³-50 mortars, normalized by the flow value.

9.4.2 Paste

Figure 9.24 shows the amount of superplasticizer required to reach a flow close to PC. It shows an increase of the admixture content with the calcined kaolinite for both water to binder ratio. Obviously, the amount of superplasticizer needed decreases with the increase of the water to binder ratio. Since not all systems have exactly the same flow values, the amount of superplasticizer added was normalized by the flow value in Figure 9.25. As for mortars, linear trends are obtained, showing

that the calcined kaolinite content is the most critical parameter controlling the workability of LC³-50 blends.

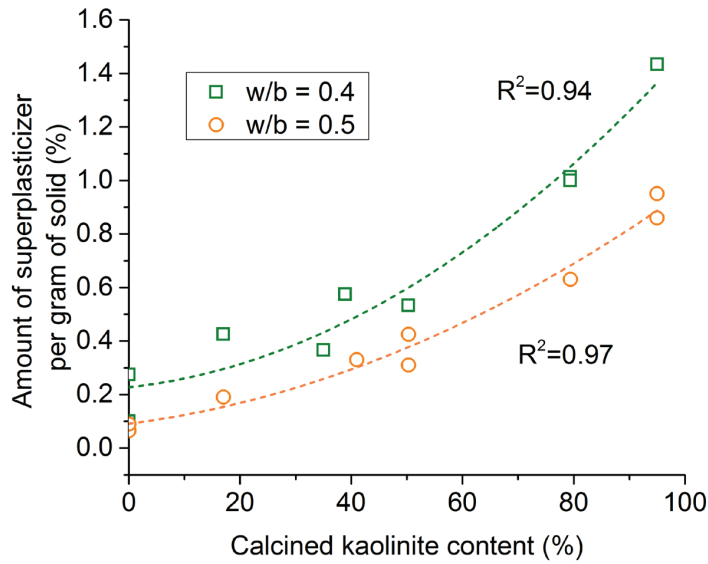


Figure 9.24. Amount of superplasticizer added in LC³-50 pastes.

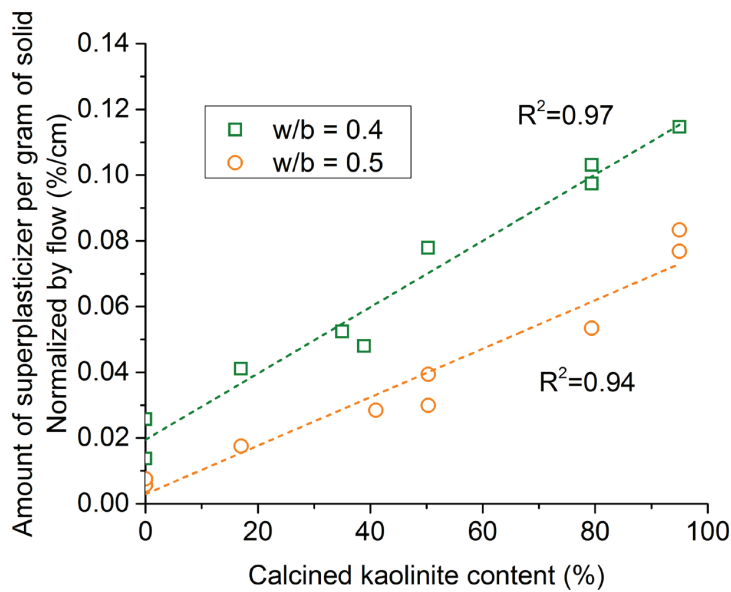


Figure 9.25. Amount of superplasticizer added in LC³-50 pastes, normalized by the flow value.

9.5 Appendix 5 – Determination of the density of C-A-S-H by $^1\text{H-NMR}$

^1H Nuclear Magnetic Resonance permits to analyse the different water populations present in a sample. A magnetic pulse leads to the excitation of the spins of hydrogen atoms (protons). The relaxation time of the hydrogen spins is recorded and gives information on the mobility of water molecules. The more tightly bound the water molecule is, the faster the relaxation time. In pores, the protons relax when they hit the surface, so the relaxation time is related to the size of the pore [115, 116].

Five main populations of water have been identified in hydrated cement pastes [80]:

- the first population with the fastest relaxation time (about 10 μs) corresponds to the chemically bound water of crystalline phases such as ettringite, portlandite and monosulfate for plain Portland cement system as well as hemi- and monocarboaluminate phases for blends containing limestone, such as LC³-50 blends. This water is called *solid* water.
- C-A-S-H interlayer water is attributed to the water population with a relaxation time of hydrogen spins of about 100 μs .
- slightly more mobile water in the gel pores of C-A-S-H is then observed with a relaxation time of 400 μs .
- the fourth water population corresponds to the water in inter-hydrate space (between C-A-S-H needles) which show a relaxation time from 1 to 10 ms.
- finally, the longest relaxation time corresponds to the water present in the capillaries, with a relaxation time from about 6 ms onwards. These last two populations represent the free water in the samples. They will be referred to as capillary water in the next sections.

Using the quantitative information on the different water populations from $^1\text{H-NMR}$ measurements, mass and volume balance can be applied to determine the density of C-A-S-H, according to Equations 9.5 and 9.6, adapted from [80]. These Equations are based on 100g of anhydrous binder. w and b refer to the initial amounts of water and binder, respectively. α refers to the hydration degree of clinker (cl), limestone (ls) and calcined clay(cc), I is the intensity fraction of the different water signals. β , γ and δ are the inverse mass fraction of water in the different crystalline phases, in the C-A-S-H and in the gel and capillary space, respectively.

$$w + b = b \left((1 - \alpha_{cl}) + (1 - \alpha_{cc}) + (1 - \alpha_{ls}) \right) + w \left(\beta_{CH} I_{CH} + \beta_{AFt} I_{AFt} + \beta_{Hc} I_{Hc} + \beta_{Mc} I_{Mc} + \gamma I_{CASH} + \delta (I_{gel} + I_{cap}) \right) \quad \text{Eq. 9.5}$$

$$\frac{w}{\rho_w} + b \left(\frac{m_{cl}}{\rho_{cl}} + \frac{m_{cc}}{\rho_{cc}} + \frac{m_{ls}}{\rho_{ls}} \right) = b \left(\frac{(1 - \alpha_{cl})}{\rho_{cl}} + \frac{(1 - \alpha_{cc})}{\rho_{cc}} + \frac{(1 - \alpha_{ls})}{\rho_{ls}} \right) + w \left(\frac{\beta_{CH} I_{CH}}{\rho_{CH}} + \frac{\beta_{AFt} I_{AFt}}{\rho_{AFt}} + \frac{\beta_{Hc} I_{Hc}}{\rho_{Hc}} + \frac{\beta_{Mc} I_{Mc}}{\rho_{Mc}} + \frac{\gamma I_{CASH}}{\rho_{CASH}} + \delta \frac{(I_{gel} + I_{cap} + I_{void})}{\rho_w} \right) \quad \text{Eq. 9.6}$$

The degree of hydration of clinker and limestone are obtained by X-Ray Diffraction (XRD) combined with Rietveld method. The degree of reaction of metakaolin in calcined clay is obtained according to Chapter 3.

The signal of the water present in the crystalline phases can be expressed as $I_{\text{solid}} = I_{\text{CH}} + I_{\text{AFt}} + I_{\text{Hc}} + I_{\text{Mc}}$. XRD-Rietveld was used to determine the amounts of portlandite, ettringite, hemi-, monocarboaluminate and monosulfoaluminate phases. The inverse water contents of portlandite, ettringite, hemi- and monocarboaluminate and monosulfate are obtained from the stoichiometric compositions of each phase, i.e. $\beta_{\text{CH}} = 74.09/18.01$, $\beta_{\text{AFt}} = 1255.11/576.51$, $\beta_{\text{Hc}} = 564.45/216.19$, $\beta_{\text{Mc}} = 568.29/198.18$ and $\beta_{\text{Ms}} = 622.52/216.19$. For the volume balance, the contribution of the chemical shrinkage I_{void} is measured separately. Thus, the remaining unknowns from Equations 1 and 2 are the inverse water content of the C-A-S-H γ and the C-A-S-H density $\rho_{\text{C-A-S-H}}$. Equation 9.5 permits to determine γ and $\rho_{\text{C-A-S-H}}$ is obtained from Equation 9.6. The C-A-S-H stoichiometric composition can be written as $\text{Ca}_z(\text{Al}_{1-y}\text{Si}_y)\text{O}_{z+1/2y+3/2}\text{H}_2\text{O}_x$. x , y and z parameters can be obtained from the Equations 9.7, 9.8 and 9.9 respectively. x is related to the inverse water content γ of C-A-S-H in Equation 3. y and z parameters are obtained experimentally by SEM-EDX from the atomic composition of C-A-S-H.

$$x = \frac{56z + 9y + 51}{18(\gamma - 1)} \quad \text{Eq. 9.7}$$

$$y = \frac{\text{Si}}{\text{Al} + \text{Si}} \quad \text{Eq. 9.8}$$

$$z = \frac{\text{Ca}}{\text{Al} + \text{Si}} \quad \text{Eq. 9.9}$$

To determine the bulk density of C-A-S-H $\rho'_{\text{C-A-S-H}}$, the C-A-S-H stoichiometric composition is modified to $\text{Ca}_z(\text{Al}_{1-y}\text{Si}_y)\text{O}_{z+1/2y+3/2}\text{H}_2\text{O}_{x'}$ to include the water present in the gel pores. x' is obtained according to Equation 9.10. The bulk density of C-A-S-H is obtained according to Equation 9.11, where $M_{\text{C-A-S-H}}$ and M_w refer to the molecular mass of solid C-A-S-H and water, respectively.

$$x' = x \frac{(I_{\text{gel}} + I_{\text{CASH}})}{I_{\text{CASB}}} \quad \text{Eq. 9.10}$$

$$\rho'_{\text{CASH}} = \frac{M_{\text{CASH}} + (x' - x)M_w}{\frac{M_{\text{CASH}}}{\rho_{\text{CASH}}} + (x' - x)M_w} \quad \text{Eq. 9.11}$$

9.6 Appendix 6 – XRD patterns of PC and LC³-50 blends in binding isotherms

The XRD patterns of PC and the LC³-50 blends after 4 months of exposure to water and NaCl solutions (after 28 days of hydration) are shown in Figures 9.26-9.28.

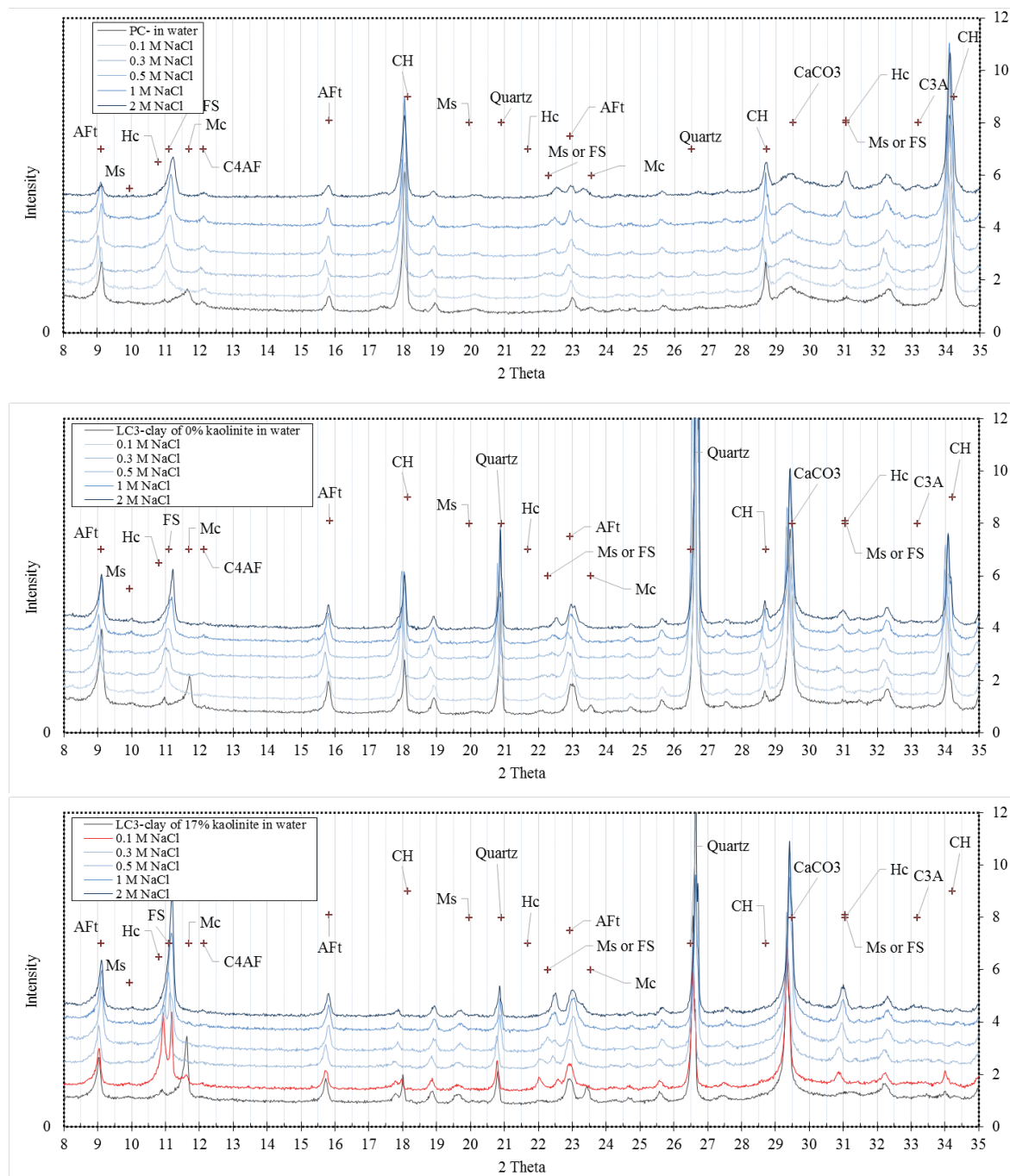


Figure 9.26. XRD patterns of PC and LC³-50 (0%) and (17.0%) blends for samples stored in water and in the different NaCl solutions.

Appendix

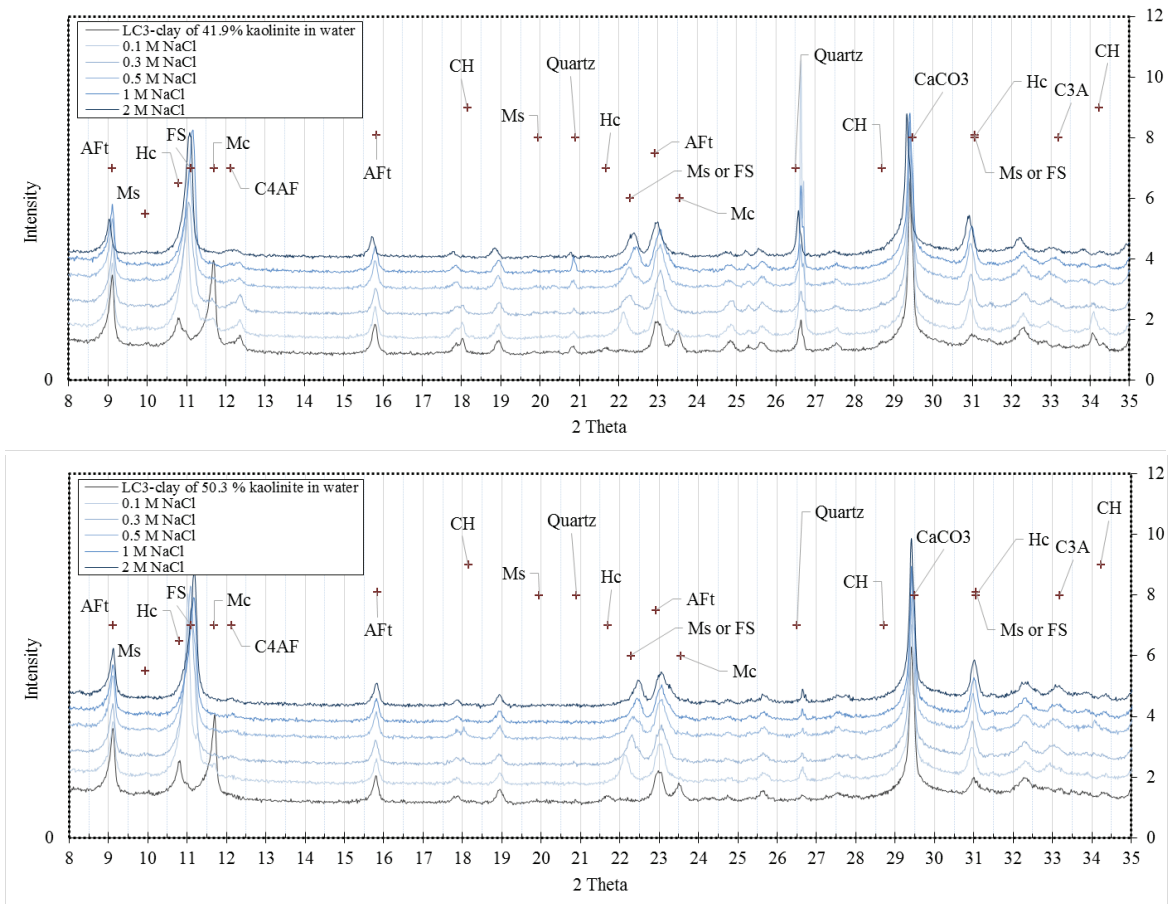


Figure 9.27. XRD patterns of LC³-50 (41.9%) and (50.3%) blends for samples stored in water and in the different NaCl solutions.

Appendix

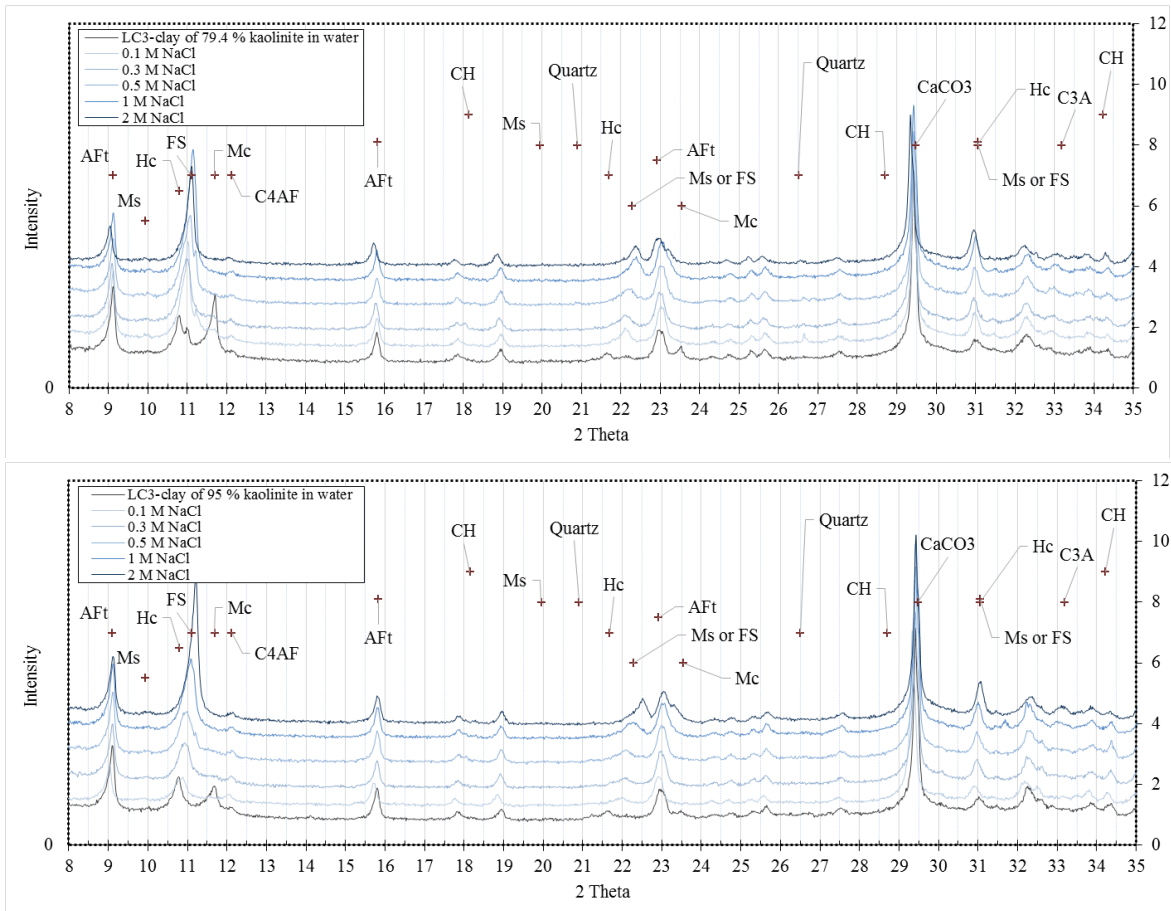


Figure 9.28. XRD patterns of LC³-50 (79.4%) and (95.0%) blends for samples stored in water and in the different NaCl solutions.

References

- [1] Cembureau, World Statistical Review 2004 - 2014, Cembureau, (2017).
- [2] N.H. Müller, J., A blueprint for a climate friendly cement industry, WWF International, (2008).
- [3] Concrete CO₂ Fact Sheet, National Ready Mixed Concrete Association, (2008).
- [4] G.P. Hammond, C.I. Jones, Embodied energy and carbon in construction materials, Proceedings of Institution of Civil Engineers: Energy, 161 (2008) 87-98.
- [5] B.D. Metz, O.; Bosch P.; Meyer L., Contribution of Working Group III to the Fourth Assessment Report of the Intergovernmental Panel on Climate Change, in: C.U. Press (Ed.), 2007.
- [6] Energy Technology Perspectives 2015 - Mobilising Innovation to Accelerate Climate Action, International Energy Agency, (2015).
- [7] R. Snellings, Assessing, Understanding and Unlocking Supplementary Cementitious Materials, RILEM Technical Letters, 1 (2016) 50-55.
- [8] Cement Roadmap targets, International Energy Agency - World Business Council for Sustainable Development, (2009).
- [9] K. Scrivener, J. Vanderley, E. Gartner, Eco-efficient cements: Potential, economically viable solutions for a low-CO₂, cement based materials industry, UNEP, (2016).
- [10] Global Soil Regions, US Department of Agriculture - Natural Resources Conservation Service, (2005).
- [11] H.H. Murray, Applied Clay Mineralogy: Occurrences, Processing and Application of Kaolins, Bentonites, Palygorskite-sepiolite, and Common Clays, Development in Clay Science, 2 (2007).
- [12] F. González Sánchez, L.R. Van Loon, T. Gimmi, A. Jakob, M.A. Glaus, L.W. Diamond, Self-diffusion of water and its dependence on temperature and ionic strength in highly compacted montmorillonite, illite and kaolinite, Applied Geochemistry, 23 (2008) 3840-3851.
- [13] H.H. Murray, Applied clay mineralogy today and tomorrow, Clay Minerals, 34 (1997) 39-49.
- [14] W. Gruner John, The Crystal Structure of Kaolinite, Zeitschrift für Kristallographie - Crystalline Materials, 1932, pp. 75.
- [15] A. Shvarzman, K. Kovler, G.S. Grader, G.E. Shter, The effect of dehydroxylation/amorphization degree on pozzolanic activity of kaolinite, Cement and Concrete Research, 33 (2003) 405-416.
- [16] A. Alujas, R. Fernández, R. Quintana, K.L. Scrivener, F. Martirena, Pozzolanic reactivity of low grade kaolinitic clays: Influence of calcination temperature and impact of calcination products on OPC hydration, Applied Clay Science, 108 (2015) 94-101.
- [17] C.Y. Chen, G.S. Lan, W.H. Tuan, Microstructural evolution of mullite during the sintering of kaolin powder compacts, Ceramics International, 26 (2000) 715-720.
- [18] P. Ptáček, F. Frajkorová, F. Šoukal, T. Opravil, Kinetics and mechanism of three stages of thermal transformation of kaolinite to metakaolinite, Powder Technology, 264 (2014) 439-445.
- [19] R.C. MacKenzie, M. Society, The Differential Thermal Investigation of Clays, Mineralogical Society (Clay Minerals Group) 1957.
- [20] J. Rocha, J. Klinowski, Festkörper-NMR-Untersuchungen zur Struktur und Reaktivität von Metakaolinit, Angewandte Chemie, 102 (1990) 539-541.
- [21] J. Sanz, A. Madani, J.M. Serratos, J.S. Moya, S. Aza, Aluminum-27 and Silicon-29 Magic-Angle Spinning Nuclear Magnetic Resonance Study of the Kaolinite-Mullite Transformation, Journal of the American Ceramic Society, 71 (1988) C418-C421.
- [22] R. Fernandez, F. Martirena, K.L. Scrivener, The origin of the pozzolanic activity of calcined clay minerals: A comparison between kaolinite, illite and montmorillonite, Cement and Concrete Research, 41 (2011) 113-122.
- [23] J. Lambert, W. Millman, J. Fripiat, Revisiting kaolinite dehydroxylation: A silicon-29 and aluminum-27 MAS NMR study, Journal of the American Chemical Society, 111 (1989) 3517-3522.
- [24] K.L. Konan, C. Peyratout, A. Smith, J.P. Bonnet, S. Rossignol, S. Oyetola, Comparison of surface properties between kaolin and metakaolin in concentrated lime solutions, Journal of Colloid and Interface Science, 339 (2009) 103-109.
- [25] C. He, B. Osbaeck, E. Makovicky, Pozzolanic reactions of six principal clay minerals: Activation, reactivity assessments and technological effects, Cement and Concrete Research, 25 (1995) 1691-1702.
- [26] J. Ambroise, M. Murat, J. Péra, Hydration reaction and hardening of calcined clays and related minerals. V. Extension of the research and general conclusions, Cement and Concrete Research, 15 (1985) 261-268.
- [27] S. Hollanders, R. Adriaens, J. Skibsted, Ö. Cizer, J. Elsen, Pozzolanic reactivity of pure calcined clays, Applied Clay Science, 132 (2016) 552-560.

References

- [28] B. Lothenbach, K. Scrivener, R.D. Hooton, Supplementary cementitious materials, *Cement and Concrete Research*, 41 (2011) 1244-1256.
- [29] E.M.J. Berodier, Impact of the supplementary cementitious materials on the kinetics and microstructural development of cement hydration, EPFL, 2015.
- [30] W.A. Guttridge, J.A. Dalziel, Filler cement: The effect of the secondary component on the hydration of Portland cement. Part I. A fine non-hydraulic filler, *Cement and Concrete Research*, 20 (1990) 778-782.
- [31] A. Tironi, M.A. Trezza, A.N. Scian, E.F. Irassar, Assessment of pozzolanic activity of different calcined clays, *Cement and Concrete Composites*, 37 (2013) 319-327.
- [32] A.S. Silva, A. Gameiro, J. Grilo, R. Veiga, A. Velosa, Long-term behavior of lime–metakaolin pastes at ambient temperature and humid curing condition, *Applied Clay Science*, 88–89 (2014) 49-55.
- [33] J. Ambroise, M. Murat, J. Pera, Hydration reaction and hardening of calcined clays and related minerals. IV. Experimental conditions for strength improvement on metakaolinite minicylinders, *Cement and Concrete Research*, 15 (1985) 83-88.
- [34] T. H.F.W., *Cement Chemistry 2nd Edition*, (1997).
- [35] K. De Weerd, M.B. Haha, G. Le Saout, K.O. Kjellsen, H. Justnes, B. Lothenbach, Hydration mechanisms of ternary Portland cements containing limestone powder and fly ash, *Cement and Concrete Research*, 41 (2011) 279-291.
- [36] M. Zajac, A. Rossberg, G. Le Saout, B. Lothenbach, Influence of limestone and anhydrite on the hydration of Portland cements, *Cement and Concrete Composites*, 46 (2014) 99-108.
- [37] V.L. Bonavetti, V.F. Rahhal, E.F. Irassar, Studies on the carboaluminate formation in limestone filler-blended cements, *Cement and Concrete Research*, 31 (2001) 853-859.
- [38] B. Lothenbach, G. Le Saout, E. Gallucci, K. Scrivener, Influence of limestone on the hydration of Portland cements, *Cement and Concrete Research*, 38 (2008) 848-860.
- [39] G. Kakali, S. Tsvivilis, E. Aggeli, M. Bati, Hydration products of C3A, C3S and Portland cement in the presence of CaCO₃, *Cement and Concrete Research*, 30 (2000) 1073-1077.
- [40] T. Matschei, B. Lothenbach, F.P. Glasser, The role of calcium carbonate in cement hydration, *Cement and Concrete Research*, 37 (2007) 551-558.
- [41] O. Chowaniec, Limestone addition in cement, Ecole Polytechnique Fédérale de Lausanne, Thesis 5335 (2012).
- [42] C.E. Tsvivilis S., Badogiannis E., Pahoulasa G., Ilias A., A study on the parameters affecting the properties of Portland limestone cements, *Cement and Concrete Composites*, 21 (1999) 107-116.
- [43] M. Antoni, J. Rossen, F. Martirena, K. Scrivener, Cement substitution by a combination of metakaolin and limestone, *Cement and Concrete Research*, 42 (2012) 1579-1589.
- [44] M. Antoni, Investigation of cement substitution by blends of calcined clays and limestone, Ecole Polytechnique Fédérale de Lausanne, Thesis 6001 (2013).
- [45] R. Fernandez, Calcined Clayey Soils as a Potential Replacement for Cement in Developing Countries, Ecole Polytechnique Fédérale de Lausanne, Thesis 5335 (2009).
- [46] R. Snellings, K.L. Scrivener, Rapid screening tests for supplementary cementitious materials: past and future, *Mater Struct*, 49 (2016) 3265-3279.
- [47] L.J. Vicat, *Traité pratique et théorique de la composition des mortiers, ciments et gangues à pouzzolanes et de leur emploi dans toutes sortes de travaux suivi des moyens d'en apprécier la durée dans les constructions à la mer*, Imprimerie Maisonville, (1856).
- [48] J. Chapelle, *Attaque sulfo-calcique des laitiers et des pouzzolanes*, Thèse de doctorat de l'Université Aix Marseille, (1958).
- [49] N. P18-513, Additions pour béton hydraulique - Métakaolin - Spécifications et critères de conformité, Association Française de Normalisation, (2012).
- [50] N. Frattini, Ricerche sulla calce di idrolisi nelle paste di cemento, *Annali di Chimica*, 39 (1949) 616-620.
- [51] EN196-5, Methods of testing cement - Part 5: Pozzolanicity test for pozzolanic cement, European Committee for Standardization, (2013).
- [52] S. Donatello, M. Tyrer, C.R. Cheeseman, Comparison of test methods to assess pozzolanic activity, *Cement and Concrete Composites*, 32 (2010) 121-127.
- [53] M.P. de Luxán, F. Soria, Study and critical review of the pozzolanity test, *Cement and Concrete Research*, 5 (1975) 461-479.
- [54] ASTM-C618-15, Standard Specification for Coal Fly Ash and Raw or Calcined Natural Pozzolan for Use in Concrete, ASTM International, (2015).
- [55] IS-1727, Methods of test for pozzolanic materials, Bureau of Indian Standards, (1967).
- [56] NBR-5751, Materiais pozolanicos - Determinacao da atividade pozolanica com cal aos sete dias, Brazilian standards, (2015).
- [57] EN196-1, Methods of testing cement - Part 1: Determination of strength, European Committee for Standardization, (2006).
- [58] B. Lothenbach, F. Winnefeld, C. Alder, E. Wieland, P. Lunk, Effect of temperature on the pore solution, microstructure and hydration products of Portland cement pastes, *Cement and Concrete Research*, 37 (2007) 483-491.
- [59] B. Lothenbach, T. Matschei, G. Möschner, F.P. Glasser, Thermodynamic modelling of the effect of temperature on the hydration and porosity of Portland cement, *Cement and Concrete Research*, 38 (2008) 1-18.

References

- [60] E. Gallucci, X. Zhang, K.L. Scrivener, Effect of temperature on the microstructure of calcium silicate hydrate (C-S-H), *Cement and Concrete Research*, 53 (2013) 185-195.
- [61] P.S.d. Silva, F.P. Glasser, Hydration of cements based on metakaolin: thermochemistry, *Advances in Cement Research*, 1990, pp. 167-177.
- [62] R. Snellings, A. Salze, K.L. Scrivener, Use of X-ray diffraction to quantify amorphous supplementary cementitious materials in anhydrous and hydrated blended cements, *Cement and Concrete Research*, 64 (2014) 89-98.
- [63] R.B. Perkins, C.D. Palmer, Solubility of ettringite ($\text{Ca}_6[\text{Al}(\text{OH})_6]_2(\text{SO}_4)_3 \cdot 26\text{H}_2\text{O}$) at 5–75°C, *Geochimica et Cosmochimica Acta*, 63 (1999) 1969-1980.
- [64] G. Li, P. Le Bescop, M. Moranville, The U phase formation in cement-based systems containing high amounts of Na_2SO_4 , *Cement and Concrete Research*, 26 (1996) 27-33.
- [65] H. Pöllmann, Syntheses, properties and solid solution of ternary lamellar calcium aluminate hydroxi salts (AFm-phases) containing SO_4^{2-} , CO_3^{2-} , and OH^- , *Neues Jahrbuch für Mineralogie - Abhandlungen: Journal of Mineralogy and Geochemistry*, 182 (2006) 173-181.
- [66] F. Deschner, B. Lothenbach, F. Winnefeld, J. Neubauer, Effect of temperature on the hydration of Portland cement blended with siliceous fly ash, *Cement and Concrete Research*, 52 (2013) 169-181.
- [67] K.L. Scrivener, Options for the future of cement, *Indian Concr. J.*, 88 (2014) 11-21.
- [68] K.L. Scrivener, B. Lothenbach, N. De Belie, E. Gruyaert, J. Skibsted, R. Snellings, A. Vollpracht, TC 238-SCM: hydration and microstructure of concrete with SCMs, *Mater Struct.*, 48 (2015) 835-862.
- [69] Z.T. Dai, Thuan T.; Skibsted, J., Aluminum Incorporation in the C–S–H Phase of White Portland Cement–Metakaolin Blends Studied by ^{27}Al and ^{29}Si MAS NMR Spectroscopy, *Journal of the American Ceramic Society*, 97 (2014) 2662 - 2671.
- [70] W. Kunther, Z. Dai, J. Skibsted, Thermodynamic modeling of hydrated white Portland cement–metakaolin–limestone blends utilizing hydration kinetics from ^{29}Si MAS NMR spectroscopy, *Cement and Concrete Research*, 86 (2016) 29-41.
- [71] Z. Shi, M.R. Geiker, K. De Weerd, T.A. Østnor, B. Lothenbach, F. Winnefeld, J. Skibsted, Role of calcium on chloride binding in hydrated Portland cement–metakaolin–limestone blends, *Cement and Concrete Research*, 95 (2017) 205-216.
- [72] S.L. Poulsen, V. Kocaba, G. Le Saoût, H.J. Jakobsen, K.L. Scrivener, J. Skibsted, Improved quantification of alite and belite in anhydrous Portland cements by ^{29}Si MAS NMR: Effects of paramagnetic ions, *Solid State Nuclear Magnetic Resonance*, 36 (2009) 32-44.
- [73] P.T. Durdziński, M. Ben Haha, S.A. Bernal, N. De Belie, E. Gruyaert, B. Lothenbach, E. Menéndez Méndez, J.L. Provis, A. Schöler, C. Stabler, Z. Tan, Y. Villagrán Zaccardi, A. Vollpracht, F. Winnefeld, M. Zajac, K.L. Scrivener, Outcomes of the RILEM round robin on degree of reaction of slag and fly ash in blended cements, *Mater Struct.*, 50 (2017) 135.
- [74] P.T. Durdziński, M. Ben Haha, M. Zajac, K.L. Scrivener, Phase assemblage of composite cements, *Cement and Concrete Research*, 99 (2017) 172-182.
- [75] P. Durdziński, Hydration of multi-component cements containing cement clinker, slag, calcareous fly ash and limestone, *Ecole Polytechnique Fédérale de Lausanne, Thesis n°6834* (2016).
- [76] B.Z. Dilnesa, E. Wieland, B. Lothenbach, R. Dähn, K.L. Scrivener, Fe-containing phases in hydrated cements, *Cement and Concrete Research*, 58 (2014) 45-55.
- [77] Available at <http://gems.web.psi.ch/>, (2014).
- [78] Available at <http://www.empa.ch/cemdata>, cemdata 14, EMPA, (2014).
- [79] D.A. Kulik, Improving the structural consistency of C-S-H solid solution thermodynamic models, *Cement and Concrete Research*, 41 (2011) 477-495.
- [80] A.C.A. Muller, K.L. Scrivener, A.M. Gajewicz, P.J. McDonald, Densification of C–S–H Measured by ^1H NMR Relaxometry, *The Journal of Physical Chemistry C*, 117 (2013) 403-412.
- [81] K. Scrivener, R. Snellings, B. Lothenbach, *A Practical Guide to Microstructural Analysis of Cementitious Materials*, Taylor & Francis 2016.
- [82] H.F.W. Taylor, *Cement Chemistry*, Thomas Telford 1997.
- [83] J.E. Rossen, K.L. Scrivener, Optimization of SEM-EDS to determine the C–A–S–H composition in matured cement paste samples, *Materials Characterization*, 123 (2017) 294-306.
- [84] J. Rossen, Composition and morphology of C-A-S-H in pastes of alite and cement blended with supplementary cementitious materials, *Ecole Polytechnique Fédérale de Lausanne, Thesis n°6294* (2014).
- [85] S. Lee, Y.J. Kim, H.-S. Moon, Energy-Filtering Transmission Electron Microscopy (EF-TEM) Study of a Modulated Structure in Metakaolinite, Represented by a 14 Å Modulation, *Journal of the American Ceramic Society*, 86 (2003) 174-176.
- [86] L. Trusilewicz, F. Fernández-Martínez, V. Rahhal, R. Talero, TEM and SAED Characterization of Metakaolin. Pozzolanic Activity, *Journal of the American Ceramic Society*, 95 (2012) 2989-2996.
- [87] S. Sánchez Berriel, A. Favier, E. Rosa Domínguez, I.R. Sánchez Machado, U. Heierli, K. Scrivener, F. Martirena Hernández, G. Habert, Assessing the environmental and economic potential of Limestone Calcined Clay Cement in Cuba, *Journal of Cleaner Production*, 124 (2016) 361-369.

References

- [88] L.S. Vizcaino, S.; Damas, S.; Pérez, A.; Scrivener, K.L.; Martirena, J.F., Industrial trial to produce a low clinker, low carbon cement, *Materiales de Construcción*, 65 (2015).
- [89] S.M. Bishnoi, S.; Mallik, A.; Joseph, S.; Krishnan, S., Pilot scale manufacture of limestone calcined clay cement : The Indian experience, *The Indian Concrete Journal*, 88 (2014) 22-28.
- [90] F. Avet, R. Snellings, A. Alujas Diaz, M. Ben Haha, K. Scrivener, Development of a new rapid, relevant and reliable (R3) test method to evaluate the pozzolanic reactivity of calcined kaolinitic clays, *Cement and Concrete Research*, 85 (2016) 1-11.
- [91] B.R. Ilić, A.A. Mitrović, L.R. Miličić, Thermal treatment of kaolin clay to obtain metakaolin, *Hemijska industrija*, 64 (2010) 351-356.
- [92] M. Frías, J. Cabrera, Pore size distribution and degree of hydration of metakaolin–cement pastes, *Cement and Concrete Research*, 30 (2000) 561-569.
- [93] A.C.A. Muller, K.L. Scrivener, A reassessment of mercury intrusion porosimetry by comparison with ¹H NMR relaxometry, *Cement and Concrete Research*, 100 (2017) 350-360.
- [94] T. Matschei, B. Lothenbach, F.P. Glasser, The AFm phase in Portland cement, *Cement and Concrete Research*, 37 (2007) 118-130.
- [95] R. Snellings, Solution-Controlled Dissolution of Supplementary Cementitious Material Glasses at pH 13: The Effect of Solution Composition on Glass Dissolution Rates, *Journal of the American Ceramic Society*, 96 (2013) 2467-2475.
- [96] E. Berodier, K. Scrivener, Evolution of pore structure in blended systems, *Cement and Concrete Research*, 73 (2015) 25-35.
- [97] J. Bizzozero, C. Gosselin, K.L. Scrivener, Expansion mechanisms in calcium aluminate and sulfoaluminate systems with calcium sulfate, *Cement and Concrete Research*, 56 (2014) 190-202.
- [98] M. Steiger, Crystal growth in porous materials—I: The crystallization pressure of large crystals, *Journal of Crystal Growth*, 282 (2005) 455-469.
- [99] M. Steiger, Crystal growth in porous materials—II: Influence of crystal size on the crystallization pressure, *Journal of Crystal Growth*, 282 (2005) 470-481.
- [100] E. L'Hôpital, B. Lothenbach, D.A. Kulik, K. Scrivener, Influence of calcium to silica ratio on aluminium uptake in calcium silicate hydrate, *Cement and Concrete Research*, 85 (2016) 111-121.
- [101] E. L'Hôpital, B. Lothenbach, G. Le Saout, D. Kulik, K. Scrivener, Incorporation of aluminium in calcium-silicate-hydrates, *Cement and Concrete Research*, 75 (2015) 91-103.
- [102] A. Bazzoni, Study of early of hydration mechanisms of cement by means of electron microscopy, *Ecole Polytechnique Fédérale de Lausanne*, Thesis n°6296 (2014).
- [103] F. Deschner, F. Winnefeld, B. Lothenbach, S. Seufert, P. Schwesig, S. Dittrich, F. Goetz-Neunhoeffler, J. Neubauer, Hydration of Portland cement with high replacement by siliceous fly ash, *Cement and Concrete Research*, 42 (2012) 1389-1400.
- [104] V. Kocaba, Development and evaluation of methods to follow microstructural development of cementitious systems including slags, EPFL, 2009.
- [105] S. Adu-Amankwah, M. Zajac, C. Stabler, B. Lothenbach, L. Black, Influence of limestone on the hydration of ternary slag cements, *Cement and Concrete Research*, 100 (2017) 96-109.
- [106] M.D. Andersen, H.J. Jakobsen, J. Skibsted, Incorporation of Aluminum in the Calcium Silicate Hydrate (C–S–H) of Hydrated Portland Cements: A High-Field ²⁷Al and ²⁹Si MAS NMR Investigation, *Inorganic Chemistry*, 42 (2003) 2280-2287.
- [107] M.D. Andersen, H.J. Jakobsen, J. Skibsted, Characterization of white Portland cement hydration and the C-S-H structure in the presence of sodium aluminate by ²⁷Al and ²⁹Si MAS NMR spectroscopy, *Cement and Concrete Research*, 34 (2004) 857-868.
- [108] I.G. Richardson, G.W. Groves, The structure of the calcium silicate hydrate phases present in hardened pastes of white Portland cement/blast-furnace slag blends, *Journal of Materials Science*, 32 (1997) 4793-4802.
- [109] C.A. Love, I.G. Richardson, A.R. Brough, Composition and structure of C–S–H in white Portland cement–20% metakaolin pastes hydrated at 25 °C, *Cement and Concrete Research*, 37 (2007) 109-117.
- [110] I.G. Richardson, The nature of C-S-H in hardened cements, *Cement and Concrete Research*, 29 (1999) 1131-1147.
- [111] A. Muller, K. Scrivener, A. Gajewicz, P. McDonald, Use of bench-top NMR to measure the density, composition and desorption isotherm of C–S–H in cement paste, *Microporous and Mesoporous Materials*, 178 (2013) 99-103.
- [112] A. Müller, Characterization of porosity & C-S-H in cement pastes by ¹H NMR, *Ecole Polytechnique Fédérale de Lausanne*, Thesis (2014).
- [113] J. Zhang, G.W. Scherer, Comparison of methods for arresting hydration of cement, *Cement and Concrete Research*, 41 (2011) 1024-1036.
- [114] L. Konecny, S.J. Naqvi, The effect of different drying techniques on the pore size distribution of blended cement mortars, *Cement and Concrete Research*, 23 (1993) 1223-1228.
- [115] J.P. Korb, NMR and nuclear spin relaxation of cement and concrete materials, *Current Opinion in Colloid & Interface Science*, 14 (2009) 192-202.

References

- [116] A. Valori, P.J. McDonald, K.L. Scrivener, The morphology of C–S–H: Lessons from 1H nuclear magnetic resonance relaxometry, *Cement and Concrete Research*, 49 (2013) 65-81.
- [117] X. Chen, S. Wu, J. Zhou, Influence of porosity on compressive and tensile strength of cement mortar, *Construction and Building Materials*, 40 (2013) 869-874.
- [118] B. Mota Gassó, Impact of alkali salts on the kinetics and microstructural development of cementitious systems, EPFL, 2015.
- [119] A.M. Ramezani-pour, R.D. Hooton, A study on hydration, compressive strength, and porosity of Portland-limestone cement mixes containing SCMs, *Cement and Concrete Composites*, 51 (2014) 1-13.
- [120] M. Ben Haha, B. Lothenbach, G. Le Saout, F. Winnefeld, Influence of slag chemistry on the hydration of alkali-activated blast-furnace slag — Part II: Effect of Al₂O₃, *Cement and Concrete Research*, 42 (2012) 74-83.
- [121] K.L. Watson, A simple relationship between the compressive strength and porosity of hydrated portland cement, *Cement and Concrete Research*, 11 (1981) 473-476.
- [122] I. Odler, M. Rößler, Investigations on the relationship between porosity, structure and strength of hydrated Portland cement pastes. II. Effect of pore structure and of degree of hydration, *Cement and Concrete Research*, 15 (1985) 401-410.
- [123] R. Sersale, R. Cioffi, G. Frigione, F. Zenone, Relationship between gypsum content, porosity and strength in cement. I. Effect of SO₃ on the physical microstructure of Portland cement mortars, *Cement and Concrete Research*, 21 (1991) 120-126.
- [124] T.C. Powers, Structure and Physical Properties Of Hardened Portland Cement Paste, *Journal of the American Ceramic Society*, 41 (1958) 1 - 6.
- [125] T.C. Powers, T.L. Brownyard, Studies of the Physical Properties of Hardened Portland Cement Paste, *Journal Proceedings*, 43 (1948).
- [126] L. Lam, Y.L. Wong, C.S. Poon, Degree of hydration and gel/space ratio of high-volume fly ash/cement systems, *Cement and Concrete Research*, 30 (2000) 747-756.
- [127] P. Termkhajornkit, Q.H. Vu, R. Barbarulo, S. Daronnat, G. Chanvillard, Dependence of compressive strength on phase assemblage in cement pastes: Beyond gel–space ratio — Experimental evidence and micromechanical modeling, *Cement and Concrete Research*, 56 (2014) 1-11.
- [128] M. Balonis, F.P. Glasser, The density of cement phases, *Cement and Concrete Research*, 39 (2009) 733-739.
- [129] G. Constantinides, F.-J. Ulm, The effect of two types of C-S-H on the elasticity of cement-based materials: Results from nanoindentation and micromechanical modeling, *Cement and Concrete Research*, 34 (2004) 67-80.
- [130] Z. He, C. Qian, Y. Zhang, F. Zhao, Nanoindentation characteristics of calcium hydroxide-metakaolin blended with sodium hydroxide solutions, *Journal of Wuhan University of Technology-Mater. Sci. Ed.*, 29 (2014) 185-189.
- [131] P. Shukla, S. Taneja, C. Sondergeld, C. Rai, Nanoindentation Measurements on Rocks, in: J. Carroll, S. Daly (Eds.) *Fracture, Fatigue, Failure, and Damage Evolution, Volume 5: Proceedings of the 2014 Annual Conference on Experimental and Applied Mechanics*, Springer International Publishing, Cham, 2015, pp. 99-105.
- [132] K. Velez, S. Maximilien, D. Damidot, G. Fantozzi, F. Sorrentino, Determination by nanoindentation of elastic modulus and hardness of pure constituents of Portland cement clinker, *Cement and Concrete Research*, 31 (2001) 555-561.
- [133] W. Zhu, J.J. Hughes, N. Bicanic, C.J. Pearce, Nanoindentation mapping of mechanical properties of cement paste and natural rocks, *Materials Characterization*, 58 (2007) 1189-1198.
- [134] R. Loser, B. Lothenbach, A. Leemann, M. Tuchschnid, Chloride resistance of concrete and its binding capacity – Comparison between experimental results and thermodynamic modeling, *Cement and Concrete Composites*, 32 (2010) 34-42.
- [135] C. Arya, Y. Xu, Effect of cement type on chloride binding and corrosion of steel in concrete, *Cement and Concrete Research*, 25 (1995) 893-902.
- [136] C. Arya, N.R. Buenfeld, J.B. Newman, Factors influencing chloride-binding in concrete, *Cement and Concrete Research*, 20 (1990) 291-300.
- [137] N.J.P. Coleman, C.L. , Aspects of the pore solution chemistry of hydrated cement pastes containing MK, *Cement and Concrete Research*, 27 (1997) 147 - 154.
- [138] R.K. Dhir, M.A.K. El-Mohr, T.D. Dyer, Chloride binding in GGBS concrete, *Cement and Concrete Research*, 26 (1996) 1767-1773.
- [139] R. Luo, Y. Cai, C. Wang, X. Huang, Study of chloride binding and diffusion in GGBS concrete, *Cement and Concrete Research*, 33 (2003) 1-7.
- [140] K. De Weerd, A. Colombo, L. Coppola, H. Justnes, M.R. Geiker, Impact of the associated cation on chloride binding of Portland cement paste, *Cement and Concrete Research*, 68 (2015) 196-202.
- [141] M. Balonis, B. Lothenbach, G. Le Saout, F.P. Glasser, Impact of chloride on the mineralogy of hydrated Portland cement systems, *Cement and Concrete Research*, 40 (2010) 1009-1022.
- [142] M.D.A. Thomas, R.D. Hooton, A. Scott, H. Zibara, The effect of supplementary cementitious materials on chloride binding in hardened cement paste, *Cement and Concrete Research*, 42 (2012) 1-7.
- [143] Y. Elakneswaran, T. Nawa, K. Kurumisawa, Electrokinetic potential of hydrated cement in relation to adsorption of chlorides, *Cement and Concrete Research*, 39 (2009) 340-344.

References

- [144] K. De Weerd, D. Orsáková, M.R. Geiker, The impact of sulphate and magnesium on chloride binding in Portland cement paste, *Cement and Concrete Research*, 65 (2014) 30-40.
- [145] H. Zibara, R.D. Hooton, M.D.A. Thomas, K. Stanish, Influence of the C/S and C/A ratios of hydration products on the chloride ion binding capacity of lime-SF and lime-MK mixtures, *Cement and Concrete Research*, 38 (2008) 422-426.
- [146] M. Shekarchi, A. Bonakdar, M. Bakhshi, A. Mirdamadi, B. Mobasher, Transport properties in metakaolin blended concrete, *Construction and Building Materials*, 24 (2010) 2217-2223.
- [147] E. Badogiannis, E. Aggeli, V.G. Papadakis, S. Tsivilis, Evaluation of chloride-penetration resistance of metakaolin concrete by means of a diffusion – Binding model and of the k-value concept, *Cement and Concrete Composites*, 63 (2015) 1-7.
- [148] A. Boddy, R.D. Hooton, K.A. Gruber, Long-term testing of the chloride-penetration resistance of concrete containing high-reactivity metakaolin, *Cement and Concrete Research*, 31 (2001) 759-765.
- [149] C.S. Poon, S.C. Kou, L. Lam, Compressive strength, chloride diffusivity and pore structure of high performance metakaolin and silica fume concrete, *Construction and Building Materials*, 20 (2006) 858-865.
- [150] A. Souiri, H. Kazemi-Kamyab, R. Snellings, R. Naghizadeh, F. Golestani-Fard, K. Scrivener, Pozzolanic activity of mechanochemically and thermally activated kaolins in cement, *Cement and Concrete Research*, 77 (2015) 47-59.
- [151] Z. Shi, M.R. Geiker, B. Lothenbach, K. De Weerd, S.F. Garzón, K. Enemark-Rasmussen, J. Skibsted, Friedel's salt profiles from thermogravimetric analysis and thermodynamic modelling of Portland cement-based mortars exposed to sodium chloride solution, *Cement and Concrete Composites*, 78 (2017) 73-83.
- [152] M.K. Moradillo, B. Sudbrink, Q. Hu, M. Aboustait, B. Tabb, M.T. Ley, J.M. Davis, Using micro X-ray fluorescence to image chloride profiles in concrete, *Cement and Concrete Research*, 92 (2017) 128-141.
- [153] C. He, E. Makovicky, B. Osbæk, Thermal stability and pozzolanic activity of calcined kaolin, *Applied Clay Science*, 9 (1994) 165-187.
- [154] M. Murat, C. Comel, Hydration reaction and hardening of calcined clays and related minerals. III. Influence of calcination process of kaolinite on mechanical strengths of hardened metakaolinite, *Cement and Concrete Research*, 13 (1983) 631-637.

Curriculum Vitae

François Avet

Date of birth: 04th February 1990

Nationality: French

Education

- Oct 2013 – 2017 PhD thesis at the Swiss Federal Institute of Technology of Lausanne (EPFL) on the investigation and the demonstration of the feasibility of using various grades of calcined kaolinitic clays in Limestone Calcined Clay Cement (LC³ project)
- Jan – Sept 2013 Master's thesis at Siam Cement Group in Saraburi (Thailand) on the study of hydration products of Portland Limestone Cement, to understand how limestone quality influences cement hydration. Also determined the limitations of using lower grade limestone in cement
- July – Dec 2012 Internship at Siam Cement Group in Saraburi (Thailand) to investigate the changes caused by inter-grinding time and limestone content on Portland Composite Cement hydration. Pointed out fineness and phase assemblage influences on porosity
- Spring 2012 Research project at the Laboratory of Construction Materials at EPFL to study the microstructure evolution in slag- and quartz-cement systems and to quantify filler effect
- Fall 2011 Applied project at the Laboratory of Polymer and Composite Technology at the EPFL on the production of shape memory polymer membranes used as actuators
- Spring 2011 Research project at the Laboratory of Construction Materials at the EPFL on the use of small doses of calcite as fluxing agent in fired clay bricks to reduce the calcination temperature
- 2011 Bachelor in Materials Science and Engineering at the EPFL, Lausanne
- 2007 French high school diploma, scientific option with 1st rank honors

Professional & Associative Experience

- Summer 2011 Student assistant of Prof. L.Zuppiroli, director of the Laboratory of Optoelectronics of Molecular Materials at the EPFL. Worked on matter and material history in different civilizations
- 2010 – 2011 Responsible for the sponsoring committee of the "MX On Tour" organization – coordinated fund raising for the annual study trip to Chicago (IL, USA)
- 2009 – 2010 Coach and Webmaster of the materials section coaching at the EPFL

Publications

- 2017 Avet F., Scrivener K. Use of various grades of calcined kaolinitic clays in Limestone Calcined Clay Cement (LC³). International Conference on Advances in Construction Materials and Systems, Chennai, India
- 2017 Avet F., Scrivener K. Evaluation of the potential of calcined kaolinitic clays as clinker substitute in Limestone Calcined Clay Cement (LC³). XVI International Clay Conference, Granada, Spain
- 2017 Avet F., Maraghechi H., Scrivener K. Analysis of chloride transport and binding in limestone calcined clay binders with various kaolinite content. 14th International Conference on Durability of Building Materials and Components. Ghent, Belgium
- 2017 Avet F., Boehm-Courjault E., Scrivener K. Morphology and composition of C-A-S-H in Limestone Calcined Clay Cement (LC³). EMABM2017, Les Diablerets, Switzerland
- 2016 Avet F., Snellings R., Alujas A. Ben Haha M., Scrivener K. Development of a new Rapid, relevant and reliable (R³) testing method to evaluate the pozzolanic reactivity of calcined clays. Cement and Concrete Research 85 (2016) 1-11
- 2016 Avet F., Scrivener K. Investigation of the reactivity of various grades of kaolinitic calcined clays used as partial clinker substitute. 2nd International Conference on Advances in Cement and Concrete in Africa. Dar Es Salaam, Tanzania
- 2016 Avet F., Scrivener K. Difference in kinetics of hydration for various grades of kaolinitic calcined clays in Limestone Calcined Clay Cement (LC³) systems. International Symposium of Chemistry, Santa Maria, Cuba
- 2015 Avet F., Snellings R, Alujas A., Ben Haha, M., Scrivener K. Development of a new Rapid, relevant and reliable (R³) testing method to evaluate the pozzolanic reactivity of calcined clays. 1st International Conference on Calcined Clays for Sustainable Concrete, Lausanne, Switzerland
- 2014 Avet F., Scrivener K. Benchmark test of Low Carbon Cement (LCC) - strength and porosity. 2nd International Congress on Durability of Concrete. New Delhi, India

